Title

Development of Fluorescent and Bioluminescent Hybrid Voltage Imaging Strategies for Voltage Sensitive Dyes

Author

Benlian, Brittany

Publication Date

2021

Peer reviewed|Thesis/dissertation

Development of Fluorescent and Bioluminescent Hybrid Voltage Imaging Strategies for Voltage Sensitive Dyes

By

Brittany Renee Benlian

A Dissertation submitted in partial satisfaction of the
requirements for the degree of
Doctor of Philosophy
In
Molecular and Cell Biology
In the
Graduate Division
of the
University of California, Berkeley

Committee in charge:

Professor Evan W. Miller, Chair
Professor David Savage
Professor Diana Bautista
Professor Daniela Kaufer

Fall 2021

Development of Fluorescent and Bioluminescent Hybrid Voltage Imaging Strategies for Voltage Sensitive Dyes

By Brittany Renee Benlian

Abstract

Development of Fluorescent and Bioluminescent Hybrid Voltage Imaging Strategies for Voltage Sensitive Dyes

By

Brittany Renee Benlian

Doctor of Philosophy in Molecular and Cell Biology
University of California, Berkeley
Professor Evan W. Miller, Chair

Understanding the broader implications and functions of membrane potential in the brain, heart, and body requires accurate and simultaneous membrane-associate voltage measurements on a large array of single cells. Achieving high spatial resolution and millisecond time resolution with minimal perturbation to live cells is a long-standing challenge, especially within the field of neurobiology. Direct imaging of membrane potential changes with fluorescence-based voltage indicators has become a powerful and most popular approach to mapping electrical changes yet several challenges addressing indicator speed, brightness, sensitivity, and localization remain. The Miller lab focuses on addressing these issues using a relatively new class of small molecule voltage indicators, VoltageFlours, that depend on a photo-induced electron transfer (PeT) mechanism. The intramolecular electron transfer modulates fluorescence intensity based on the surrounding electric field and results in sub-microsecond response kinetics with high voltage sensitivity. As with all organic indicators, the cellular spatial resolution in dense tissue samples is limited since VoltageFluors indiscriminately stain all membrane types. Our group has worked on addressing this limitation by combining VoltageFluors with genetically encoded self-labeling enzymes like the well-known Halo- and SNAP-tag proteins. Portions of this dissertation will focus specifically on the SNAP-tag covalent tethering approach with fluorescein and rhodamine-based VoltageFluors. The remainder of this thesis is primarily focused on a new branch of voltage imaging using bioluminescence which has never been explored within our group. Fluorescent indicators are dependent on externally applied illumination leading to unavoidable light-induced damage, *especially* at shorter wavelengths, which alters cell physiology and confounds data. There are relatively few examples of bioluminescent indicators relative to fluorescent indicators, and even fewer that are voltage sensitive. This dissertation will explore the development of the first ever quenching bioluminescent voltage indicator, limitations to single cell bioluminescent voltage imaging, and other potential approaches to functionalize bioluminescence at the membrane.

Table of Contents

Chapter 1:
Introduction to Covalent Targeting of VoltageFluors and Bioluminescent Voltage Sensing

Membrane potential is a crucial component of cellular physiology. Cells maintain an electrochemical gradient of unequal ion distributions through variable ion permeabilities across a lipid bilayer. This gradient creates a resting membrane potential in all cell types and holds an important role in cellular signaling and homeostasis (**Figure 1-1**). For example, a change in resting potential of epithelial or other non-excitable cells can impact cell migration, division, and proliferation[1–3] especially within cancer biology[4,5]. In excitable cells, like neurons and cardiomyocytes, rapid millisecond changes in membrane potential can generate an action potential. The pattern and frequency of action potential firing events relays specific information within complex communication networks of the brain to control behavior, emotion, perception, and so much more. Within the heart, pacemaker cells generate electrical potentials responsible for triggering cardiac muscle contraction[6]. Deeper understanding of the broader implications and functions of membrane potential on cell signaling pathways in the brain, heart, and body requires rapid, accurate, and simultaneous measurements on a large array of cells.

For a long time, electrophysiological recordings have remained the gold standard for studying membrane potential and the technique been incredibly impactful to the field. Yet as our knowledge grows, electrode-based measurements have true limitations and challenges which impede their use in certain instances. For example, the sheer invasiveness of the method precludes any study of cellular movement and migration in relation to membrane potential regulation in cancer cells. Electrophysiological techniques are also challenging to master, destructive to the cell membrane, low throughput, and while the temporal resolution is excellent it suffers from poor spatial resolution. Fluorescence-based indicators are a very attractive alternative to electrode-based methods. The optical approach offers high throughput means to study changes in membrane potential with increased spatial resolution, decreased invasiveness, and temporal resolution comparable to electrophysiology. The indicators themselves are typically small molecules, genetically encoded protein sensors, or a hybrid of the two.

Florescence-based organic dyes with spectral voltage-sensitive properties where discovered in the early 1970's[7,8]. Over the decades numerous fast- and slow-sensing synthetic indicators have been discovered, and new strategies continue to be investigated to this day[9,10]. Electrochromic dyes are among the first well known "fast" voltage indicators due to their rapid color change modulated by changes in the electric field[11]. On the other hand, the mechanism of "slow" dyes is dependent on accumulation or redistribution relative to membrane potential[11–13]. These traditional types of voltage-indicators have laid the foundation for voltage imaging however neither are perfect: fast dyes suffer low sensitivity from only a small spectral shift[14] (few nanometers) and while slow dyes have higher sensitivity, the slower response mechanism cannot resolve action potential dynamics and/or adds a capacitive load to the membrane[11–15].

More recently, our group has developed a new series of voltage indicators, VoltageFlours, with both fast response kinetics and high voltage sensitivity by way of a photo-induced electron transfer (PeT) mechanism (**Figure 1-2**). The structural composition of our traditional VoltageFluors combines a hydrophobic phenylene vinylene molecular wire coupled to a bright xanthene fluorophore. Fluorophore quenching is dependent on the rate of PeT between the electron donor and acceptor coupled to the wire, which is in turn modified by the membrane potential. With the indicator resting within the membrane, a hyperpolarized resting state accelerates the rate of PeT and fluorescence quenching. Upon depolarization, the rate of PeT is reduced resulting in a large fluorescence turn-on with excellent voltage sensitivity ranging from 10% to 60% $\Delta F/F$ per 100 mV depending on the dye). VoltageFluors have been incredibly useful molecules in studying the mechanistic insights between membrane potential and biological observations both *in vitro* and

in vivo[16–19]. For instance, sRhoVR imaging in live mice showed transmembrane depolarizations at varying depths within the somatosensory cortex, connecting physical brain structures to a functional output[19].

Transitioning VoltageFluor applications into complex tissues has highlighted the challenge and necessity of single-cell resolution. As with all synthetic indicators, VoltageFluors indiscriminately stain all membranes, limiting the spatial resolution in dense and heterogeneous samples. To address this problem, our group has more recently focused on hybrid targeting approaches using VoltageFlours (**Figure 1-3**). One promising approach covalently links VoltageFluors to a self-labeling enzyme, non-reversibly anchoring the dye into cell membranes expressing the exogenous protein[20–22]. We have also explored fluorogenic uncaging to enzymatically activate, or turn on the dye without anchoring it to the protein [23]. Each targeting system has shown varying results in protein expression, targeting efficiency, and retention of voltage sensitivity relative to the untargeted parent VF derivative.

Our covalent targeting method using the SpyTag/SpyCatcher system with VoltageSpy (VF2.1.Cl coupled to the SpyTag peptide) gave contrast ratios up to 35-fold in HEK cells with a slight decrease in cultured neurons to 25-fold[20]. VoltageSpy maintained good voltage sensitivity (12% ΔF/F) albeit lower than the unmodified VF2.1.Cl scaffold (27% ΔF/F)[24]. Covalent targeting of voltage indicators can also be adapted to other fluorophore scaffolds, including rhodamine and silicon-rhodamines, by coupling RhoVR1[17] and BeRST[25] rhodamine based VoltageFluors to a HaloTag ligand. BeRST-HaloTag had 3x better contrast than RhoVR1-HaloTag in HEK cells with a 30-fold difference in fluorescence intensity for HaloTag expressing cells compared to non-expressing[21,22]. BeRST-HaloTag was also the only targeted VoltageFluor that retained the same voltage sensitivity as its non-targeted derivative (BeRST 24% ΔF/F and BeRST-HaloTag 21% ΔF/F)[22]. RhoVR1-HaloTag has the largest voltage response of all our targeted dyes (34% ΔF/F), but we did encounter a 13 percentage-point decrease relative to the parent RhoVR1 (47% ΔF/F)[21]. Additionally, not only could we see successful cell-specific labeling for BeRST and RhoVR1 HaloTag VoltageFlours, but both dyes were able to record single trial action potentials in cortical neurons from mouse brain slices sparsely expressing cell-surface HaloTag.

We also found success with fluorogenic targeting over a series of VF-EX dyes by coupling methylcyclopropylacetoxymethyl ether groups to our prototypical VF2.1.Cl scaffold. The labile ether drastically reduces fluorescence until hydrolysis by porcine liver esterase (PLE) exogenously expressed at the cell membrane. Contrast in fluorescence between PLE-expressing and non-expressing cells was up to 17-fold in HEK cells and a 4-fold in cultured neurons[23]. Similarly to the covalently targeted VF2.1.Cl derivatives (VoltageSpy), VF-EX maintained a good voltage sensitivity (21% ΔF/F) but which was also lower than the unmodified VF2.1.Cl (27% ΔF/F)[26].

Experiments are also underway to expand this covalent tethering approach to fluorescein and rhodamine-based VoltageFluors using the well know SNAP-tag system[27,28]. The SNAP-tag protein is a mutant form of the human DNA repair enzyme, O6-alkylguanine-DNA transferase (hAGT), which reacts specifically and non-reversibly with a wide variety of benzylguanine (BG) derivatives[29]. In 2011, further mutations of the SNAP-tag mutant, now referred to as $SNAP_f$, improved its reactivity by 10-fold and demonstrated fast, wash free labeling at the cell surface after just 5 minutes[30]. With its fast reactivity and proven membrane targetability, we were interested in exploring how the SNAP-tag system would compare to Halo- and SpyTag VoltageFluor targeting. We found improved protein expression and enhanced fluorescence contrast of transfected cells using $SNAP_f$ compared to the original SNAP-tag protein. The fluorescein and rhodamine-based derivatives show excellent labeling and voltage sensitivity, however contrast with the rhodamine-

SNAP-tag ligand drastically improves the contrast (40-fold) likely due to the reduced autofluorescence from using a more spectrally red-shifted indicator. Chapter 2 and Appendix 1 of this thesis will focus in more detail on the development, synthesis, and characterization of hybrid VoltageFluor/SNAP-tag approaches to cell-specific targeting.

The remainder of this thesis is primarily focused on a new branch of voltage imaging using bioluminescence and has never been explored within our group. Many of the best and most used fluorescent probes in cell biology require blue excitation light. This short wavelength of light considerably increases tissue autofluorescence from endogenous chromophores which reduces the signal-to-noise ratio and prevents simultaneous imaging with other indicators or actuators within the same spectral region. Additionally, extended periods of exposure (seconds to minutes) under intense incident radiation necessary to excite fluorophores causes light-induced damage, *especially* at shorter wavelengths, altering cell physiology and confounding experimental data[31–33]. Eliminating the incident radiation used in fluorescence microscopy, and instead utilizing an alternative excitation energy source, would reduce these effects and expand experimental time courses from seconds to minutes and hours.

Bioluminescent methods avoid the use of excitation light, relying instead on the luciferase-catalyzed promotion of a luciferin substrate into the excited state. A number of luciferase–luciferin pairs have been deployed in a range of applications from protein-protein interaction assays[34], visualization of gene expression[35], whole-organism imaging[36,37], Ca^{2+} dynamics[38], adenosine 5′-triphosphate (ATP)[39] and cyclic adenosine monophosphate (cAMP) dynamics[40] through either a pure bioluminescent or bioluminescence resonance energy transfer (BRET) approach[41]. However, there are relatively few examples of bioluminescent indicators and reporters compared to the number of fluorescent indicators and reporters, and even fewer to measure voltage changes at the plasma membrane.

To date, very few bioluminescent voltage indicators exist: LOTUS-V[42], AMBER[43], and the first ever hybrid bioluminescent indicator developed by our group, Q-BOLT[44] (**Figure 1-4**). LOTUS-V utilizes bioluminescence resonance energy transfer (BRET) changes between the NanoLuc luciferase and fluorescent protein, Venus. The distance dependent BRET efficiency is modulated by conformational changes of the voltage sensing domain (VSD) from the phosphatase of *Ciona intestinalis* with a sensitivity of 21% $\Delta R/R$ per 100 mV[42]. Similarly, the Autonomous Molecular BioluminEscent Reporter (AMBER) utilizes the functionality of the same VSD but couples the N- and C-terminals to a flavin reductase phosphate (FRP) and a bacterial luciferase/yellow fluorescence protein BRET pair, LuxAB/YFP, respectively. Unlike other bioluminescent systems, AMBER encodes both luciferase and luciferin genes and uses the voltage dependent conformational change of the VSD to modulate the enzymatic activity of the luciferase. At more positive membrane potentials the proximity between FRP and luciferase decreases, improving substrate availability and resulting in an increased probability of photon emission[43]. Simultaneous whole-cell electrophysiology and optical characterization in HEK293T did not show a linear increase within a physiologically relevant range between -70 to +40 mV, however the group was able to identify neuronal activity in live *Caenorhabditis elegans*.

Our lab developed the first ever quenching bioluminescent voltage indicator (Q-BOLT) inspired by fluorescent hybrid voltage sensors (hVOSs) and two-component oxonol–coumarin systems. The bioluminescent properties of Q-BOLT, however, eliminate the need for illumination and associated issues of photobleaching, phototoxicity, and background fluorescence. Luminescence from an extracellular membrane-targeted luciferase, NanoLuc (NLuc), is quenched by a nonfluorescent voltage sensor, dipicrylamine (DPA). The energy transfer mechanism between

the luciferin and DPA is similar to the well-established Förster resonance energy transfer (FRET) theory but is classified more specifically as quenching resonance energy transfer (QRET) due to the nonfluorescent absorber. Lipophilic and anionic properties allow DPA to localize and redistribute within the membrane bilayer in a voltage-dependent manner. Q-BOLT also includes the self-labeling HaloTag protein fused to the N-terminus of NLuc. The addition of a fluorescent HaloTag ligand incorporates a second energy acceptor, which allows BRET and QRET to occur simultaneously. We show that DPA can quench bioluminescence at hyperpolarized membrane potentials and this quenching is reduced upon depolarization, resulting in an increased bioluminescent and BRET signal.

Q-BOLT demonstrated a real ability to measure single-cell voltage changes without illumination but was not without its limitations. We hypothesize one of the biggest challenges in resolving *fast* ratio metric single-cell bioluminescent voltage changes is photon emission and collection. Efforts to improving the BRET signal are underway and initial explorations are discussed within the appendices. Chapters 3 and 4 focus on the development of Q-BOLT and alternative chemical-genetic approaches to bioluminescent voltage indicators using a 2-acceptor RET system. The interesting ratio-metric readout using a 2-acceptor RET system may be a promising approach for absolute membrane potential determination. However, with Q-BOLT the dynamic range in the difference between raw ratio values at -60 mV and +60 mV was not large enough to predict mV values with accuracy. Initial efforts to explore alternative acceptor/donor/acceptor combinations to achieve a larger dynamic range are also discussed in Appendices 2 and 3 but need further investigation.

This thesis describes the design, synthesis, and characterization of SNAP-tag mediated covalent targeting of fluorescein VoltageFluors in Chapter 2 and rhodamine VoltageFluors in Appendix 1. The remainder of the thesis focuses primarily on exploring bioluminescent voltage imaging. Chapter 3 describes the development of our groups first ever hybrid small-molecule bioluminescent voltage indicator, Q-BOLT, and its application in cardiomyocytes. The chapter also discusses the interesting 2-acceptor RET system and its potential as a new and novel technique for ratiometric measurements. Chapter 4 further explores the abilities of bioluminescent voltage imaging using VoltageFluors and alternative genetically encoded voltage indicators. Appendices 2 and 3 describe efforts to further explore alternative fluorescent- and bioluminescent-based ratiometric voltage indicators using the 2-acceptor and 1 donor configuration. Appendix 4 explains initial efforts to apply Q-BOLT to intracellular organelle membranes, and Appendix 5 explores the possibility of bioluminolysis to uncage VoltageFluors modified with a photolabile quencher.

Figures and Schemes

Figure 1-1. *Membrane potential exists in all cell types*

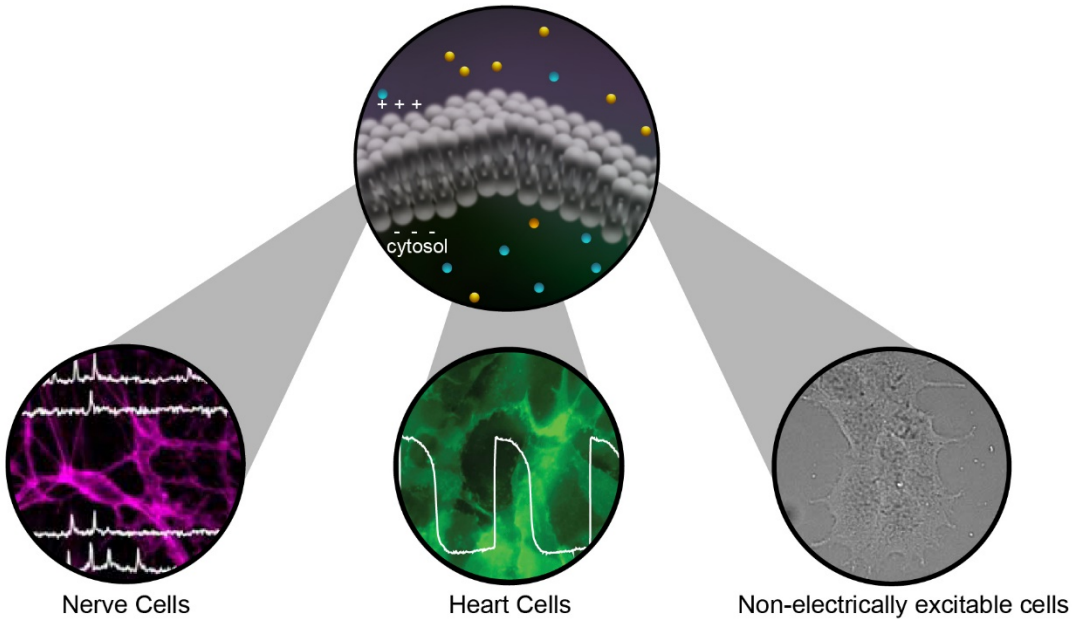

Figure 1-1. Scheme of membrane potential and relevance in various cell types. Membrane potential within a cell is more negative (- - -) relative to the extracellular environment. This difference is a result of ion concentration gradients across a selectively permeable bilayer. Higher sodium concentrations exist outside the cell (orange) and high potassium concentrations exist inside the cell (blue). Rapid depolarization events generate action potentials which can be optically measured with fluorescent VoltageFluors (white voltage traces transposed over images). Action potential spikes in nerve cells (magenta) occur within milliseconds, whereas heart cell (green) action potentials last the duration of a few hundred milliseconds. Non-electrically excitable cells do not elicit action potentials, but still maintain a resting membrane potential important for normal cellular processes.

Figure 1-2. *Fluorescence photoinduced electron transfer-based voltage sensing*

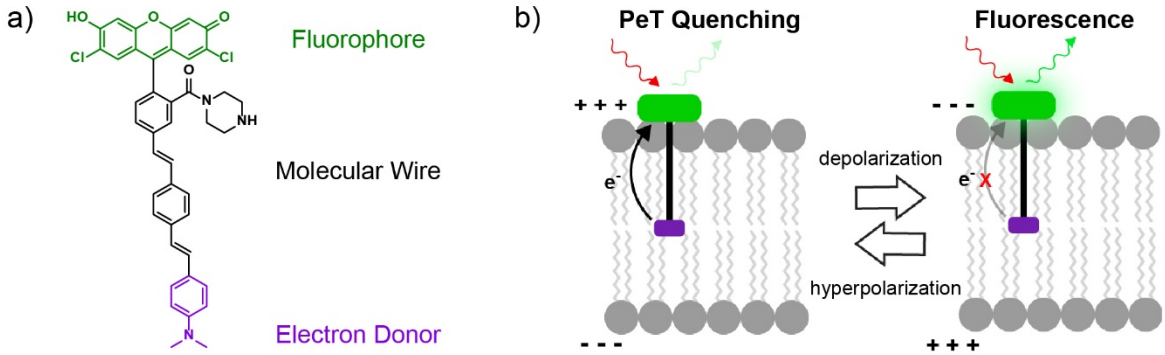

Figure 1-2. Structure and voltage sensing scheme employed by VoltageFlours. a) All VoltageFluors are composed of an electron poor fluorescent head group (green), a hydrophobic molecular wire (black), and an electron donating group (magenta). The molecule wire **b)** anchors the dye into the membrane while the slight negative charge of the fluorophore at pH 7 helps to prevent internalization. At rest, the increased rate of electron transfer from the electron donating group quenches the fluorescence (PeT quenching). Changes in the membrane-associated electric field during a depolarization event reduce the rate of electron transfer resulting a bright fluorescence turn on.

Figure 1-3. *Hybrid targeting approaches using VoltageFlours*

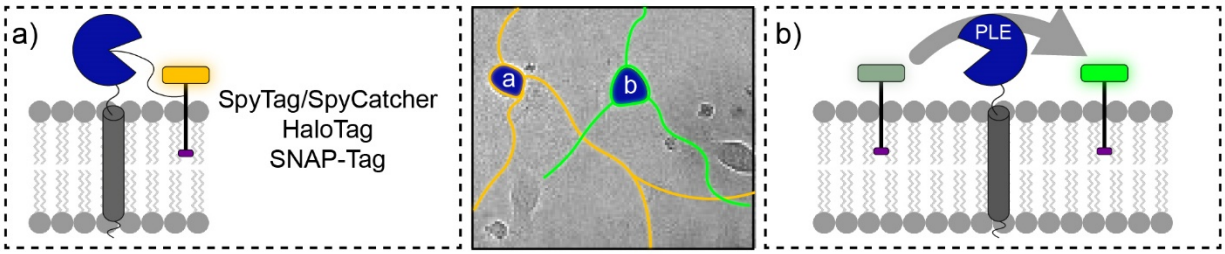

Figure 1-3. Hybrid strategies used for cell-specific targeting of VoltageFlours. a) Non-reversible Covalent tethering of VoltageFluors to a self-labeling enzyme like SpyCatcher, HaloTag, or SNAP-tag expressed at the cell surface. **b)** Enzymatic fluorogenic uncaging to activate a capped VoltageFluor, for example using porcine liver esterase (PLE).

Figure 1-4. *Bioluminescent voltage indicators*

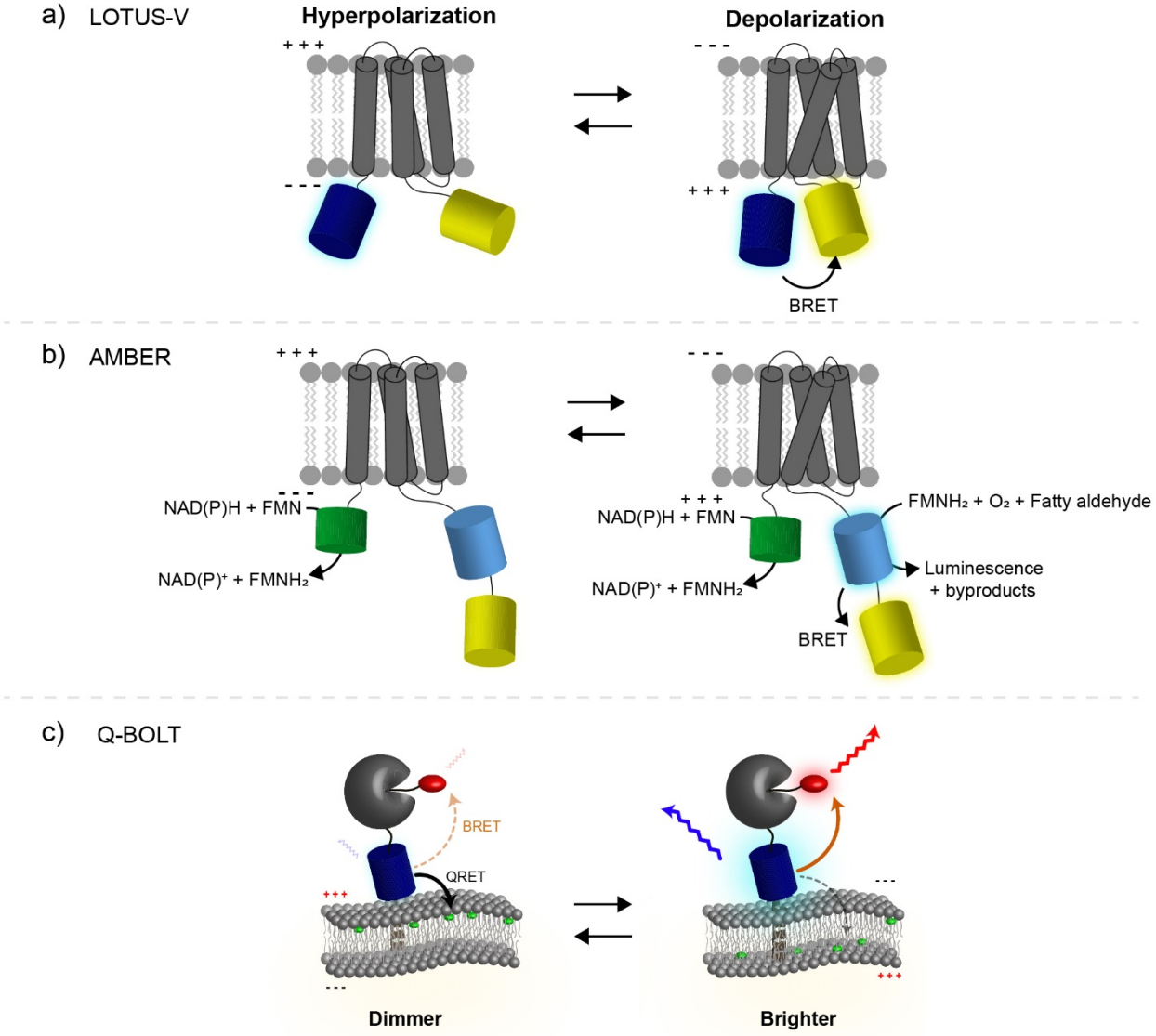

Figure 1-4. Overview of current bioluminescent voltage indicators. a) Bioluminescence resonance energy transfer (BRET) of LOTUS-V is dependent on conformational changes from the *Ciona intestinalis* phosphatase voltage sensing domain (VSD). The BRET efficiency between NanoLuc luciferase (blue, NLuc) and the fluorescent protein, Venus (yellow) increases at depolarization and decreases when a cell is at rest, or hyperpolarized. **b)** The Autonomous Molecular BioluminEscent Reporter (AMBER) uses the same VSD but couples the N- and C-terminals to a flavin reductase phosphate (FRP, green) and a bacterial luciferase/yellow fluorescence protein BRET pair, LuxAB (cyan) and YFP (yellow), respectively. For clarity, the mechanism of action is abbreviated in this scheme, but in general the luminescence and BRET output is dependent on substrate availability ($FMNH_2$) which is increased at depolarized membrane potentials due to the increased FRP and luciferase proximity. **c)** QRET voltage sensing mechanism with HaloTag (grey) fused to the N-terminal of NLuc (blue) and anchored to the plasma membrane through a transmembrane domain (brown). At negative membrane potentials DPA (green) quenches luminescence. Depolarizations redistribute DPA closer to the inner leaflet, leading to a decrease in QRET, and an increase bioluminescence at BRET emission.

References

1. Blackiston, D. J., McLaughlin, K. A. & Levin, M. Bioelectric controls of cell proliferation: ion channels, membrane voltage and the cell cycle. *Cell Cycle* **8**, 3519–3528 (2009).
2. Sundelacruz, S., Levin, M. & Kaplan, D. L. Role of membrane potential in the regulation of cell proliferation and differentiation. *Stem Cell Rev. Reports* **5**, 231–246 (2009).
3. Jiménez-Pérez, L. *et al.* Molecular determinants of Kv1.3 potassium channels-induced proliferation. *J. Biol. Chem.* **291**, 3569–3580 (2016).
4. Yang, M. & Brackenbury, W. J. Membrane potential and cancer progression. *Frontiers in Physiology* **4 JUL**, (2013).
5. Pardo, L. A., Brüggemann, A., Camacho, J. & Stühmer, W. Cell cycle-related changes in the conducting properties of r-eag K+ channels. *J. Cell Biol.* **143**, 767–775 (1998).
6. Fozzard, H. A. & Gibbons, W. R. Action potential and contraction of heart muscle. *Am. J. Cardiol.* **31**, 182–192 (1973).
7. Salzberg, B. M., Davila, H. V. & Cohen, L. B. Optical Recording of Impulses in Individual Neurones of an Invertebrate Central Nervous System. **246**, 508–509 (1973).
8. Davila, H. V, Salzberg, B. M., Cohen, L. B. & Waggoner, A. S. A Large Change in Axon Fluorescence that Provides a Promising Method for Measuring Membrane Potential. *Nat. New Biol.* **241**, 159–160 (1973).
9. Terai, T. & Nagano, T. Small-molecule fluorophores and fluorescent probes for bioimaging. *Pflugers Arch. Eur. J. Physiol.* **465**, 347–359 (2013).
10. Kulkarni, R. U. & Miller, E. W. Voltage Imaging: Pitfalls and Potential. *Biochemistry* **56**, 5171–5177 (2017).
11. Peterka, D. S., Takahashi, H. & Yuste, R. Imaging Voltage in Neurons. *Neuron* **69**, 9–21 (2011).
12. González, J. E. & Tsien, R. Y. Improved indicators of cell membrane potential that use fluorescence resonance energy transfer. *Chem. Biol.* **4**, 269–277 (1997).
13. González, J. E. & Tsien, R. Y. Voltage sensing by fluorescence resonance energy transfer in single cells. *Biophys. J.* **69**, 1272–1280 (1995).
14. Kuhn, B. & Fromherz, P. Anellated hemicyanine dyes in a neuron membrane: Molecular Stark effect and optical voltage recording. *J. Phys. Chem. B* **107**, 7903–7913 (2003).
15. Miller, E. W. Small molecule fluorescent voltage indicators for studying membrane potential. *Curr. Opin. Chem. Biol.* **33**, 74–80 (2016).
16. Rodrigues, G. M. C. *et al.* Defined and Scalable Differentiation of Human Oligodendrocyte Precursors from Pluripotent Stem Cells in a 3D Culture System. *Stem Cell Reports* **8**, 1770–1783 (2017).
17. Deal, P. E., Kulkarni, R. U., Al-Abdullatif, S. H. & Miller, E. W. Isomerically Pure Tetramethylrhodamine Voltage Reporters. *J. Am. Chem. Soc.* **138**, 9085–9088 (2016).
18. Walker, A. S. *et al.* Imaging Voltage in Complete Neuronal Networks Within Patterned Microislands Reveals Preferential Wiring of Excitatory Hippocampal Neurons. *Front. Neurosci.* **15**, 1–14 (2021).
19. Kulkarni, R. U. *et al.* In Vivo Two-Photon Voltage Imaging with Sulfonated Rhodamine Dyes. *ACS Cent. Sci.* **4**, 1371–1378 (2018).
20. Grenier, V., Daws, B. R., Liu, P. & Miller, E. W. Spying on Neuronal Membrane Potential with Genetically Targetable Voltage Indicators. *J. Am. Chem. Soc.* **141**, 1349–1358 (2019).
21. Deal, P. E. *et al.* Covalently Tethered Rhodamine Voltage Reporters for High Speed Functional Imaging in Brain Tissue. *J. Am. Chem. Soc.* **142**, 614–622 (2020).

22. Ortiz, G. *et al.* A Silicon-Rhodamine Chemical-Genetic Hybrid for Far Red Voltage Imaging from Defined Neurons in Brain Slice A silicon-rhodamine chemical-genetic hybrid for far red voltage imag- ing from defined neurons in brain slice. **8**, (2020).
23. Liu, P., Grenier, V., Hong, W., Muller, V. R. & Miller, E. W. Fluorogenic Targeting of Voltage-Sensitive Dyes to Neurons. *J. Am. Chem. Soc.* **139**, 17334–17340 (2017).
24. Miller, E. W. *et al.* Optically monitoring voltage in neurons by photo-induced electron transfer through molecular wires. *Proc. Natl. Acad. Sci.* **109**, 2114–2119 (2012).
25. Huang, Y. L., Walker, A. S. & Miller, E. W. A Photostable Silicon Rhodamine Platform for Optical Voltage Sensing. *J. Am. Chem. Soc.* **137**, 10767–10776 (2015).
26. Miller, E. W. *et al.* Optically monitoring voltage in neurons by photoinduced electron transfer through molecular wires. *Proc. Natl. Acad. Sci. U. S. A.* **109**, 2114–2119 (2012).
27. Rudd, A. K., Valls Cuevas, J. M. & Devaraj, N. K. SNAP-tag-reactive lipid anchors enable targeted and spatiotemporally controlled localization of proteins to phospholipid membranes. *J. Am. Chem. Soc.* (2015). doi:10.1021/jacs.5b00040
28. Comps-Agrar, L. *et al.* Cell-surface protein-protein interaction analysis with time-resolved FRET and snap-tag technologies: Application to G protein-coupled receptor oligomerization. *Methods Mol. Biol.* (2011). doi:10.1007/978-1-61779-160-4_10
29. Keppler, A. *et al.* A general method for the covalent labeling of fusion proteins with small molecules in vivo. (2002). doi:10.1038/nbt765
30. Sun, X. *et al.* Development of SNAP-tag fluorogenic probes for wash-free fluorescence imaging. *ChemBioChem* **12**, 2217–2226 (2011).
31. Laissue, P. P., Alghamdi, R. A., Tomancak, P., Reynaud, E. G. & Shroff, H. Assessing phototoxicity in live fluorescence imaging. *Nat. Methods* **14**, 657–661 (2017).
32. Dixit, R. & Cyr, R. Cell damage and reactive oxygen species production induced by fluorescence microscopy: Effect on mitosis and guidelines for non-invasive fluorescence microscopy. *Plant J.* **36**, 280–290 (2003).
33. Boggess, S. C., Gandhi, S. S., Benlian, B. R. & Miller, E. W. Vinyl-Fluorene Molecular Wires for Voltage Imaging with Enhanced Sensitivity and Reduced Phototoxicity. *J. Am. Chem. Soc.* **143**, 11903–11907 (2021).
34. Dixon, A. S. *et al.* NanoLuc Complementation Reporter Optimized for Accurate Measurement of Protein Interactions in Cells. *ACS Chem. Biol.* **11**, 400–408 (2016).
35. Chen, Z. H., Zhao, R. J., Li, R. H., Guo, C. P. & Zhang, G. J. Bioluminescence Imaging of DNA Synthetic Phase of Cell Cycle in Living Animals. *PLoS One* **8**, (2013).
36. Zhao, H. *et al.* Emission spectra of bioluminescent reporters and interaction with mammalian tissue determine the sensitivity of detection in vivo. *J. Biomed. Opt.* **10**, 041210 (2005).
37. Iwano, S. *et al.* Single-cell bioluminescence imaging of deep tissue in freely moving animals. *Science (80-.).* **359**, 935 LP – 939 (2018).
38. Suzuki, K. *et al.* Five colour variants of bright luminescent protein for real-time multicolour bioimaging. *Nat. Commun.* **7**, 13718 (2016).
39. Pellegatti, P., Falzoni, S., Pinton, P., Rizzuto, R. & Di Virgilio, F. A Novel Recombinant Plasma Membrane-targeted Luciferase Reveals a New Pathway for ATP Secretion. *Mol. Biol. Cell* **16**, 3659–3665 (2005).
40. French, A. R., Tesmer, A. L. & Tantama, M. Dual-Mode FRET and BRET Sensors for Detecting cAMP Dynamics. *ACS Omega* **4**, 15504–15511 (2019).
41. Wang, A., Feng, J., Li, Y. & Zou, P. Beyond Fluorescent Proteins: Hybrid and

Bioluminescent Indicators for Imaging Neural Activities. *ACS Chem. Neurosci.* (2018). doi:10.1021/acschemneuro.7b00455

42. Inagaki, S. *et al.* Genetically encoded bioluminescent voltage indicator for multi-purpose use in wide range of bioimaging. *Sci. Rep.* **7**, 1–11 (2017).
43. Srinivasan, P. *et al.* An Autonomous Molecular Bioluminescent Reporter (AMBER) for voltage imaging in freely moving animals Department of Electrical and Computer Engineering , Harold Frank Hall , University of Department of Molecular , Cellular and Developmental Biology and t. (2019).
44. Benlian, B. R. *et al.* Small Molecule-Protein Hybrid for Voltage Imaging via Quenching of Bioluminescence. *ACS Sensors* (2021). doi:10.1021/acssensors.1c00058

Chapter 2:
Genetic Targeting of VoltageFluors

Portions of this work were performed in collaboration with the following persons:

Synthesis was assisted by Vincent Grenier and Jonathon Maza
Molecular cloning and imaging for Drosophila performed by Molly Kirk.

Abstract

Membrane potential (V_{mem}) changes across neurons within a complex circuit is fundamental to understanding how the brain encodes and computes sensory behavior, learning, memory, and cognition. Being able to measure these rapid signals may allow us to better understand the differences between normal and disease neurological states. However, being able to monitor and record these changes with high fidelity in complex tissues has been a long-standing challenge in neuroscience. Optical methods offer improved spatial resolution relative to traditional electrode-based measurements, and in some instances can still maintain excellent temporal resolution. For example, voltage-sensitive fluorophores, or VoltageFlours (VFs), utilize a photoinduced electron transfer voltage sensing mechanism capable of resolving sub-millisecond electrical events. However, within complex tissues the application of VFs results in non-specific staining of all membranes making it challenging to isolate voltage changes from single cells or specific cell types. Here we have extended the versatility of VFs by incorporation of a reactive O^6-benzylguanine (BG) handle which allows for covalent labeling of cells expressing the modified DNA methyltransferase $SNAP_f$ protein. The BG VoltageFlour, mSNAP2, provides a ~20X turn on with a ΔF/F of 19% per 100 mV in HEK293T cells. Using previously characterized *Drosophila* reporter line, $SNAP_f$-CD4 (unpublished, Molly Kirk) in combination with mSNAP2 voltage-sensitive dye, we show that mSNAP2 is capable of labeling genetically defined subpopulations of neurons in vivo. mSNAP2 robustly reports drug-evoked depolarizations in live *Drosophila* explant brains.

Introduction

Billions of neurons connect and intertwine to form complex neural circuits. These circuits coordinate action potentials through differential ion permeabilities to ultimately control behavior, perception, emotion, and more. However, being able to successfully monitor these events to understand neuronal communication has been a long-standing challenge in neuroscience. Traditional electrode measurements restrict our ability to interrogate multiple cells within a network, the size of the electrode is often too large to measure activity at smaller projections, and the method is not a trivial skill to learn. The development of optical techniques to directly monitor changes in membrane potential (V_{mem}) has proven powerful, offering a less invasive alternative to electrode measurements with improved spatial resolution.

One approach uses protein based genetically encoded voltage indicators (GEVIs) which can be targeted to distinct cell populations by leveraging cell type-specific promoters.[1,2] GEVIs have become a popular technique for probing cells *in vitro* and *in vivo* given their genetic targetability however overall improvements to brightness, response kinetics, and plasma membrane localization are still needed. For instance, suboptimal protein localization contributes to non-functional intracellular fluorescence coming from protein not yet trafficked to the plasma membrane, incorrect trafficking to intracellular membranes, or even cellular aggregation. On the other hand, synthetic indicators like VotlageFlours (VFs) localize *only* to the plasma membrane and cannot typically distinguish cell type specificity. However, targeting a small molecule to a specific cell of interest is much more challenging but without this targetability the usefulness of organic dyes becomes extremely limited in more complex studies *in vivo* or in dense tissue preparations. Both optical approaches have their advantages but are not without their limitations.

Other challenges to consider with both GEVIs and synthetic indicators include toxicity, added membrane excitability or capacitance, physiologically relevant dynamic range or voltage sensitivity, and rapid kinetics capable of detecting sub-millisecond events. VFs sense electrical

changes via a photoinduced electron transfer (PeT) mechanism where at resting membrane potentials, the more negative intracellular environment promotes an intramolecular electron transfer to the fluorescent reporter thereby quenching fluorescence. Membrane depolarization reduces the rate of electron transfer resulting in a linear fluorescence turn-on response. Additionally, these indicators do not induce membrane excitability, contribute to additional membrane capacitance, have linear voltage responses within a physiological range (-100 to +100 mV), and can detect sub-microsecond electrical events.[3] Here we report a chemical-genetic hybrid approach to combine the speed, sensitivity, and brightness of our VoltageFluor (VF) dyes with the cell-specificity of genetic targeting through covalent targeting with a self-labeling enzyme. Previous work in our group showed success with SpyTag/SpyCatcher systems in mammalian HEK cells and dissociated rat hippocampal neurons.[4,5] The contrast between SpyCatcher expressing and non-expressing cells was as large as 35-fold using a VoltageFluor2.1.Cl[6] derived SpyTag indicator (VoltageSpy) in HEK cells and maintained a high contrast ratio and voltage sensitivity when transferred into cultured neurons. Similarly, HaloTag VoltageFluor systems not only showed successful cell-specific labeling for BeRST and RhoVR1 HaloTag VFs, but both dyes were able to record single trial action potentials within brain slices.[7–9]

We have now expanded this approach by synthetically incorporating a reactive O^6-benzylguanine (BG) handle which covalent reacts with the modified DNA methyltransferase $SNAP_f$ protein (**Scheme 2-1**).[10] The $SNAP_f$ protein is an improved version of the original SNAP-tag protein derived from the human DNA repair enzyme, O6-alkylguanine-DNA transferase (hAGT), which reacts specifically and non-reversibly with a wide variety of benzylguanine (BG) derivatives.[11] We show the $SNAP_f$ VF effectively labels transfected dissociated hippocampal neurons and the antenna-lobe in $SNAP_f$ transgenic *drosophila melanogaster*. By expanding our toolbox of genetically tractable indicators, we hope more complicated neurological circuits could be studied by combining orthogonal VF tagging systems, for example using a rhodamine-HaloTag and fluorescein-SNAP-tag to simultaneously record excitatory and inhibitory neuronal activity.

Results and Discussion

Synthesis of Piperazine-Cysteic Acid VoltageFluor Dyes

The presence of a charged sulfonate group at the 3 position on the meso aromatic ring of VoltageFluor2.1.Cl (VF2.1Cl) is excellent for maintaining cellular impermeability. However, the aryl sulfonate does not allow for further covalent modifications. We previously reported both rhodamine- and fluorescein-based voltage indicators in which the sulfonate is replaced with a sarcosine amide (**1,2**) creating an easily accessible synthetic handle for the addition of chemical ligands. Our previous work has shown success in genetic targeting with the addition of Halo-tag and SpyTag ligands which react with HaloTag and SpyCatcher enzymes expressed at the cell surface, respectively. Here we synthesize new fluorescein-based O^6-benzylguanine VoltageFluors. These derivatives should react specifically with the self-labeling SNAP-tag protein, forming an irreversible covalent bond. HATU-mediated piperazine (pip) couplings to isomerically pure 5- and 6-bromo-2',7'-dichlorofluorescein (**3** or **4**) yields tert-butyl ester protected intermediates **5** and **6** in 78 and 93% yield, respectively. Heck coupling of an aniline donating phenylene vinylene molecular wire (**7**) to compounds **5** and **6** gives boc-protected VF-piperazine compounds 8 and 9 in yields ranging from 55 to 61%. Removal of the tert-butyl ester via TFA deprotection gives VF-pip **10** and **11** in moderate to good yield (~65%) after preparative TLC purification. HATU-mediated couplings with boc-protected cysteic acid gives compounds **12** and **13** (43 and 67% yield, respectively) and probes **14** and**15** after TFA deprotection (~95-100% yield). All VF dyes display

similar optical properties, with absorption and emission maxima centered at 525 and 540 nm respectively (**Table 2-1**). Quantum yields for the new dyes range from 0.6% to 29.7%, in line with typical values for fluorescein-type VoltageFluors (**Table 2-1**).[6,12]

In Cellulo Characterization of Piperazine-Cysteic Acid VoltageFlours

All newly synthesized VFs label plasma membranes of HEK293T cells (**Fig. 2-1** and **Fig. 2-2a-d**). In line with previous VF structural comparisons between meta- and para- wire placements, the meta- derivatives are 2x brighter (**Fig. 2-1e**). Relative to the free piperazine VFs (VF-pip), the addition of the cysteic acid moiety (VF-pip-cya) improved fluorescence roughly 1.5 to 2-fold (**Fig. 2-1**). Voltage sensitivities were determined via dual optical and patch-clamp electrophysiology with voltage steps applied in 20 mV increments from +100 to -100 mV (**Fig. 2-2**). VFs display fractional fluorescence changes ranging from 14-21% ΔF/F per 100 mV, with the most sensitive VF being pVF-pip-cya (**14**) (21% ΔF/F per 100 mV, **Fig. 2-2p**) and the least sensitive pVF-pip (**10**) (14% ΔF/F per 100 mV, **Fig. 2-2o**). Compound **15** (mVF-pip-cya) has largest relative signal-to-noise ratio, 2.2x greater than pVF-pip (**10**, **Table 2-1**).

Synthesis of SNAP VoltageFlours

The O^6-benzylguanine SNAP ligand was functionalized with a reactive alkyne handle synthesized following previously published protocols[11]. The SNAP-tag ligand was coupled to VFs **2**, **14** and **15** via a flexible $PEG_{11/12}$ linker long enough to allow VF dye incorporation into the cell membrane. In previous findings in our group found longer linkers (> 5 units) showed improved voltage sensitivity in HaloTag-tethered RhoVR compounds. However, with Spy Tag tethered VoltageSpy the voltage sensitivities were consistent across varying PEG_3 to PEG_{35} linkers. We hypothesize smaller proteins may bring the active site closer to the membrane surface, and therefore require less distance between the VF and reactive ligand. Taken together, we reasoned the $PEG_{11/12}$ linkers would allow for proper membrane insertion and orientation given the $SNAP_f$ protein is closer in size to Spy Tag (19.4 kDa and 15 kDa, respectively) relative to the larger HaloTag protein (33 kDa). Amide coupling of VFs with heterobifunctional PEG linkers terminating with amino and azido groups providess VF-$PEG_{11/12}$-N_3 intermediates **16-18** in 21% to 55% yields. Copper catalyzed azide-alkyne cyclization of compounds **16-18** with O^6-benzylguanine-alkyne (BG-SNAP) gives VF-$PEG_{11/12}$-SNAP-tags **19, 20, and 21** in low yields (1-9%) after semi-preparative HPLC or preparative TLC purification. For convenience, the 6' sarcosine derivative (**19**) is referred to as mSNAP1, while 5' and 6' piperazine-cysteic acid derivatives (**20** and **21**) are referred to as pSNAP2 and mSNAP2, respectively (**Scheme 2-1**).

Optimization of SNAP-tag expression and VF targeting in HEK293T cells

The structure of VFs makes them inherently 'sticky', due to the largely hydrophobic molecular wire, which in turn promotes VF labeling of all cell membranes. A major goal for targeting VFs to a specific cell or cell type is to gain a large contrast between labeled and unlabeled cells, in other words a large turn-on ratio. The turn-on ratio is defined as the fluorescence intensity of transfected over non-transfected cells. In initial experiments we transfected HEK293T cells with the SNAP protein fused to a single pass alpha helical transmembrane domain (**Scheme 2-1a**). Transfected cells bath loaded with 25 nM mSNAP1 in HBSS had a low turn-on (~1.5x) after a 15-minute incubation (**Fig. 2-3a**). A slight increase in the turn-on ratio to about ~2.5x was achieved with mSNAP2 at the same concentration (**Fig. 2-3a**). Further optimization was continued only with mSNAP2. Increasing the loading concentration of mSNAP2 did not further improve fluorescence turn-on (**Fig. 2-3b**), nor did multiple variations in loading times ranging from 10 minutes to an hour, with or without wash steps, in the presence of 0.02% pluronic F-127 surfactant,

or in alternative media containing FBS (data not shown). To determine if the structure of mSNAP2 hindered protein reactivity, we compared membrane fluorescence to a well-known SNAP Surface AlexaFluor-4 88(SS-A488, NEB) substrate. Both mSNAP2 and SNAP-AlexaFluor-488 show similar membrane fluorescence values (**Fig. 2-3c**) suggesting mSNAP2 is a comparable substrate for the self-reactive SNAP protein. Given these results, we reasoned the poor turn-on ratios could be limited by the amount of protein successfully expressed at the cell surface and/or enzyme efficiency.

To optimize the SNAP-VF labeling system, we replaced the original SNAP protein with an improved $SNAP_f$ variant[13]. $SNAP_f$ has a 10-fold faster rate of reaction with benzylguanine substrates relative to the original SNAP-tag mutant protein.[13] We find that cells expressing the faster $SNAP_f$ enzyme and treated with mSNAP2 showed a 4-fold improvement under identical conditions using the original SNAP protein (~8-10x turn-on, **Fig. 2-4a** and **b,** and **Fig. 2-5a-d**). While these findings are consistent with literature improvements, it is unclear if increased labeling is due to improved reactivity specifically. We hypothesize it could be a combination of factors including improved protein folding or secretion, resulting in higher levels of $SNAP_f$ on the cell surface compared to the original SNAP.

Replacing the single-pass α-helical transmembrane domain with a GPI-anchor (decay accelerating factor or DAF, **Scheme 2-1b**) improved the ratio 8- to 10- fold (~20-25x turn-on, **Fig. 2-4c** and **d, Fig. 2-5a,b** and **e,f**) compared to the original SNAP-pDisplay/mSNAP2 system (**Fig. 2-4a**), suggesting further improvements to functional protein expression and/or reactivity at the plasma membrane. Increasing the concentration and loading time duration of VF dye provided little enhancement to the turn-on ratio (**Fig. 2-4c-f**). The average fluorescence intensity remained relatively constant with increasing VF concentration (**Fig. 2-4d**, green) while non-specific labeling increased (**Fig. 2-4d,** grey), reducing the turn-on ratio by 2-fold (**Fig. 2-4c,** compare 15 and 150 nM). Additionally, increasing the time available for protein expression from 15 to 72 hours post-transfection did not significantly improve the turn-on ratio suggesting there is little improvement in membrane protein expression with extended time (data not shown). Single cell loading kinetics also suggest fluorescence saturation at the membrane occurs within 5-10 minutes (**Fig. 2-4e**). Covalent labeling with mSNAP2 is highly dependent on protein availability at the membrane and can be blocked with pre-incubation of a non-fluorescent O^6-benzylguanine derivative (**Fig. 2-4g**). We chose to further characterize mSNAP2 paired with the $SNAP_f$ protein and a GPI membrane anchoring motif given this combination yields the best results with a fluorescence turn-on of 20x in HEK cells, relative to non-expressing cells. Additionally, we chose to focus on mSNAP2 over pSNAP2 to achieve maximum signal to noise in future, more complex tissue preparations, rather than maximum voltage sensitivity. Typically, 5' VFs have a larger voltage response but a lower signal to noise ratio relative to 6' VFs. We see this trend when comparing (**14**) and (**15**) and would expect this comparison to extend to pSNAP2 and mSNAP2.

Voltage Sensing with a SNAPf-VoltageFluor

In transfected HEK293T cells, the voltage response for mSNAP2 was 19.1% ± 0.9% per 100 mV (**Fig. 2-6a-d**). While the addition of the polyethylene glycol linker and BG moiety to mVF-pip-cya improves the reported voltage response from ~17% to ~19% ΔF/F, the difference was not statistically significant (**Fig. 2-6e**, one way ANOVA; p=0.6488). In our previously synthesized RhoVR-HaloTag and VoltageSpy VFs we found the voltage response of targeted dyes to be reduced by half the original response relative to the parent VF scaffold (which does not contain a reactive ligand or PEG linker). We speculate the reason for this drop in sensitivity could be due to improper VF orientation, which might suggest mSNAP2 (**21**) is able to properly load

into the membrane similarly to its parent VF (**18**) and that the linker and targeting moiety have little effect in loading.

Preliminary experiments in rat hippocampal neurons transfected with the original SNAP-pDisplay construct under a neuron specific synapsin promoter show cell-specific labeling using mSNAP2 (**Fig. 2-6f**). The targeted VoltageFluor can also reliably detect spontaneous actional potentials with a 5% ΔF/F (**Fig. 2-6g**). We reasoned the contrast between transfected and non-transfected cells would be improved using the optimized $SNAP_f$-DAF fusion, however cloning the fusion under a synapsin promoter is still in progress. However, transfection of neurons using the same construct used for HEK cell characterization driven under the non-specific cmv promoter shows mSNAP2 labeling (**Fig. 2-6h-j**). Further optimization and characterization within neurons is still needed, but these preliminary results show mSNAP2 can be specifically targeted to cells of interest and still maintain a good voltage sensitive response.

In vivo dye loading in Drosophila melanogaster.

Having determined that we could target voltage-sensitive dyes with high contrast in HEK293T cells. We sought to transition mSNAP2 to more complex living tissues. Leveraging the genetic tractability, simplistic nervous system and ease of stimulation, we selected *Drosophila melanogaster* as the optimal model organism to develop these probes. Our group had previously developed an extracellularly trafficked $SNAP_f$ fusion protein which consisted of 5' PAT-3 secretion signal and a 3' hCD4 transmembrane domain anchor (Molly Jane Kirk, Thesis 2021-Chapter 2). This construct was used to generate stable transgenic *Drosophila* reporter lines which express the $SNAP_f$-CD4 fusion under the Gal4/UAS system. $SNAP_f$-CD4 had been shown to robustly target dyes to the extracellular surface in live *Drosophila* brains. Yet to further confirm this finding, we expressed $SNAP_f$-CD4 in a subset of neurons. Crossing UAS-$SNAP_f$-CD4 to the GH146-Gal4[14] driver line, expressed $SNAP_f$-CD4 in a subpopulation of olfactory projection neurons in the antennal lobe. When loaded with SS-A488 in live brain tissue the antennal lobe projection neurons: glomeruli, cell bodies and axonal projections **(Fig. 2-7a)** were highly visible and SS-A488 staining localized well to the extracellular surface (**Fig. 2-7 b**). Further quantification revealed that SS-A488 was targeted to *Drosophila* olfactory projection neurons with an approximately 40-fold increase in fluorescence intensity over non-targeted regions of protocerebrum (**Fig. 2-7 c)**.

We further evaluated the ability of $SNAP_f$-CD4 to target mSNAP2 voltage-sensitive dye. Using GH146-Gal4>$SNAP_f$-CD4 we expressed $SNAP_f$-CD4 again in olfactory projection neurons. We then loaded brains with varying concentrations of mSNAP2 and found that 500nM yielded the highest intensity staining with minimal background fluorescence (**Fig. 2-8a and b**).

Functional imaging in Drosophila melanogaster

To evaluate the voltage-sensitivity of mSNAP2 *in vivo*, we again expressed $SNAP_f$-CD4 in olfactory projection neurons under the GH146-Gal4 driver line. Our group had previously shown that PNs can be readily and robustly stimulated with carbachol (CCH), a non-hydrolysable acetylcholine mimic.[15] Loading mSNAP2 (500 nM) in live flies, we then removed the brain and imaged in explants using epifluorescence microscopy. We imaged mSNAP2 responses to three individual carbachol stimuli and found that mSNAP2 showed robust voltage responses in the positive direction as expected for these turn-on probes (**Fig. 2-9a and b**). The chemical-genetic hybrid approach of mSNAP2 enables additional controls to be carried out with in the exact same Drosophila genotype. Loading brains with non-voltage-sensitive SS-A488 and stimulating with carbachol yielded little to no response to the carbachol stimulation (**Fig. 2-9 c**). The use of a non-

voltage sensitive dye permits control experiments to be run in the same transgenic animals, eliminating unwanted confounds from the use of various transgenes or genetic backgrounds. Similar experiments with genetically encoded indicators/actuators (like ArcLight or GCaMP) would require the generation of separate transgenic animals which express and inactive indicator. Ultimately these studies remain preliminary in nature and require the addition of a no drug stimulation control as well as increased replicates but show promise that the dye is voltage-sensitive in *Drosophila.*

Experimental Methods

General Synthetic and Analytical Methods

Chemical reagents and solvents (dry) were purchased from commercial suppliers and used without further purification. Syntheses of 5- and 6-2',7-dichlorofluorescein, and molecular wire **(7)** were adapted from existing procedures.[1,2] Thin layer chromatography (TLC) (Silicycle, F254, 250 μm) and preparative thin layer chromatography (PTLC) (Silicycle, F254, 1000 μm) was performed on glass backed plates pre-coated with silica gel and visualized by fluorescence quenching under UV light. Flash column chromatography was performed on Silicycle Silica Flash F60 (230–400 Mesh) using a forced flow of air at 0.5–1.0 bar.

High performance liquid chromatography (HPLC) and low resolution ESI Mass Spectrometry were performed on an Agilent Infinity 1200 analytical instrument coupled to an Advion CMS-L ESI mass spectrometer. The column used for analytical HPLC was Phenomenex Luna 5 μm C18(2) (4.6 mm I.D. × 150 mm) with a flow rate of 1.0 mL/min. The column used for preparative HPLC was Phenomenex Luna 5 μm C18(2) (10 mm I.D. x 150 mm) with a flow rate of 5.0 mL/min. In both cases water (eluent A) and acetonitrile (eluent B) were employed as the mobile phase, with 0.05% trifluoroacetic acid present as an additive. For analytical HPLC the mobile phase was ramped from 10 to 100% eluent A water over eight minutes, then held at 100% A for two minutes at a flow rate of 1.0 mL/minute.

Spectroscopic studies

Stock solutions of dyes were prepared in DMSO and diluted with PBS (10 mM KH2PO4, 30 mM Na2HPO4·7H2O, 1.55 M NaCl, pH 7.2) solution containing 0.10 % (w/w) Triton X-100 (1:100-1:1000 dilution). UV-Vis absorbance and fluorescence spectra were recorded using a Shimadzu 2501 Spectrophotometer (Shimadzu) and a Quantamaster Master 4 L-format scanning spectrofluorometer (Photon Technologies International). The fluorometer is equipped with an LPS-220B 75-W xenon lamp and power supply, A-1010B lamp housing with integrated igniter, switchable 814 photon-counting/analog photomultiplier detection unit, and MD5020 motor driver. Samples were measured at room temperature in 1-cm path length quartz cuvettes (Starna Cells).

Cell culture, transfection, and dye loading

All animal procedures were approved by the UC Berkeley Animal Care and Use Committees and conformed to the NIH Guide for the Care and Use of Laboratory Animals and the Public Health Service (PHS) Policy.

Human embryonic kidney 293T (HEK) cells were maintained in Dulbecco's modified eagle medium (DMEM) supplemented with 4.5 g/L D-glucose, 10% fetal bovine serum (FBS; Thermo Scientific) and 1% GlutaMax (Invitrogen) at 37 °C in a humidified incubator with 5 % CO_2. Cells were plated in high glucose DMEM (as above) at a density of 500 000 per well in a 6-well plate, transfected near ~75-80% confluency, then plated onto 12mm glass coverslips pre-treated with Poly-D-Lysine (PDL; 1 mg/ml; Sigma-Aldrich). Transfections were carried out using

Lipofectamine 3000 (Invitrogen) and cells were left untouched 10-12 hours after addition of lipofectamine/DNA solutions and then then split in either high glucose DMEM (as above) or low glucose DMEM (1 g/L D-glucose, 10% FBS, 1% GlutaMax, for electrophysiology) at a density of 50 000 to 75 000 cells per well in a 24-well plate, or 200 000 to 500 000 cells per well in a 6 well plate (for electrophysiology), and imaged ~24 h following transfection.

Hippocampi were dissected from embryonic day 18 Sprague Dawley rats (Charles River Laboratory) in cold, sterile HBSS (zero Ca^{2+}, zero Mg^{2+}, phenol red). All dissection products were supplied by Invitrogen, unless otherwise stated. Hippocampal tissue was treated with trypsin (2.5%) for 15 min at 37 °C. The tissue was triturated using fire polished Pasteur pipettes, in minimum essential media (MEM) supplemented with 5% FBS, 2% B-27, 2% 1M dextrose (Fisher Scientific) and 1% GlutaMax. The dissociated cells were plated onto 12 mm diameter coverslips (Fisher Scientific) pre-treated with PDL (as above) at a density of 25-30,000 cells per coverslip in MEM supplemented media (as above). Neurons were maintained at 37 °C in a humidified incubator with 5 % CO_2. At 1 day in vitro (DIV) half of the MEM supplemented media was removed and replaced with Neurobasal media containing 2% B-27 supplement and 1% GlutaMax. Transfection of plasmids was carried out using Lipofectamine 3000 (without P3000 reagent) at 6-7 DIV. Imaging was performed on mature neurons 13-16 DIV.

Unless stated otherwise, for loading of HEK cells and hippocampal neurons, DMSO stock solutions of dyes were diluted in HBSS to working concentrations. All imaging experiments were performed in HBSS at room temperature.

Epifluorescence microscopy

Imaging was performed on an AxioExaminer Z-1 (Zeiss) equipped with a Spectra-X Light engine LED light (Lumencor), controlled with Slidebook (v6, Intelligent Imaging Innovations). Images were acquired with a W-Plan-Apo 20x/1.0 water objective (20x; Zeiss) and focused onto an OrcaFlash4.0 sCMOS camera (sCMOS; Hamamatsu). More detailed imaging information for each experimental application is explained below. Dual imaging during electrophysiology experiments was performed on an inverted epifluorescence microscope AxioObserver Z-1 (Zeiss), equipped with a Spectra-X Light engine LED light (Lumencor), controlled using μManager (V1.4, open-source, Open Imaging). Images were acquired using Plan-Apochromat 20/0.8 air objective (20x, Zeiss) and captured on an OrcaFlash4.0 sCMOS camera (sCMOS; Hamamatsu).

Electrophysiology

Pipettes were pulled from borosilicate glass with filament (Sutter Instruments, Novato, CA) resistances ranging from 4 to 7 MΩ with a P97 pipette puller (Sutter Instruments). The internal solution composition is as follows, in mM (pH 7.25, 285 mOsmol/L): 125 potassium gluconate, 10 KCl, 5 NaCl, 1 EGTA, 10 HEPES, 2 ATP sodium salt, 0.3 GTP sodium salt. EGTA (tetraacid form) was prepared as a stock solution in either 1 M KOH or 10 M NaOH before addition to the internal solution. Pipettes were positioned with an MP-225 micromanipulator (Sutter Instruments).

Recordings were obtained with an Axopatch 200B amplifier at room temperature. The signals were digitized with a Digidata 1550B (Molecular Devices), sampled at 50 kHz and recorded with pCLAMP 10 software (Molecular Devices) on a PC. Fast capacitance was compensated in cell-attached configuration. For all electrophysiology experiments, recordings were only pursued if series resistance in voltage clamp were less than 20 MΩ. For whole-cell, voltage clamp recordings, HEK 293T cells were held at -60 mV until hyper- and de- polarizing steps were applied (from -100 to +100 mV) in 20 mV increments.

Image analysis

For image intensity measurements, regions of interest (ROIs) were drawn around HEK or neuronal cell bodies and the mean fluorescence calculated in ImageJ (FIJI, NIH). These reported values were background corrected by subtracting the fluorescence intensity of a region with no cells from the fluorescence intensity value of labeled cells. The turn on ratio of SNAP-tag expressing cells was calculated by taking the ratio of background corrected transfected and non-transfected cell fluorescence values. At least 15-20 cells were quantified for each coverslip and 2-3 coverslips were examined to get the average contrast.

Analysis of voltage sensitivity in HEK cells was performed using ImageJ (FIJI). Fluorescence intensities were calculated using ROIs described above. A baseline fluorescence value (F_{base}) was calculated from the average of frames held at -60 mV and subtracted from each timepoint of the background subtracted trace to yield a ΔF trace. The ΔF was then divided by F_{base} to give $\Delta F/F$ traces. No averaging was applied to voltage traces. For analysis of voltage responses in neurons, regions of interest encompassing cell bodies (all approximately the same size) were drawn in ImageJ and the mean fluorescence intensity for each frame extracted.

Live-fly brain dye loading with HT-TMR and voltage-sensitive dyes

Live-fly preparations were performed in the following way: 10-20 day old flies were briefly anesthetized on ice and placed into a small slit on a custom-built plastic mount at the cervix so that the head was isolated from the rest of the body. The head was then immobilized using clear nail polish, which was allowed to set for 15 minutes. The head cuticle was then removed using sharp forceps in calcium-magnesium free Artificial Hemolymph solution, AHL-/-, (NaCl 108.0 mM, KCl 5.0 mM, $NaHCO_3$ 4.0 mM, $NaH_2PO_4 \cdot H_2O$ 1.0 mM, Trehalose 2 H_2O 5.0 mM, Sucrose 10.0 mM and HEPES 5.0 mM, perfused at 5 mL/min)[16], and the esophagus was cut to eliminate autofluorescence. The AHL was then replaced with calcium-magnesium free AHL containing 0.2% Pluronic F127, and either 500nM mSNAP2-Halo or 1 µM SS-A488 (for functional imaging experiments, this was lowered to 5 nM SS-A488 to match fluorescence intensity with mSNAP2), and the glial sheath was punctured manually over the optic lobes to permit dye access. DMSO concentrations were maintained below 3% vol/vol in the dye loading solutions. Following a 45-minute loading period in the dark at room temperature, the brains were removed and then imaged via confocal or epifluorescent microscopy. When imaged under confocal microscopy, brains were mounted onto glass coverslips with spacers to prevent sample loss and deformation. When imaged under epifluorescent microscopy, brains were adhered to PDL- (Poly-D-Lysine), or PLL- treated (Poly-L-Lysine) coverslips and bathed in AHL-/-.

Confocal microscopy

We performed confocal imaging using an LSM710 upright confocal microscope maintained by the Biological Imaging Facility at UC Berkeley. mSNAP2 images were acquired under 488 nm laser illumination focused on the sample using a 20x air objective and collecting 548-685 nm wavelengths using a 54 µm pinhole. Brains were scanned in the z-direction beginning at the top of the brain for 15 planes with 3µm steps. Each image totals the first 45 µm of the brain tissue.

Epifluorescent microscopy

We performed epifluorescent microscopy on varying concentrations of the mSNAP2 voltage sensitive dye in live loaded drosophila brains. Imaging was performed on an AxioExaminer Z-1 (Zeiss) equipped with a Spectra-X Light engine LED light (Lumencor), controlled with Slidebook (v6, Intelligent Imaging Innovations). Images were acquired with a W-Plan-Apo 20x/1.0 water objective (20x; Zeiss) and focused onto an OrcaFlash4.0 sCMOS camera (sCMOS; Hamamatsu).

The optical setup for imaging with each dye is described below. Fluorescein dyes were excited using a cyan LED (455-495 nm) and fluorescence collected through a QUAD emission filter set (430/32, 508/14, 586/30, 708/98 BP) and long pass dichroic (432/38, 509/22, 586/40, 654).

Epifluorescent image analysis

Epifluorescent images from live loaded brain samples focused on the middle of the antennal lobes were analyzed in the following way. Fluorescence intensity was measured for the antennal lobe and a region of non-labeled protocerebrum from each brain. The ratio of the AL region's intensity and the nontargeted protocerebrum was then calculated and displayed as fold change above background.

Carbachol ArcLight functional imaging

GH146-Gal4, $SNAP_f$-CD4; Tm2/TM6b flies had their cuticle removed as described in the section above and then loaded with 500 nM mSNAP2 or 5 nM SS-A488 in the presence of 0.2% Pluronic F127 at room temperature for 45 minutes. Post loading, brains were immediately removed from the cuticle placed a perfusion chamber where they were mounted onto a PDL-coated coverslip. Samples were incubated for 3 minutes at room temperature with constant perfusion of AHL+/+ (NaCl 108.0 mM, KCl 5.0 mM, $NaHCO_3$ 4.0 mM, $NaH_2PO_4 \cdot H_2O$ 1.0 mM, Trehalose 2 H_2O 5.0 mM, Sucrose 10.0 mM, HEPES 5.0 mM, $CaCl_2$ 2 H_2O 2.0 mM, $MgCl_2$ 6 H_2O 8.2 mM, perfused at 5 mL/min) before imaging was performed. Perfusion was maintained throughout the experiment. Imaging was performed on an AxioExaminer Z-1 (Zeiss) equipped with a Spectra-X Light engine LED light (Lumencor), controlled with Slidebook (v6, Intelligent Imaging Innovations). Images were acquired with a W-Plan-Apo 20x/1.0 water objective (20x; Zeiss) and focused onto an OrcaFlash4.0 sCMOS camera (sCMOS; Hamamatsu). The acquisition rate of 1 Hz for each experiment with 125 ms exposure times and light power (19.7 mW/mm^2) were maintained across all experiments independent of acquisition frequency. A baseline was obtained for one minute, and then brains were stimulated for 30 seconds, followed by a 5-minute recovery period between stimulations.

Functional imaging data analysis

We extracted fluorescence intensity values over time for the antennal lobe using an in-house MATLAB code, and background-subtracted these values. We used these traces to calculate the % $\Delta F/F_0$, where F_0 was defined as the average of frames 2 to 50 from each video. These were then subsequently plotted and displayed using Prism Graph Pad as Mean and Standard Error of the Mean.

DNA constructs

For expression in HEK cells, SNAP- or $SNAP_f$-tag and the C-terminal decay accelerating factor (DAF) or an alpha helical domain (pDisplay) were subcloned into a pCAGS vector. Nuclear targeted mCherry or GFP was inserted downstream, separated by an internal ribosome entry (IRES) or self-cleaving T2A sequence.

The following sequences were used (5' to 3'):

SNAP

GGGGCCCAGCCGGCCAGATCTATGAAGCGCACCACCCTGGATAGCCCTCTGGGCAA
GCTGGAACTGTCTGGGTGCGAACAGGGCCTGCACGAGATCAAGCTGCTGGGCAAAG
GAACATCTGCCGCCGACGCCGTGGAAGTGCCTGCCCCAGCCGCCGTGCTGGGCGGA

CCAGAGCCACTGATGCAGGCCACCGCCTGGCTCAACGCCTACTTTCACCAGCCTGAG
GCCATCGAGGAGTTCCCTGTGCCAGCCCTGCACCACCCAGTGTTCCAGCAGGAGAG
CTTTACCCGCCAGGTGCTGTGGAAACTGCTGAAAGTGGTGAAGTTCGGAGAGGTCAT
CAGCTACCAGCAGCTGGCCGCCCTGGCCGGCAATCCCGCCGCCACCGCCGCCGTGA
AAACCGCCCTGAGCGGAAATCCCGTGCCCATTCTGATCCCCTGCCACCGGGTGGTGT
CTAGCTCTGGCGCCGTGGGGGGCTACGAGGGCGGGCTCGCCGTGAAAGAGTGGCTG
CTGGCCCACGAGGGCCACAGACTGGGCAAGCCTGGGCTGGGTCCTGCAGGTATAGT
CGAC

SNAP$_f$

ATGGACAAAGACTGCGAAATGAAGCGCACCACCCTGGATAGCCCTCTGGGCAAGCT
GGAACTGTCTGGGTGCGAACAGGGCCTGCACCGTATCATCTTCCTGGGCAAAGGAA
CATCTGCCGCCGACGCCGTGGAAGTGCCTGCCCCAGCCGCCGTGCTGGGCGGACCA
GAGCCACTGATGCAGGCCACCGCCTGGCTCAACGCCTACTTTCACCAGCCTGAGGCC
ATCGAGGAGTTCCCTGTGCCAGCCCTGCACCACCCAGTGTTCCAGCAGGAGAGCTTT
ACCCGCCAGGTGCTGTGGAAACTGCTGAAAGTGGTGAAGTTCGGAGAGGTCATCAG
CTACAGCCACCTGGCCGCCCTGGCCGGCAATCCCGCCGCCACCGCCGCCGTGAAAA
CCGCCCTGAGCGGAAATCCCGTGCCCATTCTGATCCCCTGCCACCGGGTGGTGCAGG
GCGACCTGGACGTGGGGGGCTACGAGGGCGGGCTCGCCGTGAAAGAGTGGCTGCTG
GCCCACGAGGGCCACAGACTGGGCAAGCCTGGGCTGGGT

DAF

CCAAATAAAGGAAGTGGAACCACTTCAGGTACTACCCGTCTTCTATCTGGGCACACG
TGTTTCACGTTGACAGGTTTGCTTGGGACGCTAGTAACCATGGGCTTGCTGACTTAG

pDisplay

GCTGTGGGCCAGGACACGCAGGAGGTCATCGTGGTGCCACACTCCTTGCCCTTTAAG
GTGGTGGTGATCTCAGCCATCCTGGCCCTGGTGGTGCTCACCATCATCTCCCTTATCA
TCCTCATCATGCTTTGGCAGAAGAAGCCACGTTAG

T2A

GAGGGTCGGGGCTCTCTGCTCACATGTGGCGACGTCGAGGAGAATCCCGGACCGGC
CCCGGGGTCGACA

IRES

GCCCCTCTCCCTCCCCCCCCCCTAACGTTACTGGCCGAAGCCGCTTGGAATAAGGCC
GGTGTGCGTTTGTCTATATGTTATTTTCCACCATATTGCCGTCTTTTGGCAATGTGAG
GGCCCGGAAACCTGGCCCTGTCTTCTTGACGAGCATTCCTAGGGGTCTTTCCCCTCTC
GCCAAAGGAATGCAAGGTCTGTTGAATGTCGTGAAGGAAGCAGTTCCTCTGGAAGC
TTCTTGAAGACAAACAACGTCTGTAGCGACCCTTTGCAGGCAGCGGAACCCCCCACC
TGGCGACAGGTGCCTCTGCGGCCAAAAGCCACGTGTATAAGATACACCTGCAAAGG
CGGCACAACCCCAGTGCCACGTTGTGAGTTGGATAGTTGTGGAAAGAGTCAAATGG
CTCTCCTCAAGCGTATTCAACAAGGGGCTGAAGGATGCCCAGAAGGCACCCCATTG
TATGGGATCTGATCTGGGGCCTCGGTGCACATGCTTTACATGTGTTTAGTCGAGGTT
AAAAAAACGTCTAGGCCCCCCGAACCACGGGGACGTGGTTTTCCTTTGAAAAACAC
GATGATAATATGGCCACA

NLS-mCherry

ATGGTGCCCAAGAAGAAGAGGAAAGTCGTGAGCAAGGGCGAGGAGGACAACATGG
CCATCATCAAGGAGTTCATGCGCTTCAAGGTGCACATGGAGGGCTCCGTGAACGGC
CACGAGTTCGAGATCGAGGGCGAGGGCGAGGGCCGCCCCTACGAGGGCACCCAGA
CCGCCAAGCTGAAGGTGACCAAGGGCGGCCCCCTGCCCTTCGCCTGGGACATCCTGT

CCCCTCAGTTCATGTACGGCTCCAAGGCCTACGTGAAGCACCCCGCCGACATCCCCG
ACTACTTGAAGCTGTCCTTCCCCGAGGGCTTCAAGTGGGAGCGCGTGATGAACTTCG
AGGACGGCGGCGTGGTGACCGTGACCCAGGACTCCTCCCTGCAGGACGGCGAGTTC
ATCTACAAGGTGAAGCTGCGCGGCACCAACTTCCCCTCCGACGGCCCCGTAATGCA
GAAGAAGACCATGGGCTGGGAGGCCTCCTCCGAGCGGATGTACCCCGAGGACGGCG
CCCTGAAGGGCGAGATCAAGCAGAGGCTGAAGCTGAAGGACGGCGGCCACTACGA
CGCCGAGGTCAAGACCACCTACAAGGCCAAGAAGCCCGTGCAGCTGCCCGGCGCCT
ACAACGTCAACATCAAGCTGGACATCACCTCCCACAACGAGGACTACACCATCGTG
GAACAGTACGAGCGCGCCGAGGGCCGCCACTCCACCGGCGGCATGGACGAGCTGTA
CAAG

NLS-GFP

ATGGTGCCCAAGAAGAAGAGGAAAGTCAGCAAGGGCGAGGAGCTGTTCACCGGGG
TGGTGCCCATCCTGGTCGAGCTGGACGGCGACGTAAACGGCCACAAGTTCAGCGTG
TCCGGCGAGGGCGAGGGCGATGCCACCTACGGCAAGCTGACCCTGAAGTTCATCTG
CACCACCGGCAAGCTGCCCGTGCCCTGGCCCACCCTCGTGACCACCCTGACCTACGG
CGTGCAGTGCTTCAGCCGCTACCCCGACCACATGAAGCAGCACGACTTCTTCAAGTC
CGCCATGCCCGAAGGCTACGTCCAGGAGCGCACCATCTTCTTCAAGGACGACGGCA
ACTACAAGACCCGCGCCGAGGTGAAGTTCGAGGGCGACACCCTGGTGAACCGCATC
GAGCTGAAGGGCATCGACTTCAAGGAGGACGGCAACATCCTGGGGCACAAGCTGGA
GTACAACTACAACAGCCACAACGTCTATATCATGGCCGACAAGCAGAAGAACGGCA
TCAAGGTGAACTTCAAGATCCGCCACAACATCGAGGACGGCAGCGTGCAGCTCGCC
GACCACTACCAGCAGAACACCCCCATCGGCGACGGCCCCGTGCTGCTGCCCGACAA
CCACTACCTGAGCACCCAGTCCGCCCTGAGCAAAGACCCCAACGAGAAGCGCGATC
ACATGGTCCTGCTGGAGTTCGTGACCGCCGCCGGGATCACTCTCGGCATGGACGAGC
TGTACAAGTAA

Drosophila DNA constructs:

Transgenic generation, the insert Pat3-HaloTag-CD4 was assembled into pJFRC7[29] backbone via restriction digest (CD8::GFP was removed by XhoI and XbaI) and Gibson assembly (Addgene). All constructs were sequence confirmed by the UCB Sequencing Facility. Sequences used for all constructs can be found below.

Pat3

ATGCCACCTTCAACATCATTGCTGCTCCTCGCAGCACTTCTTCCATTCGCTTTACCAG
CAAGCGATTGGAAGACTGGAGAAGTCACTG

HA epitope tag

TATCCATATGATGTTCCAGATTATGCT

SNAP$_f$-CD4

ATGGACAAAGACTGCGAAATGAAGCGCACCACCCTGGATAGCCCTCTGGGCAAGCT
GGAACTGTCTGGGTGCGAACAGGGCCTGCACCGTATCATCTTCCTGGGCAAAGGAA
CATCTGCCGCCGACGCCGTGGAAGTGCCTGCCCCAGCCGCCGTGCTGGGCGGACCA
GAGCCACTGATGCAGGCCACCGCCTGGCTCAACGCCTACTTTCACCAGCCTGAGGCC
ATCGAGGAGTTCCCTGTGCCAGCCCTGCACCACCCAGTGTTCCAGCAGGAGAGCTTT
ACCCGCCAGGTGCTGTGGAAACTGCTGAAAGTGGTGAAGTTCGGAGAGGTCATCAG
CTACAGCCACCTGGCCGCCCTGGCCGGCAATCCCGCCGCCACCGCCGCCGTGAAAA
CCGCCCTGAGCGGAAATCCCGTGCCCATTCTGATCCCCTGCCACCGGGTGGTGCAGG
GCGACCTGGACGTGGGGGGCTACGAGGGCGGGCTCGCCGTGAAAGAGTGGCTGCTG
GCCCACGAGGGCCACAGACTGGGCAAGCCTGGGCTGGGT

SNAP Tag

GGGGCCCAGCCGGCCAGATCTGCTGGGCAAAGGAACATCATGAAGCGCACCACCCT
GGATAGCCCTCTGGGCAAGCTGGAACTGTCTGGGTGCGAACAGGGCCTGCACGAGA
TCAAGCTGCTGGGCAAAGGAACATCTGCCGCCGACGCCGTGGAAGTGCCTGCCCCA
GCCGCCGTGCTGGGCGGACCAGAGCCACTGATGCAGGCCACCGCCTGGCTCAACGC
CTACTTTCACCAGCCTGAGGCCATCGAGGAGTTCCCTGTGCCAGCCCTGCACCACCC
AGTGTTCCAGCAGGAGAGCTTTACCCGCCAGGTGCTGTGGAAACTGCTGAAAGTGG
TGAAGTTCGGAGAGGTCATCAGCTACCAGCAGCTGGCCGCCCTGGCCGGCAATCCC
GCCGCCACCGCCGCCGTGAAAACCGCCCTGAGCGGAAATCCCGTGCCCATTCTGATC
CCCTGCCACCGGGTGGTGTCTAGCTCTGGCGCCGTGGGGGGCTACGAGGGCGGGCT
CGCCGTGAAAGAGTGGCTGCTGGCCCACGAGGGCCACAGACTGGGCAAGCCTGGGC
TGGGTCCTGCAGGTATAGTCGACGAACAAAAACTCATCTCAGAAGAGGATCTG

Linker

GGTGGCGGCGGAAGTGGAGGTGGAGGCTCG

CD4

TTCCAGAAGGCCTCCAGCATAGTCTATAAGAAAGAGGGGGAACAGGTGGAGTTCTC
CTTCCCACTCGCCTTTACAGTTGAAAAGCTGACGGGCAGTGGCGAGCTGTGGTGGCA
GGCGGAGAGGGCTTCCTCCTCCAAGTCTTGGATCACCTTTGACCTGAAGAACAAGGA
AGTGTCTGTAAAACGGGTTACCCAGGACCCTAAGCTCCAGATGGGCAAGAAGCTCC
CGCTCCACCTCACCCTGCCCCAGGCCTTGCCTCAGTATGCTGGCTCTGGAAACCTCA
CCCTGGCCCTTGAAGCGAAAACAGGAAAGTTGCATCAGGAAGTGAACCTGGTGGTG
ATGAGAGCCACTCAGCTCCAGAAAAATTTGACCTGTGAGGTGTGGGGACCCACCTC
CCCTAAGCTGATGCTGAGCTTGAAACTGGAGAACAAGGAGGCAAAGGTCTCGAAGC
GGGAGAAGGCGGTGTGGGTGCTGAACCCTGAGGCGGGGATGTGGCAGTGTCTGCTG
AGTGACTCGGGACAGGTCCTGCTGGAATCCAACATCAAGGTTCTGCCCACATGGTCC
ACCCCGGTGCAGCCAATGGCCCTGATTGTGCTGGGGGGCGTCGCCGGCCTCCTGCTT
TTCATTGGGCTAGGCATCTTCTTCTGTGTCAGGTGCCGGCACCGAAGGCGCTAG

Synthesis

5' and 6' Sarcosine VFs previously synthesized in Grenier et al. 2019[5].

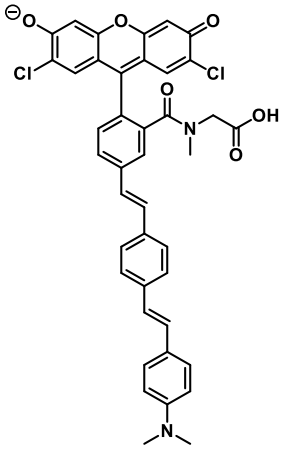

(1)

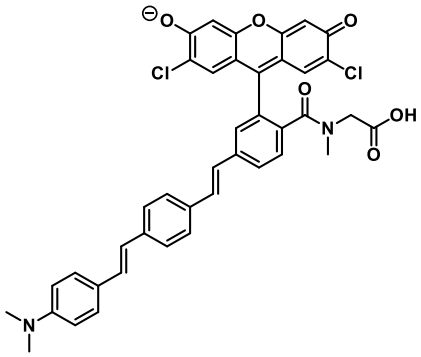

(2)

Synthesis of 5 (BD3-09)

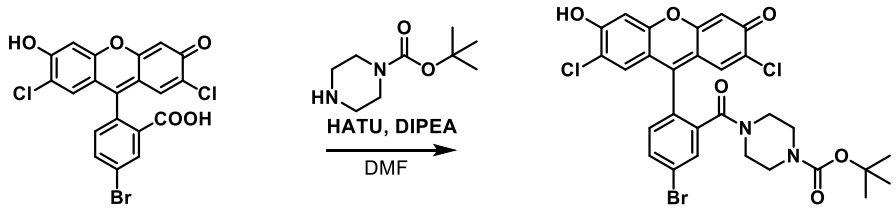

(3) (5)

5-bromo-2',7'-dichlorofluorescein (3) (300 mg, 625 µmol, 1.0 equiv.), 1-boc piperazine (128 mg) and HATU (261 mg) were dissolved in 7.8 mL anhydrous DMF, followed by the addition of 550 µL of DIPEA, turning the reaction dark red. The reaction was allowed to proceed overnight at room temperature and completion was verified via LC-MS (m/z = 649),. The crude reaction was dried under reduced pressure, redissolved in minimal chloroform, and purified via PTLC (10% MeOH/DCM). Isolated product (5) was filtered, dried under reduced pressure until it was a fine red powder (316 mg) giving a 78% yield.

Synthesis of 6 (BD3-20, JCM-57)

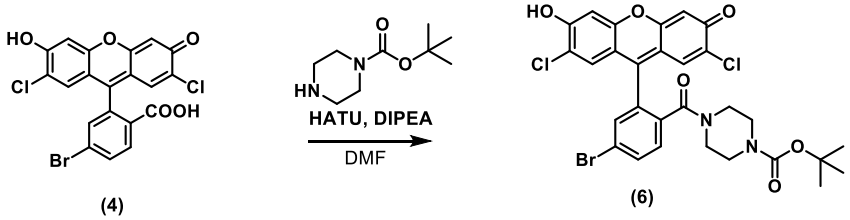

(4) (6)

6-bromo-2',7'-dichlorofluorescein (4) (400 mg, 883 µmol, 1.0 equiv.), 1-boc piperazine (170 mg) and HATU (348 mg) were dissolved in 10 mL anhydrous DMF, followed by the addition of 725 µL of DIPEA. The reaction was allowed to proceed overnight at room temperature, verified via LC-MS (m/z = 649), purified following the procedure in the synthesis of (5), and resulted in a 93 % yield (500 mg).

Synthesis of 8 (BD3-10 and BD3-22, JCM-43)

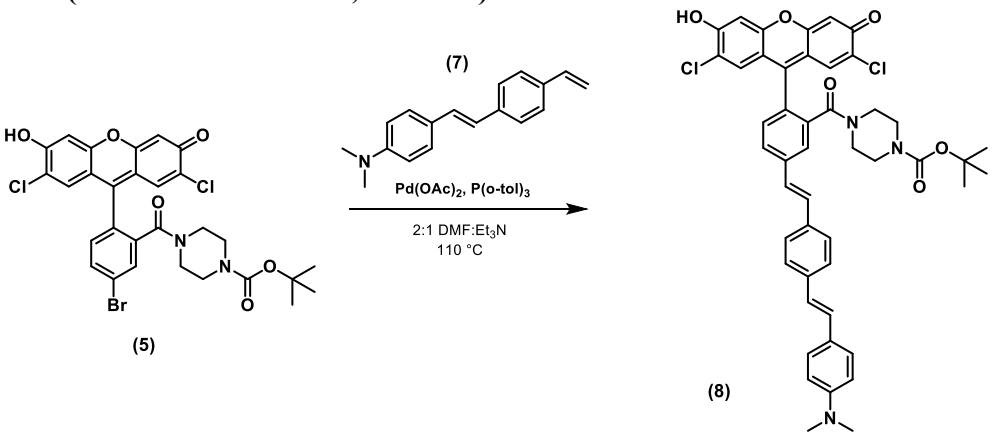

A round bottom was flame dried and left under N_2 to dry and cool for 1 hour. Compound (5) (100 mg, 154 µmol, 1.0 equiv.), compound (7) (65.4 mg, 1.7 equiv.), $Pd(oAc)_2$ (0.07 equiv.), and $P(o\text{-}Tol)_3$ (0.04 equiv.) were then added the flask which was then purged and backfilled with fresh N_2 three times followed by the addition of dry DMF (2 mL) and Et_3N (1 mL). The reaction was stirred at 110°C under N_2 overnight (~22 hrs) and completion was verified via LCMS (m/z = 816). The crude reaction was filtered through a celite pad and washed with portions of 20% isopropanol in DCM. The filtrate was concentrated *in vacuo* and purified using preparatory TLC plates run in 10% MeOH in DCM. The most intense band was cut out and extracted in 10% MeOH in DCM. 69 mgs of a dark red powder were obtained (55% yield).

Synthesis of 9 (BD3-23 and BD3-91)

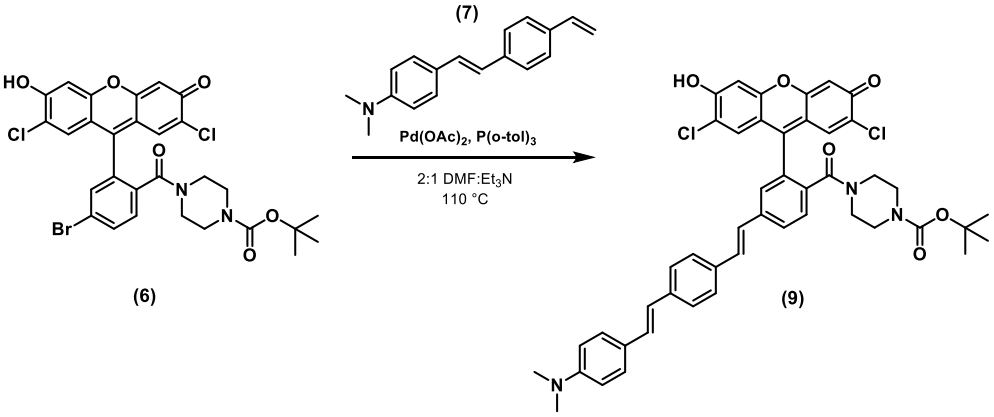

Compound (**2**) (300 mg, 1 equiv.) and a phenylene vinylene aniline wire (1.7 equiv.) were combined with $Pd(oAc)_2$ (0.07 equiv.), and of $P(o\text{-}Tol)_3$ (0.04 equiv.) in an oven dried schlenk flask with a stir bar. The flask was purged and backfilled with fresh N_2 three times followed by the addition of dry DMF (6 mL) and Et_3N (3 mL). The reaction was stirred at 110°C under N_2 overnight (~22 hrs). Reaction completion was verified via LCMS (m/z = 816). The crude reaction was filtered through a celite pad and washed with portions of 20% isopropanol in DCM. The filtrate was concentrated *in vacuo* and purified using preparatory TLC plates run in 10% MeOH in DCM. The most intense top band was cut out and extracted in 10% MeOH in DCM. Compound 9 was obtained as a dark red powder (378 mg, 61% yield).

Synthesis of 10 (pVF-pip) and 12 (BD3-10, BD3-13, BD3-17 and BD3-22)

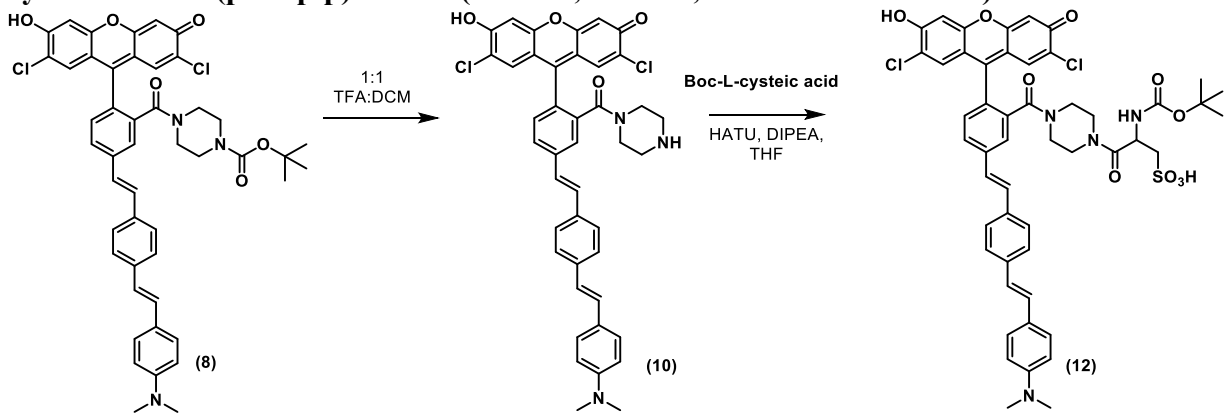

Compound (8) (26.8 mgs, 32.8 μmol, 1.0 equiv.) was dissolved in 1 mL 1:1 DCM/TFA solution. The reaction was stirred at room temperature for ~1 hr when quantitative boc deprotection was observed via LCMS. The TFA/DCM mixture was blown off using N_2. Ether was added to the resulting film, sonicated, filtered off, and the dried product was used immediately for cysteic acid HATU coupling (~100% yield). L-NBoc-cysteic acid (9.51 mg, 1.1 equiv.) and HATU (13.5 mg, 1.1 equiv.) were added directly to the product vial containing ~23 mg of (10). The solids were dissolved in 1.5 mL of dry DMF followed by the addition of dry DIPEA (28 μL, 5 equiv.). The reaction was stirred overnight at room temperature (~ 16 hrs) and product conversion verified via LCMS (m/z = 966.7). The reaction was neutralized with AcOH before removing solvent and the desired product was isolated via preparatory TLC using 10% MeOH:DCM. The dark red bottom band was cut out and product was eluted using 10% MeOH in DCM, concentrated and placed on the high vac for ~1 hr to remove residual AcOH. The film that formed was then dissolved in DCM and filtered through a fluorinated syringe tip filter to remove any additional contaminants. 13.4 mg of (12) were collected giving a 43.2% yield and used immediately for the synthesis of (14) and (16).

Synthesis of 11 (mVF-pip) and 13 (BD3-23, BD3-28 and BD3-93)

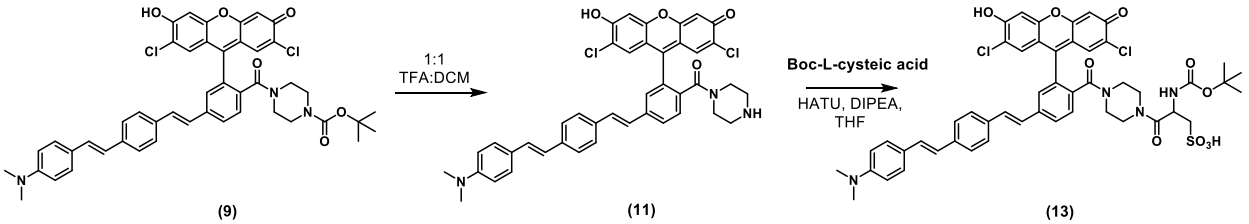

Compound 9 (69 mg, 84.5 μmol, 1.0 equiv.) was dissolved in 1 mL of DCM followed by the addition of TFA (1 mL). The reaction was stirred at room temperature for ~1 hr when quantitative boc deprotection was observed via LCMS. The TFA/DCM mixture was blown off using N_2. Ether was added to the resulting film, sonicated, filtered off, and the dried product was isolated in ~88% yield and used immediately for cysteic acid HATU coupling. L-NBoc-cysteic acid (34 mg, 1.1 equiv.) and HATU (48 mg, 1.1 equiv.) were added directly to the product vial. The solids were dissolved in 1 mL of dry DMF followed by the addition of dry DIPEA (100 μL, 5 equiv.). The reaction was stirred overnight at room temperature (~ 16 hrs) and product conversion verified via LCMS (m/z = 966.7). The reaction was neutralized with AcOH before removing solvent and drying on the high vac for ~1 hr. The desired product was isolated via preparatory TLC using 15% MeOH, 8% AcOH in DCM. The dark red band was cut out and product was eluted using 15% MeOH in DCM. The product was concentrated down *in vacuo* and placed on the high vac for ~1 hr to remove residual AcOH. The film that formed was then dissolved in DCM and filtered through a fluorinated syringe tip filter to remove any additional contaminants. The filtrate was then concentrated *in vacuo*, giving 88 mg of a dark red powder (67% yield).

Synthesis of 14 (pVF-pip-cya) and 16 (BD3-13 and JCM-62,63)

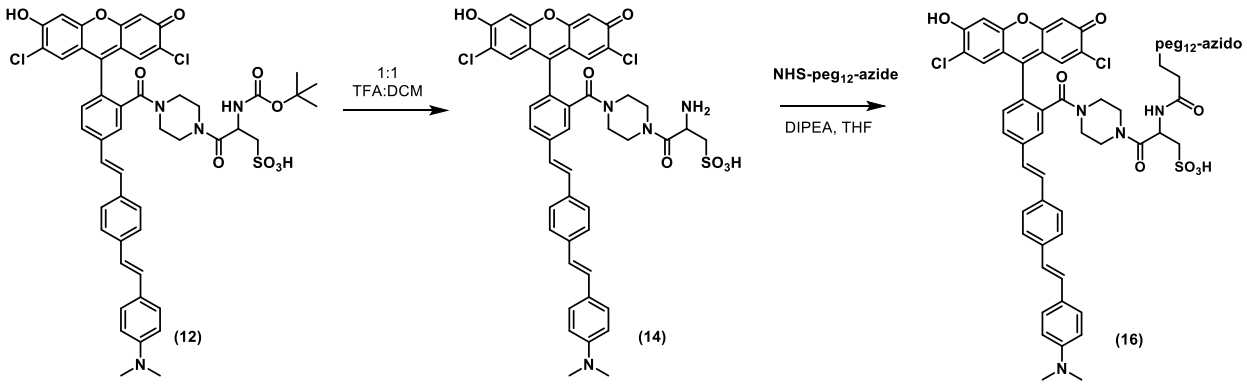

Compound (12) was dissolved (13.4mg) in a 1 mL 1:1 DCM/TFA (500 µL: 500 µL) solution and stirred at room temperature for ~1 hr, after which LCMS showed quantitative boc deprotection. The TFA/DCM mixture was blown off the reaction using N_2. Ether was added to the resulting film that formed and then sonicated and filtered off. After drying, 25.6 mgs of deprotected product (14) were collected (0.0295 mmol, 57.8% yield). Compound 14 was added to a flame dried 8 mL vial and stir (1 equiv.) which was subsequently dissolved in 1 mL of dry DMF. A tared glass pipet was then used to measure out 1.5 equivalents of NHS-PEG_{12}-N_3 (measured over 3 glass pipets), followed by the addition of 10 µL dry DIPEA (2 equiv.). The top of the vial was wrapped with Teflon tape and N_2 was blown into the vial for 30 sec and rapidly capped. The reaction was stirred at room temperature for a day (~29 hrs), rotovapped down, and allowed to sit on the high vac overnight. The desired product was isolated via preparatory TLC using 15% MeOH, 2% AcOH in DCM as the solvent. The dark red band was cut out and eluted in 15% MeOH in DCM. The eluent was then filtered through a fluorinated syringe filter, rotovapped down, then placed on the high vac for ~1 hr to remove residual AcOH. 16.2 mgs of a dark red powder were collected (MW = 1493.46, 0.0108 mmol, ~21% yield over two steps).

Synthesis of 15 (mVF-pip-cya) and 17 (BD2-44 and BD3-93)

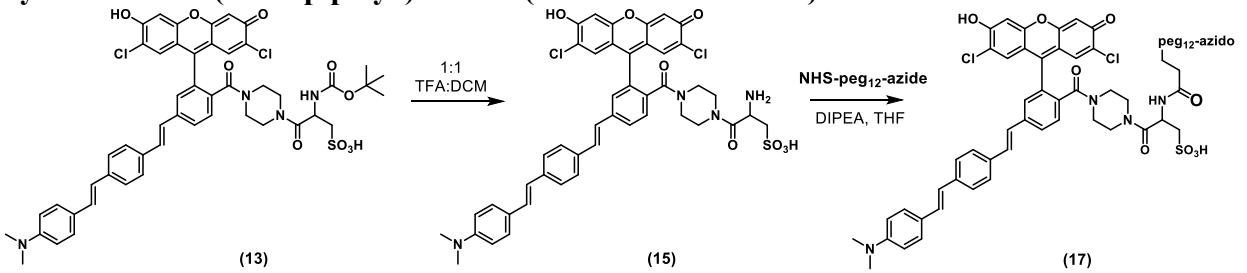

Compound (13) was dissolved (60 mg) in 1 mL DCM followed by the addition of TFA (1:1). The solution was stirred for ~3 hrs, after which LCMS showed quantitative deprotection. The TFA/DCM mixture was blown off using N_2 and ether was added to the resulting film, sonicated, and then filtered off giving an 88.7% yield. Additional purification steps via preparatory TLC were done in previous preparations, however this step was generally omitted since it typically decreased the overall yield (~30%). Compound (15) was then dissolved (50 mg, 1.0 equiv.), in 2 mL dry DMF. A tared glass pipet was used to measure NHS-PEG_{12}-N_3 (60 mg, 1.5 equiv.). Dry DIPEA was added to the vial (20 µl, 2 equiv.) and the top of the vial was wrapped with Teflon tape. N_2 was blown into the vial for ~30 sec and rapidly capped. The reaction proceeded at room temperature for one day, reaction completion verified by LCMS, solvents removed, and the crude reaction dried under high vac overnight. The desired product was isolated via preparatory TLC using 15% MeOH, 2% AcOH in DCM as the solvent. The dark red band was removed and eluted in 15% MeOH in DCM. The eluent was then filtered through a fluorinated syringe filter, evaporated and left under high vac for ~1 hr to remove residual AcOH. The addition of the PEG linker made it challenging to isolate (17) in a powdered form, but rather a 'gooey' film. The purified product was dissolved in 1 mL DMSO and estimated using UV-vis absorbance ($\varepsilon = 90000$ cm^{-1} M^{-1}) to contain 33.8 mg resulting in 42% yield.

Synthesis of mSNAP1 (BD-51 and BD-71 & 74)

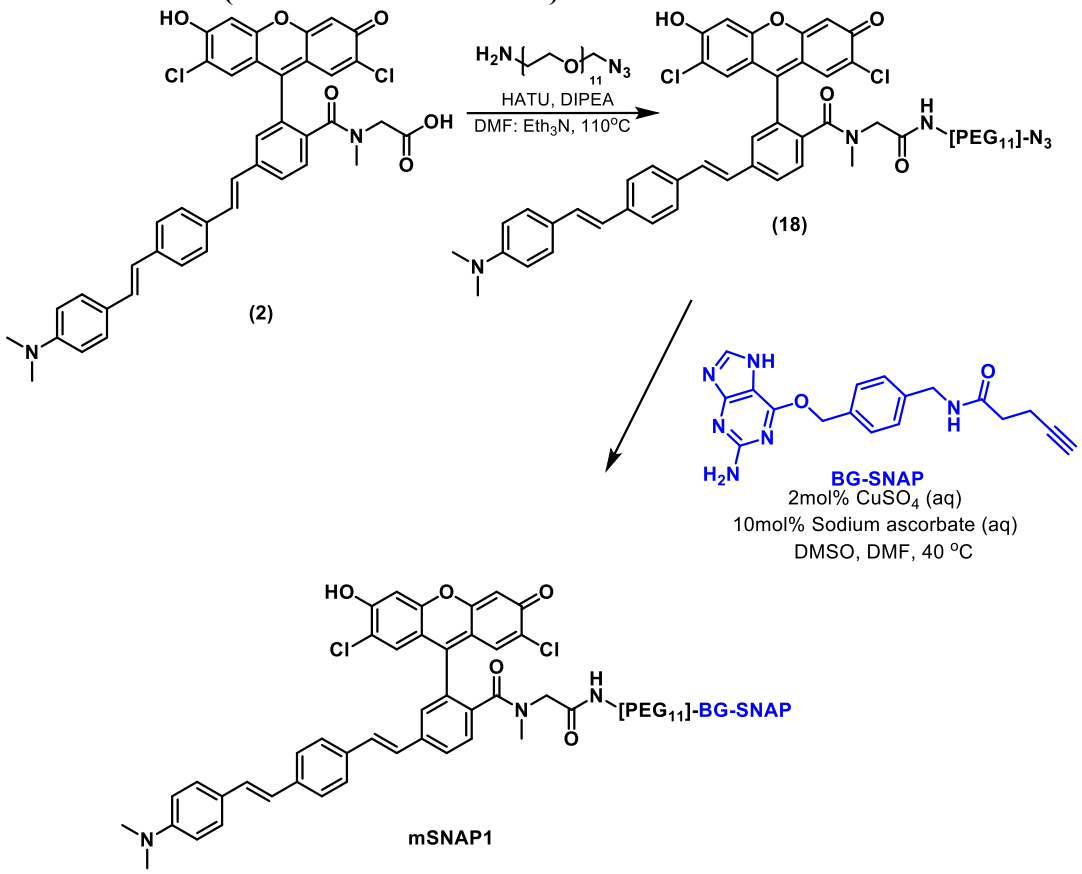

HATU (4 mg, 10 µmol, 1.1 equiv.) and **(2)** (7.0 mg, 9.7 µmol, 1 equiv.) were added to a small dram vial and taken up in 1 mL DMF. About 1.1 equiv. of the polyethylene glycol linker (6.1 mg, 10.7 µmol) was measured using a tared pipette and added to the solution followed by the addition of DIPEA (8.5 µL, 48.6 µmol, 5 equiv.). The reaction mixture was left to stir overnight and monitored the following day using LC-MS (m/2 = 626). The crude mixture was dried under low pressure and re-dissolved in minimal amounts of chloroform to purify via preparatory TLC. The pegylated azide was recovered giving a 56% yield (6.9 mg) and used to make a 25 mM solution in DMF for the following reaction. All aqueous solutions used for the synthesis of mSNAP1 were made fresh. In a 1.5 mL eppendorf tube, 50 µL of a 25 mM compound (**18**) in DMF was combined with 25 µL of a 100 mM benzyl guanine alkyne solution in DMSO. In separate glass vials, 3.2 mg and 19.8 mg of CuSO4and sodium ascorbate, respectively, were dissolved in 1.0 mL of milliQ water and left at room temperature for ~5 minutes. 50µL from each solution was then added to the eppendorf tube followed by the addition of DMSO to a total volume of 1.0 mL. The reaction was left on a shaker at 40°C and monitored hourly by LC-MS. Following completion, the reaction was diluted with 1.0 mL DMSO, centrifuged, and the supernatant removed and filtered into an HPLC vial. The product was then further purified by semi-preparative HPLC (4% yield).

Synthesis of mSNAP2 and pSNAP2 (mSNAP2; BD-133, BD2-49, BD2-44, pSNAP2; JCM-56))

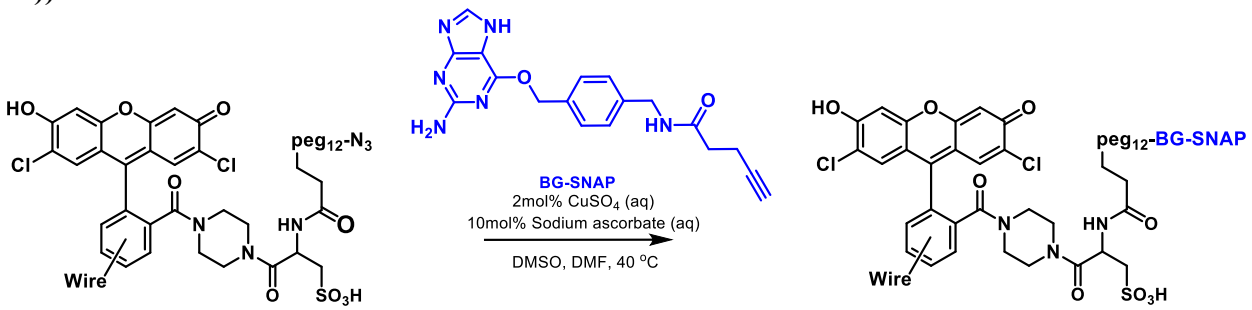

(16) = 5' VF-pip-cys-PEG12-azide
(17) = 6' VF-pip-cys-PEG12-azide

pSNAP2.0 = 5' VF-pip-cys-PEG12-BG
mSNAP2.0 = 6' VF-pip-cys-PEG12-BG

25 mM solutions of (**16**) and (**17**) were made in dry DMSO. The following were added to a 1.5 mL epi: 50 µL of ~2 mol% $CuSO_4$ (prepared fresh in MilliQ water), and 50 µL of ~10 mol% Na Ascorbate (prepared fresh in MilliQ water), 50 µL of a 25 mM solution of **(16)** or **(17)**, 25 µL of BG-SNAP at 100 mM in DMSO, and at least 125 µL of DMSO. Additional DMSO was added to the reaction to ensure it was all dissolved (300 uL). The reaction was left overnight at 40°C and 300 rpm (~15 hrs). The next morning, the reaction was diluted to 1.5 mL with DMSO and 10 µL injected onto the LCMS. A peak was observed with mass corresponding to m/z (1842) and m/2z (922) with a retention time of ~4.5 mins (in MeCN/H_2O with 0.05% TFA). The product was purified using semi-preparatory HPLC and the single product (mSNAP2 = 9% yield, pSNAP2 =9% yield estimated by absorbance) was stored as a 250 µM solution in DMSO at -20 °C. Additionally, aliquots stored at room temperature for a week did not show signs of decomposition via LCMS (single peak around 4.8 min. with m/2z = 922)
QY =16.1%

Spectra

Spectrum 2-1. HPLC of 5

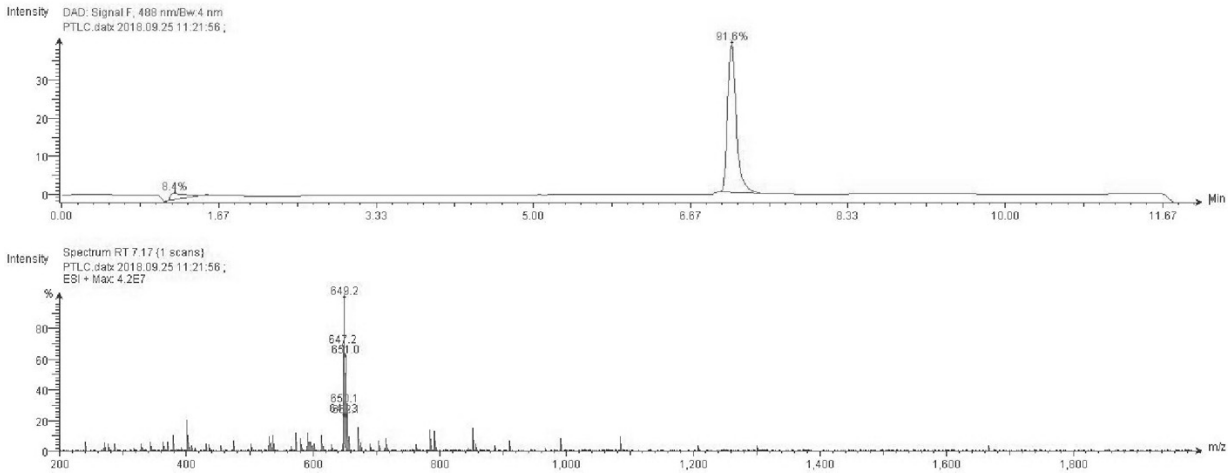

Low-resolution ESI(+) mass spectrum of **5**
Calculated for Calculated for [M+H]+ 649.007276; Found 649.2.

Spectrum 2-2. **Crude HPLC of 6**

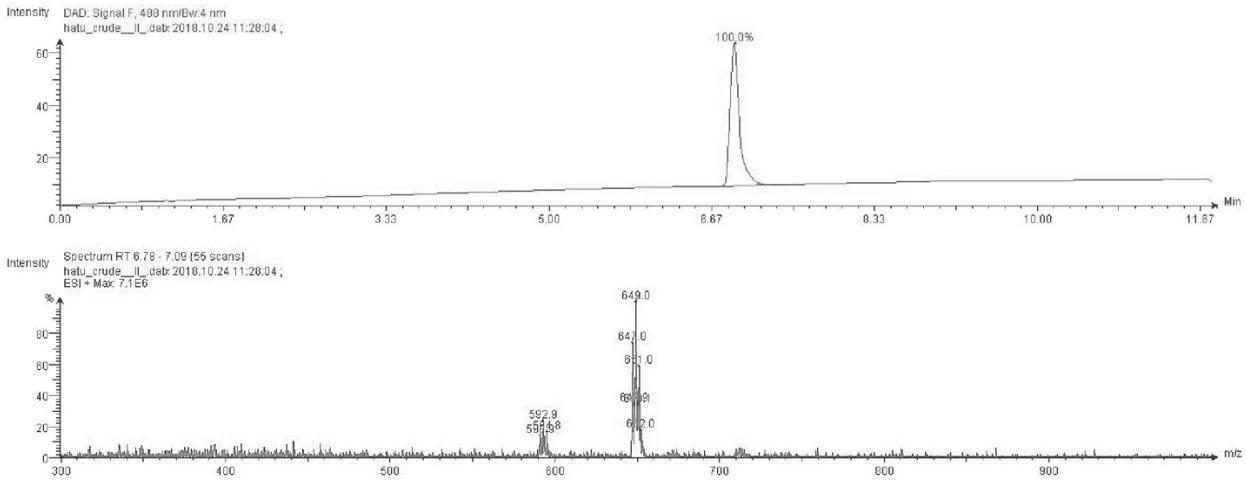

Low-resolution ESI(+) mass spectrum of **6** before purification
Calculated for [M+H]+ 649.007276; Found 649.0.

Spectrum 2-3. HPLC of 8

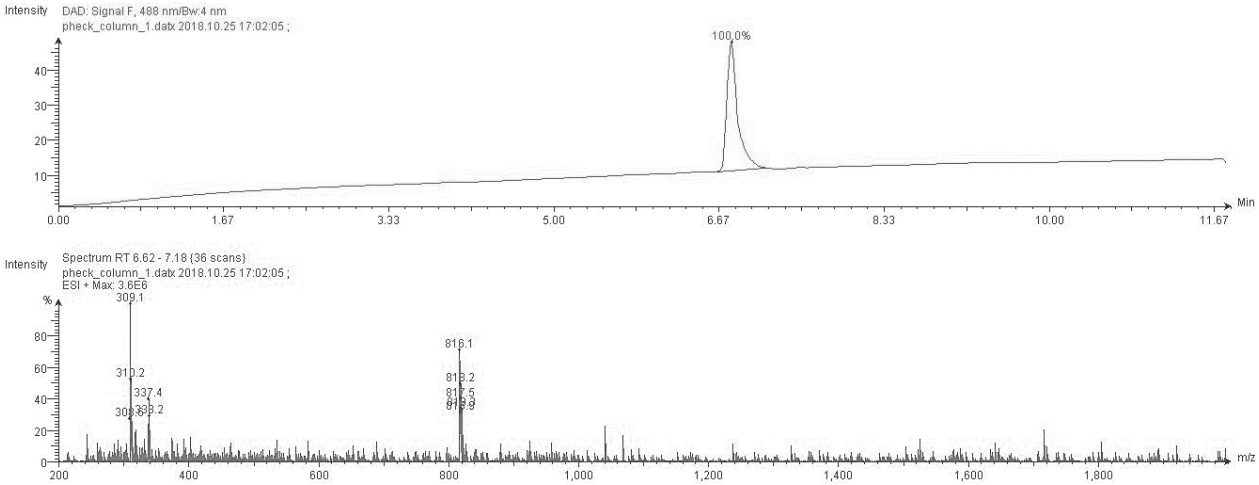

Low-resolution ESI(+) mass spectrum of **8**
Calculated for [M+H]+ 816.007276; Found 816.1.

Spectrum 2-4. Crude HPLC of 9

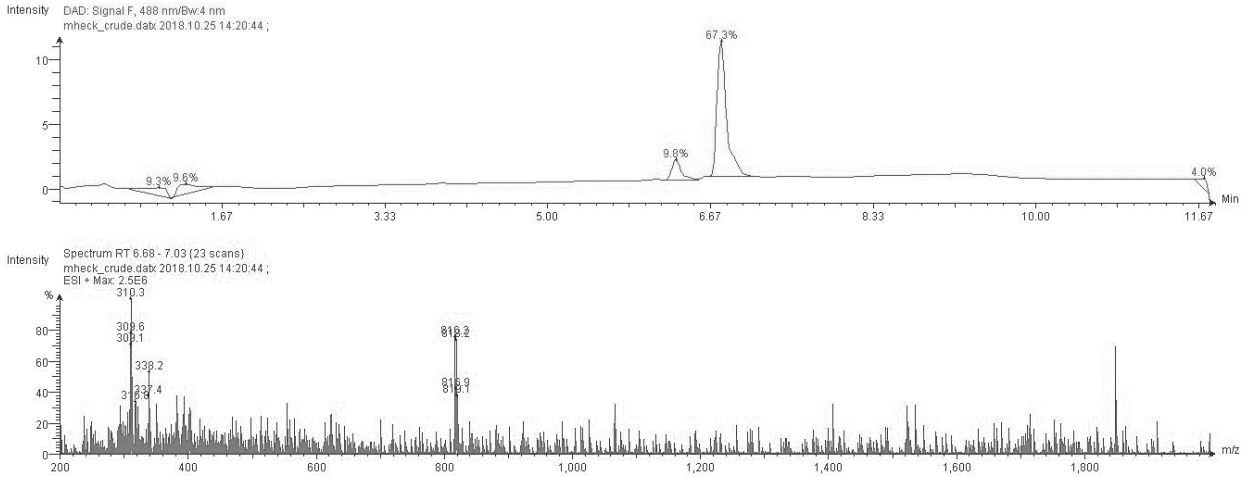

Low-resolution ESI(+) mass spectrum of **9** before purification
Calculated for [M+H]+ 816.007276; Found 816.2.

Spectrum 2-5. Crude HPLC of 10

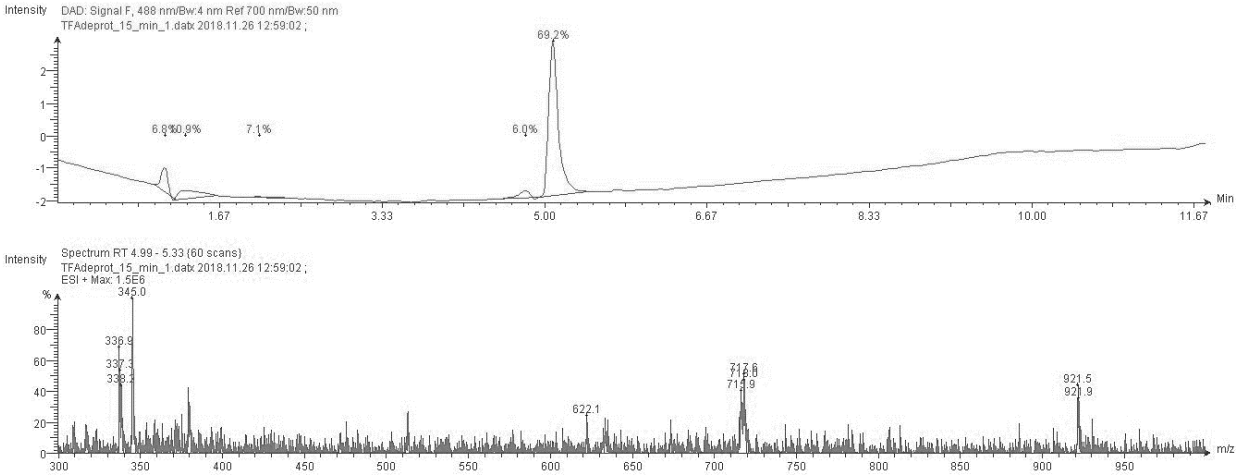

Low-resolution ESI(+) mass spectrum of **10** before purification
Calculated for [M+H]+ 716.007276; Found 716.2.

Spectrum 2-6. **HPLC of 11**

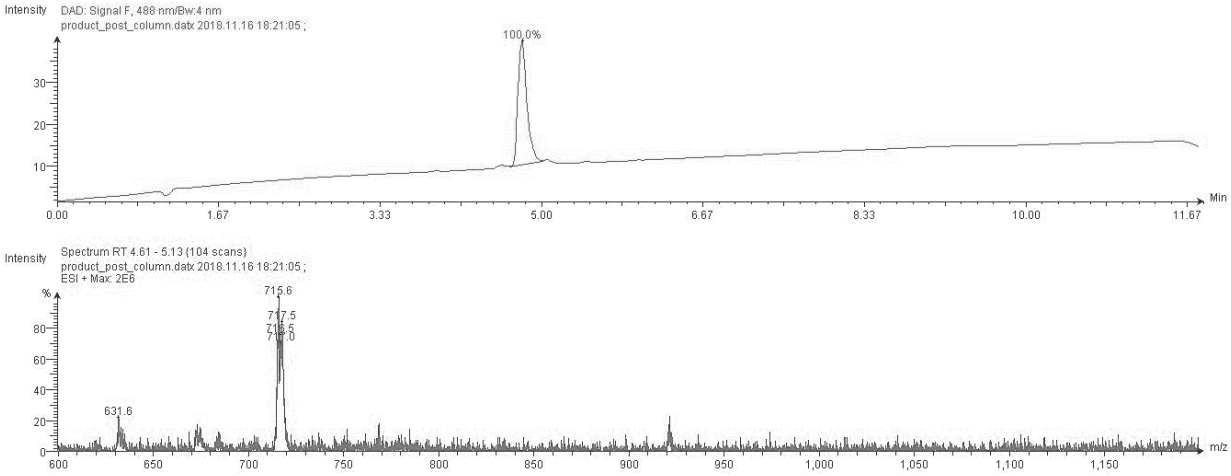

Low-resolution ESI(+) mass spectrum of **11**
Calculated for [M+H]+ 716.007276; Found 715.6

Spectrum 2-7. **HPLC of 13**

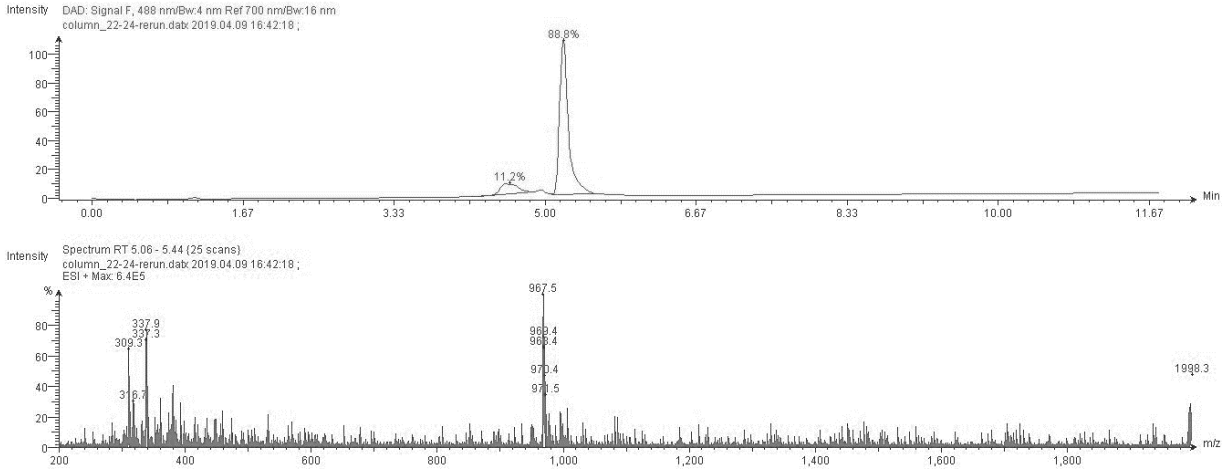

Low-resolution ESI(+) mass spectrum of **13**
Calculated for [M+H]+ 967.007276; Found 967.5.

Spectrum 2-8. Crude HPLC of 14

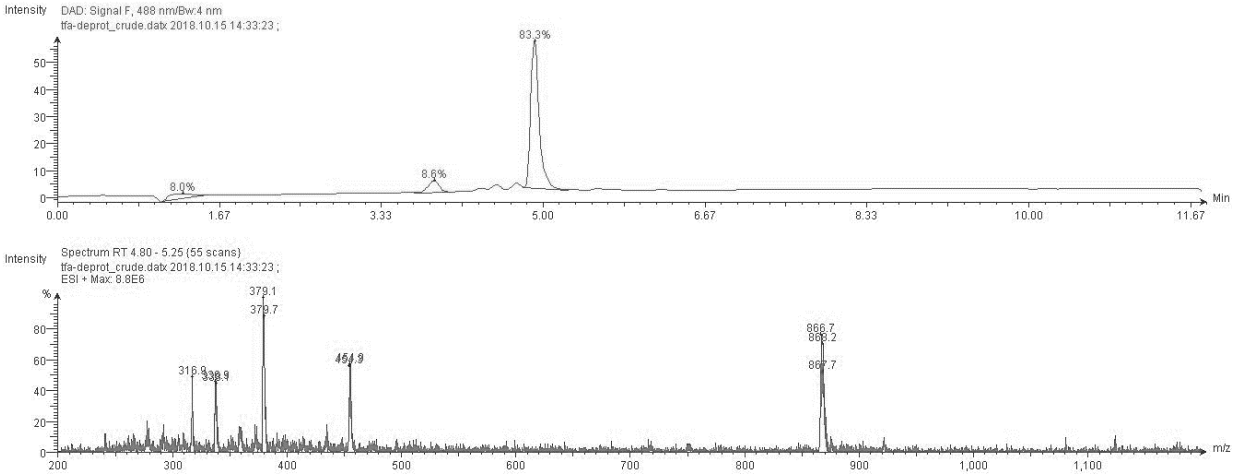

Low-resolution ESI(+) mass spectrum of **14**
Calculated for [M+H]+ 867.007276; Found 866.7 and 867.7.

Spectrum 2-9. HPLC of 15

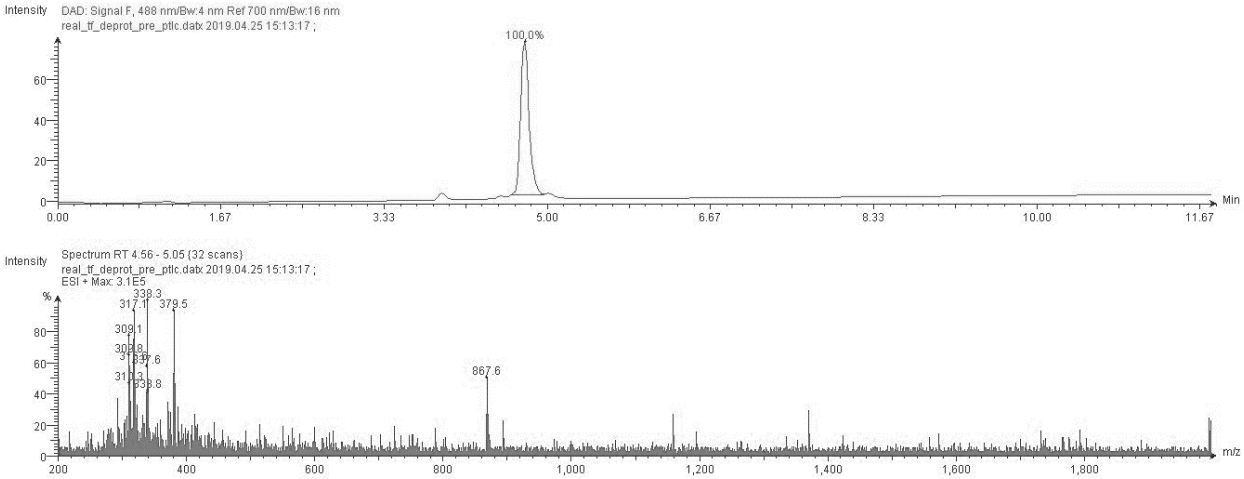

Low-resolution ESI(+) mass spectrum of **15**
Calculated for [M+H]+ 867.007276; Found 867.6.

Spectrum 2-10. **HPLC of 16**

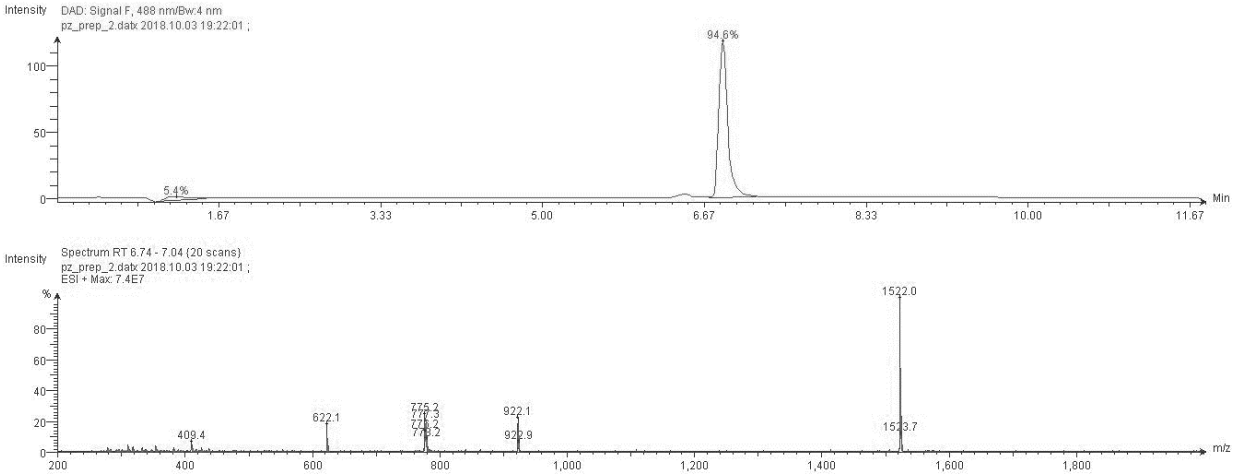

Low-resolution ESI(+) mass spectrum of **16**
Calculated for [M+H]+ 922.007276; Found 922.1.

Spectrum 2-11. HPLC of 17

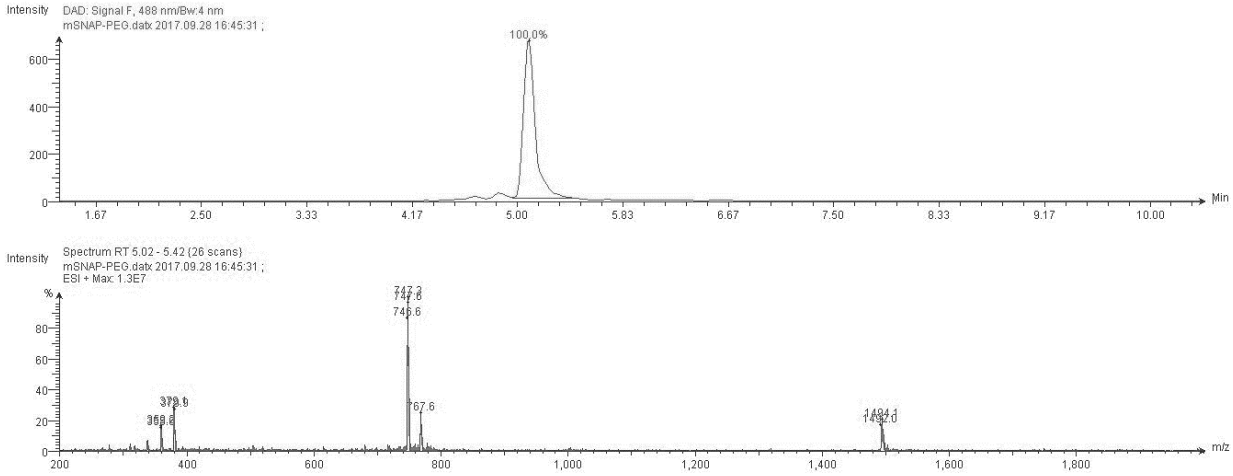

Low-resolution ESI(+) mass spectrum of **17**
Calculated for [M+H]+ 1494.467276; Found 1494.1

Spectrum 2-12. HPLC of 18

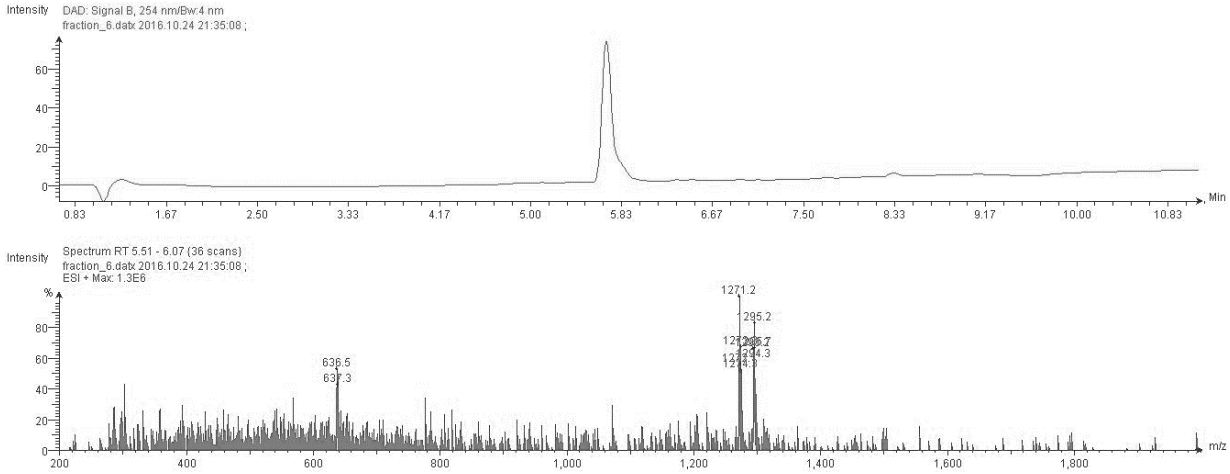

Low-resolution ESI(+) mass spectrum of **18**
Calculated for [M/2+2H]+ 636.75; Found 636.5
Calculated for [M+H]+ 1272.5; Found 1271.2 and 1272.1

Spectrum 2-13. **HPLC of 19, mSNAP1**

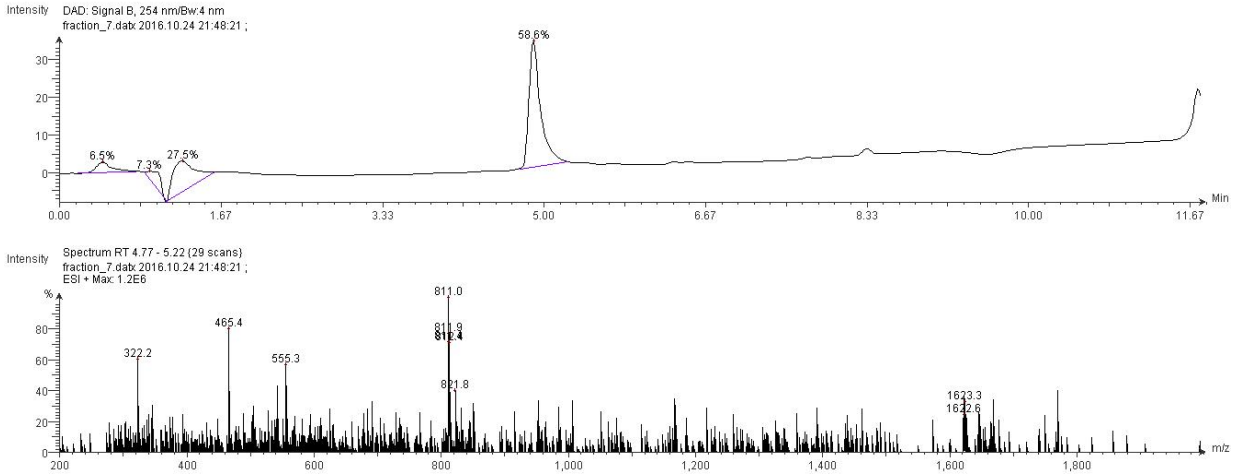

Low-resolution ESI(+) mass spectrum of **19**
Calculated for [M/2+2H]+ 812.5; Found 812.4
Calculated for [M+H]+ 1624.00; Found 1623.4

Spectrum 2-14. HPLC of mSNAP2

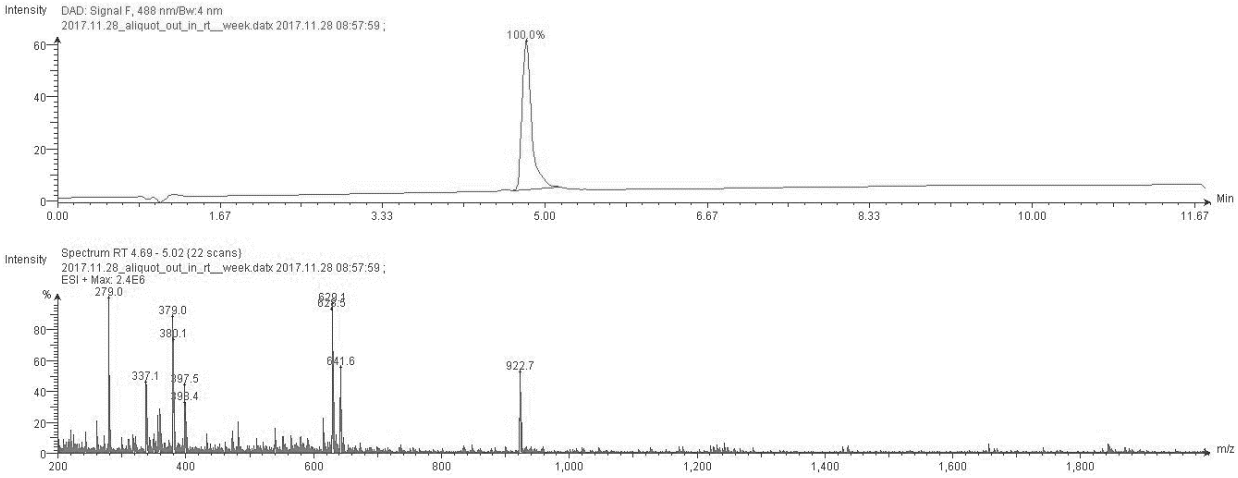

Low-resolution ESI(+) mass spectrum of **mSNAP2**
Calculated for [M+H]+ 1842.007276 and [M/2+ 2H]+ 921.507276; Found 922.7.

Spectrum 2-15. **^{1}H NMR of 6**

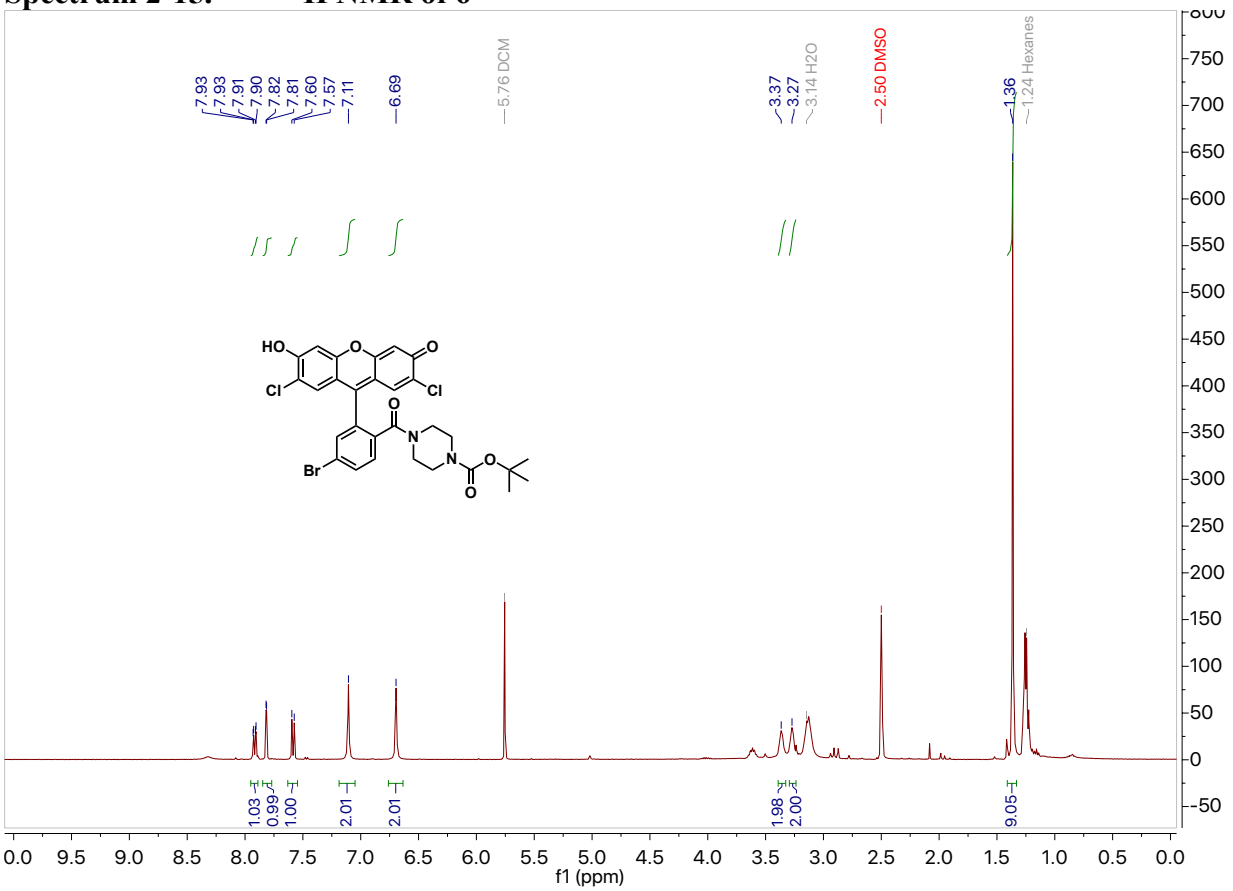

^{1}H NMR (400 MHz, DMSO-d_6) δ 7.92 (dd, J = 8.3, 1.9 Hz, 1H), 7.82 (d, J = 1.9 Hz, 1H), 7.59 (d, J = 8.3 Hz, 1H), 7.11 (s, 2H), 6.69 (s, 2H), 3.37 (s, 2H), 3.27 (s, 2H), 1.36 (s, 9H).

Spectrum 2-16. **^{1}H NMR of 8 (pVF-pip-boc)**

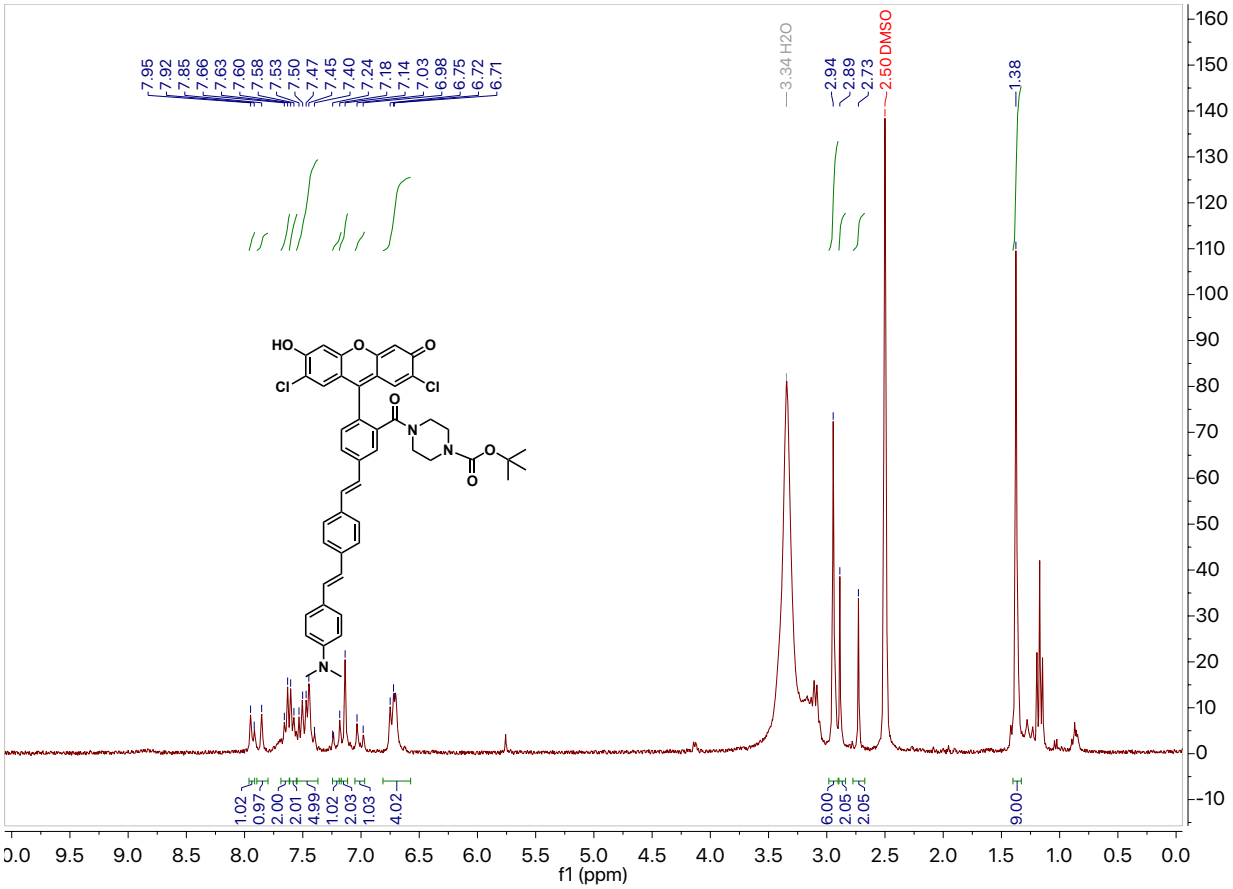

^{1}H NMR (300 MHz, DMSO-d_6) δ 7.93 (d, J = 9.4 Hz, 1H), 7.85 (s, 1H), 7.64 (d, J = 8.4 Hz, 2H), 7.59 (d, J = 8.4 Hz, 2H), 7.53 – 7.40 (m, 5H), 7.21 (d, J = 18.2 Hz, 1H), 7.14 (s, 2H), 7.01 (d, J = 15.9 Hz, 1H), 6.81 – 6.57 (m, 4H), 2.94 (s, 6H), 2.89 (s, 2H), 2.73 (s, 2H), 1.38 (s, 9H).

Spectrum 2-17. **^{1}H NMR of 15 (mVF-pip-cya)**

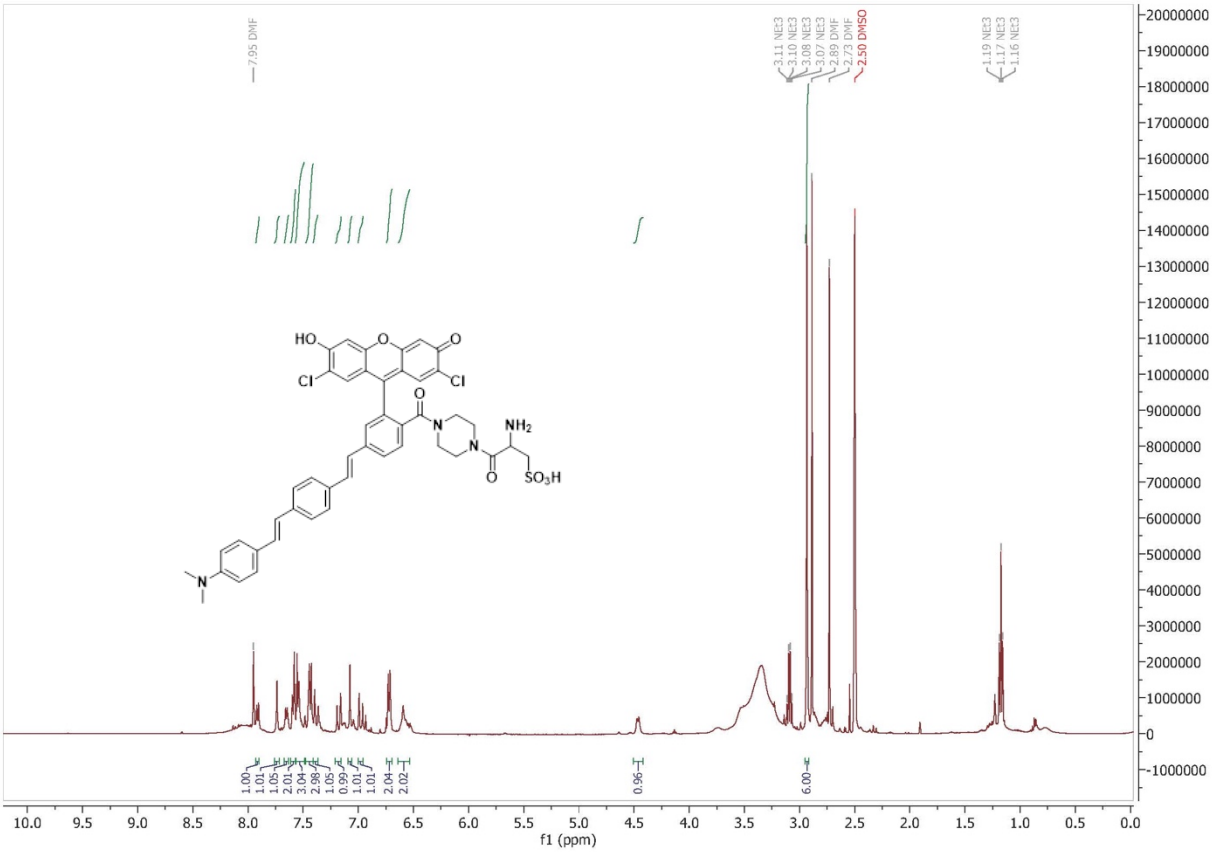

^{1}H NMR (600 MHz, d_6-DMSO) δ 8.03 (s, 3H), 7.93 (d, J = 8.2 Hz, 1H), 7.77 (s, 1H), 7.68 (d, J = 8.1 Hz, 1H), 7.61 – 7.50 (m, 3H), 7.50 – 7.30 (m, 4H), 7.18 (d, J = 16.3 Hz, 2H), 6.98 (d, J = 16.3 Hz, 1H), 6.73 (d, J = 8.5 Hz, 2H), 4.47 (s, 1H), 3.66 – 3.54 (m, 6H), 3.17 – 3.06 (m, 2H), 2.94 (s, 6H).

Figures, Schemes and Tables

Scheme 2-1. *SNAP-tag membrane anchoring designs and chemical structures of VF-SNAP ligands and derivatives.*

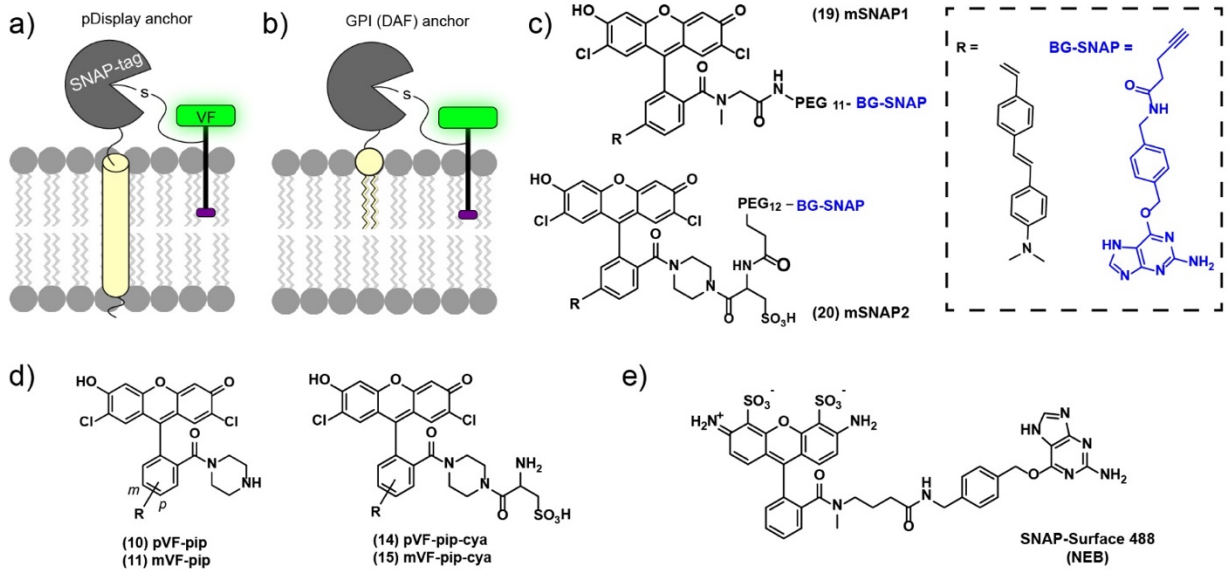

Figure 2-1. *Piperazine-cysteic acid VoltageFluor labeling in HEK293T cells*

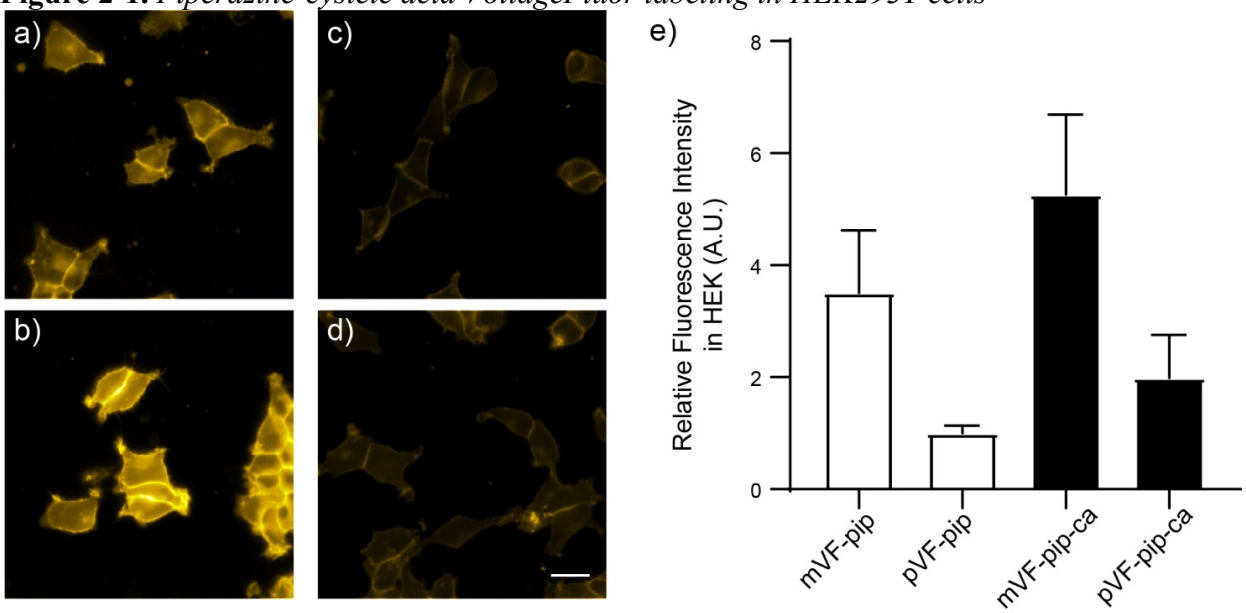

Figure 2-1. VoltageFluor labeling in HEK293T cells. Epifluorescence images of cells labeled with 500 nM **a)** mVF-pip **11**, **b)** mVF-pip-cya **15**, **c)** pVF-pip **10**, and **d)** pVF-pip-cya **14** in HBSS. All images are normalized to (**b**) mVF-pip-cya, **15**. **e)** Average background corrected fluorescence of VFs imaged in **a-d** relative to the average value of pVF-pip, **11** (the dimmest = 1). Scale bar is 20 μm. Error bars are the standard deviation of the mean with n = 10-20 cells per condition.

Figure 2-2. *Characterization of piperazine and cysteic acid VoltageFluors.*

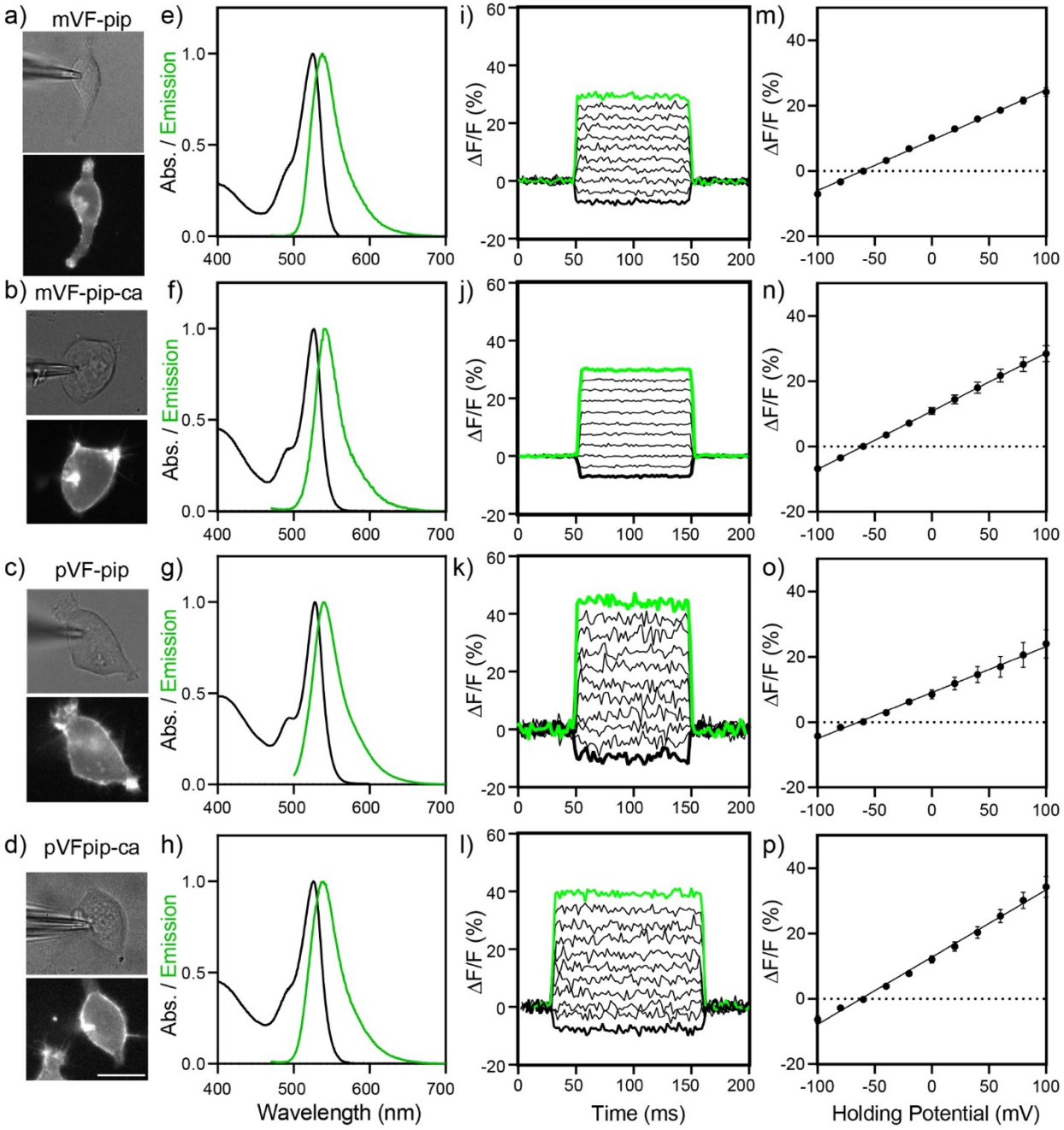

Figure 2-2. Characterization of piperazine and cysteic acid VoltageFluors. Widefield transmitted and epifluorescent images of HEK293T cells loaded with **a)** mVF-pip (**11**), **b)** mVF-pip-cya (**15**), **c)** pVF-pip (**10**), and **d)** pVF-pip-cya (**14**). Scale bar is 15 μm. **e-g)** Plot of normalized absorbance and emission intensity of 500 nM mVF-pip, mVF-pip-cya, pVF-pip and pVF-pip-cya, respectively, in phosphate-buffered saline (PBS with 0.1% Triton X-100, pH 7.2). **i-l)** Plot of relative change in fluorescence (% ΔF/F) vs. time of the same VFs in HEK 293T cells under whole-cell patch -clamp electrophysiology. **m-p)** Plot of fractional change in fluorescence (% ΔF/F) vs. membrane potential for the same VF dyes in a-d). Data are mean ± SEM for n = 5-7 determinations.

Figure 2-3. *mSNAP1 & 2 fluorescence turn-on in SNAP-pDisplay expressing HEK293T cells*

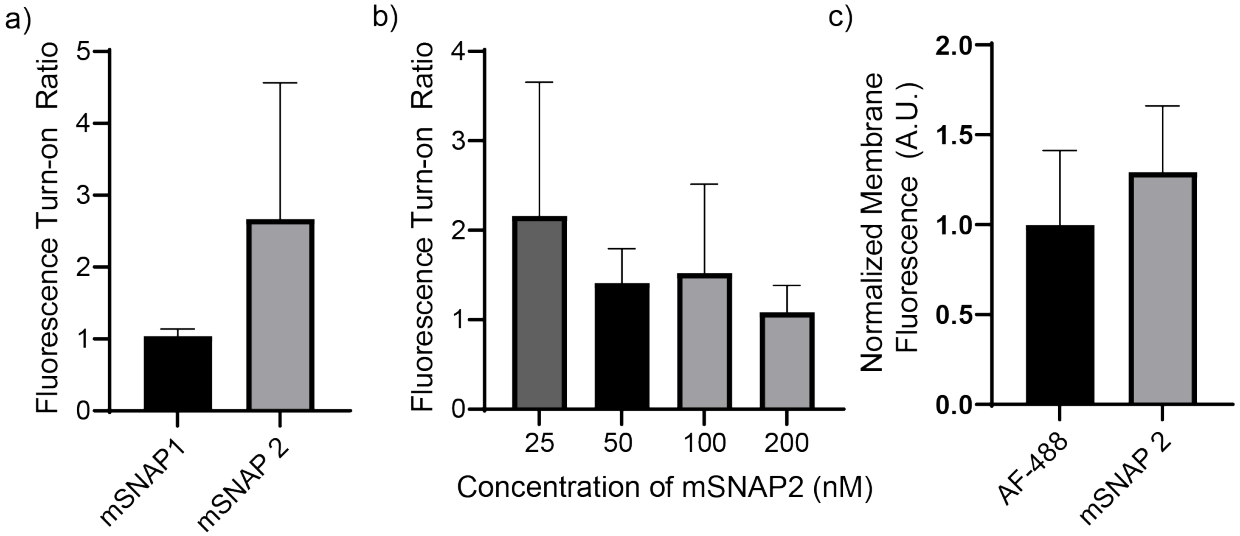

Figure 2-3. mSNAP1 & 2 fluorescence turn-on in SNAP-pDisplay expressing HEK293T cells. **a)** Average fluorescence turn-on ratio of transfected to non-transfected cells labeled with 25 nM mSNAP1 or mSNAP2 for 15 minutes, n = 3-4 ROIs each with 3-9 transfected cells. **b)** Loading concentration effects on the turn-on ratio for HEK293T cells labeled with mSNAP2 only, ranging from 25 to 200 nM, n = 3-7 ROIs each with 3-9 transfected cells. **c)** mSNAP2 membrane fluorescence relative to SNAP-Surface-488 (SS-488), n=39-65 cells. Error bars represent standard deviation of the mean.

Figure 2-4. *Optimization of SNAP$_f$tag expression and labeling using mSNAP2*

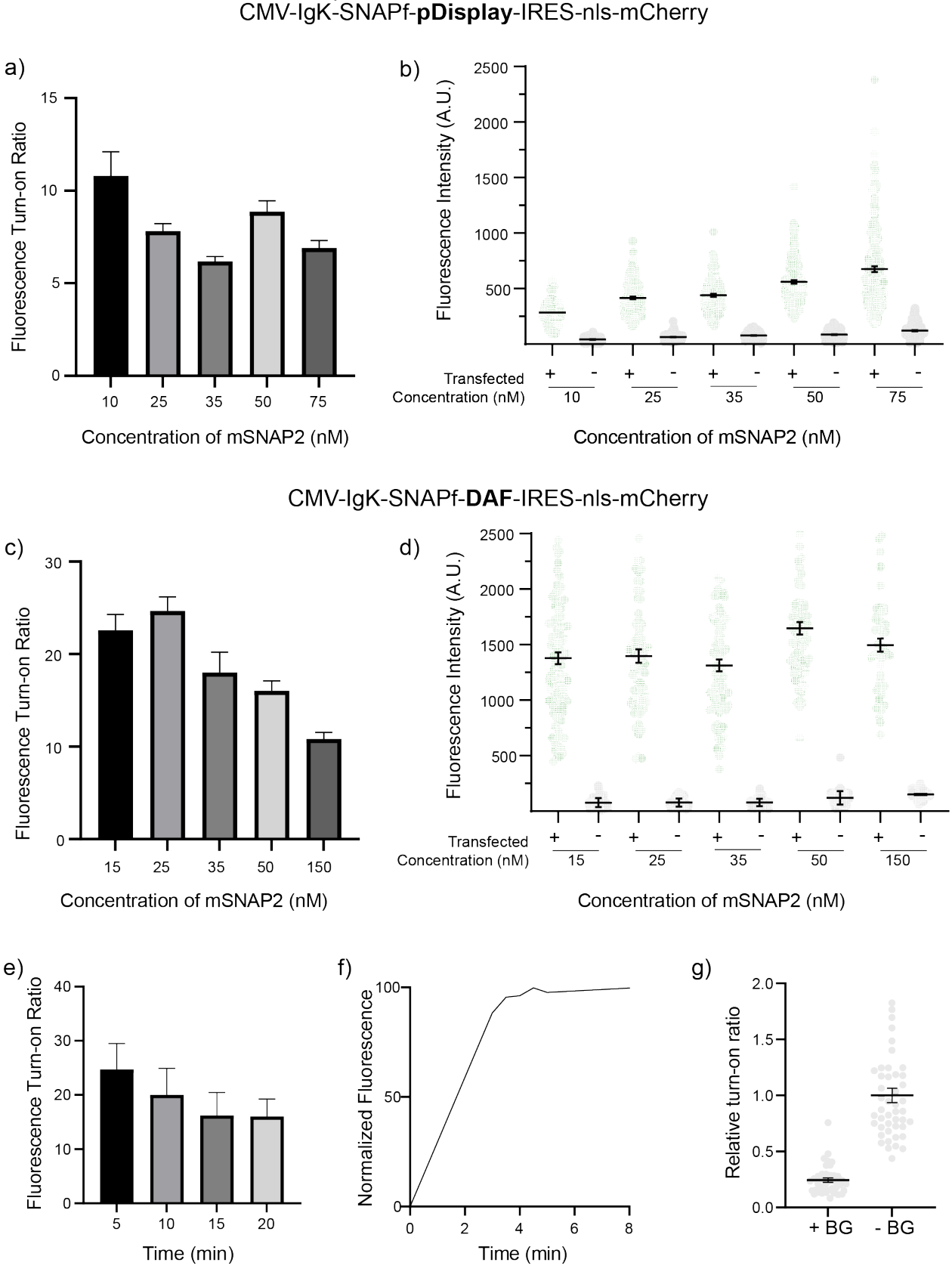

Figure 2-4. Optimizing SNAP-tag expression constructs with mSNAP2 labeling. a) and **c)** Average turn on ratio of HEK293T cells expressing $SNAP_f$ and labeled with varying concentrations of mSNAP2, ranging from 10 – 150 nM, for 25 minutes. Ratios are based on background corrected values shown in (**b**) and (**d**), respectively, of transfected (light green) and non-transfected (light grey) cells. SNAPf was targeted to the plasma membrane with an alpha helical transmembrane domain (pDisplay) for (**a**) and (**b**) and targeted using a GPI-anchor (DAF) for figures **c-g. e)** Average turn on ratio of HEK cells loaded with 25 nM mSNAP2 for 5, 10, 15, or 20 minutes without washing. **f)** Fluorescence time course of membrane localized emission of a single transfected cell loaded with 25 nM mSNAP2 using epifluorescence microscopy. Time points were taken roughly every 1-2 minutes and values were normalized to the initial fluorescence recorded at t=0 min. **g)** Relative turn-on ratio of cells with (+BG) and without (-BG) pre-incubation of a non-fluorescent O^6-benzylguanine substrate (100 nM) prior to bath loading 100 nM mSNAP2. All error bars are represented as the mean ± SEM.

Figure 2-5. *mSNAP2 contrast between expressing and non-expressing cells using different $SNAP_f$ expression constructs*

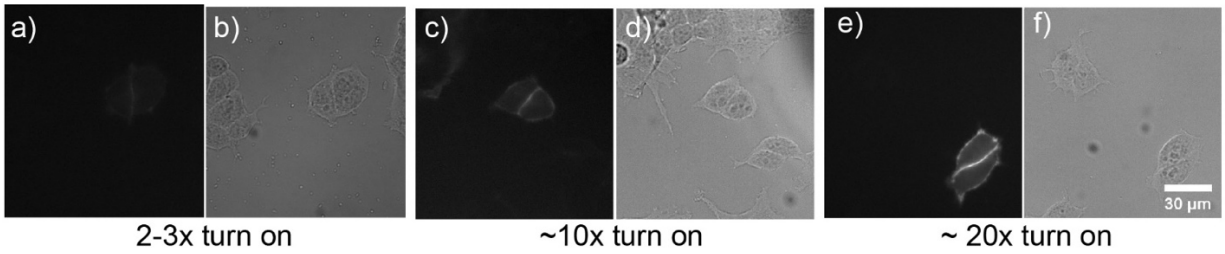

Figure 2-5. mSNAP2 labeling in different $SNAP_f$ expression constructs. Turn-on improvements of mSNAP2 in HEK239T cells expressing SNAP-pDisplay (**a** and **b**), $SNAP_f$-pDisplay (**c** and **d**), and $SNAP_f$-DAF (**e** and **f**). Cells in both pDisplay constructs (**a-d**) were labeled with 50 nM mSNAP2. Cells expressing $SNAP_f$-DAF (**e** and **f**) were labeled with 25 nM mSNAP2. Fluorescent images are normalized to $SNAP_f$-DAF intensity (**e**). Scale bar is 30 μm.

Figure 2-6. *mSNAP2 voltage sensitivity in HEK cells and cultured neurons*

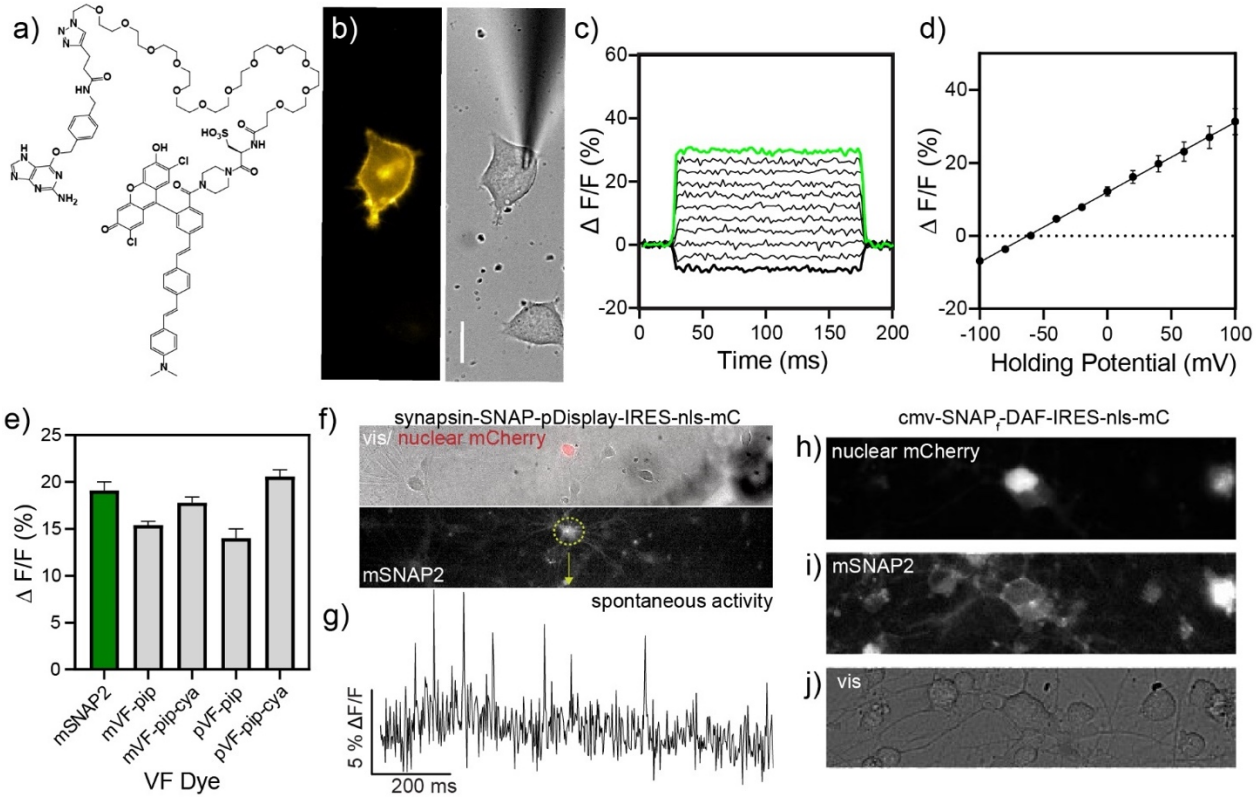

Figure 2-6. mSNAP2 voltage sensitivity in HEK cells. a) Synthetic structure of mSNAP2 (VF-pip-cya-PEG12-BG). **b)** Epifluorescent and transmitted image of a voltage-clamped HEK cell expressing membrane localized SNAP-tag protein loaded with 25 nM mSNAP2 in HBSS. **c)** Fractional change in fluorescence from a single cell held at -100 mV (bold) to +100 mV (green) with 20 mV increment steps. **d)** Average fractional change in fluorescence from n=7 cells with a voltage response of 19.1% ± 0.9% ΔF/F per 100 mV. **e)** Average voltage sensitivity (% ΔF/F) in HEK cells for mSNAP2 and VF-pip-cya derivatives (compounds **10**,**11**,**14** and **15**) Scale bar is 15 µm. All error bars are SEM. **f)** Live cell images of dissociated rat hippocampal neurons expressing SNAP-tag using a pDisplay transmembrane anchor and nuclear localized mCherry separated by an internal ribosome entry site sequence (IRES) under the neuron specific synapsin promoter. The red labeled cell in the vis image indicates positive SNAP-tag expression, also seen by mSNAP2 labeling. **g**) Below the images are fractional changes in the fluorescence signal of the transfected cell from non-evoked spontaneous activity. Live cell images of neurons expressing $SNAP_f$ using the GPI anchor, DAF, and **h**) nuclear localized mCherry. **i**) mSNAP2 labeling and **j**) transmitted light image of the same field of view.

Figure 2-7. *Dye loading in Live Drosophila brains*

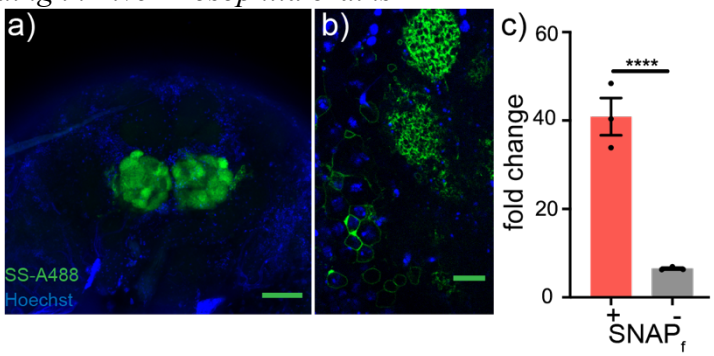

Figure 2-7. **Live brain dye loading in Drosophila**. Confocal maximum z-projection of live brain SS-A488 (1 µM) dye loading in GH146-Gal4 driven a) SNAPf-CD4 expressing Drosophila nervous tissue. High magnification single confocal plane of b) SNAPf-CD4 expressing olfactory projection neurons treated with SS-A488 (1 µM). c) Plot of relative fluorescence intensity of antennal lobe region expressing SNAPf-CD4 vs. non transgene expressing regions. Non transgene expressing regions were selected as large non-antennal lobe regions of protocerebrum. Data are mean ± SEM for n = 3 individually loaded brains. Data points represent the relative fluorescence intensity of the antennal lobe region or protocerebral region.

Figure 2-8. *Voltage-sensitive dye loading in Drosophila brains*

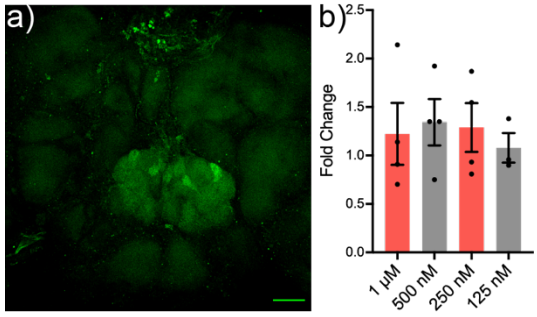

Figure 2-8. Voltage-sensitive dye loading in *Drosophila* brains. Confocal maximum z-projection of live brain mSNAP2 (100 nM) dye loading in GH146-Gal4 driven **a)** SNAP-CD4 expressing *Drosophila brains.* **b)** Plot of normalized relative fluorescence intensity of antennal lobe region expressing SNAP-CD4 across various concentrations of mSNAP2. Data are mean ± SEM for n = 3-4 individually loaded brains. Data points represent the relative fluorescence intensity of the antennal lobe region normalized to background protocerebral fluorescence intensity.

Figure 2-9. *mSNAP2 voltage reporting in live Drosophila brain tissue*

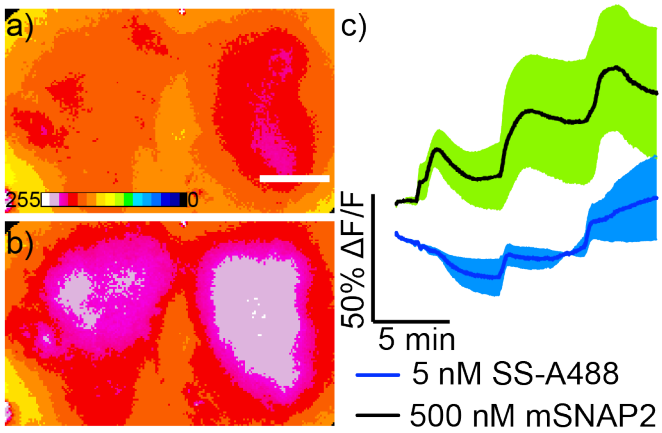

Figure 2-9. mSNAP2 voltage reporting in live Drosophila brain tissue. Epifluorescence images of explant Drosophila brain expressing SNAPf-CD4 in olfactory projection neurons (GH146-GAL4 /CyO>SNAPf-CD4::) **a)** immediately before and **b)** at peak fluorescence response to the carbachol stimulation. Scale bar is 50 µm. Image is pseudo-colored, and the color scale bar indicates 8-bit pixel grey values. **c)** Plot of mSNAP2 (Green, n=3, 500 nM) or SS-A488(blue, n=3, 5 nM) fluorescence (ΔF/F) vs. time for individual fly brains in response to three 100 µM carbachol stimulations. Data are mean ± SEM. Black bars represent the addition of carbachol.

Table 2-1 *Properties of sarcosine and piperazine VF dyes, PEGylated intermediates and SNAP-tag indicators*

Dye	Isomer	PEG units	λ_{max} (abs)[a]	λ_{max} (em)[a]	% Φ [a]	Relative SNR [b]	%ΔF/F[b,c]
1[d]	5	--	525	540	2.7	--	27.2 ± 0.2
2[d]	6	--	525	540	3.9	--	22.7 ± 0.1
10 pVF-pip	5	--	527	539	29.7	1	15.5 ± 0.4
11 mVF-pip	6	--	525	538	1.5	1.3	14.0 ± 1.0
14 pVF-pip-cya	5	--	526	539	2.5	1.3	17.8 ± 0.6
15 mVF-pip-cya	6	--	526	540	0.6	2.2	20.6 ± 0.7
16 pVF-pip-cya-PEG_{12}-N_3	5	12	--	--	3.1	--	--
17 mVF-pip-cya-PEG_{12}-N_3	6	12	--	--	2.6	--	--
19 mSNAP1	6	11			7.0	--	
20 mSNAP2	6	12	524	540	16.1	--	19.1 ± 0.9
21 pSNAP2	5	12	524	542	16.3	--	--

[a] Acquired in PBS, pH 7.4 with 0.1% Triton X-100. [b] Measured in HEK293T cells. [c] Measured per 100 mV, optically sampled at 500 Hz. [d] Values taken from Grenier, et al. 2019

References

1. Walther, W. & Stein, U. Cell type specific and inducible promoters for vectors in gene therapy as an approach for cell targeting. *J. Mol. Med. (Berl).* **74**, 379–392 (1996).
2. Chhatwal, J. P., Hammack, S. E., Jasnow, A. M., Rainnie, D. G. & Ressler, K. J. Identification of cell-type-specific promoters within the brain using lentiviral vectors. *Gene Ther.* **14**, 575–583 (2007).
3. Beier, H. T., Roth, C. C., Bixler, J. N., Sedelnikova, A. V. & Ibey, B. L. Visualization of Dynamic Sub-microsecond Changes in Membrane Potential. *Biophys. J.* **116**, 120–126 (2019).
4. Zakeri, B. *et al.* Peptide tag forming a rapid covalent bond to a protein, through engineering a bacterial adhesin. *Proc. Natl. Acad. Sci. U. S. A.* **109**, (2012).
5. Grenier, V., Daws, B. R., Liu, P. & Miller, E. W. Spying on Neuronal Membrane Potential with Genetically Targetable Voltage Indicators. *J. Am. Chem. Soc.* **141**, 1349–1358 (2019).
6. Miller, E. W. *et al.* Optically monitoring voltage in neurons by photo-induced electron transfer through molecular wires. *Proc. Natl. Acad. Sci.* **109**, 2114–2119 (2012).
7. Ortiz, G. *et al.* A Silicon-Rhodamine Chemical-Genetic Hybrid for Far Red Voltage Imaging from Defined Neurons in Brain Slice A silicon-rhodamine chemical-genetic hybrid for far red voltage imag- ing from defined neurons in brain slice. **8**, (2020).
8. Deal, P. E. *et al.* Covalently Tethered Rhodamine Voltage Reporters for High Speed Functional Imaging in Brain Tissue. *J. Am. Chem. Soc.* **142**, 614–622 (2020).
9. Los, G. V *et al.* HaloTag: a novel protein labeling technology for cell imaging and protein analysis. *ACS Chem Biol* **3**, 373–382 (2008).
10. Sun, X. *et al.* Development of SNAP-tag fluorogenic probes for wash-free fluorescence imaging. *ChemBioChem* **12**, 2217–2226 (2011).
11. Keppler, A. *et al.* A general method for the specific and covalent labeling of fusion proteins with small molecules in vivo - Supplementary Experimental Protocols. *Nat. Biotechnol.* **21**, 6–12 (2003).
12. Woodford, C. R. *et al.* Improved PeT Molecules for Optically Sensing Voltage in Neurons. *J. Am. Chem. Soc.* **137**, 1817–1824 (2015).
13. Sun, X. *et al.* Development of SNAP-tag fluorogenic probes for wash-free fluorescence imaging. *ChemBioChem* **12**, 2217–2226 (2011).
14. Stocker, R. F., Heimbeck, G., Gendre, N. & De Belle, J. S. Neuroblast ablation in Drosophila P[GAL4] lines reveals origins of olfactory interneurons. *J. Neurobiol.* **32**, 443–456 (1997).
15. Kirk, M. J. *et al.* Voltage imaging in Drosophila using a hybrid chemical-genetic rhodamine voltage reporter. (2021).
16. Wang, J. W., Wong, A. M., Flores, J., Vosshall, L. B. & Axel, R. Two-photon calcium imaging reveals an odor-evoked map of activity in the fly brain. *Cell* **112**, 271–282 (2003).

Chapter 3:
Voltage Imaging via Bioluminescence Quenching

This work was published in the following scientific journal:
Benlian, B. R.; Klier, P. E.; Martinez, K. N.; Schwinn, M. K.; Kirkland, T. A.; Miller, E. W. "Small Molecule-Protein Hybrid for Voltage Imaging via Quenching of Bioluminescence" *ACS sensors* **2021** 6(5), 1857-1863.

Abstract

We report a small molecule enzyme pair for optical voltage sensing via quenching of bioluminescence. This Quenching Bioluminescent Voltage Indicator, or Q-BOLT, pairs the dark absorbing, voltage-sensitive dipicrylamine with membrane-localized bioluminescence from the luciferase NanoLuc (NLuc). As a result, bioluminescence is quenched through resonance energy transfer (QRET) as a function of membrane potential. Fusion of HaloTag to NLuc creates a two-acceptor bioluminescence resonance energy transfer (BRET) system when a tetramethylrhodamine (TMR) HaloTag ligand is ligated to HaloTag. In this mode, Q-BOLT is capable of providing direct visualization of changes in membrane potential in live cells via three distinct readouts: change in QRET, BRET, and the ratio between bioluminescence emission and BRET. Q-BOLT can provide up to a 29% change in bioluminescence (ΔBL/BL) and >100% ΔBRET/BRET per 100 mV change in HEK 293T cells, without the need for excitation light. In cardiac monolayers derived from human induced pluripotent stem cells (hiPSC), Q-BOLT readily reports on membrane potential oscillations. Q-BOLT is the first example of a hybrid small molecule – protein voltage indicator that does not require excitation light and may be useful in contexts where excitation light is limiting.

Introduction

Membrane potential (Vm) plays a crucial role in signaling for both excitable and non-excitable cells. In electrically excitable cells like neurons or cardiomyocytes, millisecond changes in voltage trigger Ca^{2+} release and muscle contraction. Slower and smaller changes in resting V_m are also associated with essential cell physiology, including mitotic growth, cell proliferation,[1] differentiation,[2] and DNA synthesis in non-electrically excitable cell types.[3–6] However, the precise mechanisms underlying their relationships to V_m remain incompletely characterized.[3,7]

Optical methods to directly measure changes in V_m with fluorescent indicators are attractive because they avoid the invasiveness and low-throughput of electrode-based measurements while providing the spatial resolution of an imaging technique. In the last decade, substantial improvements to and new mechanisms for fluorescent voltage indicators have increased voltage sensitivity, enhanced brightness, and enabled imaging across the visible spectrum for a range of protein and small molecule based fluorescent indicators. However, all fluorescent indicators are dependent on externally applied illumination leading to unavoidable autofluorescence from cells and tissues, increased photobleaching and phototoxic effects, and overlap with optical actuators.[8,9]

Bioluminescent methods circumvent this problem. They avoid the use of excitation light, relying instead on the luciferase-catalyzed promotion of a luciferin substrate into the excited state. A number of luciferase-luciferin pairs have been deployed in heterologous hosts to enable a range of applications from visualizing gene expression[10] to whole-organism imaging.[11] More recently, bioluminescent methods have expanded to include indicators capable of monitoring Ca^{2+} dynamics,[12,13] protein-protein or protein-ligand interactions,[14] ATP,[15] cAMP,[16] and more[9,17] through either a pure bioluminescent or bioluminescent resonance energy transfer (BRET) approach. However, there are relative few examples of bioluminescent indicators and reporters compared to the number of fluorescent indicators and reporters.

Here we present a general approach to create a bioluminescence-based voltage indicator, Q-BOLT (Quenching Bioluminescent Voltage Sensor), which exploits two energy transfer processes as a function of voltage. Q-BOLT contains an extracellular membrane targeted luciferase, NanoLuc (NLuc),[18] whose luminescence (after the addition of its coelenterazine-based substrate furimazine) is quenched by a non-fluorescent voltage sensor, dipicrylamine (DPA).[19] The energy

transfer mechanism between the luciferin and DPA is similar to the well-established Förster resonance energy transfer (FRET) theory but is classified more specifically as quenching resonance energy transfer (QRET) due to the non-fluorescent absorber. DPA is both lipophilic and anionic, allowing the small molecule to localize and redistribute within the membrane bilayer in a V_m-dependent manner.[20] At depolarized potentials, the DPA migrates to the inner leaflet of the membrane resulting in decreased QRET and increased bioluminescence. This configuration was inspired by fluorescent hVOS[21–23] and two-component oxonol-coumarin systems;[24,25] however, the bioluminescent properties of Q-BOLT eliminate the need for illumination and associated issues of photobleaching, phototoxicity, and background fluorescence. Q-BOLT also includes the self-labeling HaloTag protein fused to the N-terminus of NLuc (**Scheme 3-1**). The addition of a fluorescent HaloTag ligand incorporates a second energy acceptor, which allows BRET and QRET to occur simultaneously. Here we show DPA can quench bioluminescence at hyperpolarized membrane potentials and this quenching is reduced upon depolarization, resulting in an increased bioluminescent and BRET signal.

Results

DPA quenches bioluminescence at the plasma membrane

While most bioluminescence resonance energy transfer (BRET) systems pair a luciferase with a bright fluorescent reporter to increase the optical signal, quenching of bioluminescence using an organic small molecule has not been previously demonstrated. For this reason, we first investigated whether Q-BOLT would enable voltage dependent quenching of bioluminescence. A HaloTag-NLuc fusion with a pDisplay α-helical transmembrane domain was expressed to the cell surface using a cellular secretory signal sequence (**Fig. 3-1a**). Cells expressing HaloTag-NLuc-pDisplay and treated with furimazine show strong bioluminescence signal localized to the periphery of the cell (**Fig. 3-1b-e**). Under whole-cell voltage clamp, NLuc expressing cells with 250 nM DPA show a increase in bioluminescence intensity upon depolarization with a ΔBL/BL of 39% ± 2% per 100 mV, (**Fig. 3-1c** and **3-1f**). Strategies for improving deviations from linearity, and possible reasons for it, are discussed in further detail later. There is no bioluminescent voltage response in cells without DPA (**Fig. 3-1d-f**). In contrast to similar fluorescent voltage indicators that rely on DPA, we were able to report larger fractional changes in luminescence with far lower concentrations of DPA. For example, a hVOS indicator typically requires >2 μM DPA and reports a 26% ΔF/F per 100 mV,[22,23,26,27] while our bioluminescent indicator reports voltage changes of 100 mV with 29% and 39% ΔBL/BL using 250 or 500 nM DPA, respectively.

We also tested an alternative protein configuration which swaps the order of the NLuc and HaloTag proteins, placing the luciferase farther from the cell membrane (**Fig. 3-2a** and **3-2b**). We hypothesized DPA would minimally quench bioluminescence using the NLuc-HaloTag fusion due to an increased distance between NLuc and the membrane/DPA. Both fusion proteins show membrane localized bioluminescence (**Fig. 3-3c** and **3-3e**) and the addition of DPA decreased this luminescence (**Fig. 3-3d** and **3-3f-h**). However, moving the luciferase farther from the membrane decreased the quenching resonance energy transfer (QRET) efficiency resulting in a lower and non-linear voltage response of 29% ± 2% per 100 mV (NLuc-HaloTag-pDisplay, **Fig. 3-4a** and **Table 3-1**). This is consistent with the distance dependence of energy transfer.[23]

Design of a Dual BRET/QRET Voltage Reporter

The emission from bioluminescent proteins is typically much less than that of fluorescent proteins.[8] Consequently, bioluminescent imaging is limited by low sensitivity and dynamic range,

and in general is not comparable to the temporal resolution achievable with fluorescence. To address this, bioluminescent probes typically pair a bright and stable luciferase with a compatible protein or small molecule BRET acceptor[8,28]. Here we chose to pair NLuc with the self-labeling HaloTag for easy modulation of bright and tunable fluorophore acceptors. We wondered if the addition of a cell impermeant HaloTag ligand[29] would be an efficient BRET acceptor with a voltage dependent emission.

A rhodamine acceptor with a small overlap integral with NLuc,[29] tetramethylrhodamine-PEG_X-HaloTag (TMR-PEG_X-HaloTag, ex/em 575/590), was chosen to increase BRET sensitivity based on previous studies.[30] Cells expressing our best construct, Q-BOLT, which incorporates an additional 10 residue gly-ser linker between HaloTag and NLuc in the HaloTag-NLuc-pDisplay configuration (**Fig. 3-5a**), show TMR emission from BRET located at the plasma membrane (**Fig. 3-5b**). BRET efficiency was optimized by increasing the TMR PEG linker length from PEG_0 to PEG_{13} (**Fig. 3-6b**). However, increasing the length to PEG_{25} had diminishing returns on the BRET ratio, likely from increased distance and TMR flexibility. Voltage sensitivities were not compared across different PEG linkers and all reported values are with TMR- PEG_{13}-HaloTag.[29]

Similar to initial experiments, bioluminescence signal increases with depolarizing voltage steps as in **Fig. 3-1d**, however the voltage sensitivity was reduced to 22% ± 3% ΔBL/BL per 100 mV (**Fig. 3-5c** and **3-5d**) compared to 29% ΔBL/BL without TMR**.** There was also a robust change in TMR emission, from BRET, resulting in a 114% ± 10% ΔBRET/BRET per 100 mV (**Fig. 3-5e).** We also observed a voltage dependent change in the ratio of BRET emission to bioluminescence emission, or BRET ratio (ΔR/R), of 81% ± 7% per 100 mV (**Fig. 3-5f**). We hypothesize the voltage-dependent change in ratio is the result of a switch between a two acceptor and a one acceptor RET system (**Scheme 3-2**), explained in more detail below.

We compared four fusion protein configurations. Improving BRET efficiency between NLuc and HaloTag did not necessarily improve voltage sensitivity. We examined BRET efficiency based on orientation between NLuc / TMR (**Fig. 3-2a** and **3-2b**) and found BRET to be more efficient in the NLuc-HaloTag-pDisplay configuration compared to HaloTag-NLuc-pDisplay, as determined by either widefield microscopy (**Fig. 3-6a**) or a microplate reader (**Fig. 3-6b** and **3-6d vs. 3-6e**). The more BRET-efficient NLuc-HaloTag-pDisplay orientation is not the more voltage sensitive construct (**Fig. 3-7a** and **3-7b**, **Table 3-1**). Use of microscopy or a microplate reader gave qualitatively similar estimates of BRET efficiency (**Fig. 3-6c**) for the different NLuc / HaloTag configurations (**Fig. 3-2**).

Using the more voltage sensitive, but less RET efficient protein, HaloTag-NLuc-pDisplay, we also investigated how BRET distance would affect voltage sensitivity (**Fig. 3-2b-d**). The BRET distance was increased by inserting another 10 amino acid residues between HaloTag and NLuc (**Fig. 3-2b** and **3-2c, Q-BOLT**). Increasing the distance between the two proteins resulted in a decreased BRET efficiency, consistent with the distance dependence of RET (**Fig. 3-6c**, **3-6e** vs. **3-6f**, blue vs. orange). However, there is a substantial increase in indicator voltage sensitivity with this sacrifice in RET efficiency (**Table 3-1**, **Fig. S5b** vs. **3-7c**): Q-BOLT has the largest voltage response (ΔBRET/BRET = 114% ± 10%), yet this probe has the lowest BRET efficiency based on relative BRET ratios (**Fig. 3-6**, Q-BOLT in orange vs. all other constructs).

We also swapped the membrane anchoring motif from pDisplay to a glycosyl phosphatidylinositol (GPI) anchor from decay accelerating factor or DAF,[31] which could bring the luciferase closer to membrane and DPA (**Fig. 3-2c** vs. **3-2d)**. This shorter distance could also influence the dipole orientation of excited state furimazine in the luciferase active site[32] and lead to an increase in the QRET efficiency and voltage response. Interestingly, the BRET ratio between Q-BOLT and

the analogous DAF construct are equivalent (**Fig. 3-6c**, **3-6f** and **3-6g**); however, their voltage sensitivities are very different (**Table 3-1, Fig. 3-7c** and **3-7d**). This is likely due to a difference in QRET based on the increased ΔBL with the DAF anchor compared to pDisplay (~48% and ~20% ΔBL/BL, respectively, **Table 3-1**), suggesting the DAF anchor may bring NLuc closer to the membrane and DPA. This increase in QRET makes the ΔBL and ΔBRET responses nearly equivalent, resulting in a nearly constant ΔR.

Voltage sensitivity can also be modulated by changing the concentration of DPA. At a low DPA concentration of 250 nM, the ΔBL/BL response of Q-BOLT to voltage was relatively linear. Above +40 mV, however, the increase in bioluminescence signal plateaus (**Fig. 3-7c**). When NLuc is farther from the membrane, the onset of non-linearity occurs earlier, at -20 mV for NLuc-HaloTag-pDisplay (**Fig. 3-7a**). At the low DPA concentration used in these experiments the probability of enough DPA molecules within the Förster radius required to achieve QRET is negligible, owing to the voltage-dependent Boltzman distribution of DPA in the bilayer.[19,21,23] This loss of quenching is seen at more negative potentials for NLuc-HaloTag-pDisplay, because the luciferase is farther from the membrane and DPA than the luciferase of Q-BOLT (HaloTag-NLuc-pDisplay). Consistent with this hypothesis, higher concentrations of DPA improve the linear response at more positive membrane potentials (**Table 3-1**, also compare **Fig. 3-5** and **Fig. 3-7c**).

Voltage sensitivity is a direct result of DPA and NanoLuc interactions

We suspect the voltage sensing mechanism of Q-BOLT involves changes in resonance energy transfer efficiencies which switch between a one-acceptor and two-acceptor system (**Scheme 3-2**). To support this hypothesis, we wanted to determine if direct interactions between DPA and TMR were contributing to voltage sensitivity. The addition of DPA to cells expressing either Q-BOLT or NLuc-HaloTag-pDisplay, labeled with TMR-PEG_{13}-Halo but not furimazine, does not result in quenching of TMR fluorescence (**Fig. 3-8i**). This suggests DPA is unable to interact with TMR either because of physical separation and/or the spectral overlap between the two chromophores is poor. To account for variations in fluorescence intensity from cell to cell, we imaged (1) *identical cells* before and after the addition of DPA, (2) used the lowest possible LED light intensity to reduce photobleaching, and (3) included an additional control comparing cells before and after the addition of buffer solution not containing DPA. With direct LED excitation of TMR, electrophysiology measurements reveal only a modest fluorescence response in cells expressing NLuc-HaloTag-pDisplay with a ΔF/F per 100 mV of ~3.7% (**Fig. 3-8h)**.

The response in HEK 293Tcells expressing Q-BOLT, however, was even lower: ~1.2% ΔF/F per 100 mV (**Fig. 3-8a** and **3-8b**). Moreover, the Q-BOLT sensor is oriented with the HaloTag relatively far from the membrane, further supporting the idea that DPA quenching of TMR is likely not a contributing factor to the robust voltage readout, ΔBRET/BRET = 91% per 100 mV, of Q-BOLT (**Fig. 3-8a, 3-8c,** and **3-8d**). It is also possible that some changes in the TMR signal may be due to donor bleed-through. However, in the absence of TMR, we found bioluminescence bleed-through was minimal (~ 2%, **Fig. 3-10**). Taken together, the robust voltage sensitivity of Q-BOLT cannot be explained by additional quenching of TMR by DPA or by bioluminescence bleed-through. Based on these controls and the results from structural modifications, we suspect the voltage sensing mechanism involves changes in energy transfer efficiencies between a one-acceptor and two-acceptor system (**Scheme 3-2**).

We hypothesize that under hyperpolarized conditions, the proximity of DPA to NLuc creates a "2-Acceptor State" where either QRET (NLuc → DPA) or BRET (NLuc → TMR) can both occur (**Scheme 3-2, "**2s-Acceptor State"). Upon depolarization, the probability of QRET decreases as a function of distance **(Scheme 3-2, "**1-Acceptor State"). This decrease in quenching increases

the probability of energy transferred to A_1 (solid red arrow) and energy emitted as luminescence (solid blue arrow). Because the distance between donor and A_1 is constant (solid black line), resonance energy transfer efficiency is dependent on R_0 which changes between the 1- and 2-acceptor states. Based on Eq. 1 and Eq. 2, this increase in Φ_{NLuc} would explain the voltage dependent change in BRET efficiency,

$$E_{A1} = \frac{1}{1+\left(\frac{r_1}{R_0^{A1}}\right)^6} \quad (1)$$

$$R_0 = 0.021\sqrt[6]{J\Phi_D n^{-4}\kappa^2}\ (nm) \quad (2)$$

Where E_{A1} is the energy transfer efficiency from the donor to acceptor 1 (A1), $r_1$is the distance from donor to A1, and R_0 is the Förster distance, defined in Eqn. 2, where J is the overlap integral between the donor emission and acceptor absorbance, Φ_{NLuc} is the bioluminescence quantum efficiency of NLuc, n is the refractive index, and κ is the orientation factor between the transition dipoles of the donor and acceptor.

Q-BOLT can detect action potentials from human induced pluripotent stem cell–derived cardiomyocytes (hiPSC-CMs)

Since prolonged light exposures can often disrupt cardiac action potentials (cAPs) or cause cessation of beating[33–36] we thought Q-BOLT would be a good candidate for imaging membrane potential dynamics in cardiomyocytes. Q-BOLT possesses high voltage sensitivity (>29% ΔBL/BL per 100 mV), requires only sub-micromolar DPA, and does not need exogenously added excitation light to optically sense voltage changes thereby reducing the chance of light induced cell damage. We transiently expressed Q-BOLT in human induced pluripotent stem cell-derived cardiomyocytes (hiPSC-CMs), treated the hiPSC-CMs with furimazine and DPA, and monitored bioluminescence using a plate reader. We observed robust oscillations in the bioluminescence signal from hiPSC-CMs expressing Q-BOLT and treated with furimazine and DPA (**Fig. 3-9a** and **Fig. 3-12**). These rhythmic oscillations in bioluminescence intensity appear only in the presence of DPA (**Fig. 3-9a**); without DPA, the bioluminescence signal of Q-BOLT is flat (**Fig. 3-9b**). No oscillations are seen in non-electrically excitable HEK 293T cells with or without DPA (**Fig. 3-9e-f**). Analysis of the dominant frequencies in these optical recordings via fast Fourier transform (FFT) reveal a frequency band around 1.5 Hz which is present only in hiPSC-CMs with DPA (**Fig. 3-9c-d**). This is expected for cardiomyocytes beating every 1 to 2 times per second with a typical action potential duration averaging ~500 ms.[18] Dominant frequencies are not present in non-electrically excitable cells regardless of the presence of DPA (**Fig. 3-9g-h**). As a control, we also used a previously developed fluorescent voltage indicator, BeRST, which senses V_m using a photoinduced electron transfer mechanism, independent of DPA.[37] Using BeRST we found similar dominant frequencies at about 1 Hz in hiPSC-CMs and no oscillations in non-excitable cells (**Fig. 3-13**). We also verified that DPA at concentrations up to 5 μM had no apparent toxic effects on the cardiac action potential duration or shape (**Fig. 3-11**). Action potential durations were within 10% of the baseline action potential duration, demonstrating minimal effects of DPA on iPSC-CM action potential durations at these concentrations.

Conclusion

In summary, Q-BOLT represents a new class of hybrid voltage indicator that functions via quenching of bioluminescence. It provides robust bioluminescence responses to changes in membrane potential of up to 39% ΔBL/BL, while using sub-micromolar DPA concentrations, more

than an order of magnitude less than typical concentrations used for fluorescent hVOS methods.[21,22] At the same time, Q-BOLT provides a large change in BRET, approximately 100% ΔBRET/BRET per 100 mV when paired with TMR-HaloTag. Our investigations into the mechanism of this voltage sensitivity suggest a direct quenching interaction between DPA and furimazine emission and subsequent voltage-dependent switching between a two-acceptor state at hyperpolarized potentials, in which either DPA or TMR can act as an acceptor, and one-acceptor state at depolarized potentials in which TMR is the primary acceptor (**Scheme 3-2**).

While Q-BOLT, and other bioluminescent probes, offer an advantage over fluorescence imaging by eliminating the need for harmful incident radiation, the primary limitation to Q-BOLT is the low photon emission from bioluminescence. Q-BOLT produces enough photons to enable single-cell imaging of membrane potential changes via bioluminescence or BRET at the plasma membrane (**Figure 3-1**). However, the long photon collection times (0.1 to 1 s), limit single-cell imaging of rapid neuronal action potentials. In systems where cells have a uniform change in membrane potential, like the cardiomyocyte syncytium, Q-BOLT can readily detect changes and oscillations in membrane potential (**Figure 3-9**), presaging its utility, for example, in phenotypic assays of hiPSC-CMs, where phototoxicity is often a limiting factor.[33,38,39] In these contexts, slow-release or cell impermeant versions[40] of the NLuc substrate, furimazine, may aid long-term imaging, and improve signal-to-noise; tethered DPA-fluorophore pairs[41] may also improve performance. We are currently investigating methods to improve the photon output of Q-BOLT by screening[42] pairs of HaloTag-NLuc fusions that show both enhanced BRET and voltage sensitivity and combining these constructs with even brighter[43] synthetic fluorophore-HaloTag ligands.

Experimental Methods

General synthetic methods

Chemical reagents and solvents (dry) were purchased from commercial suppliers and used without further purification. Synthesis of BOC-haloamine (compound 1) and TMR-pip-cys (compound 3) was carried out as previously reported . Thin layer chromatography (TLC) (Silicycle, F254, 250 μm) and preparative thin layer chromatography (PTLC) (Silicycle, F254, 1000 μm) were performed on glass backed plates pre-coated with silica gel and were visualized by fluorescence quenching under UV light. Flash column chromatography was performed on Silicycle Silica Flash F60 (230–400 Mesh) using a forced flow of air at 0.5–1.0 bar. NMR spectra were measured on Bruker AVB-400 MHz, 100 MHz, AVQ-400 MHz, 100 MHz, Bruker AV-600 MHz, 150 MHz. Variable temperature NMR experiments were measured on the Bruker AV-600 with the assistance of Hasan Celik. Chemical shifts are expressed in parts per million (ppm) and are referenced to CDCl3 (7.26 ppm, 77.0 ppm) or DMSO (2.50 ppm, 40 ppm). Coupling constants are reported as Hertz (Hz). Splitting patterns are indicated as follows: s, singlet; d, doublet; t, triplet; q, quartet; dd, doublet of doublet; m, multiplet. High-resolution mass spectra (HR-ESI-MS) were measured by the QB3/Chemistry mass spectrometry service at University of California, Berkeley. High performance liquid chromatography (HPLC) and low resolution ESI Mass Spectrometry were performed on an Agilent Infinity 1200 analytical instrument coupled to an Advion CMS-L ESI mass spectrometer. The column used for the analytical HPLC was Phenomenex Luna 5 μm C18(2) (4.6 mm I.D. × 150 mm) with a flow rate of 1.0 mL/min. The mobile phases were MQ-H2O with 0.05% trifluoroacetic acid (eluent A) and HPLC grade acetonitrile with 0.05% trifluoroacetic acid (eluent B). Signals were monitored at 254, 380 and 545 nm over 10 min with a gradient of 10-100% eluent B. The column used for preparative HPLC was Phenomenex Luna 10 μm C18(2) (21.2 mm I.D. x

250 mm) with a flow rate of 30.0 mL/min. The mobile phases were MQ-H2O with 0.05% trifluoroacetic acid (eluent A) and HPLC grade acetonitrile with 0.05% trifluoroacetic acid (eluent B). Signals were monitored at 545 over 20 min with a gradient of 30-70% eluent B.

Cell culture

HEK293T cell lines were obtained from the UC Berkeley Cell Culture Facility and discarded after 25 passages. Cells were dissociated during passages using 0.05% Trypsin-EDTA with phenol red (Thermo Fisher Scientific) at 37°C, and then maintained in Dulbecco's Modified Eagle Medium (DMEM) with 4.5 g/L D-glucose supplemented with 10% FBS (Seradigm (VWR); Radnor, PA) and 2 mM 668 GlutaMAX (Gibco) in a 5% CO2 incubator at 37°C.

For all imaging experiments, cells were plated onto 8 well chambered cover glass (57x25 mm). For patching experiments, cells were plated on 25 mm diameter #1.5 glass coverslips (Electron Microscopy Sciences) in 6 well tissue culture plates (Corning; Corning, NY). To maximize cell attachment, coverslips were treated before use with 1-2 M HCl for 2-5 hours and washed overnight three times with 100% ethanol and three times with deionized water. Coverslips were sterilized by heating to 150°C for 2-3 hours. Before use, coverslips were incubated with poly-D-lysine (Sigma-Aldrich, made as a 0.1 mg/mL solution in phosphate-buffered saline with 10 mM Na_3BO_3) for 2-10 hours at 37°C and then washed twice with water and twice with Dulbecco's phosphate buffered saline (dPBS, Gibco). HEK293T cells were seeded 9-24 hours before microscopy experiments. To ensure the presence of single cells for whole-cell voltage clamp electrophysiology, HEK293T cells were seeded in reduced glucose (1 g/L) DMEM with 10% FBS, 2 mM GlutaMAX, and 1 mM sodium pyruvate.

NanoLuc substrate, DPA, and dye loading

For experiments imaging TMR-HaloTag, cells were loaded with 500nM dye in HBSS for 15-20 minutes at 37°C and 5% CO2. Cells were washed 2x with HBSS and replaced with fresh HBSS for imaging. For experiments without TMR-HaloTag, cells were rinsed 2x to remove residual media and replaced with fresh HBSS before proceeding. Cells were used immediately after loading the dye and no cells remained at room temperature for longer than an hour.

After loading TMR-HaloTag and placing cells in fresh HBSS, furimazine substrate (Promega) was added to NanoGlo buffer, mixed, and pipetted directly into the dish to be imaged. The final substrate concentration was kept at 2x (~5-10uM) and cells were not imaged for longer than an hour to ensure a relatively stable bioluminescence signal throughout each experiment. It was noted, however, that voltage sensitivities remained the same across very bright and dim emitting cells alike. For experiments using DPA, a fresh working solution was made every time from a 20 mM DPA stock in DMSO (source) and made up in the same furimazine/buffer solution.

Whole-cell patch clamp electrophysiology

Pipettes were pulled from borosilicate glass with filament (Sutter Instruments, Novato, CA) resistances ranging from 4 to 7 MΩ with a P97 pipette puller (Sutter Instruments). The internal solution composition is as follows, in mM (pH 7.25, 285 mOsmol/L): 125 potassium gluconate, 10 KCl, 5 NaCl, 1 EGTA, 10 HEPES, 2 ATP sodium salt, 0.3 GTP sodium salt. EGTA (tetraacid form) was prepared as a stock solution in either 1 M KOH or 10 M NaOH before addition to the internal solution. Pipettes were positioned with an MP-225 micromanipulator (Sutter Instruments).

Electrophysiology recordings were made with an Axopatch 200B amplifier and digitized with a Digidata 1550B (Molecular Devices). Signals were filtered with a 5 kHz low-pass Bessel filter. Correction for pipette capacitance was performed in the cell attached configuration. Images were acquired while in voltage-clamp mode at the designated holding potential for 2-4 seconds.

Holding potentials applied varied from -80mV to +80 mV, with +20 mV increments and a -60mV holding potential between each step. Potentials were applied in random order, and a membrane test was conducted between each step to verify the quality of the patch. Recordings of single cells were only included if they maintained a 10:1 ratio of membrane resistance (Rm) to access resistance (Ra) and an Ra value below 30 MΩ throughout the recording, although most recordings maintained a 20:1 ratio or better. Occasionally, -80 mV and +80mV holding potentials resulted in an unstable patch (<10:1 ratio, and ultimately a lost patch) and for this reason some of those data points were not included in analysis.

Dual-view microscopy

All imaging was performed on an inverted epifluorescence microscope AxioObserver Z-1 (Zeiss), equipped with a Spectra-X Light engine LED light (Lumencor), controlled using μManager (V1.4, open-source, Open Imaging). Images were acquired using Plan-Apochromat 20/0.8 air objective (20x, Zeiss) and captured on an Evolve 128 EMCCD camera (Photometrics). Emission was collected with a dichroic used in conjunction with a Dual-View emission splitter (Optical Insights). The Dual-View was equipped with a 585dcxr dichroic (Chroma), 460/30 nm (Semrock) and 610/75 nm (Chroma) emission filters to separate the bioluminescent and BRET signals. Imaging for electrophysiology experiments were performed at 1 Hz when collecting bioluminescence and/or BRET data, and 100 Hz for experiments using 550/15 nm LED excitation light. Exposure times for all other (non-electrophysiology) experiments measuring bioluminescence/BRET were kept at 0.5 seconds (2 Hz).

All images were analyzed using FIJIs ImageJ. Hand drawn regions of interest were limited to intensities at the cell periphery, avoiding internal bioluminescent signals, and were background subtracted to a region without any cells.

CLARIOstar Plus+ microplate reader

Bulk actional potential measurements were taken with a CLARIOstart plus plate reader (courtesy of the Martin Lab at UC Berkeley). Bioluminescence values (466/64 nm) were measured over 10-20 second intervals without excitation light. Fluorescence emission from BeRST (636/21 LED excitation, 100 ms exposure) was collected using a 698/29 nm emission filter and 665 nm dichroic also over 10-20 second intervals. Exposure times for measuring bioluminescence and fluorescence were kept at 0.1 seconds (10 Hz). Emission scans (Figure S4d-g) were collected from 400 – 650 nm at 10 Hz after adding furimazine substrate to wells with and without 500 nM TMR-peg_{13}-HaloTag. All spectra were normalized to the peak emission at 460 nm. Fast Fourier Transforms (FFT) of luminesence signals were performed in Matlab (R2019a, Mathworks).

DPA dose-response in hiPSC-CMs

Induced pluripotent stem cell-derived cardiomyocytes (hiPSC-CMs)[33] were incubated with 1 μM BeRST 1 in RPMI 1640 minus Phenol Red (Gibco) plus B27 supplement media for 20 min at 37 °C. Baseline cardiac activity was recorded in three regions of interest per cell, prior to addition of DPA (631/28 nm bandpass, 66.6 mW/mm2, emission collected with a quadruple emission filter (430/32, 508/14, 586/30, 708/98) after passing through a quadruple dichroic mirror (43/38, 509/22, 586/40, 654 nm LP), 5 ms exposure). DPA stocks were made in DMSO and added as a 1:1000 dilution in a 100 μL addition of RPMI 1640 (minus Phenol Red) plus B27 supplement media. As a vehicle control, 0.1% DMSO in a 100 μL addition of RPMI 1640 (minus Phenol Red) plus B27 supplement media was added. Cardiomyocytes were incubated with added DPA/DMSO control in media for 15 min at 37 °C preceding imaging in three regions of interest per well. An in-well dose escalation was performed, and the DPA concentration was raised through subsequent

addition of media containing DPA. The vehicle control was matched to add the same percentage of DMSO. This protocol was followed for the following concentrations of DPA: 250 nM, 1 μM, 2 μM, and 5 μM. Dose response curves were acquired in GraphPad using cardiac data extracted from .tiff stacks using an in-house MATLAB script.

Cloning and transient transfections

HEK293T cells plated in a 6 well tissue culture dish were incubated at 37°C in a humidified incubator for at least 24 hours prior to transfection. Once cells reached ~60-75% confluency, transfections were performed with Lipofectamine 3000, using half the recommended p3000 and a quarter of the lipofectamine volumes suggested from the manufacturer's protocol (Thermo Fisher Scientific). We found reducing the amount of lipofectamine significantly increased cell health without dramatically reducing the transfection efficiency. Cells were allowed to grow an additional 5-10 hours after transfection before being plated onto glass coverslips for microscopy experiments (described above).

After differentiation from hi-PSCs, and lactate purification,[33] hiPSC-CMs were plated at ~40k onto glass bottom 96-well ibidi dishes pre-treated with Matrigel. After 3-4 days of recovery, beating cells were transfected using Lipofectamine according to the manufacturers protocol. hiPSC-CMs were imaged 1-4 days later.

For expression in HEK293T cells, all constructs were sub-cloned into a pCDNA3 vector with the HaloTag/NLuc fusions sandwiched by an IgK secretion signal and a single pass pDisplay transmembrane domain (or a GPI-anchor, the decay accelerating factor, DAF). The name of each construct and corresponding order of each domain is as follows:

01: IgK – NLuc – (short GS linker) – HaloTag – pD
02: IgK – HaloTag – (long GS linker) – NLuc – pD
02.2: IgK – HaloTag – (short GS linker) – NLuc – pD
03: IgK – HaloTag – (long GS linker) – NLuc – DAF
04: IgK – NLuc – (short GS linker) – HaloTag – pD – IRES – nls – mCherry
05: IgK – HaloTag – (long GS linker) – NLuc – pD – IRES – nls – mCherry

Constructs 04 and 05 are identical to 01 and 02, respectively, but have an additional nuclear localized (NLS) fluorescent reporter. These constructs were used in all experiments which did not include the addition of TMR in order to identify transfected cells rather than using bioluminescence alone.

Synthesis

Synthesis of tert-butyl succinate halo amide, 2:

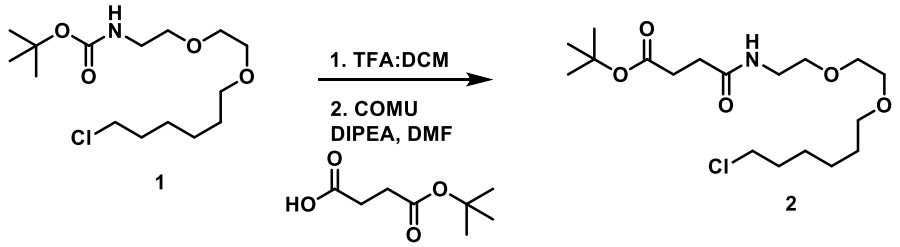

BOC-haloamine (543 mg, 1.68 mmol) was stirred in 2 mL of a 1:1 mixture of trifluoroacetic acid (TFA) and dichloromethane (DCM) for 2 hours at room temperature. Solvent was then removed under a stream of nitrogen and the remaining acid was quenched with 2mL of a saturated solution of potassium carbonate in methanol. In a separate flask, mono-tert-butyl succinate (344 mg, 1.97 mmol) was stirred with COMU (1.08g, 2.52 mmol) and diisopropylethylamine (DIPEA) (1.5 mL, 8.61 mmol) in ~3 mL dimethylformamide (DMF) for 20 minutes at room temperature. The solution was then cooled to 0oC and the solution of deprotected haloamine added dropwise. The reaction was then stirred for 30 minutes at room temperature, concentrated under reduced pressure, extracted 5x with DCM and 5% LiCl, dried with sodium sulfate, filtered, and concentrated under reduced pressure. Crude material was purified via flash chromatography to yield 315 mg of compound 2 (49% yield).

^{1}H NMR (400 MHz, Chloroform-d) δ 4.51 (q, J = 7.2 Hz, 2H), 4.44 (q, J = 7.1 Hz, 1H), 3.54 (q, J = 7.1 Hz, 3H), 2.91 (dd, J = 7.5, 5.7 Hz, 2H), 2.73 (dd, J = 7.5, 5.8 Hz, 2H), 2.70 – 2.61 (m, 1H), 2.58 (ddd, J = 7.6, 5.8, 1.4 Hz, 1H), 1.48 (s, J = 2.5 Hz, 9H), 1.48 (m, J = 2.5 Hz, 8H), 1.46 – 1.40 (m, 4H), 1.25 (t, J = 7.0 Hz, 5H)

Synthesis of TMR-pip-cys-succ-HaloTag, 4:

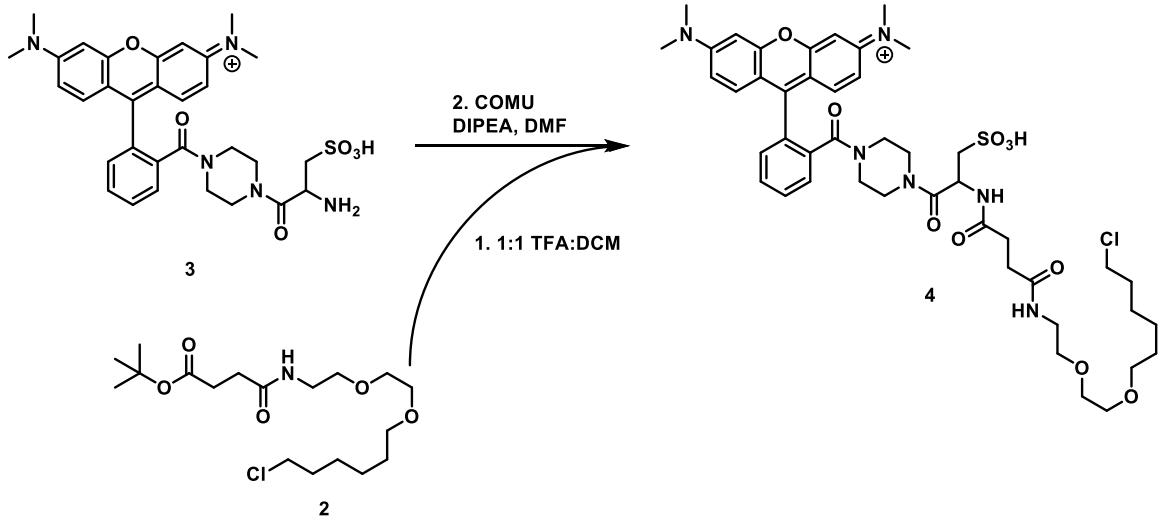

Tert-butyl succinate halo amide (compound 2, 19 mg, 0.050 mmol) was stirred in 2 mL of a 1:1 mixture of TFA:DCM for 2 hours. Solvent was then removed under a stream of nitrogen and compound was redissolved in DMF with DIPEA (30 µL, 0.17 mmol), COMU (17 mg, 0.040 mmol), and TMR-pip-cys (compound 3, 20 mg, 0.033 mmol) and stirred for 30 minutes at room temperature. Solvent was then removed under reduced pressure and the crude material was extracted 5x with 0.1 M HCl and DCM. Organic phase was then evaporated under reduced pressure and crude material was purified via preparative TLC (10% MeOH in DCM) to yield compound 4 (5 mg, 18% yield).

^{1}H NMR (600 MHz, DMSO) δ 8.25 – 8.04 (m, 2H), 7.84 (s, 1H), 7.82 – 7.73 (m, 1H), 7.53 (s, 1H), 7.25 – 7.07 (m, 3H), 6.99 – 6.88 (m, 1H), 4.94 (s, 1H), 3.62 (tq, J = 6.6, 3.6 Hz, 3H), 3.55 – 3.43 (m, 3H), 3.15 (qd, J = 7.3, 4.3 Hz, 2H), 1.70 (dq, J = 8.4, 6.7 Hz, 2H), 1.49 (p, J = 6.7 Hz, 2H), 1.40 (d, J = 7.2 Hz, 2H), 1.31 – 1.23 (m, 14H).

HRMS (ESI+) Calculated for $C_{45}H_{60}{}^{35}ClN_6O_{10}S$ $[M+Na-H]^+$: 933.3594; Found 933.3594

Synthesis of TMR-pip-cys-PEG$_{25}$-HaloTag, 5:

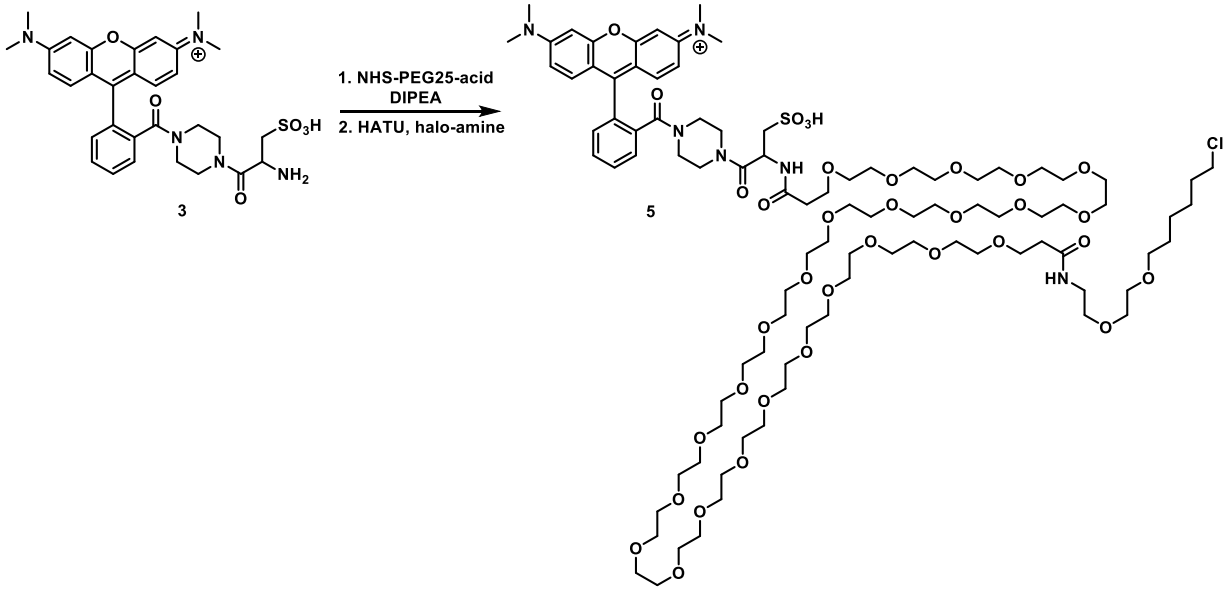

TMR-pip-cys (compound 3, 40 mg, 0.066 mmol) was dissolved in DMF with DIPEA (75 µL, 0.043 mmol) and NHS-PEG$_{25}$-acid (Quanta BioDesign) (100 mg, 0.076 mmol) and stirred for 2 hours at room temperature. Concurrently for 2h, BOC-haloamine (compound 1, 27 mg, 0.083 mmol) was deprotected in 2 mL of a 1:1 mixture of TFA:DCM and then the solvent was evaporated under nitrogen. Deprotected haloamine, HATU (32 mg, 0.083 mmol) and DIPEA (75 µL, 0.043 mmol) were added to the reaction and the reaction was stirred overnight. The solvent was then removed under reduced pressure and the crude material was extracted 5x with 0.1 M HCl and DCM. The organic layer was then removed under reduced pressure and the crude material purified via preparative HPLC (30-70% MeCN in H20 with 0.05% TFA) to yield compound 5 (4 mg, 3% yield).

^{1}H NMR (600 MHz, DMSO) δ 8.78 – 8.74 (m), 8.47 (d, J = 8.1 Hz), 8.26 (s), 7.99 – 7.58 (m), 7.59 – 7.39 (m), 7.24 – 7.05 (m), 6.98 – 6.89 (m), 6.61 (s), 3.62 (s,), 3.50 (d, J = 2.9 Hz), 3.11 (q, J = 7.4 Hz), 3.02 – 2.85 (m), 2.30 (ttd, J = 14.2, 10.0, 9.6, 5.9 Hz), 2.27 – 2.11 (m), 1.91 (s), 1.24 (dd, J = 11.6, 7.0 Hz), 1.20 (d, J = 6.4 Hz).

HRMS (ESI+) Calculated for $C_{95}H_{160}{}^{35}ClN_6O_{10}S$ $[M+Na]^{2+}$: 1017.5110; Found 1017.5114

Spectra

Spectrum S1. *[1]H spectrum of 2 (tert-butyl succinate halo amide):*

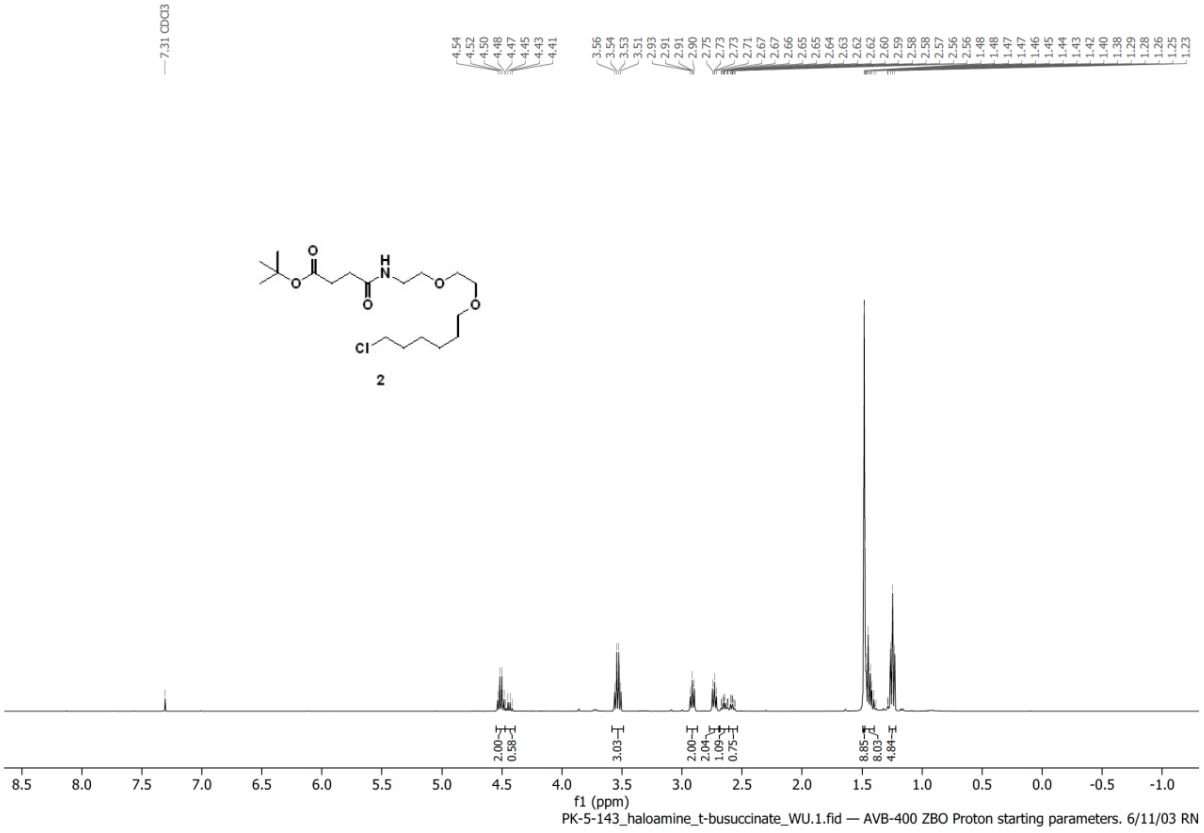

Spectrum S2. *[1]H spectrum of 4 (TMR-pip-cys-succ-HaloTag):*

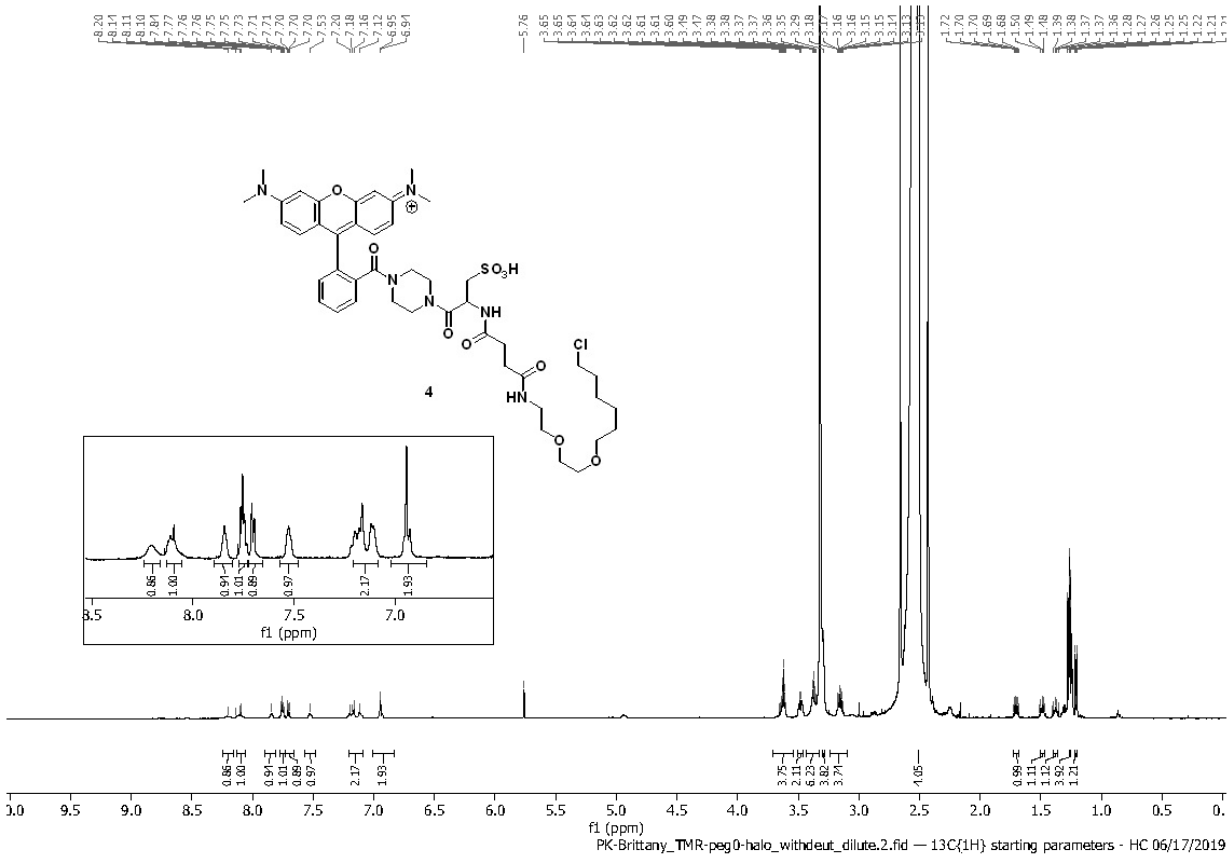

Spectrum S3. *^{1}H spectrum of 5 (**TMR-pip-cys-PEG$_{25}$-HaloTag**):*

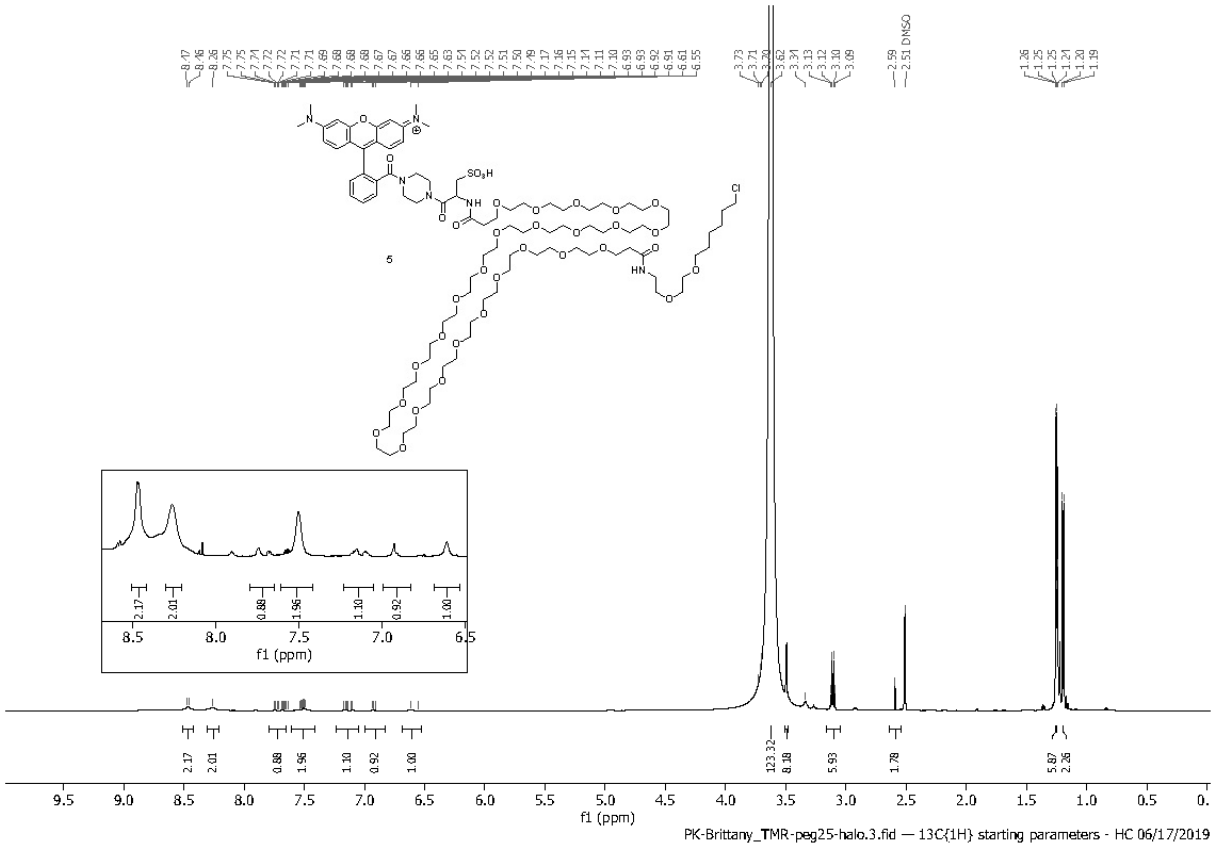

Spectrum S4. *HPLC of 4 (TMR-piperazine-cysteic acid-succinate-halo):*

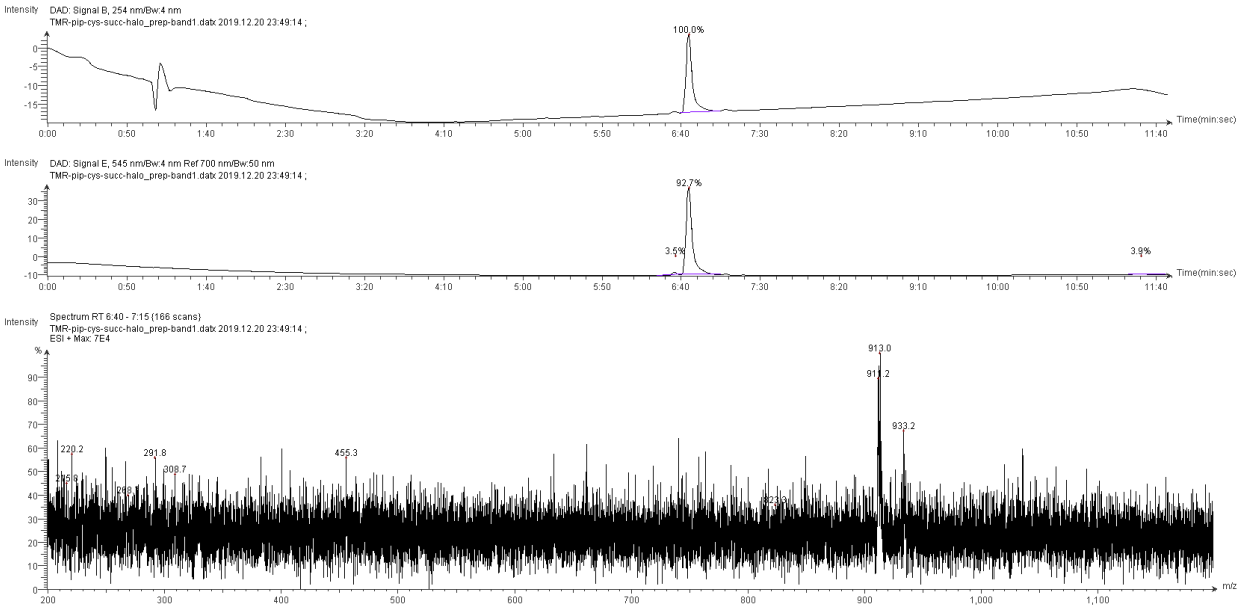

Low-resolution ESI(+) mass spectrum of **4** (TMR-piperazine-cysteic acid-succinate-halo)

Calculated for $C_{45}H_{60}{}^{35}ClN_6O_{10}S$ $[M]^+$: 911.38
Calculated for $C_{45}H_{60}{}^{37}ClN_6O_{10}S$ $[M]^+$: 913.38

Calculated for $[M]^+$, ^{35}Cl = 911.38
Found: 911.2

Calculated for $[M]^+$, ^{37}Cl = 913.38
Found: 913.0

Calculated for $[M + Na^+ - H^+]^+$, ^{35}Cl = 933.36
Found: 933.2

Spectrum S5. *HPLC of 5 (TMR-piperazine-cysteic acid-PEG25-halo):*

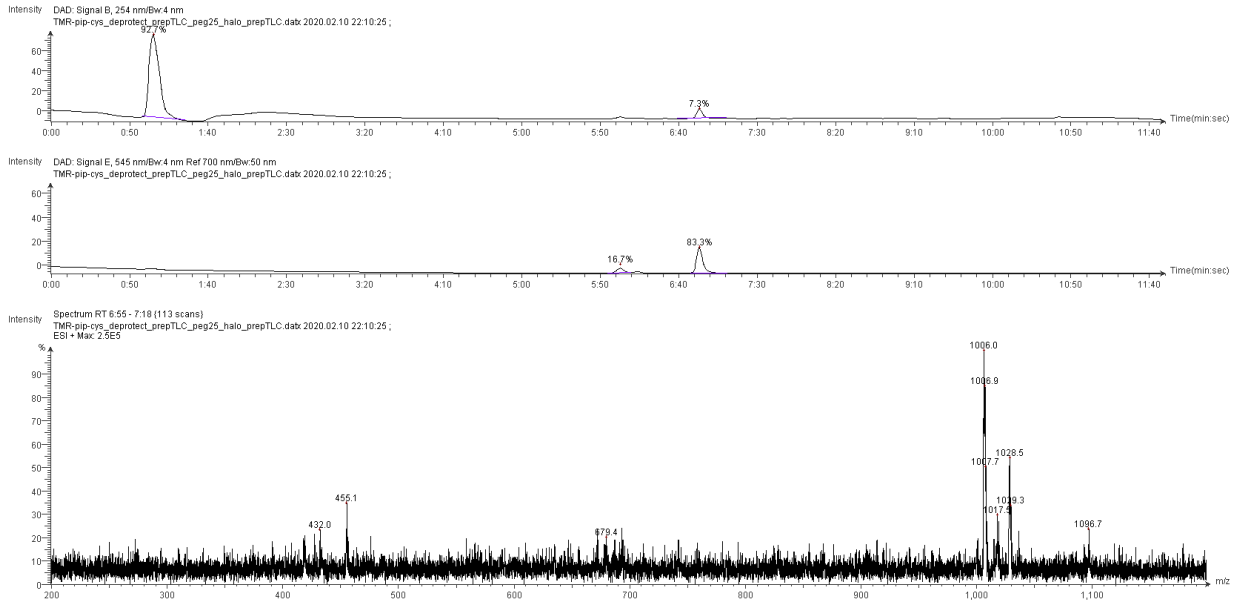

Low-resolution ESI(+) mass spectrum of **5**(TMR-piperazine-cysteic acid-PEG25-halo)

Calculated for $[M+H]^{2+}$, ^{35}Cl = 1006.5
Found: 1006.0

Calculated for $[M+H]2^{+}$, ^{13}C average = 1007.0
Found: 1006.9

Calculated for $[M + 2Na^{+} - H^{+}]^{2+}$, ^{35}Cl = 1028.5
Found: 1028.5

Calculated for $[M + 3Na^{+} - H^{+} + TFA-]^{2+}$, ^{35}Cl = 1096.5
Found: 1096.7

Figures, schemes and tables

Scheme 3-1. *A small molecule-protein hybrid for voltage imaging via quenching of bioluminescence*

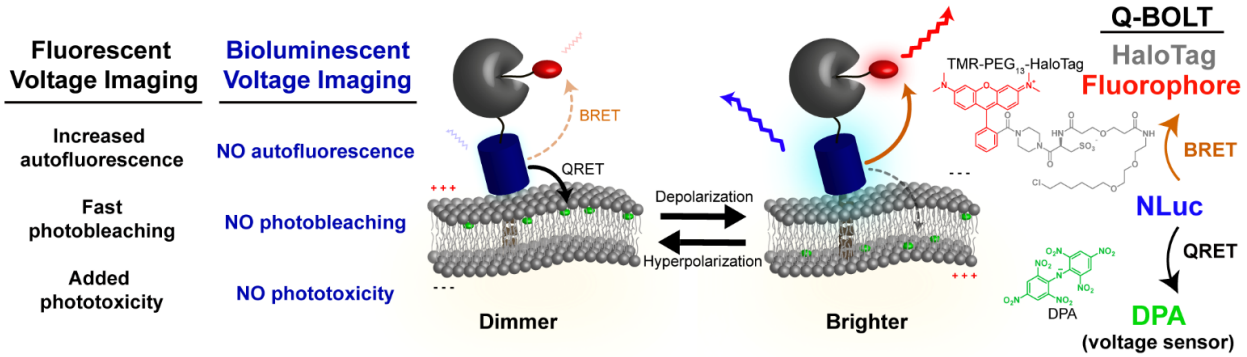

Scheme 3-1. *Proposed dual QRET/BRET voltage sensing mechanism.*

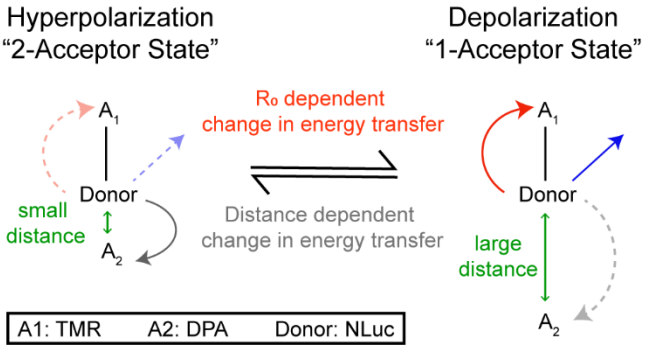

Figure 3-1. *Voltage dependent bioluminescent quenching in Q-BOLT*

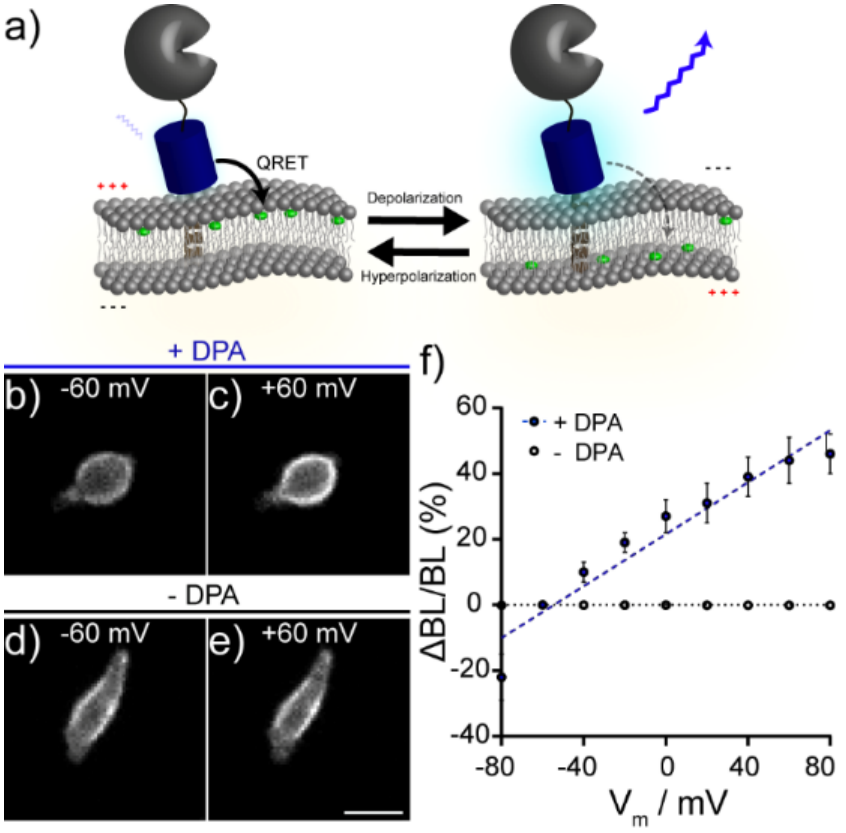

Figure 3-1. Voltage dependent bioluminescent quenching in Q-BOLT. a) QRET voltage sensing mechanism with NLuc close to the membrane. HaloTag (grey) is fused to the N-terminal of NLuc (blue) and anchored to the plasma membrane through a transmembrane domain (brown). At negative membrane potentials DPA (green) quenches luminescence. Depolarizations redistribute DPA closer to the inner leaflet, leading to a decrease in QRET, and an increase bioluminescence. **b)** and **c)** Bioluminescent images of voltage clamped HEK293T cells loaded with 250 nM DPA held at **b)** -60 mV and **c)** +60 mV. **d)** and **e)** Bioluminescent images of HEK 293T cells without DPA held at **d)** -60 mV and **c)** +60 mV. Scale bar is 20 µm. **f)** Plot of ΔBL/BL (%) versus holding membrane potential with DPA (blue, n = 10 cells, error bars are SEM, 500 nM DPA) and without DPA (black, n = 6 cells, error bars are SEM but not visible). Data for **b-f** were acquired with a 10 ms exposure time.

Figure 3-2. *Illustrations of HaloTag/NanoLuc constructs*

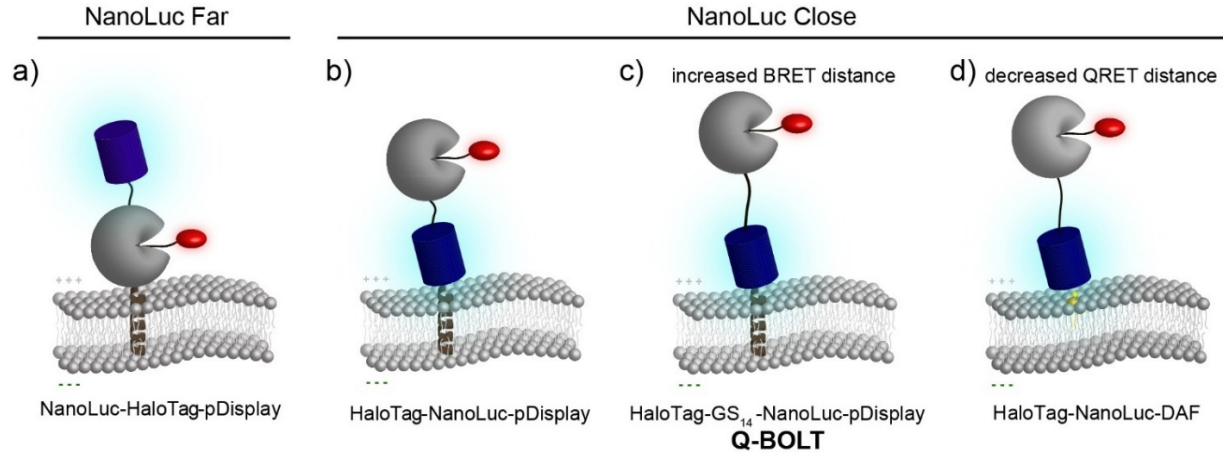

Figure 3-2. **Illustrations of HaloTag/NanoLuc constructs.** NLuc (blue) and HaloTag (grey) are abbreviated NL and HT, respectively. The fusion proteins are expressed on the extracellular leaflet and anchored to the plasma membrane by a single-pass transmembrane domain (pDisplay or pD, brown) or a DAF anchor (yellow). Starting from left to right, the first two constructs only vary in the orientation of NL and HT, one with **a)** NL far (left) and the other with **b)** NL close to the membrane (right). The third construct, or Q-BOLT **c)** maintains the orientation of NL close to the membrane but varies only in the linker length between the HT and NL proteins. The last construct **d)** maintains the orientation and longer linker length between NL and HT but is anchored to the membrane with a DAF-anchor.

Figure 3-3. *DPA quenches membrane bioluminescence*

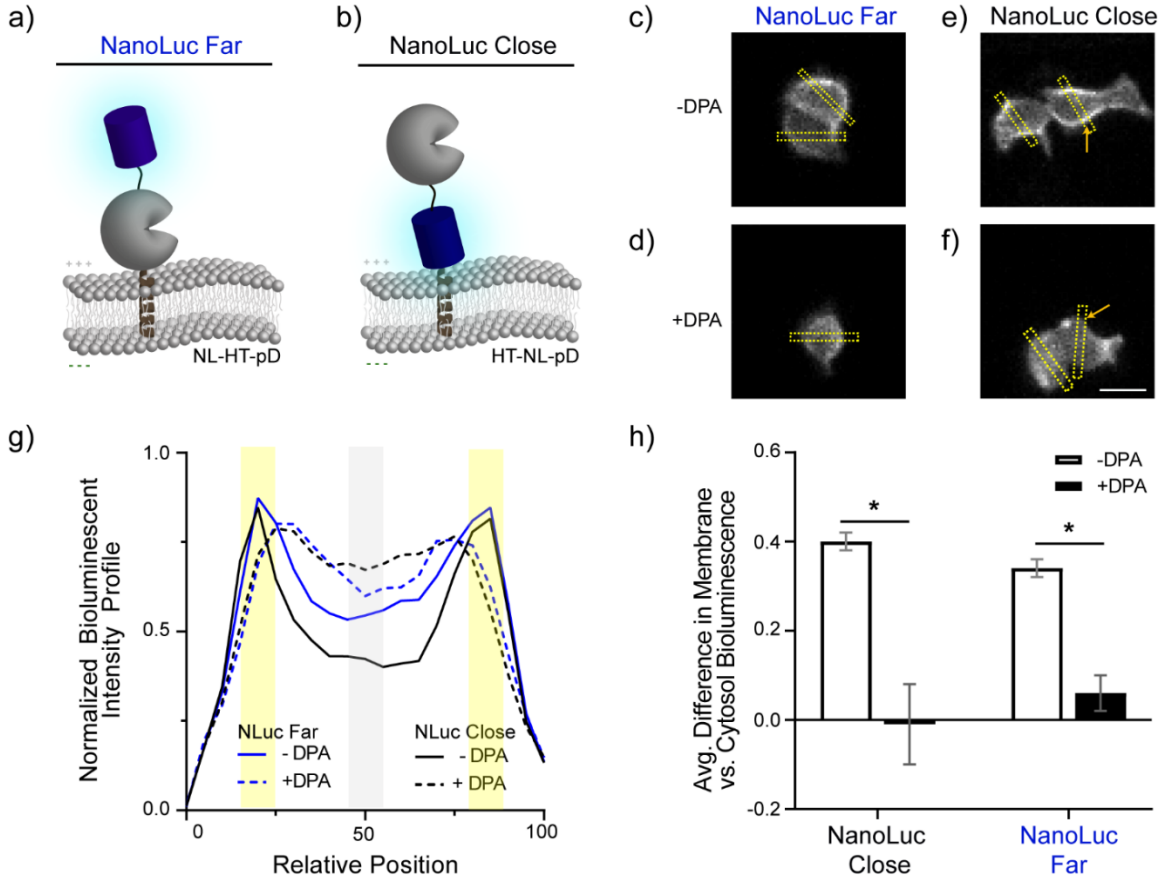

Figure 3-3. DPA quenches membrane bioluminescence. Scheme of bioluminescent constructs compared with the luciferase (blue) **a)** far **and b)** close to the membrane. The HaloTag protein (grey) is present in all constructs however a fluorescent ligand was omitted for these experiments. Bioluminescence images of HEK cells expressing NLuc Far constructs (panel a) **c)** without DPA and **d)** after the addition of 1 µM DPA or HEK cells expressing NLuc Close (panel b) **e)** without DPA and **f)** after addition of 1 µM DPA. Orange arrows highlight the decrease in membrane localized luminescence after DPA addition. Scale bar is equal to 20 µm. **g)** Average luminescence profile across HEK cells with (dashed) and without (solid) DPA with NL far (blue) and close (black) to the membrane. Rectangles in (c-f) are representative of areas used to obtain line profiles. **h)** Average difference between the edge and center (yellow and grey shaded regions in (g), respectively) normalized luminescence values. Without DPA (white) there is a large difference in the edge vs. center intensity indicating bright luminescence at the cell membrane. Addition of DPA (solid black) reduces this difference due to quenched bioluminescence at the membrane. The error bars represent the standard error of the mean (4-5 replicates per condition, n = 22-23 total cells per condition). Students t-test used to determine statistical significance, *$p<0.05$.

Figure 3-4. *Distance dependent bioluminescent voltage response to DPA quenching*

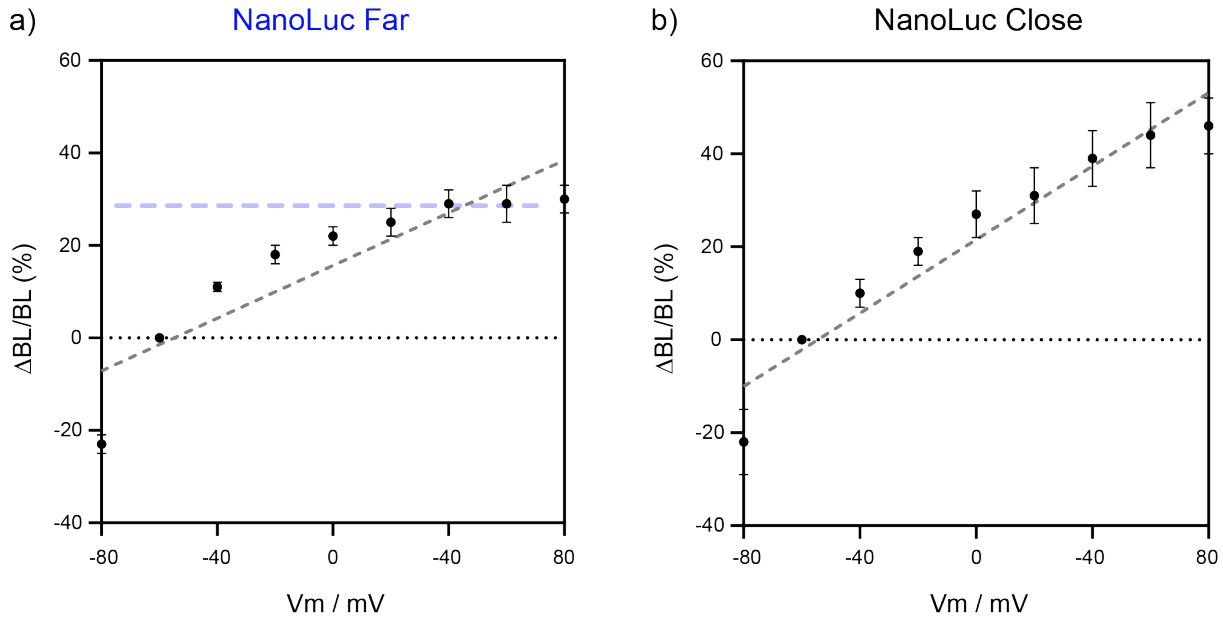

Figure 3-4. Distance dependent bioluminescent voltage response to DPA quenching. Fractional changes in bioluminescence of HEK cells expressing NLuc constructs under whole-cell voltage clamp. a) Average fractional change of bioluminescence as a function of holding potential for cells expressing NL far from the membrane. The blue dashed line highlights the plateau in intensity likely due to the lack of DPA molecules within an acceptable radius to appreciably quench bioluminescence. The voltage sensitivity is 29% ± 2% per 100 mV from the slope of the line (R^2 =0.80, n = 11 cells, error bars are SEM, 250 nM DPA). Data from Panel b) are reproduced from Figure 1b in the main text for comparison. Cells expressing NL close to the membrane have a voltage sensitivity of 39% ± 2% per 100 mV from the slope of the line (R^2 = 0.93, n = 9 cells, error bars are SEM, 250 nM DPA).

Figure 3-5. *Q-BOLT voltage response in HEK293T cells*

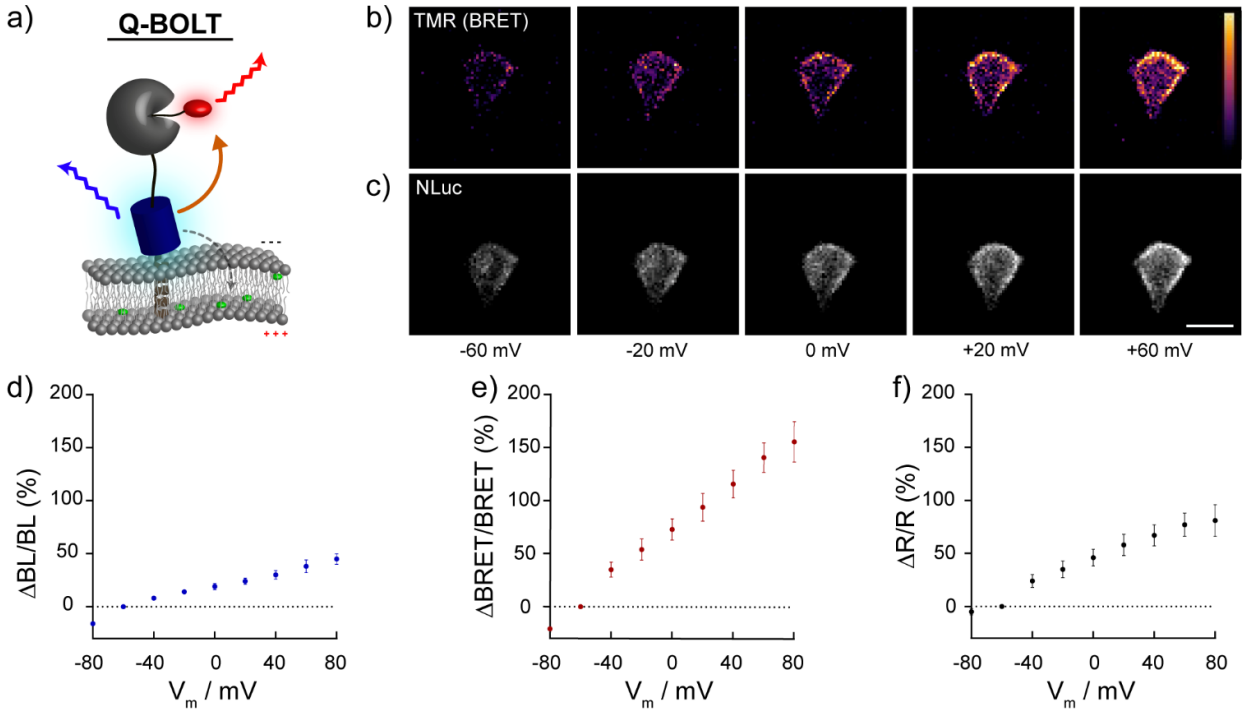

Figure 3-5. Q-BOLT voltage response in HEK293T cells. a) Schematic of Q-BOLT emission at positive membrane potentials. Color scheme is the same as Fig. 1 with the addition of TMR-PEG_{13}-HaloTag (red). **b)** Representative images of a voltage dependent BRET and **c)** bioluminescence emission from -60 mV to +60 mV. BRET and bioluminescent images are normalized to their respective -60 mV images. Scale bar is 20 µm. Exposure time is 10 ms. Percent changes in **d)** ΔBL/BL, **e**) ΔBRET/BRET, and **f)** the fractional change in BRET emission/NLuc bioluminescence ratio, ΔR/R, in HEK 293T cells with 500 nM DPA plotted against holding membrane potential under whole-cell voltage clamp for n = 10 cells, error bars represent SEM.

Figure 3-6. *Characterization of HaloTag-NLuc fusions at the cell membrane using different imaging techniques*

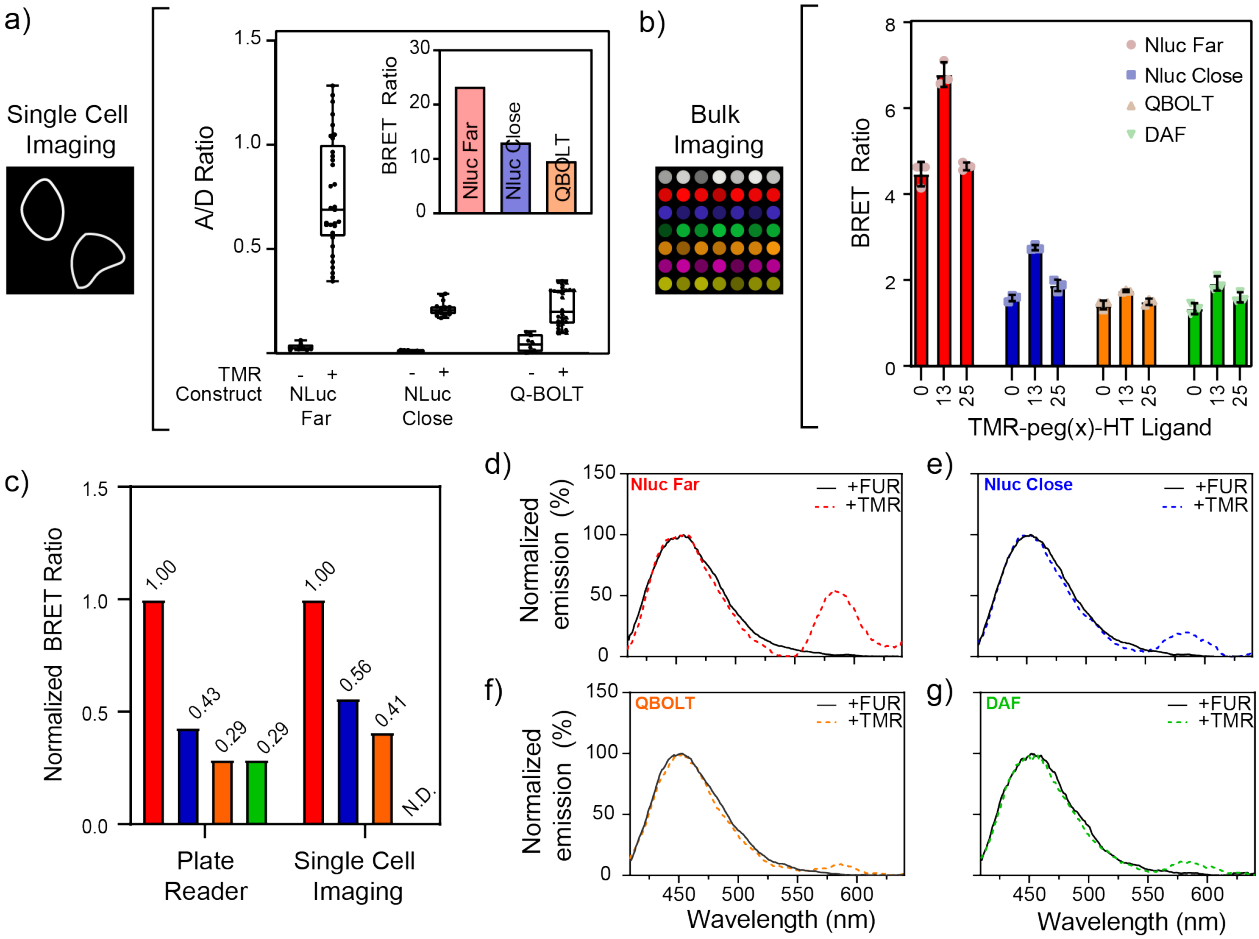

Figure 3-6. Characterization of HaloTag-NLuc fusions at the cell membrane using different imaging techniques. a) Single cell A/D ratios of TMR:NLuc emission at the membrane using epifluorescence microscopy in the presence and absence of 500 nM TMR-HaloTag for each DNA construct. The inset shows the BRET ratio determined by single cell microscopy, which is defined as the A/D ratio in the presence TMR divided by the A/D ratio in the absence of TMR. **b)** BRET ratios for varying PEG linker lengths using bulk imaging on a plate reader. BRET ratios were measured for PEG_0, PEG_{13}, and PEG_{25} across the same constructs used in **(a)**. **(c)** Side-by-side comparison of the average BRET ratios normalized to NLuc Far (red). The BRET ratio values across the two imaging techniques differ in (a) and (b). However, normalized values show the same trend regardless of a single cell or bulk imaging approach. **d-g)** Normalized emission spectra for **d)** NLuc Far, **e)** NLuc Close, **f)** Q-BOLT, and **g)** DAF DNA constructs without (black) and with (colored) TMR-PEG_{13}-HaloTag.

Figure 3-7. *Comparison of voltage sensitivities for all probes using 250 nM DPA.*

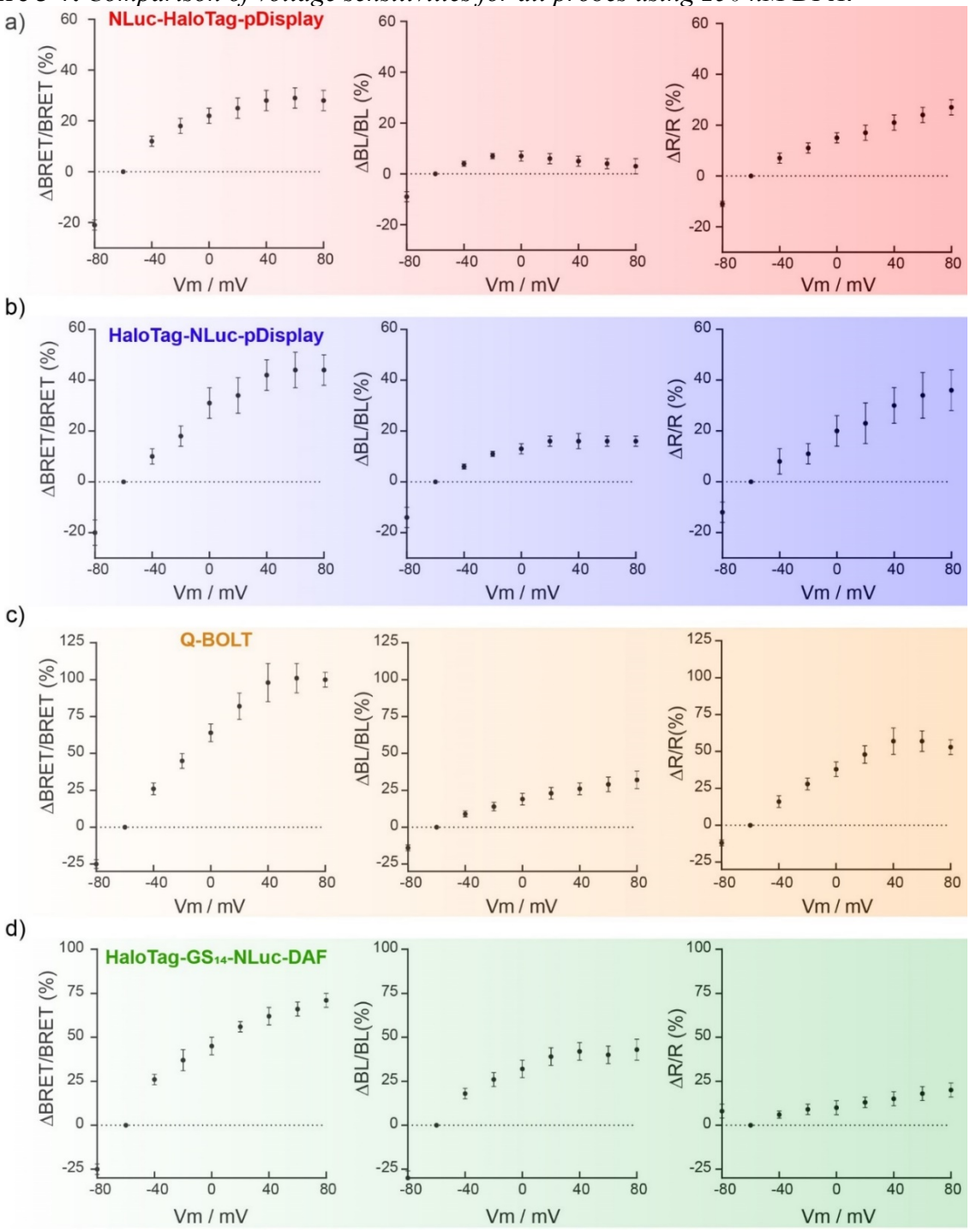

Figure 3-7. Comparison of voltage sensitivities for all probes using 250 nM DPA. Plot of voltage sensitive readouts for the change in BRET (left), bioluminescence (middle, BL), and ratio (right, R) for probes with **a)** NLuc-HaloTag-pDisplay (NLuc far), **b)** HaloTag-NLuc-pDisplay (NLuc close), **c)** Q-BOLT, and **d)** NLuc close with a DAF membrane anchor. Reference supplementary figure 1 for construct schemes. All HEK cells were labeled with 500 nM TMR-peg13-HT and voltage clamped after the addition of 2x furimazine and 250nM DPA. Note that %ΔBL/BL plots in (a) and (b) differ from supplemental figure 3 due to the presence of an additional acceptor

(TMR). The voltage response for QBOLT (S5.c) also plateaus, unlike Fig. 2, because of the lower DPA concentration (250 nM used in comparison of all constructs (this figure) vs 500 nM DPA used in the main figure).

Figure 3-8. *Evaluation of DPA and TMR interactions without bioluminescence.*

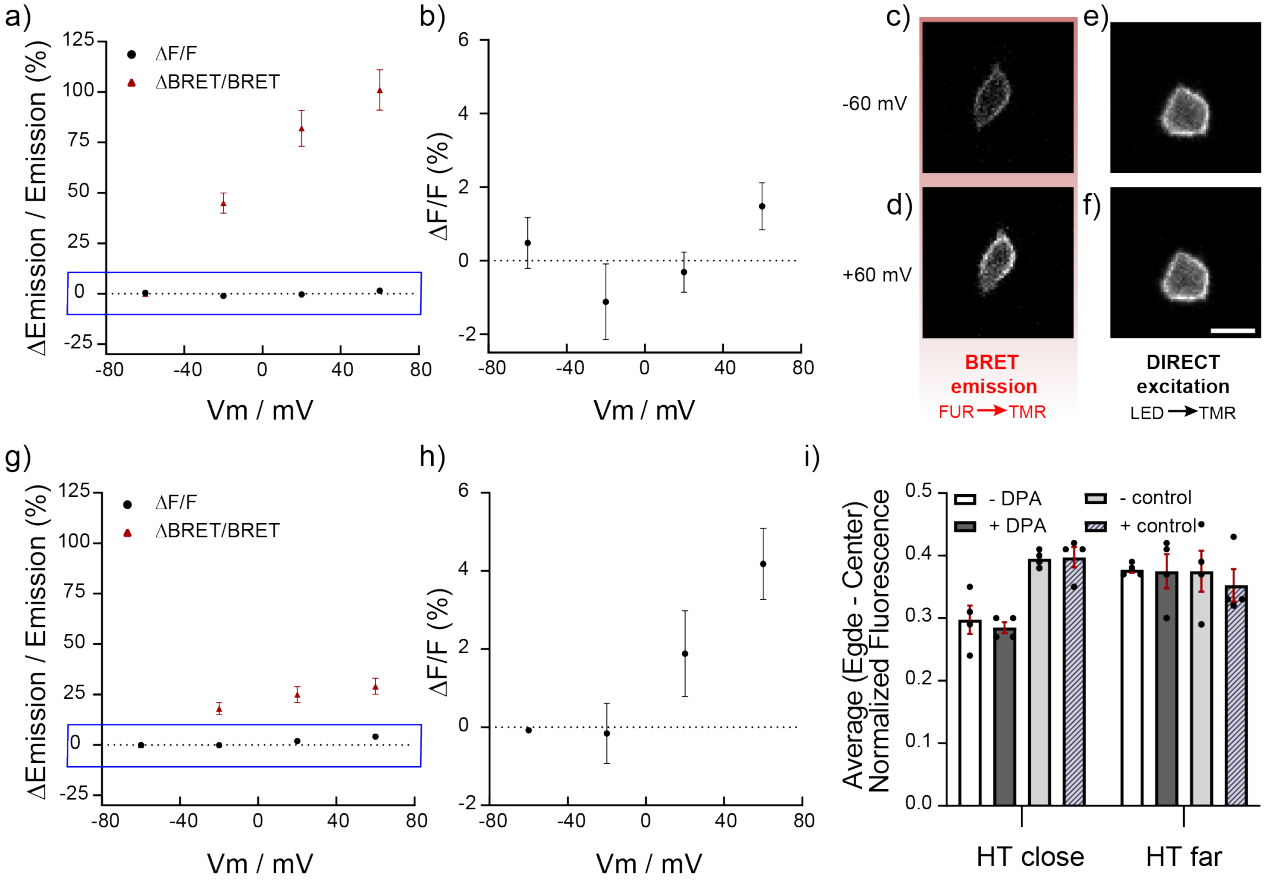

Figure 3-8. Evaluation of DPA and TMR interactions without bioluminescence. Plot of TMR fluorescence voltage sensitivity (black) compared the BRET response (red, same data in supplemental figure 5) for cells expressing **a)** HaloTag-NLuc-pDisplay (NLuc close) and **g)** NLuc-HaloTag-pDisplay (NLuc far). Panels **(b)** and **(h)** provide a closer look at the data points within the blue boxes of (a) and (g), respectively. **c-f)** Representative images of the change in emission seen with NLuc close upon a +120 mV step, scale bar is 20 μm. **c)** and **d)** BRET images, taken without LED excitation, show an increase in TMR emission with depolarization. However, **e)** and **f)** fluorescence images show no obvious change with fluorescence with increasing V_m. **i)** Results of line profile analysis (same analysis explained in supplemental figure 2c and 2d). Bars represent the average difference between the edge and center normalized luminescence values of cells expressing the constructs with HT close or far) from the membrane. No significant change in membrane fluorescence is seen after the addition of DPA (compare white and dark grey bars). As a control, no significant change in fluorescence is seen after the addition of only buffer (no DPA, compare light grey and striped bars). The error bars represent the standard error of the mean.

Figure 3-9. *Imaging membrane potential dynamics in human induced pluripotent stem cell-derived cardiomyocytes (hiPSC-CMs) with Q-BOLT.*

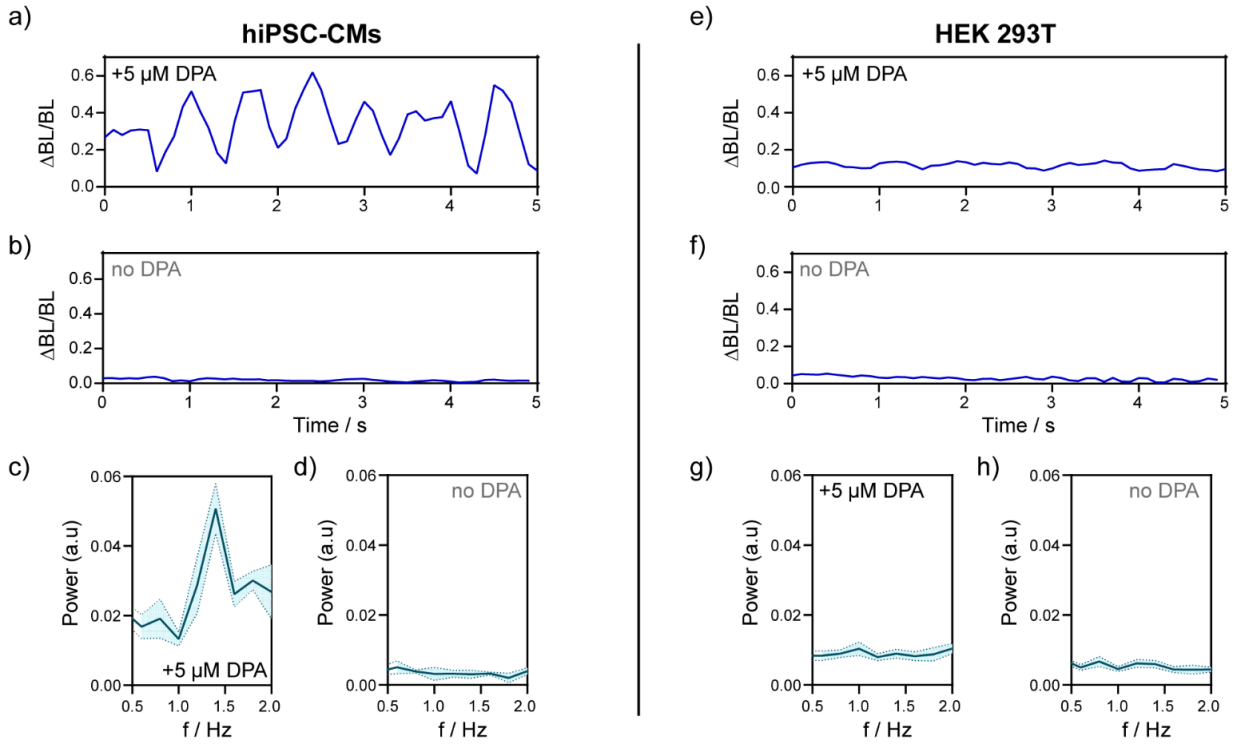

Figure 3-9. Imaging membrane potential dynamics in human induced pluripotent stem cell-derived cardiomyocytes (hiPSC-CMs) with Q-BOLT. Representative plots of bioluminescence (ΔBL/BL) vs. time in beating hiPSC-CMs expressing Q-BOLT and incubated with a) 5 µM DPA or b) no DPA. Optical sampling rate was 10 Hz. Power spectrum analysis/FFT of all data for hiPSC-CMs expressing Q-BOLT and treated c) with 5 µM DPA or d) without DPA. Data are mean ± S.E.M. (shaded region) for n = 6 independent experiments for DPA; 3 for no DPA. Representative plots bioluminescence (ΔBL/BL) vs. time in non-electrically excitable HEK 293T cells expressing Q-BOLT and incubated with either e) 5 µM DPA or f) no DPA. Optical sampling rate was 10 Hz. Power spectrum analysis/FFT (resolution 0.2 Hz) of all data for HEK 293T cells expressing Q-BOLT and treated g) with 5 µM DPA or h) without DPA. Data are mean ± S.E.M. (shaded region) for n = 18 independent experiments for DPA; 11 for no DPA.

Figure 3-10. *Bioluminescence bleed-through is minimal.*

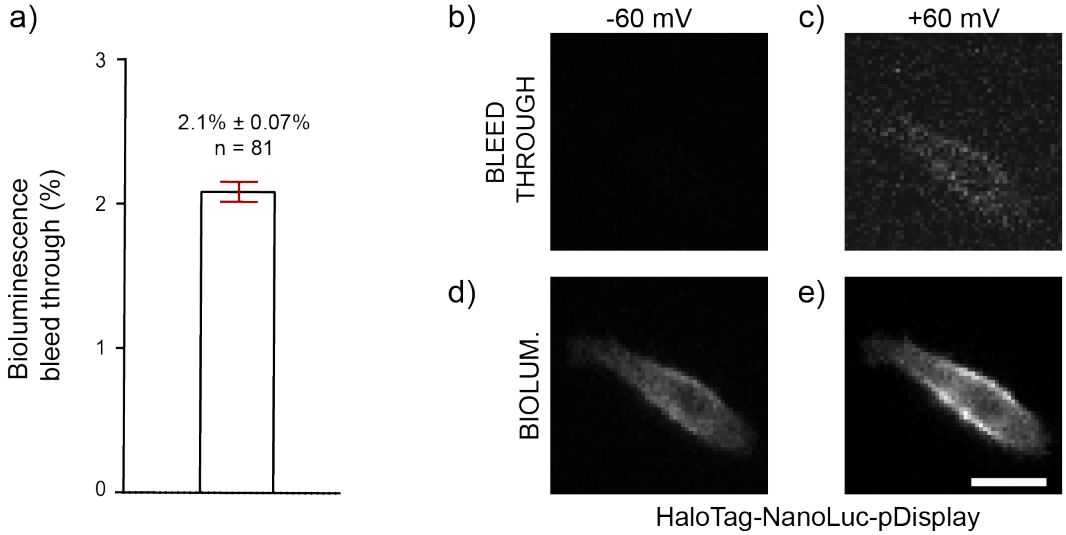

Figure 3-10. Bioluminescence bleed-through is minimal. Bar graph of the **a)** average bleed-through signal from NLuc bioluminescence into the TMR channel is 2.1 ± 0.07% (610/75 nm emission filter). Error bar is SEM, n = 81 cells. **b-e)** Normalized images of Q-BOLT expressing HEK cells using a dual view inverted epifluorescence microscope. Bioluminescence bleed-through at **b)** -60 mV and **c)** +60 mV using a 610/75 nm emission filter. **d-e)** Bioluminescence images of the same cell held at -60 and +60 mV, respectively, using a 460/30 emission filter. Scale bar is 20 μm.

Figure 3-11. *DPA toxicity in hiPSC-CMs*

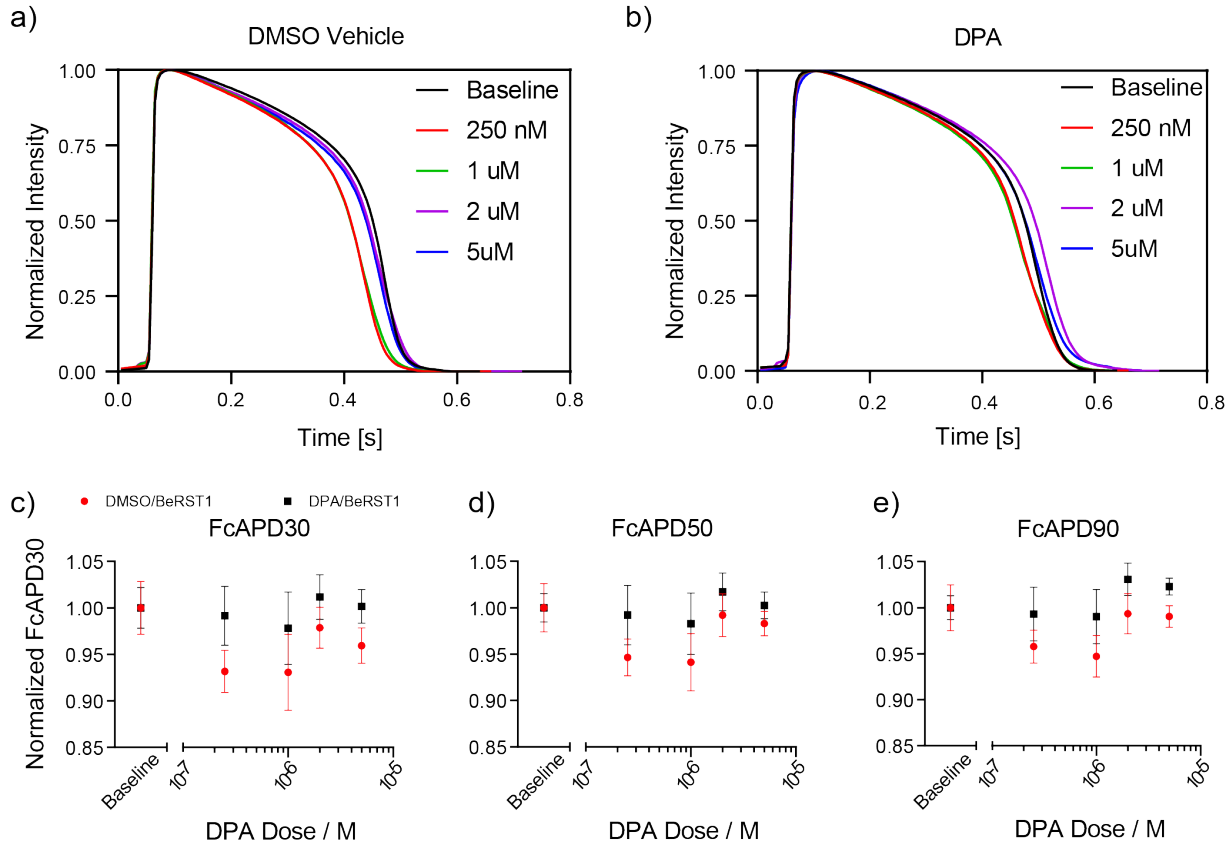

Figure 3-11. DPA toxicity in hiPSC-CMs. Plot of fluorescent voltage responses from BeRST during an in-well dose escalation experiment on iPSC-CMs testing 0 nM, 250 nM, 1 µM, 2 µM, and 5 µM **a)** DMSO vehicle control or **b)** DPA dosages. **c-e)** Plot of the Fridericia corrected action potential duration vs. dosage of DMSO or DPA for **(c)** FcAPD30, **(d)** FcAPD50, and **(e)** FcAPD90). Error bars are shown in standard deviation. No statistical difference between DMSO and DPA conditions were found using unpaired t-tests ($p > 0.1$ for all analyses).

Figure 3-12. *QBOLT voltage sensing and frequency analysis in hiPSC-CMs and HEK cells.*

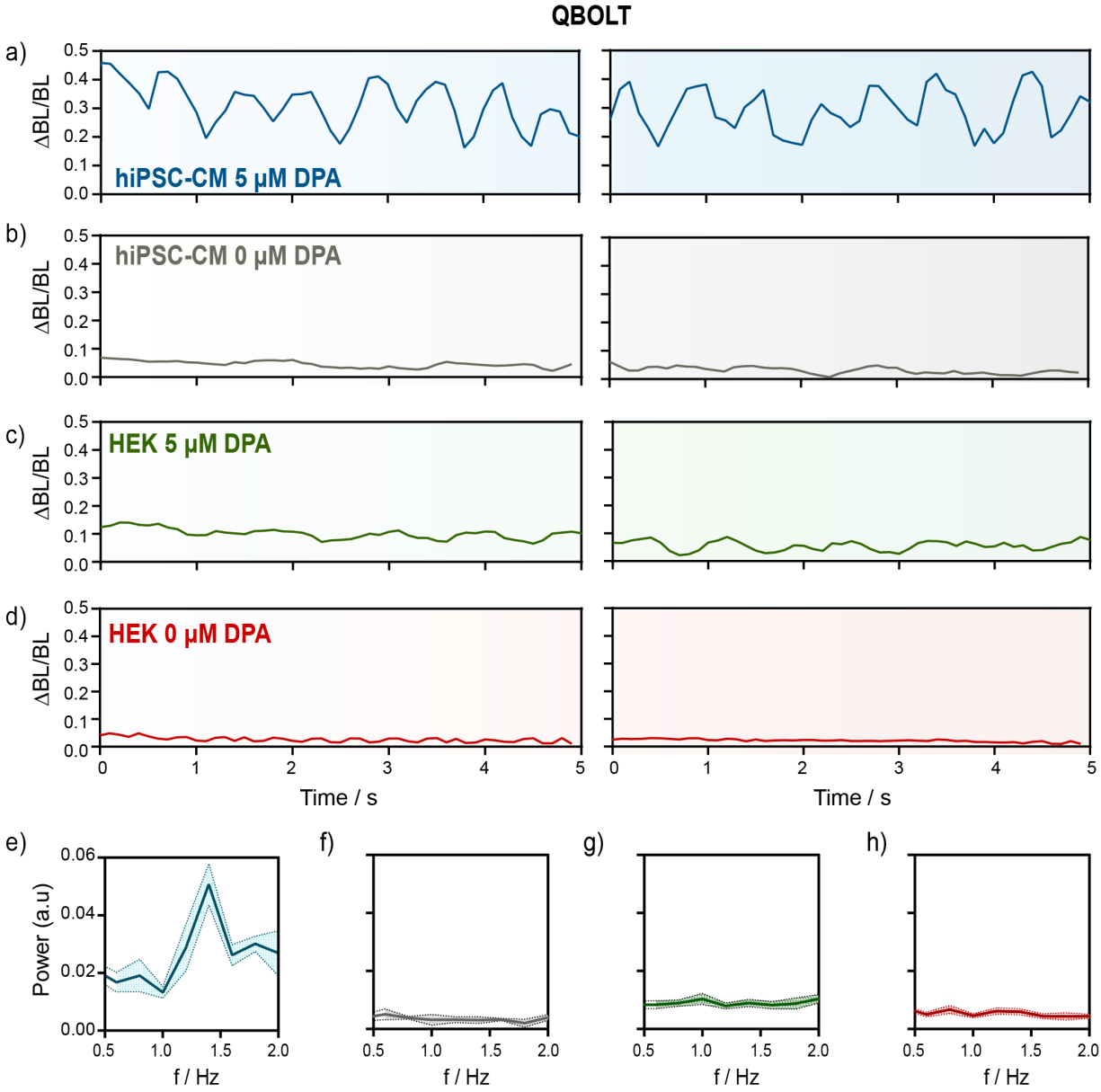

Figure 3-12. QBOLT voltage sensing and frequency analysis in hiPSC-CMs and HEK cells. Additional examples of the fractional change in bioluminescence emission from hiPSC-CMs with **a)** 5 µM DPA (blue) **b)** without DPA (grey), **c)** HEK cells with 5 µM DPA (green), and **d)** HEK cells without DPA (red). Each trace is a 5 second plate reader recording at 10 Hz taken from a single well in a 96-well plate. **e-h)** Fast Fourier transforms of the 4 conditions with the shaded regions representing SEM: **e)** hiPSC-CMs with 5 µM DPA (n = 6 wells), **f)** hiPSC-CMs without DPA (n = 3 wells), **g)** HEK cells with 5 µM DPA (n = 18 wells), and **h)** HEK cells without DPA (n = 11 wells).

Figure 3-13. *BeRST voltage sensing and frequency analysis in hiPSC-CMs and HEK cells.*

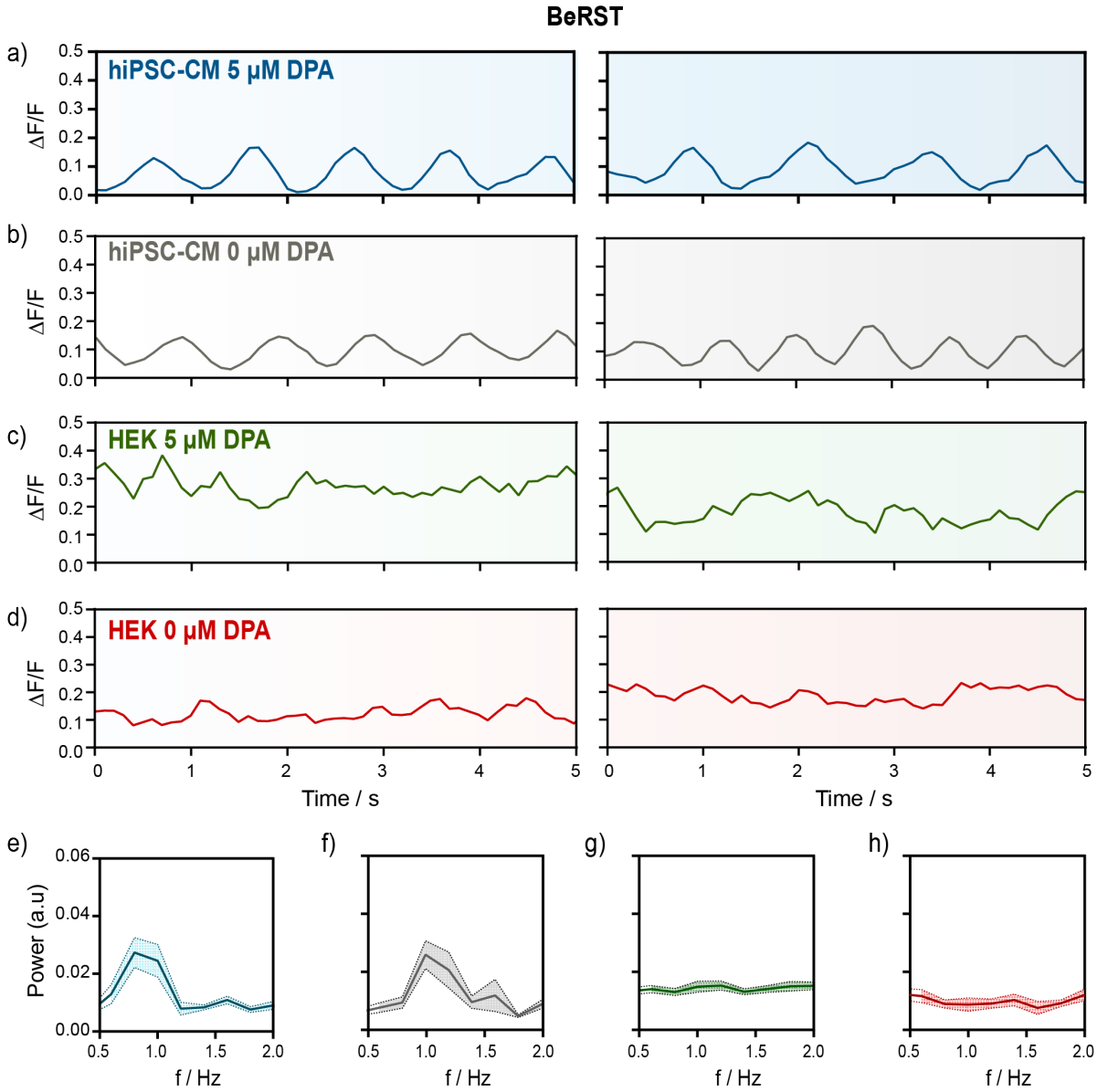

Figure 3-13. BeRST voltage sensing and frequency analysis in hiPSC-CMs and HEK cells. Fractional fluorescence change of BeRST in **a)** hiPSC-CMs with 5µM DPA (blue), **b)** hiPSC-CMs without DPA (grey), **c)** HEK cells with 5 µM DPA (green), and **d)** HEK cells without DPA (red). The voltage sensing mechanism of BeRST is independent of DPA. Each trace is a 5 second plate reader recording at 10 Hz taken from a single well in a 96-well plate**. e-h)** Fast Fourier transforms of the 4 conditions with the shaded regions representing SEM: **e)** hiPSC-CMs with 5 µM DPA (n = 13 wells), **f)** hiPSC-CMs without DPA (n = 8 wells), **g)** HEK cells with 5 µM DPA (n = 28 wells), and **h)** HEK cells without DPA (n = 8 wells).

Sensor Modifications	ΔBL/BL (-TMR)	ΔBL/BL (+ TMR)	ΔBRET/BRET	ΔR/R	BL‡ SNR	BRET‡ SNR	ΔF/F (direct excitation)	Sample Size (cells)
NLuc-HaloTag-pD	29% ± 2%	6% ± 2%	28% ± 3%	22% ± 2%	0.04**	0.2	3.7% ± 0.7%	19
HaloTag-GS_{14}-NLuc-pD (QBOLT)	39% ± 2%	28% ± 5%	91% ± 10%	48% ± 6%	0.4	1.3	1.2% ± 0.7%	14
HaloTag-GS_{14}-NLuc-pD (QBOLT)*	-	22% ± 3%	114% ± 10%	81% ± 7%	0.4	1.4	-	10
HaloTag-GS_4-NLuc-pD	-	17% ± 2%	41% ± 5%	32% ± 8%	0.6	0.3	-	10
HaloTag-GS_{14}-NLuc-DAF	-	40% ± 4%	56% ± 1%	13% ± 4%	0.7	1.1	-	6

Table 3-1. *Properties of Q-BOLT voltage indictors*

‡SNR is the difference between the signal at +40 mV and -60mV divided by the standard deviation of -60mV signals
**Ratio reported is the largest signal change occurring at -20mV due to deviation from linearity
*500nM DPA

References

1. Blackiston, D. J., McLaughlin, K. A. & Levin, M. Bioelectric controls of cell proliferation: ion channels, membrane voltage and the cell cycle. *Cell Cycle* **8**, 3519–3528 (2009).
2. Sundelacruz, S., Levin, M. & Kaplan, D. L. Role of membrane potential in the regulation of cell proliferation and differentiation. *Stem Cell Rev. Reports* **5**, 231–246 (2009).
3. Yang, M. & Brackenbury, W. J. Membrane potential and cancer progression. *Frontiers in Physiology* **4 JUL**, (2013).
4. Pérez-García, M. T., Cidad, P. & López-López, J. R. The secret life of ion channels: Kv1.3 potassium channels and proliferation. *Am. J. Physiol. Physiol.* **314**, C27–C42 (2018).
5. Pardo, L. A., Brüggemann, A., Camacho, J. & Stühmer, W. Cell cycle-related changes in the conducting properties of r-eag K+ channels. *J. Cell Biol.* **143**, 767–775 (1998).
6. Urrego, D. *et al.* Potassium channels in cell cycle and cell proliferation. *Phil. Trans. R. Soc. B 2014* 1–9 (2014). doi:10.1098/rstb.2013.0094
7. McCaig, C. D., Rajnicek, A. M., Song, B. & Zhao, M. Controlling cell behavior electrically: current views and future potential. *Physiol. Rev.* **85**, 943–978 (2005).
8. Saito, K. *et al.* Luminescent proteins for high-speed single-cell and whole-body imaging. *Nat. Commun.* **3**, (2012).
9. Wang, A., Feng, J., Li, Y. & Zou, P. Beyond Fluorescent Proteins: Hybrid and Bioluminescent Indicators for Imaging Neural Activities. *ACS Chem. Neurosci.* (2018). doi:10.1021/acschemneuro.7b00455
10. Contag, C. H. *et al.* Visualizing Gene Expression in Living Mammals Using a Bioluminescent Reporter. *Photochem. Photobiol.* **66**, 523–531 (1997).
11. Iwano, S. *et al.* Single-cell bioluminescence imaging of deep tissue in freely moving animals. *Science (80-.).* **359**, 935 LP – 939 (2018).
12. Suzuki, K. *et al.* Five colour variants of bright luminescent protein for real-time multicolour bioimaging. *Nat. Commun.* **7**, 13718 (2016).
13. Los, G. V *et al.* HaloTag: a novel protein labeling technology for cell imaging and protein analysis. *ACS Chem Biol* **3**, 373–382 (2008).
14. Dixon, A. S. *et al.* NanoLuc Complementation Reporter Optimized for Accurate Measurement of Protein Interactions in Cells. *ACS Chem. Biol.* **11**, 400–408 (2016).
15. Pellegatti, P., Falzoni, S., Pinton, P., Rizzuto, R. & Di Virgilio, F. A Novel Recombinant Plasma Membrane-targeted Luciferase Reveals a New Pathway for ATP Secretion. *Mol. Biol. Cell* **16**, 3659–3665 (2005).
16. French, A. R., Tesmer, A. L. & Tantama, M. Dual-Mode FRET and BRET Sensors for Detecting cAMP Dynamics. *ACS Omega* **4**, 15504–15511 (2019).
17. Inagaki, S. *et al.* Genetically encoded bioluminescent voltage indicator for multi-purpose use in wide range of bioimaging. *Sci. Rep.* **7**, 1–11 (2017).
18. Hall, M. P. *et al.* Engineered luciferase reporter from a deep sea shrimp utilizing a novel imidazopyrazinone substrate. *ACS Chem. Biol.* **7**, 1848–1857 (2012).
19. Fernandez, J. M., Taylor, R. E. & Bezanilla, F. Induced capacitance in the squid giant axon. Lipophilic ion displacement currents. *J. Gen. Physiol.* **82**, 331–346 (1983).
20. Fernández, J. M., Taylor, R. E. & Bezanilla, F. Induced capacitance in the squid giant axon. Lipophilic ion displacement currents. *J. Gen. Physiol.* **82**, 331–46 (1983).
21. Chanda, B. *et al.* A hybrid approach to measuring electrical activity in genetically specified neurons. *Nat. Neurosci.* **8**, 1619–1626 (2005).

22. Wang, D., Zhang, Z., Chanda, B. & Jackson, M. B. Improved probes for hybrid voltage sensor imaging. *Biophys. J.* **99**, 2355–2365 (2010).
23. Sjulson, L. & Miesenböck, G. Rational optimization and imaging in vivo of a genetically encoded optical voltage reporter. *J. Neurosci.* **28**, 5582–5593 (2008).
24. González, J. E. & Tsien, R. Y. Voltage sensing by fluorescence resonance energy transfer in single cells. *Biophys. J.* **69**, 1272–1280 (1995).
25. González, J. E. & Tsien, R. Y. Improved indicators of cell membrane potential that use fluorescence resonance energy transfer. *Chem. Biol.* **4**, 269–277 (1997).
26. Ma, Y., Bayguinov, P. O. & Jackson, M. B. Action Potential Dynamics in Fine Axons Probed with an Axonally Targeted Optical Voltage Sensor. *eneuro* **4**, (2017).
27. Ghitani, N., Bayguinov, P. O., Ma, Y. & Jackson, M. B. Single-trial imaging of spikes and synaptic potentials in single neurons in brain slices with genetically encoded hybrid voltage sensor. *J. Neurophysiol.* **113**, (2015).
28. Takai, A. *et al.* Expanded palette of Nano-lanterns for real-time multicolor luminescence imaging. *Proc. Natl. Acad. Sci.* **112**, 4352–4356 (2015).
29. Deal, P. E. *et al.* Covalently Tethered Rhodamine Voltage Reporters for High Speed Functional Imaging in Brain Tissue. *J. Am. Chem. Soc.* **142**, 614–622 (2020).
30. Machleidt, T. *et al.* NanoBRET-A Novel BRET Platform for the Analysis of Protein-Protein Interactions. *ACS Chem. Biol.* (2015). doi:10.1021/acschembio.5b00143
31. Lublin, D. M. & Atkinson, J. P. Decay-accelerating factor: biochemistry, molecular biology, and function. *Annu. Rev. Immunol.* **7**, 35–58 (1989).
32. Windisch, B., Bray, D. & Duke, T. Balls and chains - A mesoscopic approach to tethered protein domains. *Biophys. J.* **91**, 2383–2392 (2006).
33. Boggess, S. C. *et al.* New Molecular Scaffolds for Fluorescent Voltage Indicators. *ACS Chem. Biol.* **14**, 390–396 (2019).
34. Xiao-Xu, X. X. *et al.* Rapamycin and CHIR99021 coordinate robust cardiomyocyte differentiation from human pluripotent stem cells via reducing p53-dependent apoptosis. *J. Am. Heart Assoc.* **6**, (2017).
35. Mathur, A. *et al.* Human iPSC-based cardiac microphysiological system for drug screening applications. *Sci. Rep.* **5**, 1–7 (2015).
36. Huebsch, N. *et al.* Miniaturized iPS-Cell-Derived Cardiac Muscles for Physiologically Relevant Drug Response Analyses. *Sci. Rep.* **6**, 1–12 (2016).
37. Huang, Y. L., Walker, A. S. & Miller, E. W. A Photostable Silicon Rhodamine Platform for Optical Voltage Sensing. *J. Am. Chem. Soc.* **137**, 10767–10776 (2015).
38. Rohr, S. & Salzberg, B. M. Multiple site optical recording of transmembrane voltage (MSORTV) in patterned growth heart cell cultures: assessing electrical behavior, with microsecond resolution, on a cellular and subcellular scale. *Biophys. J.* **67**, 1301–1315 (1994).
39. Suzuki, K. *et al.* Uninterrupted monitoring of drug effects in human-induced pluripotent stem cell-derived cardiomyocytes with bioluminescence Ca2+ microscopy. *BMC Res. Notes* **11**, 1–6 (2018).
40. Hall, M. P. *et al.* Cell impermeable coelenterazine analogues. US 2018/0155350 A1 (2018).
41. Yan, P., Acker, C. D. & Loew, L. M. Tethered Bichromophoric Fluorophore Quencher Voltage Sensitive Dyes. *ACS Sensors* **3**, 2621–2628 (2018).

42. Villette, V. *et al.* Ultrafast Two-Photon Imaging of a High-Gain Voltage Indicator in Awake Behaving Mice. *Cell* **179**, 1590-1608.e23 (2019).
43. Grimm, J. B. *et al.* A general method to improve fluorophores for live-cell and single-molecule microscopy. *Nat. Methods* **12**, 244–250 (2015).

Chapter 4:
Investigation of Alternative Resonance Energy Transfer (RET) based Voltage Probes for Measuring Membrane Potential

Introduction

Our previously reported bioluminescence-based voltage indicator, Q-BOLT (Quenching Bioluminescent Voltage Sensor) senses membrane potential (V_m) changes using dual resonance energy transfer processes. Q-BOLT is a chemical-genetic hybrid indicator that contains an extracellular membrane targeted luciferase, NanoLuc (NLuc)[1], fused to the C-terminus of the self-labeling HaloTag protein. Briefly, when paired with a non-fluorescent voltage sensor, dipicrylamine (DPA), bioluminescence from the oxidation of the NanoLuc coelenterazine-based substrate, furimazine, is quenched. While similar in principle to Förster resonance energy transfer (FRET), this energy transfer prosses is classified more specifically as quenching resonance energy transfer (QRET). DPA is a lipophilic, anionic small molecule that redistributes within the membrane leaflets in V_m dependent manner. Upon depolarization DPA molecules redistribute towards the inner leaflet of the plasma membrane, thereby reducing QRET in a distance dependent fashion. The addition of a fluorescent HaloTag ligand incorporates a second energy acceptor, which allows bioluminescence resonance energy transfer (BRET) and QRET to occur simultaneously. In this mode, Q-BOLT can provide direct visualization of changes in membrane potential via three distinct readouts: change in QRET, BRET, and the ratio between bioluminescence emission and BRET. Q-BOLT can provide up to a 29% change in bioluminescence (ΔBL/BL) and >100% ΔBRET/BRET per 100 mV change in HEK 293T cells, without the need for excitation light[2].

Q-BOLT laid the foundation in demonstrating bioluminescence quenching can be sensitive to membrane voltage changes. It was reasoned that if DPA could quench bioluminescence in a voltage dependent manner, then so too could alternative synthetic molecules or proteins. When used in thicker tissue samples, one drawback to using DPA is the extremely large concentrations (2-10 μM) needed to achieve a reliable optical signal which can contribute to added membrane capacitance[3–5]. This added capacitance could perturb true physiological electrical events and confound data interpretation, regardless of bioluminescent or fluorescent based approaches. To investigate the limits of functional bioluminescence imaging and eliminate the use of DPA in Q-BOLT, we wanted to explore alternative approaches to designing and creating bioluminescent voltage indicators.

Here we describe two independent approaches which replace the voltage sensor, DPA, of Q-BOLT with either a VoltageFluor (VF) or a protein-based genetically encoded voltage indicator (GEVI). In the system most similar to Q-BOLT, we aimed to simplify the voltage sensing mechanism by replacing the TMR-HaloTag/DPA pair with previously reported RhoVR-HaloTag VoltageFluors (VFs, Scheme 4-1)[6,7]. VFs utilize an intramolecular photo-induced electron transfer mechanism (PeT) to sense changes in V_m. For this reason, we expect replacement of DPA with VFs would resemble a similar dual QRET/BRET sensing mechanism, however the voltage sensitive quenching would be faster and reduce capacitance given voltage sensing in VF dyes does not rely on slow molecular diffusion, but rather on fast electron transfer. This chemical-genetic hybrid probe would also simplify the number of components in the system from 3 to 2 (protein + TMR + DPA versus protein + VF), by eliminating the need for exogenously added DPA.

In a completely alternative approach to voltage imaging using bioluminescence, we also turned to the voltage-sensitive rhodopsin based GEVIs Positron and Voltron[8,9] (**Scheme 4-3a**). We made four bioluminescent variations of these GEVIs by either replacing the HaloTag protein with NanoLuc or by adding NanoLuc onto the C-terminus (**Scheme 4-3b** and **c**). The voltage sensing mechanism of Positron and Voltron is the same: The absorbance spectrum of the central chromophore within the Ace2N rhodopsin domain is dependent on transmembrane voltage

changes[10–12]. The changes in absorption in turn modulate fluorescence quenching (FRET, or more specifically QRET) of the nearby covalently bound HaloTag dye (JF_{525}) in a voltage-dependent fashion. The only difference between Positron and Voltron is the positive or negative going FRET response to a depolarization event, where Voltron is considered a 'turn-off' sensor and Positron a 'turn-on' sensor. For a cell at rest, the Voltron absorption spectrum is low, resulting in little FRET and bright fluorescence. Upon depolarization the rhodopsin absorbance increases, increasing FRET and quenching dye fluorescence. The exact opposite is true for Positron.

Results

I. BRET-VFs

Energy transfer between NanoLuc and untethered RhoVR VFs

We wondered if resonance energy transfer would be sufficient to detect membrane potential changes using the NanoLuc (NLuc) luciferase donor and an untethered-VF accepter. We hypothesized with no affinity between the A/D pair the presumably long distances (>10 nm) and unrestricted orientations between the two would limit the BRET signal. We found HEK293T cells expressing extracellular NLuc (NLuc-EGFR, Promega) and labeled with 0-10 μM RhoVR1 (**Scheme 4-2**, compound **7**) show membrane localized bioluminescence but minimal BRET (**Fig. 4-1a-d**). Initial efforts were confounded by bleed-through of bioluminescence signal into the BRET emission channel at longer wavelengths (**Fig. 4-1a)**. Plotting the photon count in the long wavelength channel (where we would expect a BRET signal) relative to the bioluminescence emission shows no statistical difference between the BRET emission data collected using 0-10 μM dye, even though there looks to be an increase in BRET at 10 μM VF (**Fig. 4-1b**). As an additional control we also expressed NLuc on the intracellular side of the membrane (EGFR-NLuc, Promega). We hypothesized the distance between the luciferase and VF would be too large and would therefore show no difference in the BRET emission with or without RhoVR. We found the photon emission collected in the long wavelength channel (BRET emission) remains constant between cells loaded with 0 μM or 10 μM RhoVR (**Fig. 4-1c**). Taken together, it seemed possible RhoVRs could act as BRET acceptors but not without closer proximity to NLuc.

Energy transfer between NanoLuc and HaloTag tethered RhoVRs

To bring the acceptor fluorophore closer to NLuc, we redesigned the luciferase construct to include the self-labeling HaloTag (HT) protein and replaced EGFR with a simpler, single pass alpha helical transmembrane domain, pDisplay (**Fig. 4-2a**). The HT/NLuc construct is the same as previously reported in Chapter 3[2]. Covalently tethered HT-RhoVRs were previously optimized and showed reduced voltage sensitivity and lower signal to noise (SNR) ratios with shorter polyethylene glycol linker lengths[7]. In brief, it was hypothesized that longer linker lengths (>10 PEG units) ensured complete VF insertion into the membrane as well as proper orientation. Shorter PEG linkers may prevent the entire phenylenevinylene wire from inserting into the membrane and/or restrict the VF from inserting perpendicular to the membrane and sensing electric field changes. Both factors would explain the suboptimal voltage-sensing properties. For this reason, we hypothesized the orientation of the HT and NLuc proteins would have a similar influence. More specifically, we opted to use a construct with the HT protein closer to the membrane, and NLuc fused to its N-terminal, to promote proper insertion of the VF dye.

After transient transfection, HEK293T cells were treated with 0.5 μM HaloTag ligands **1-6** (**Scheme 4-2**). The ligands vary in wire structure and polyethylene glycol linker lengths between the VF and chloroalkane HT ligand. We hypothesized that while the shortest PEG_5 linker would

have reduced voltage sensitivity relative to PEG_{25}, the shorter linker may improve the BRET efficiency by reducing the distance between the fluorescent dye head and NLuc. Cells loaded with compounds **1-4**, with PEG_{13} and PEG_{25} linkers, show very minimal BRET ratios – or ratio of BRET emission (acceptor, A) to bioluminescence emission (donor, D) – ranging from 0.039 to 0.065; however, these ratios are statistically significant relative to control groups labeled with untethered RhoVR1 (**7**) or no VF (**Fig. 4-2b;** 0.020 and 0.017, respectively). A modest increase in the BRET ratio is seen with compound **6**, likely due to the shorter PEG_5 linker (**Fig. 4-2b,** 0.089). We reasoned low BRET ratios in cells labeled with RhoVR-HT ligands is reasonable given the increased rate of PeT in cell at rest. In contrast, the BRET ratio is an order of magnitude larger (0.64) with the tetramethyl rhodamine (TMR) HT ligand in which there is no additional quenching from PeT (**Fig. 4-2b-i**). Increasing the concentration of TMR-PEG_{13}-HT to 1.5 μM did not improve the BRET ratio (**Fig. 4-2c**), suggesting 0.5 μM of dye was enough to saturate surface expressed HT and would likely not improve the BRET ratio of RhoVR-HT ligands. Even with relatively low ratios, the 10-fold difference in BRET ratios between RhoVR1-PEG_{13}-HT (~0.06 BRET ratio) and TMR-PEG_{13}-HT (0.59) provides a rough estimate of the maximum dynamic range we might expect in comparing BRET ratios of depolarized and hyperpolarized cells using RhoVR1 (where the rate of PeT would be greatly reduced in the former state, and might more closely resemble TMR, which is not quenched by a molecular wire).

Measuring changes in membrane potential with HaloTag tethered VFs

At hyperpolarized, or more negative, membrane potentials the rate of PeT in VF indicators is predicted to be much greater than at depolarized potentials. This voltage sensing mechanism ultimately results in a fluorescence turn-on response to depolarizing events. The voltage sensitive response of an indicator is typically reported as a fractional change in the fluorescence relative to the initial intensity of at rest, or at -60 mV. Similarly, we expect the change in the BRET emission from the VF to increase with the only difference being the excitation source (directed LED vs. luciferase). However, using whole-cell electrophysiology in tandem with optical measurements in HEK293T cells labeled with 0.5 μM compound (**1**) and (**6**), with the respective longest and shortest PEG linkers, we did not see a significant voltage response (**Fig. 4-3**). Indicators (**1**) and (**6**) report a fractional change in the BRET ratio (%Δ R/R) of 0% per 100 mV (**Fig. 4-3a)**. Similarly, the BRET and bioluminescence emissions from RhoVR1 and NLuc, respectively, do not show a linear change correlated with voltage steps (**Fig. 4-3b** and **c**).

Discussion and future directions

We speculate one reason for the lack of voltage sensitivity and poor BRET ratios is due to the large rate of PeT, and therefore quenching of the VFs even at depolarized potentials. The rate of PeT can be synthetically fine-tuned, to some degree, by changing the electron donating group of the VF. Reducing the initial PeT rate may improve BRET efficiency, however it would reduce the baseline voltage sensitive response of the VF. While there did not appear to be a large difference in the BRET ratio between the two wire types we tried here, a larger screen of VFs could potentially improve the system but would be challenging to systematically predict at this point. Another reason that BRET ratios are low for RhoVR-PEG-Halo compounds is because of the low brightness and presence of molecular wire. TMR-PEG_{13}-Halo (**5**) shows a reasonable BRET ratio (~0.6, Figure 4-2b), while the RhoVR-PEG_{13}-Halo **3** or **4** both show rather low BRET ratios (<0.1). The only difference between **5** and **3** or **4** is the presence of the molecular wire. This decreases the quantum yield and brightness of **3** and **4** relative to **5**. The hydrophobic molecular

wire may also put **3** and **4** in a different orientation compared to **5** – this orientation may have a low BRET efficiency with NanoLuc.

A potentially easier and more fruitful approach in optimizing BRET efficiency, without altering the voltage sensing VF, could be done from a biological standpoint through protein orientation. By bringing the NLuc and HT proteins in a 'side-by-side' orientation rather than one top of the other, the efficiency of energy transfer will most likely improve based on distance and orientation. Alternatively, using a single HT-NLuc chimera (rather than fusing two proteins through a flexible glycine-serine linker) may further improve the efficiency and reduce noise by reducing the flexibility and 'floppiness' between the A/D pair[13]. This approach, however, could make VF targeting and labeling difficult depending on the HaloTag active site.

A third, unexplored alternative to this system would be to eliminate HaloTag and utilize a split luciferase system, NanoBit[14]. NanoBit consists of a split luciferase enzyme divided into an inactive large bit (17.6 kD) and small peptide (HiBiT, 1.3 kDa).[7] RhoVR could be synthetically coupled to the optimized HiBiT peptide and added to cells expressing the inactive large bit. The enzyme only oxidizes furimazine when the two pieces reconstitute the full enzyme. This method has the added benefit of reducing internal, non-functional bioluminescence given the cell impermeable nature of VFs. The NanoBit system may also increase the BRET signal due to increased proximity and restricted orientation of the A/D pair. As with the previous approaches suggested, the BRET efficiency may be the easiest aspect to improve upon, however improving the efficiency does not guarantee an improvement to voltage sensitivity.

II. Bioluminescent Voltage Sensing Proteins

Design of bioluminescence-based Positron and Voltron fusions

Positron and Voltron GEVIs were designed with the Ace2 rhodopsin from *Acetabularia acetabulum* with the HaloTag protein fused at the C-terminus which enables covalent labeling of bright small-molecule fluorophores[8,9]. The two GEVIs function similarly by utilizing an electrochromic FRET (eFRET) voltage sensing mechanism based on the protonation state of the retinal Schiff base which modifies the rhodopsin absorbance spectra. Voltron exhibits a turn-off response, becoming dimmer at depolarized membrane potentials because of an increase in the rhodopsin absorbance, and therefore an increase fluorescence quenching. Alternatively, Positron is a turn-on sensor where the rhodopsin absorbance is high at resting membrane potentials and decreases at depolarized potentials, resulting in an increase in fluorophore emission. We reasoned the same concept could apply using bioluminescence based on our knowledge that bioluminescence could be quenched by an appropriate acceptor. We designed two constructs replacing HaloTag at the C-termini of Ace2N of Positron and Voltron with NanoLuc (**P01** and **V01**; **Scheme 4-3b**). We also wondered if bioluminescence resonance energy transfer (BRET) could act as an alternative excitation source to direct illumination of the HaloTag fluorophore and created two more constructs with NanoLuc fused to the C-terminal of the Positron and Voltron GEVIs, immediately after the HaloTag protein (**P02** and **V02; Scheme 4-3c**). Therefore, Positron and Voltron constructs P01 and V01 possess Ace2N-NanoLuc, while P02 and V02 are composed of Ace2N-HaloTag-NanoLuc.

All protein fusions successfully expressed in HEK293T cells based on bioluminescence emission (**Fig. 4-4a** and **c**), however P01 and V01 constructs appear to have poor membrane localization (data not shown). Additionally, after spending more time optimizing functional bioluminescent imaging in general, we reasoned bioluminescence emission changes alone would be challenging to interpret. Luminescence emission fluctuations could be misinterpreted or

misleading while troubleshooting voltage sensitivity. The absence of a fluorescent signal in P01 and V01 made it challenging to identify and image transfected cells, so for this reason preliminary investigations were carried out using primarily P02 and V02.

The addition of furimazine resulted in bioluminescence signal predominantly localized to the plasma membrane with minor cytosolic signal for both V02 and P02(**Fig. 4-4a-d**). Membrane localized BRET signal was seen for both constructs after the addition of a cell permeable JF-525 HaloTag ligand (JF 525, **Fig. 4-4b** and **d**). These data suggest the addition of NanoLuc to Positron and Voltron did not prohibit HaloTag or NanoLuc enzymatic activities. An emission scan of cells expressing P02 or V02 show two emission peaks with maxima at 460 nm and 550 nm corresponding to the NanoLuc luminescence and JF525 BRET emission, respectively (**Fig. 4-4e)**. In agreement with literature[8,9], bioluminescence and BRET emissions are larger in V02 transfected cells (**Fig. 4-4a-d**), suggesting a lower rhodopsin absorbance at rest with the turn-off Voltron-based probe relative to the turn-on Positron-based probe. Similarly, the V02 BRET ratio is slightly larger than P02 when assessed using either live single cell imaging (0.55 for V02 and 0.46 for P02) or bulk plate reader measurements (0.57 for V02 and 0.50 for P02; **Fig. 4-4f-h**). While this is less intuitive, the larger ratio in V02 further supports a larger resting rhodopsin absorbance in the Positron-based construct based on our investigations into the mechanisms of a two-acceptor state, where quenching of bioluminescence may influence the resonance energy transfer in a non-distance or orientation dependent manner. Given the similar but inverse voltage sensitivities of Positron and Voltron, we estimate a fractional change in the ratio could be as much as 15-20% $\Delta R/R$ per 100 mV (**Fig. 4-4f**) assuming V02 is the max turn-on ratio and P02 is the starting ratio for cells at rest.

Voltage sensitivity of bioluminescent Positron/Voltron 2-acceptor fusions

Prior to characterizing the voltage response of P02 and V02 using bioluminescence, we wanted to verify the addition of NanoLuc to the C-terminal of HaloTag did not inhibit the fluorescent voltage sensitive response using JF_{525} alone. Using dual optical patch-clamp electrophysiology, HEK cells expressing P02 or V02 show fluorescent voltage responses, $\Delta F/F$, similar but opposite in magnitude (**Fig. 4-5a**; 8.3% ± 0.8% and -10.3% ± 0.6% per 100 mV, respectively). The P02 voltage sensor also retains the same voltage sensitivity of the original Positron sensor under identical conditions (**Fig. 4-5b**; Positron $\Delta F/F$ = 10% ± 0.3% per 100 mV, Šídák's multiple comparisons test, $p > 0.05$). Comparison of Voltron the V02 has not yet been completed given limited time and resources during the COVID-19 pandemic and shutdown, however Positron and Voltron are reported to have similar but opposite voltage responses, similar to results seen with P02 and V02[8].

Preliminary electrophysiology studies of P02 using bioluminescence excitation, rather than LED illumination, are promising but need further investigation and optimization (**Fig. 4-6**). A single cell held from -60 mV to + 60 mV shows a decrease in the bioluminescence (**Fig 4-6a**; $\Delta BL/BL$ = -6.9%), a decrease in the BRET signal (**Fig 4-6b**; $\Delta BRET/BRET$ = -3.3%), and an increase in the ratio (**Fig 4-6c**; $\Delta R/R$ = 4%). Further studies are still underway, but we expect to see an opposite response in bioluminescence, BRET and the ratio using V02. For future improvements we also aim to swap the NanoLuc and HaloTag domains of these constructs. This orientation would place the single donor (NanoLuc) in between two spectrally distinct acceptors (rhodopsin and HaloTag domains) and more closely resemble the mechanism in Q-BOLT[2].

Experimental Methods

Cell Culture

HEK293T cell lines were obtained from the UC Berkeley Cell Culture Facility and discarded after 25 passages. Cells were dissociated during passages using 0.05% Trypsin-EDTA with phenol red (Thermo Fisher Scientific) at 37°C, and then maintained in Dulbecco's Modified Eagle Medium (DMEM) with 4.5 g/L D-glucose supplemented with 10% FBS (Seradigm (VWR); Radnor, PA) and 2 mM 668 GlutaMAX (Gibco) in a 5% CO2 incubator at 37°C.

For all imaging experiments, cells were plated onto 25 mm diameter #1.5 glass coverslips (Electron Microscopy Sciences) in 6 well tissue culture plates (Corning; Corning, NY). To maximize cell attachment, coverslips were treated before use with 1-2 M HCl for 2-5 hours and washed overnight three times with 100% ethanol and three times with deionized water. Coverslips were sterilized by heating to 150°C for 2-3 hours. Before use, coverslips were incubated with poly-D-lysine (Sigma-Aldrich, made as a 0.1 mg/mL solution in phosphate-buffered saline with 10 mM Na_3BO_3) for 2-10 hours at 37°C and then washed twice with water and twice with Dulbecco's phosphate buffered saline (dPBS, Gibco). HEK293T cells were seeded 9-24 hours before microscopy experiments. To ensure the presence of single cells for whole-cell voltage clamp electrophysiology, HEK293T cells were seeded in reduced glucose (1 g/L) DMEM with 10% FBS, 2 mM GlutaMAX, and 1 mM sodium pyruvate.

NanoLuc substrate and dye loading

For fluorescence and BRET imaging cells were loaded with 500 nM dye unless otherwise indicated. RhoVR and RhoVR-HaloTag substrates were previously synthesized and characterized by our group[2,6,7]. Janelia Flour 525, SE (JF_{525}) purchased from Tocris. Loading solutions were made fresh in HBSS and applied to cells for 15-20 minutes at 37°C and 5% CO2. Cells were washed 2x with HBSS and replaced with fresh HBSS prior to imaging and used immediately after loading the dye. No cells remained at room temperature for longer than an hour. For bioluminescent assays, furimazine substrate (Promega) was added to NanoGlo buffer, mixed, and pipetted directly into the dish to be imaged always following the dye loading procedure. The final substrate concentration was kept at 2x (~5-10uM) and cells were not imaged for longer than an hour to ensure a relatively stable bioluminescence signal throughout each experiment.

CLARIOstar Plus+ microplate reader

Bulk measurements were taken with a CLARIOstart plus plate reader (courtesy of the Martin Lab at UC Berkeley). Emission scans were collected from 400 – 600 nm at 10 Hz and spectra were normalized to the bioluminescence peak emission at 460 nm. Individual bioluminescence values (466/64 nm) were measured over 10-20 second intervals without excitation light. BRET emission was collected using a 599/20 filter with exposure times kept at 0.1 seconds (10 Hz). Ratios were determined by dividing these acceptor: donor emission values (collected using 466/64 nm and 599/20 filters).

Epifluorescence Microscopy

All imaging was performed on an inverted epifluorescence microscope AxioObserver Z-1 (Zeiss), equipped with a Spectra-X Light engine LED light (Lumencor), controlled using µManager (V1.4, open-source, Open Imaging). Bioluminescence emission was collected using a 460/30 nm (Semrock) emission filter (10 seconds). Tetramethyl rhodamine-based dyes were excited with 550/15 nm light and emission collected with an 650/60 nm bandpass filter paired with a 594 LP dichroic mirror (500 ms exposure). BRET emission from RhoVRs was collected using

the same filter settings, no LED excitation, and with longer exposure times (10 seconds). JF_{525} was excited using 475/34 nm light and emission was collected with a 540/50 nm BP emission filter paired with a 510 LP dichroic using the same exposure times as RhoVR images, depending on direct LED or BRET excitation. Images were acquired using Plan-Apochromat 20/0.8 air objective (20x, Zeiss) and captured on an OrcaFlash4.0 sCMOS camera (sCMOS; Hamamatsu). Imaging for electrophysiology experiments were performed at 1 Hz when collecting bioluminescence and/or BRET data and 100 Hz for experiments using direct LED excitation light. All images were analyzed using FIJIs ImageJ. Hand drawn regions of interest were limited to intensities at the cell periphery, avoiding internal bioluminescent signals, and were background subtracted to a region without any cells.

Whole-cell patch clamp electrophysiology

Pipettes were pulled from borosilicate glass with filament (Sutter Instruments, Novato, CA) resistances ranging from 4 to 7 MΩ with a P97 pipette puller (Sutter Instruments). The internal solution composition is as follows, in mM (pH 7.25, 285 mOsmol/L): 125 potassium gluconate, 10 KCl, 5 NaCl, 1 EGTA, 10 HEPES, 2 ATP sodium salt, 0.3 GTP sodium salt. EGTA (tetraacid form) was prepared as a stock solution in either 1 M KOH or 10 M NaOH before addition to the internal solution. Pipettes were positioned with an MP-225 micromanipulator (Sutter Instruments).

Electrophysiology recordings were made with an Axopatch 200B amplifier and digitized with a Digidata 1550B (Molecular Devices). Signals were filtered with a 5 kHz low-pass Bessel filter and recorded with pCLAMP 10 software (Molecular Devices) on a PC. Fast capacitance was compensated in cell-attached configuration. For all electrophysiology experiments, recordings were only pursued if series resistance in voltage clamp were less than 20 MΩ. Correction for pipette capacitance was performed in the cell attached configuration. Images were acquired while in voltage-clamp mode at the designated holding potential for 2-4 seconds, when imaging bioluminescence/BRET. Holding potentials applied varied from -80mV to +80 mV, with +20 mV increments and a -60mV holding potential between each step. Potentials were applied in random order, and a membrane test was conducted between each step to verify the quality of the patch. For fast voltage imaging using LED excitation, where photon count is not as limiting, fluorescence was sampled at 50 kHz and HEK 293T cells were held at -60 mV until hyper- and de- polarizing steps were applied (from -100 to +100 mV) in 20 mV increments.

Cloning and transient transfections

HEK293T cells plated in a 6 well tissue culture dish were incubated at 37°C in a humidified incubator for at least 24 hours prior to transfection. Once cells reached ~60-75% confluency, transfections were performed with Lipofectamine 3000, using half the recommended p3000 and a quarter of the lipofectamine volumes suggested from the manufacturer's protocol (Thermo Fisher Scientific). We found reducing the amount of lipofectamine significantly increased cell health without dramatically reducing the transfection efficiency. Cells were allowed to grow an additional 5-10 hours after transfection before being plated onto glass coverslips for microscopy experiments (described above). Links to the benchling files are below:

EGFR-NanoLuc (Promega) *https://benchling.com/s/seq-sRKmPZgpStLRoeJAvbU4*
NanoLuc-EGFR (Promega) *https://benchling.com/s/seq-j4chqZGuGgLH56xJrxbd*
NanoLuc-HaloTag-pDisplay *https://benchling.com/s/seq-3WFICua7WzU6xwexcJbP*
Positron (addgene) *https://benchling.com/s/seq-LlahuA9chi1c13J3CMFR*
Voltron (addgene) *https://benchling.com/s/seq-6w8A3GcuL9NtNweyLy0t*

P01 (Positive going Ace2N-NanoLuc) *https://benchling.com/s/seq-Qxe2SFoi6X2khc7cOtCm*
P02 (Positive going Ace2N-HaloTag-NanoLuc)*https://benchling.com/s/seq-Q4HbHAnM5BECvSkD0jNq*
V01 (Negative going Ace2N-NanoLuc) *https://benchling.com/s/seq-l8tMYxm5FqM1lMBn32rz*
V02(Negative going Ace2N-HaloTag-NanoLuc) *https://benchling.com/s/seq-IeermczBodaZQlxjjJo3*

The following sequences were used (5' to 3') for subcloning:

IgK

ATGGAGACAGACACACTCCTGCTATGGGTACTGCTGCTCTGGGTTCCAGGTTCCACT
GGTGAC

Kir2.1 trafficking and export signal

AAGAGCAGGATCACCAGCGAGGGCGAGTACATCCCCCTGGACCAGATCGACATCAA
CGTGTTCTGCTACGAGAACGAGGTGTAA

NanoLuc

GTCTTCACACTCGAAGATTTCGTTGGGGACTGGCGACAGACAGCCGGCTACAACCTG
GACCAAGTCCTTGAACAGGGAGGTGTGTCCAGTTTGTTTCAGAATCTCGGGGTGTCC
GTAACTCCGATCCAAAGGATTGTCCTGAGCGGTGAAAATGGGCTGAAGATCGACAT
CCATGTCATCATCCCGTATGAAGGTCTGAGCGGCGACCAAATGGGCCAGATCGAAA
AAATTTTTAAGGTGGTGTACCCTGTGGATGATCATCACTTTAAGGTGATCCTGCACT
ATGGCACACTGGTAATCGACGGGGTTACGCCGAACATGATCGACTATTTCGGACGG
CCGTATGAAGGCATCGCCGTGTTCGACGGCAAAAAGATCACTGTAACAGGGACCCT
GTGGAACGGCAACAAAATTATCGACGAGCGCCTGATCAACCCCGACGGCTCCCTGC
TGTTCCGAGTAACCATCAACGGAGTGACCGGCTGGCGGCTGTGCGAACGCATTCTGG
CG

HaloTag

GCAGAAATCGGTACTGGCTTTCCATTCGACCCCCATTATGTGGAAGTCCTGGGCGAG
CGCATGCACTACGTCGATGTTGGTCCGCGCGATGGCACCCCTGTGCTGTTCCTGCAC
GGTAACCCGACCTCCTCCTACGTGTGGCGCAACATCATCCCGCATGTTGCACCGACC
CATCGCTGCATTGCTCCAGACCTGATCGGTATGGGCAAATCCGACAAACCAGACCTG
GGTTATTTCTTCGACGACCACGTCCGCTTCATGGATGCCTTCATCGAAGCCCTGGGTC
TGGAAGAGGTCGTCCTGGTCATTCACGACTGGGGCTCCGCTCTGGGTTTCCACTGGG
CCAAGCGCAATCCAGAGCGCGTCAAAGGTATTGCATTTATGGAGTTCATCCGCCCTA
TCCCGACCTGGGACGAATGGCCAGAATTTGCCCGCGAGACCTTCCAGGCCTTCCGCA
CCACCGACGTCGGCCGCAAGCTGATCATCGATCAGAACGTTTTTATCGAGGGTACGC
TGCCGATGGGTGTCGTCCGCCCGCTGACTGAAGTCGAGATGGACCATTACtGCGAGC
CGTTCCTGAATCCTGTTGACCGCGAGCCACTGTGGCGCTTCCCAAACGAGCTGCCAA
TCGCCGGTGAGCCAGCGAACATCGTCGCGCTGGTCGAAGAATACATGGACTGGCTG
CACCAGTCCCCTGTCCCGAAGCTGCTGTTCTGGGGCACCCCAGGCGTTCTGATCCCA
CCGGCCGAAGCCGCTCGCCTGGCCAAAAGCCTGCCTAACTGCAAGGCTGTGGACAT
CGGCCCGGGTCTGAATCTGCTGCAAGAAGACAACCCGGACCTGATCGGCAGCGAGA
TCGCGCGCTGGCTGTCGACGCTCGAGATTTCCGGC

pDisplay

GCTGTGGGCCAGGACACGCAGGAGGTCATCGTGGTGCCACACTCCTTGCCCTTTAAG
GTGGTGGTGATCTCAGCCATCCTGGCCCTGGTGGTGCTCACCATCATCTCCCTTATCA
TCCTCATCATGCTTTGGCAGAAGAAGCCACGTTAG

Positron

ATGGCTGACGTGGAAACCGAGACCGGCATGATTGCACAGTGGATTGTCTTTGCTATT
ATGGCTGCTGCTGCTATTGCTTTTGGAGTGGCTGTGCACTTTCGGCCTTCAGAGCTGA
AGAGCGCATACTATATCAACATTGCCATCTGCACTATCGCCGCTACCGCTTACTATG
CAATGGCCGTGAACTACCAGGACCTGACAATGAATGGTGAAAGGCAGGTGGTCTAC
GCAAGATATATTGACTGGGTGCTGACCACACCACTGCTCCTGCTCAACCTCATCGTC
ATGACCAAGATGGGCGGAGTGATGATTTCTTGGGTCATCGGCGCAGACATTTTCATG

ATCGTGTTTGGTATTCTGGGCGCCTTCGAGGATGAACACAAGTTCAAATGGGTGTAC
TTTATCGCTGGATGTGTGATGCAGGCAGTCCTGACATACGGGATGTATAACGCCACT
TGGAAAGACGATCTGAAGAAAAGCCCCGAGTACCATAGCTCCTATGTCAGTCTGCTC
GTCTTCCTGTCAATCCTCTGGGTGTTTTATCCTGTCGTGTGGGCTTTCGGGTCTGGTA
GTGGCGTGCTGTCCGTC

Voltron

ATGGCTGACGTGGAAACCGAGACCGGCATGATTGCACAGTGGATTGTCTTTGCTATT
ATGGCTGCTGCTGCTATTGCTTTTGGAGTGGCTGTGCACTTTCGGCCTTCAGAGCTGA
AGAGCGCATACTATATCAACATTGCCATCTGCACTATCGCCGCTACCGCTTACTATG
CAATGGCCGTGAACTACCAGGACCTGACAATGAATGGTGAAAGGCAGGTGGTCTAC
GCAAGATATATTAACTGGGTGCTGACCACACCACTGCTCCTGCTCGATCTCATCGTC
ATGACCAAGATGGGCGGAGTGATGATTTCTTGGGTCATCGGCGCAGACATTTTCATG
ATCGTGTTTGGTATTCTGGGCGCCTTCGAGGATGAACACAAGTTCAAATGGGTGTAC
TTTATCGCTGGATGTGTGATGCAGGCAGTCCTGACATACGGGATGTATAACGCCACT
TGGAAAGACGATCTGAAGAAAAGCCCCGAGTACCATAGCTCCTATGTCAGTCTGCTC
GTCTTCCTGTCAATCCTCTGGGTGTTTTATCCTGTCGTGTGGGCTTTCGGGTCTGGTA
GTGGCGTGCTGTCCGTC

Schemes and Figures

Scheme 4-1. *BRET-VF schemes*

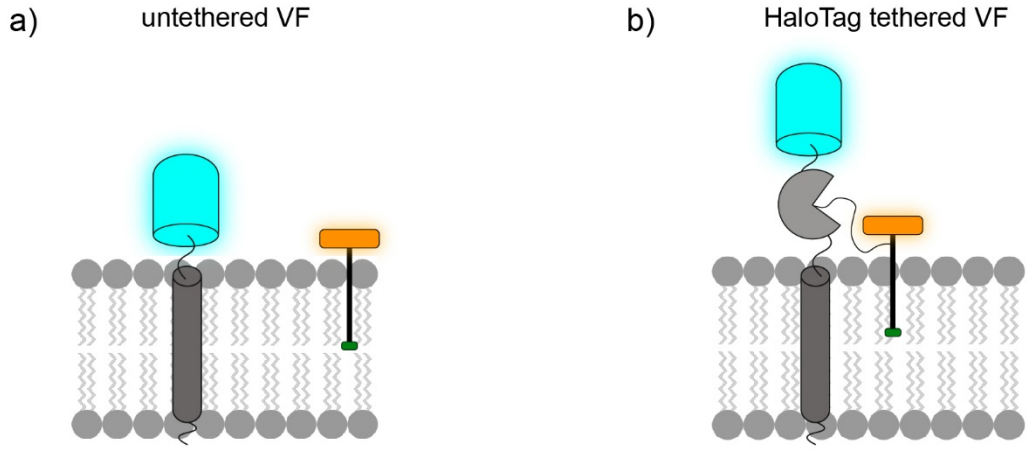

Scheme 4-1. BRET-VF schemes. Topology and orientation of BRET-VF systems using NanoLuc (blue) expressed to the extracellular surface of the plasma membrane via a transmembrane pDisplay domain (dark grey) **a)** without or **b)** with a self-labeling HaloTag domain (light grey). **a)** Without the HaloTag protein, RhoVR1 (orange) will insert into all membrane without specificity and with random distance from the luciferase. Whereas **b)** the presence of HaloTag will tether and target a RhoVR1-HaloTag ligand to transfected cells presumably decreasing the distance between the VF and luciferase to improve BRET.

Scheme 4-2. *HaloTag Ligand Chemical Structures*

a)

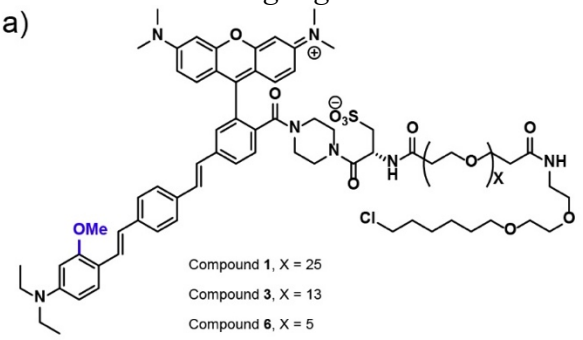

Compound **1**, X = 25

Compound **3**, X = 13

Compound **6**, X = 5

b)

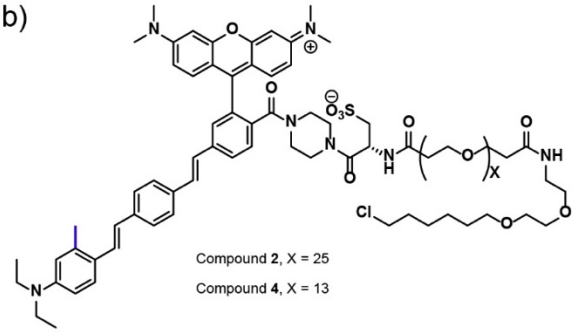

Compound **2**, X = 25

Compound **4**, X = 13

c)

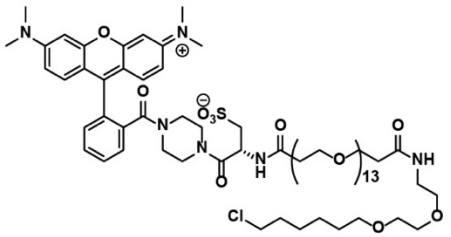

Compound **5**

d)

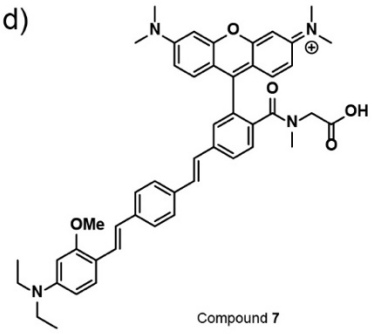

Compound **7**

Scheme 4-3. *Bioluminescent Positron and Voltron probe designs*

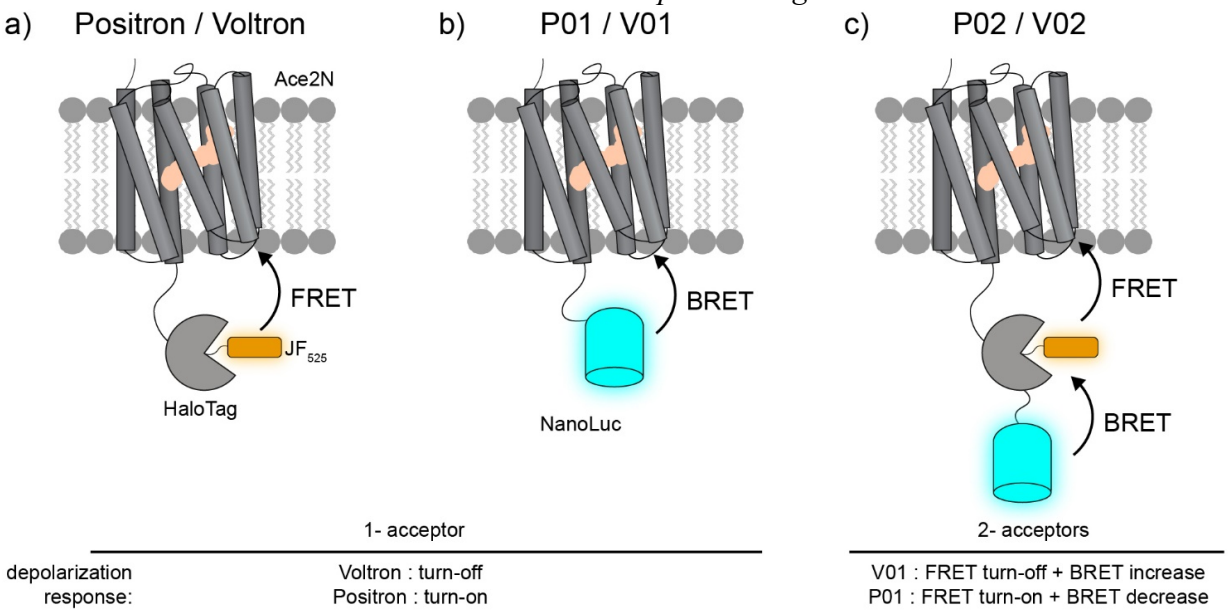

Figure 4-1. *BRET acceptor:donor ratios with untethered RhoVR1*

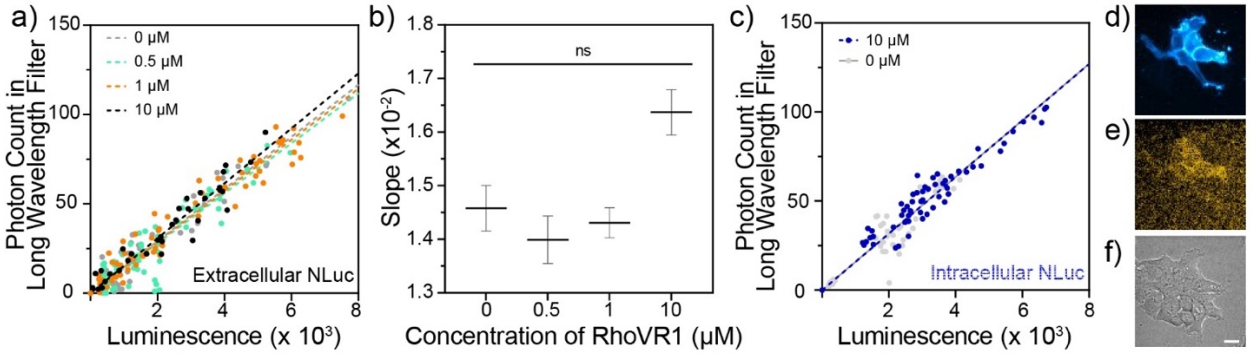

Figure 4-1. BRET acceptor:donor ratios with untethered RhoVR1. a) Long wavelength (560 nm) photon emission as a function of bioluminescence intensity in HEK cells expressing extracellular NanoLuc fused to the N terminal of EGFR. Bioluminescence bleed through and/or BRET is plotted in the presence of 0 µM (grey), 0.5 µM (aqua), 1 µM (orange), or 10 µM (black) RhoVR1 (n= 33-72 cells per condition). **b)** Slopes from a best-fit linear regression of the lines plotted in (a) with errors bars representing the standard error of the slope and statistics using a one-way ANOVA. **c)** Long wavelength (560 nm) photon emission as a function of bioluminescence intensity in HEK cells expressing *intracellular* NanoLuc fused to the C terminal of EGFR with 0 µM or 10 µM RhoVR1 (blue and grey, respectively). The solid grey line is directly underneath the dotted blue line, with an identical slope (0.0159). Epifluorescence microscopy images of membrane localized **d)** bioluminescence (blue) from HEK cells transfected with extracellular NanoLuc-EGFR, **e)** BRET from 2 µM RhoVR 1 (yellow), and **f)** transmitted light image of the same cell raft in d and e. Scale bar is 15 µm.

Figure 4-2. *BRET ratios with HaloTag tethered RhoVRs*

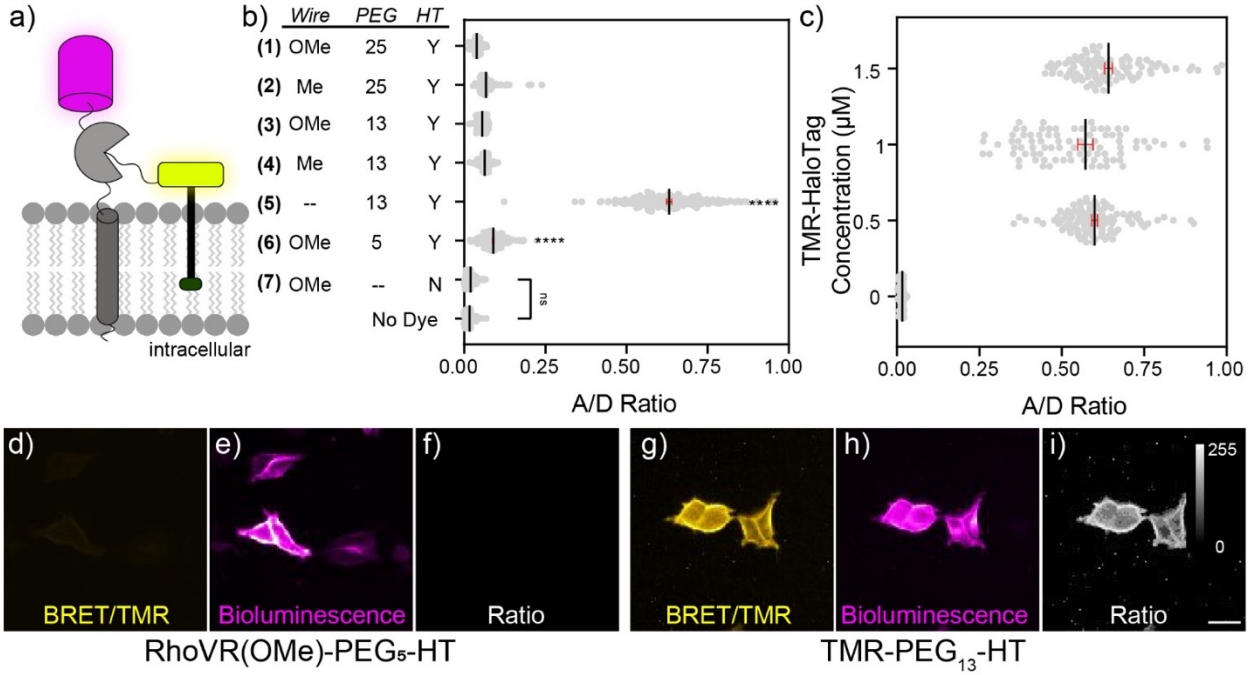

Figure 4-2. BRET ratios with HaloTag tethered RhoVRs. a) Labeling scheme of the HaloTag (HT) protein (grey) fused to the C-terminal of NanoLuc (magenta) and N-terminal of an alpha helical transmembrane domain, pDisplay (dark grey). Cells expressing the protein fusion to the plasma membrane react with RhoVR-HaloTag VF ligands (yellow dye head, black wire, green electron donating group) or a TMR-HaloTag ligand which lacks the phenylene vinylene wire and donating group (black and green) attached to the rhodamine dye head (yellow). **b)** Average BRET ratios (rhodamine dye emission divided by bioluminescence) for compounds **1-7** illustrated in **Scheme 4-2**. For convenience, differences in wire structures (-OMe and Me), and PEG linker lengths (5-25) are included. Compound **5** is not a VF and does not have a wire (denoted with --), and compound **7** is untethered RhoVR1 which lacks a PEG linker and chloroalkane ligand; n = 193-355 cells per condition; Statistical significance using Tukey's multiple comparison test, $p < 0.005$. **c)** TMR-HaloTag (**5**) BRET ratios in HEK cells loaded with 0, 0.5, 1 or 1.5 μM dye for 15-20 minutes in HBSS. **d-i)** Epifluorescent microscopy images of HEK cells labeled with 0.5 μM RhoVR(OMe)-PEG_5-HT (**d-f**) or 0.5 μM TMR-PEG_{13}-HT (**g-i**). BRET (yellow) emission from the rhodamine dye head in (**d**) is normalized to the BRET emission in (**g**). Bioluminescence images (magenta, e and h) are not normalized, but contrast adjusted to show bioluminescence. **f** and **i**) Pixel-by pixel ratio by of the acceptor channel (d and g) divided by the donor channel (e and h, respectively). Values in (f) are nearly 0 and not visible.

Figure 4-3. *Voltage sensitive response of HaloTag tethered RhoVR*

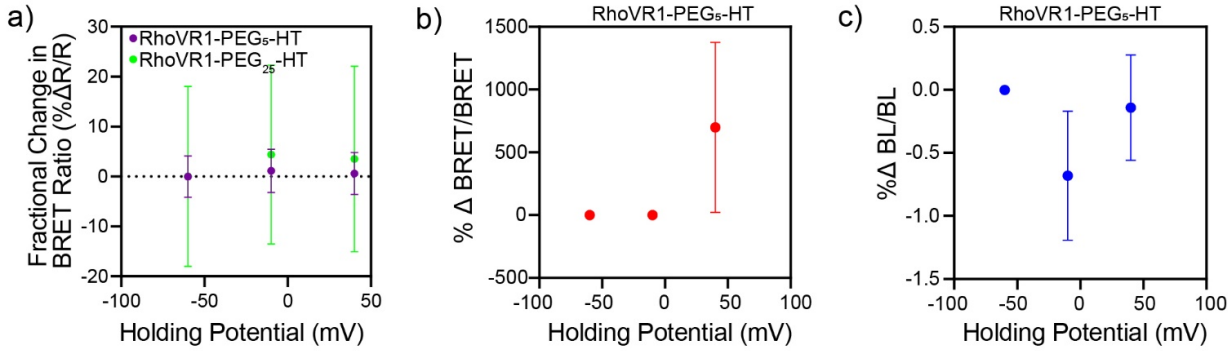

Figure 4-3. Voltage sensitive response of HaloTag tethered RhoVR1. a) Percent fractional change in the BRET ratio (%ΔR/R) of transfected HEK293T cells loaded with 0.5 µM of RhoVR1-PEG_5-HT (purple) or RhoVR1-PEG_{25}-HT (green) and voltage clamped at -60 mV, -10 mV, and +40 mV steps; n = 8 and 22 cells for PEG_{25} and PEG_5 derivatives, respectively. **b)** The average fractional change in BRET emission from RhoVR-PEG_5-HT (%Δ BRET/BRET) and **c)** bioluminescence emission (%Δ BL/BL) of the same cells used to calculate %ΔR/R in (a) at -60 mV, -10 mV, ad +40 mV holding potentials. All error bars represent the standard error of the mean.

Figure 4-4. *Ace2N-NanoLuc fusions express and localize to the cell membrane in HEK293T cells*

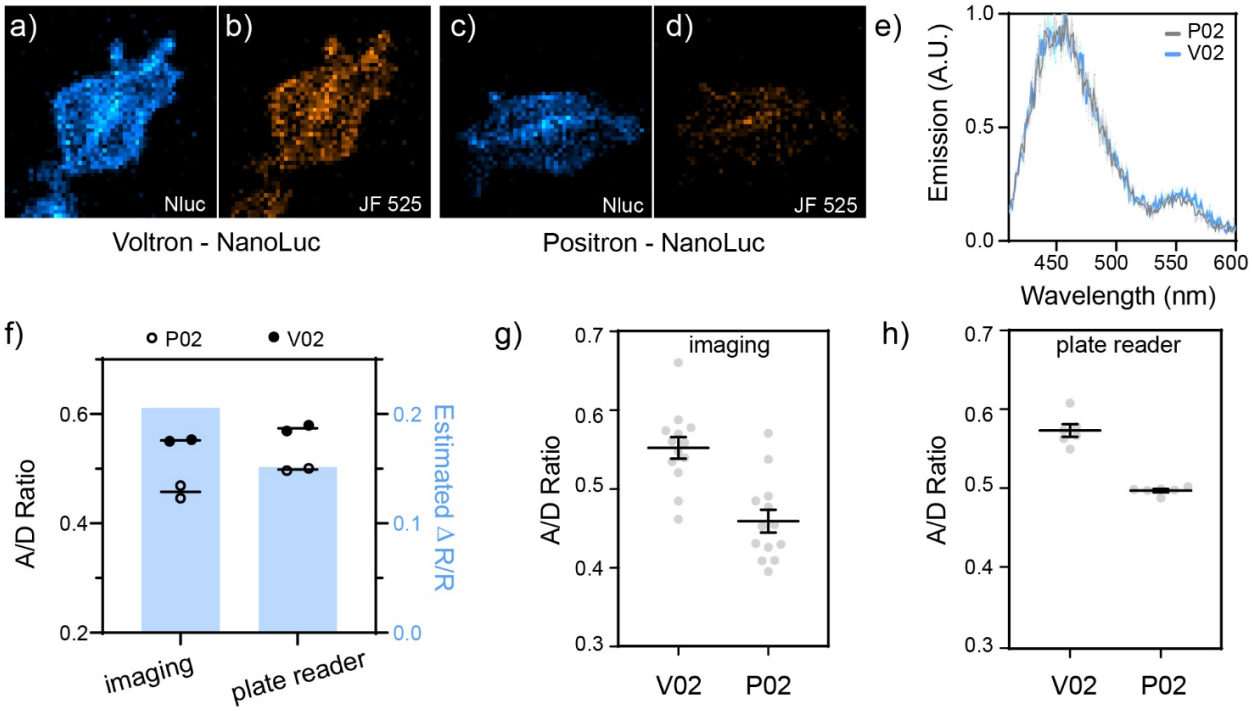

Figure 4-4. BRET evaluation of V02 and P02 fusions in HEK293T cells. Bioluminescent live cell imaging of HEK293T cells expressing **a)** V02 (Voltron-NanoLuc) or **c)** P02 (Positron-NanoLuc). **b)** and **d)** BRET emission from the same cells in (a) and (c) labeled with JF_{525} HaloTag ligand. All images are normalized to the bioluminescence in (a). **e)** Plate reader emission scan from a 96-well plate of cells expressing P02 (grey) or V02 (blue) and labeled with JF_{525}-HT. Peak emission values for NanoLuc and JF_{525} are at 460 nm and 550 nm, respectively. **f)** Left y-axis shows the average BRET ratios from 2 independent experiments, represented as black lines, from cells expressing P02 (empty circle) or V02 (solid circle) using live single cell imaging or bulk plate reader measurements. The estimated fractional change in the ratio (% ΔR/R) for each method is plotted on the right y-axis (blue) assuming V01 is the max turn-on ratio and P02 is the starting ratio for cells at rest. **g)** Average BRET ratio from live cell and **h)** plate reader imaging used for plot f.

Figure 4-5. *Fluorescent-based voltage sensitivity of rhodopsin NanoLuc fusions*

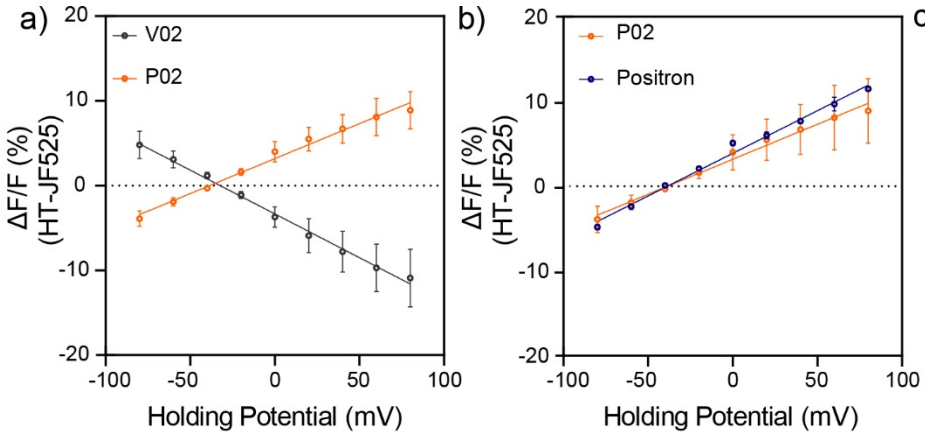

Figure 4-5. Fluorescent-based voltage sensitivity of rhodopsin NanoLuc fusions. a) Fractional change of JF_{525} fluorescence in cells expressing V02 (black), P02 (orange) or **b)** Positron (blue) under whole-cell patch clamp electrophysiology. Voltage steps were applied to HEK293T cells in 20 mV increments from -80 mV to +80 mV. The slope of the line shows a ΔF/F per 100 mV of 8.3% ± 0.8% and -10.3% ± 0.6% for P02 and V02, respectively (± SEM, n = 3-4 cells per construct). **b)** Positron shows a 10% ± 0.3% ΔF/F per 100 mV under the same experimental conditions (± SEM, n = 3 cells). The difference in P02 and Positron ΔF/F values is not statistically significant using Šídák's multiple comparisons test, $p > 0.05$.

Figure 4-6. *Preliminary bioluminescent-based voltage sensitivity of P02*

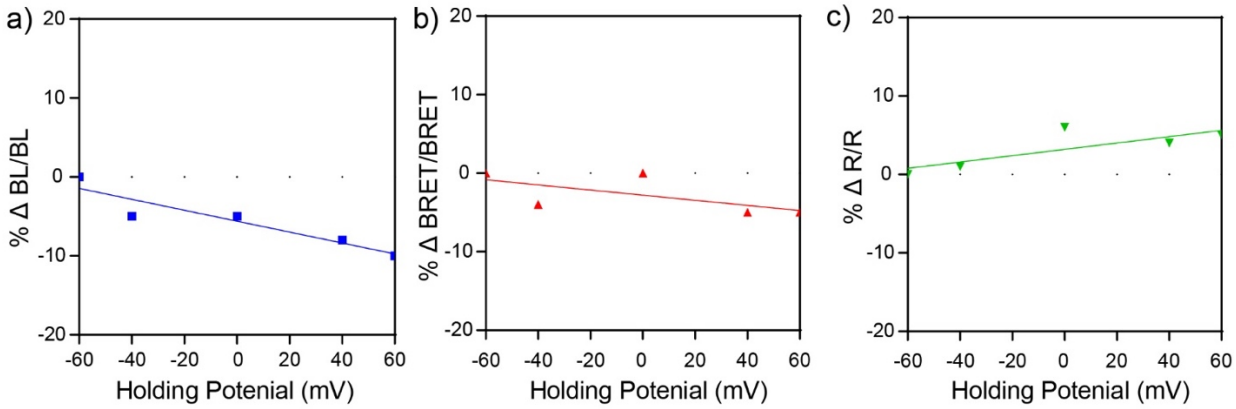

Figure 4-6. Preliminary bioluminescent-based voltage sensitivity of P02. A single HEK cell under whole-cell patch clamp electrophysiology shows **a)** a decrease in the fractional change in bioluminescence emission, ΔBL/BL = -6.9%, **b)** a decrease in the fractional change in BRET, ΔBRET/BRET = -3.3%, and **c)** an increase in the fractional change of the ratio, ΔR/R = 4%.

References

1. Hall, M. P. *et al.* Engineered luciferase reporter from a deep sea shrimp utilizing a novel imidazopyrazinone substrate. *ACS Chem. Biol.* **7**, 1848–1857 (2012).
2. Benlian, B. R. *et al.* Small Molecule-Protein Hybrid for Voltage Imaging via Quenching of Bioluminescence. *ACS Sensors* (2021). doi:10.1021/acssensors.1c00058
3. Sjulson, L. & Miesenböck, G. Rational optimization and imaging in vivo of a genetically encoded optical voltage reporter. *J. Neurosci.* **28**, 5582–5593 (2008).
4. Fernández, J. M., Taylor, R. E. & Bezanilla, F. Induced capacitance in the squid giant axon. Lipophilic ion displacement currents. *J. Gen. Physiol.* **82**, 331–46 (1983).
5. Chanda, B. *et al.* A hybrid approach to measuring electrical activity in genetically specified neurons. *Nat. Neurosci.* **8**, 1619–1626 (2005).
6. Deal, P. E., Kulkarni, R. U., Al-Abdullatif, S. H. & Miller, E. W. Isomerically Pure Tetramethylrhodamine Voltage Reporters. *J. Am. Chem. Soc.* **138**, 9085–9088 (2016).
7. Deal, P. E. *et al.* Covalently Tethered Rhodamine Voltage Reporters for High Speed Functional Imaging in Brain Tissue. *J. Am. Chem. Soc.* **142**, 614–622 (2020).
8. Abdelfattah, A. S. *et al.* A general approach to engineer positive-going eFRET voltage indicators. *Nat. Commun.* **11**, (2020).
9. Abdelfattah, A. S. *et al.* Bright and photostable chemigenetic indicators for extended in vivo voltage imaging. *Science (80-.).* **365**, 699–704 (2019).
10. Kralj, J. M., Douglass, A. D., Hochbaum, D. R., MacLaurin, D. & Cohen, A. E. Optical recording of action potentials in mammalian neurons using a microbial rhodopsin. *Nat. Methods* (2012). doi:10.1038/nmeth.1782
11. Hochbaum, D. R. *et al.* All-optical electrophysiology in mammalian neurons using engineered microbial rhodopsins. *Nat. Methods* **11**, 825–833 (2014).
12. Abdelfattah, A. S. *et al.* A Bright and Fast Red Fluorescent Protein Voltage Indicator That Reports Neuronal Activity in Organotypic Brain Slices. *J. Neurosci.* **36**, 2458–2472 (2016).
13. Chang, D. *et al.* Luciferase-Induced Photouncaging: Bioluminolysis. *Angew. Chemie - Int. Ed.* **58**, 16033–16037 (2019).
14. Dixon, A. S. *et al.* NanoLuc Complementation Reporter Optimized for Accurate Measurement of Protein Interactions in Cells. *ACS Chem. Biol.* **11**, 400–408 (2016).

Appendix 1:
Rhodamine-based SNAP-tag VoltageFluors

Introduction

Hybrid voltage imaging methodologies combining synthetic dyes with self-labeling proteins is a promising approach for labeling defined cells with fluorescent voltage reporters. Synthetic Voltage-sensitive Fluorophores (VFs) developed in the Miller lab allow for a diverse spectrum of colors all with fast response kinetics capable of resolving neuronal action potentials.[1] We have created VF targeting systems paired with HaloTag[2,3], SpyTag/Spy catcher[4], and SNAP-tag (Chapter 2) labeling proteins with both fluorescein and rhodamine-based dyes. However, one common problem we have encountered in labeling specific cells of interest is a low fluorescence turn-on of targeted cells, especially in deep tissue preparations with the fluorescein-based VFs.

One potential limitation contributing to a low turn on is the 1:1 stoichiometry of indicator and enzyme which limits the number of dye molecules within in the membrane. As a result, the fluorescence intensity is often limited by protein expression and increasing dye loading concentrations mostly leads to increased off-target labeling, or background signal. Another contributing factor is the excitation and emission profiles of the fluorescein VFs within the cyan and green regions. Excitation using cyan light excites endogenous molecules within a cell and the contributing autofluorescence further increases the background. This problem is exacerbated further when going from monolayer imaging to deep tissue or *in vivo* preparations. For example, we found with the fluorescein SNAP-tag VF (Chapter 2, mSNAP2) the turn-on ratio in dissociated cell culture was excellent (20x), however this ratio was significantly reduced when targeting neurons within a brain (2x).

While the SNAP-tag targeting system with VFs is promising, improvements in overall brightness and contrast relative to non-targeted cells are needed for *in vivo* applications. To address this limitation, we synthetically incorporated the reactive O^6-benzylguanine SNAP-tag ligand to our rhodamine voltage indicator, RhoVR1. This RhoVR-SNAP VF demonstrates a 40-50x turn-on in dissociated HEK cells (2x greater than mSNAP2) and seems a promising improvement to mSNAP2. However, synthetic challenges and molecular decomposition preclude thorough optimization and characterization of RhoVR-SNAP past HEK cells.

Results and Discussion

Synthesis of RhoVR-SNAP

The O^6-benzylguanine SNAP ligand was functionalized with a reactive alkyne handle following previously published protocols[5]. The alkyne containing SNAP-tag ligand **1** was coupled to azide **2** via copper catalyzed click reaction. The azide intermediate **2** was previously characterized during the synthesis of RhoVR-HaloTag[2]. RhoVR-SNAP (**3**) was obtained in a 2.8% yield after preparative HPLC purification (**Scheme A1-1**).

Characterization of RhoVR-SNAP targeting in HEK293T cells

We next evaluated RhoVR-SNAP in HEK cells expressing the optimized $SNAP_f$ construct containing an IgK secretion signal, GPI-membrane anchor, and a nuclear localized GFP (Chapter 2).[6] RhoVR-SNAP shows excellent membrane staining at concentrations ranging from 25 nM to 100 nM, with no internalization, and high specificity for $SNAP_f$ expressing cells (**Fig. A1-1c-e**). There is only a modest increase in the fluorescence intensity by increasing the dye concentration from 25 nM to 100 nM (**Fig A1-1a**). The increase in loading concentration also raises the baseline fluorescence of non-targeted cells, albeit very minimally (**Fig. A1-1a**). This slight increase in baseline is reflected by a decrease in the turn-on ratio; however, the there is no statistical difference in the turn-on response between the three loading concentrations evaluated (**Fig. A1-1b**). The

average turn-on response in HEK cells is 45x, more than double the 20x turn-on seen with the fluorescein based mSNAP2 VF (**Fig. A1-1b**).

Synthetic challenges and stability tests

The initial synthesis of RhoVR-SNAP gave a small batch of aliquots to start initial imaging experiments as discussed above. Applications in live *Drosophila* were also simultaneously underway and are discussed in another thesis written by fellow group member Molly Kirk. However, follow-up attempts to re-make the molecule proved challenging and halted further characterization. The successful synthesis of RhoVR-SNAP was run for only 3.5 hours at 80 °C in a mixture of H_2O:DMSO (0.46:1, by volume), but the reaction never went to completion. Variations in the solvent ratio, temperature, total reaction volume and reaction length did not improve product conversion to more than 50%. Notes on reaction conditions and results are included in detail within Table A1-1. Furthermore, even after purification without reaction conditions optimized, the stability and degradation of RhoVR-SNAP was the main obstacle. Low volume (2 μL) DMSO aliquots at 357 μM, 178 μM, and 89 μM were dried under vacuum and stored under varying atmospheric and temperature conditions. Regardless of storage conditions all aliquots resulted in a 10-20% decomposition within just 1 to 3 weeks based on LCMS analysis (Table A1-2). The decomposition products could not be determined based on mass.

The initial synthesis suggests RhoVR-SNAP can be prepared and properly stored over time, yet it is unclear what may be the cause of degradation in all follow-up attempts. An extended screen of alternative click reaction and purification conditions may provide more information. The largest contrast ratio published to date with our covalent-VF targeting systems is 30x using BeRST-HaloTag.[3] Previous findings within our group using BeRST and RhoVR-HaloTag VFs also demonstrate how well red-shifted VFs perform within dense tissue samples.[2,3] Taken together, the large 40x contrast between $SNAP_f$ expressing and non-expressing HEK cells labeled with RhoVR-SNAP is very promising and a motivating factor to continue this project. Additionally, previous reports state that the BG moiety can interact varyingly with different fluorophores[7]. Alternative rhodamine or carbofluorescien fluorophores are another option to achieve successful synthesis of a red-shifted SNAP-tag VoltageFlour and are currently being explored.

Experimental Methods

Cell culture, transient transfections, and dye loading

HEK293T cell lines were obtained from the UC Berkeley Cell Culture Facility and discarded after 25 passages. Cells were dissociated during passages using 0.05% Trypsin-EDTA with phenol red (Thermo Fisher Scientific) at 37°C, and then maintained in Dulbecco's Modified Eagle Medium (DMEM) with 4.5 g/L D-glucose supplemented with 10% FBS (Seradigm (VWR); Radnor, PA) and 2 mM 668 GlutaMAX (Gibco) in a 5% CO2 incubator at 37°C.

For all imaging experiments, cells were plated onto 12 mm diameter #1.5 glass coverslips (Electron Microscopy Sciences) in 24-well tissue culture plates (Corning; Corning, NY). To maximize cell attachment, coverslips were treated before use with 1-2 M HCl for 2-5 hours and washed overnight three times with 100% ethanol and three times with deionized water. Coverslips were sterilized by heating to 150°C for 2-3 hours. Before use, coverslips were incubated with poly-D-lysine (Sigma-Aldrich, made as a 0.1 mg/mL solution in phosphate-buffered saline with 10 mM Na_3BO_3) for 2-10 hours at 37°C and then washed twice with water and twice with Dulbecco's phosphate buffered saline (dPBS, Gibco). HEK293T cells were seeded 24 hours before microscopy experiments.

HEK293T cells were incubated at 37°C in a humidified incubator on plastic culture plates for at least 24 hours prior to transfection. Once cells reached ~60-75% confluency, transfections were performed with Lipofectamine 3000, using half the recommended p3000 and a quarter of the lipofectamine volumes suggested from the manufacturer's protocol (Thermo Fisher Scientific). We found reducing the amount of lipofectamine significantly increased cell health without dramatically reducing the transfection efficiency. Cells were allowed to grow an additional 5-10 hours after transfection before being plated onto glass coverslips for microscopy experiments (described above). Prior to imaging, fresh dye solution was made from a 100 μM stock in DMSO and diluted in Hank's Balance Salt Solution (HBSS) to the desired concentration. Cells were incubated in the dye loading solution for 15 minutes, rinsed 1x with fresh HBSS, and imaged directly after.

Epifluorescence microscopy

Imaging was performed on an AxioExaminer Z-1 (Zeiss) equipped with a Spectra-X Light engine LED light (Lumencor), controlled with Slidebook (v6, Intelligent Imaging Innovations). Images were acquired with a W-PlanApo 20x/1.0 water objective (20x; Zeiss) and focused onto an OrcaFlash4.0 sCMOS camera (sCMOS; Hamamatsu). For GFP images, the excitation light was delivered from a LED (100 ms exposure time) at 475/34 nm and emission was collected with a quadruple emission filter (430/32, 508/14, 586/30, 708/98 nm) after passing through a quadruple dichroic mirror (432/38, 509/22, 586/40, 654 nm LP). RhoVR was excited using 550/15 nm light and collected with an emission filter (650/60 nm BP; 100 ms exposure time) and 594 LP dichroic.

Synthesis

Synthesis of (2) (BD3-80)

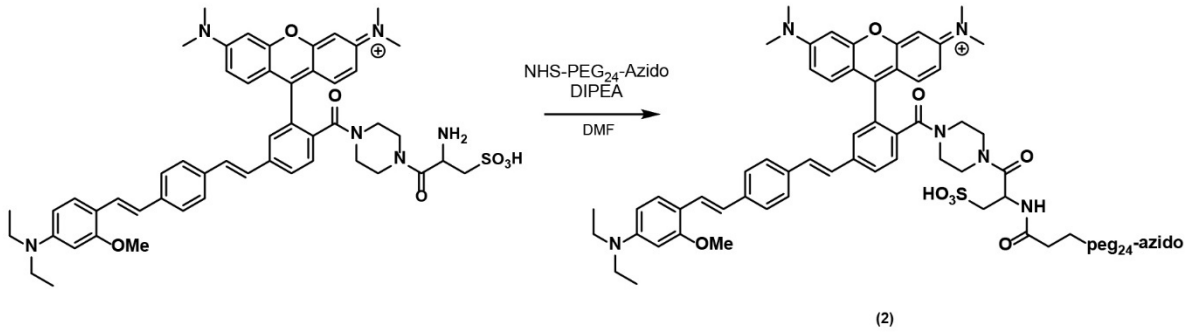

Compound (**1**) was synthesized following the procedure reported in Deal et al.[2] To a flame dried vial and stir bar, 15.5 mg (17 μmol, 1 equiv.) Compound (1) was dissolved in 500 μL of DMF followed by the addition of 20 μL DIPEA (229.4 μmol, 13.5 equiv.) and 23.7 mg NHS-PEG_{24}-azide (18.7 μmol, 1.1 equiv.). The reaction was stirred under N_2 and completion verified via LCMS after 3 hours. Solvent was removed under reduced pressure and the resulting film resuspended in minimal chloroform for purification by preparatory thin-layer chromatography (PTLC; 8% MeOH/ 2% TEA in DCM). The bottom dark red band was removed from the silica, filtered, and dried to give 16.6 mg of Compound (2) in a 47% yield.

Spectrum 1. HPLC of Compound (2)

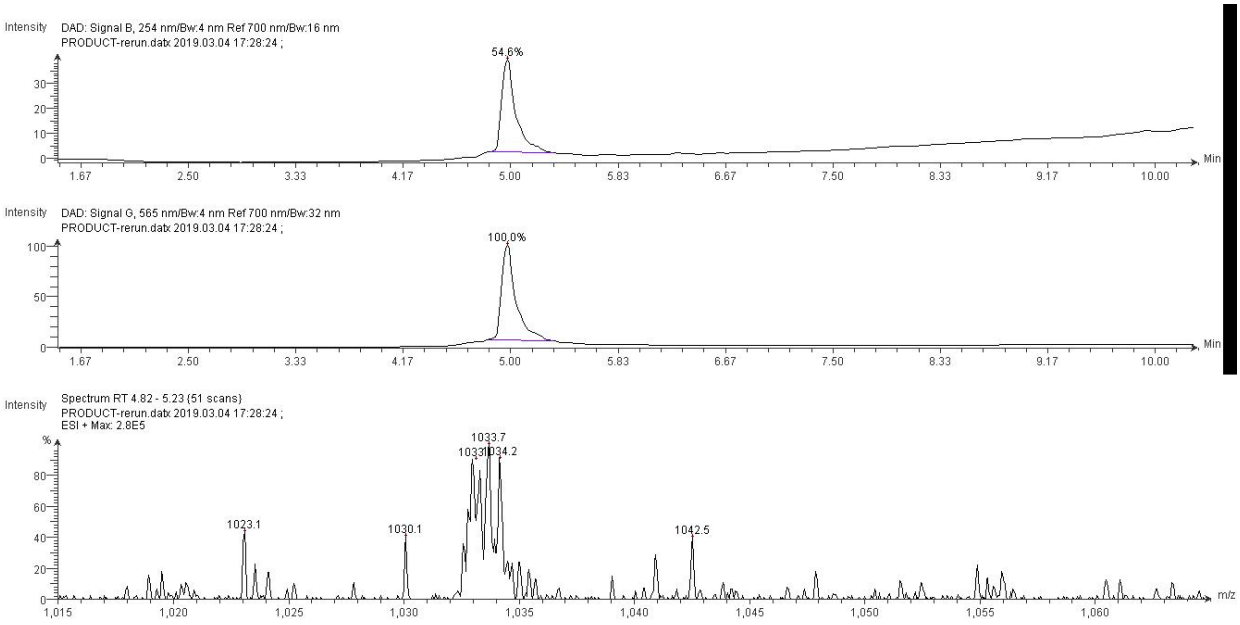

Low-resolution ESI(+) mass spectrum of **Compound (2)**
Calculated for [M/2+H]+ 1034; Found 1033.7

Synthesis of RhoVR-SNAP (BD2-105 and 107)

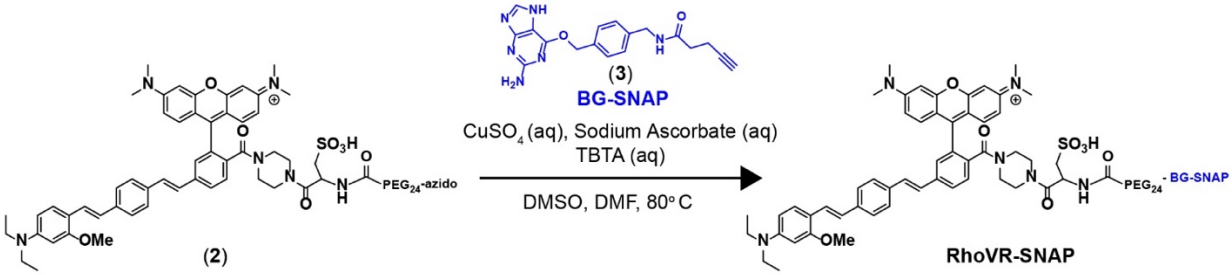

Fresh copper sulfate (25 nM) and sodium ascorbate (100 nM) solutions were prepared in MilliQ water and bubbled under N_2 for at least 30 minutes. Copper and sodium solutions were mixed together in a 1.5 mL Eppendorf tube (80 µL each) until the solution turned a pale, cloudy yellow color. Tris((1-benzyl-4-triazolyl)methyl)amine (TBTA) ligand was added (100 µL, 48 mM DMSO solution) to stabilize the copper(I) oxidation state to promote efficient cyclization between the O^6-benzylguanine (**3**) alkyne and azide (**2**). Additional replicates of this reaction indicate the addition of TBTA is not entirely necessary to generate the desired product. Following TBTA addition, Compound (**3**) was then added to the Eppendorf (50 µL, 100 mM in DMSO) followed by compound (**2**) (16 mM, 130 µL, ~4.4 mg). A slight precipitate remained and small amounts (50 µL increments) of DMSO were added until a clear homogenous solution was formed. The reaction was left to stir at 80°C and monitored by LCMS. The reaction would never go to completion and longer reaction times typically resulted to increased decomposition and/or byproducts. After 3.5 hours no increase in product formation was usually seen, and so the reaction was then filtered and purified by preparative HPLC using acetonitrile/TFA. An analytical injection showed a product peak at 6.33 minutes, however a larger injection around 300 µL must have contained too much DMSO as the product came out nearly with the solvent front at 1.5 minutes. Small injections (~100 µL) gave the best results. The final RhoVR-SNAP product was verified by LCMS and was collected in a very low yield (2.8%) determined by U.V. absorbance.

Spectrum 2. HPLC of RhoVR-SNAP

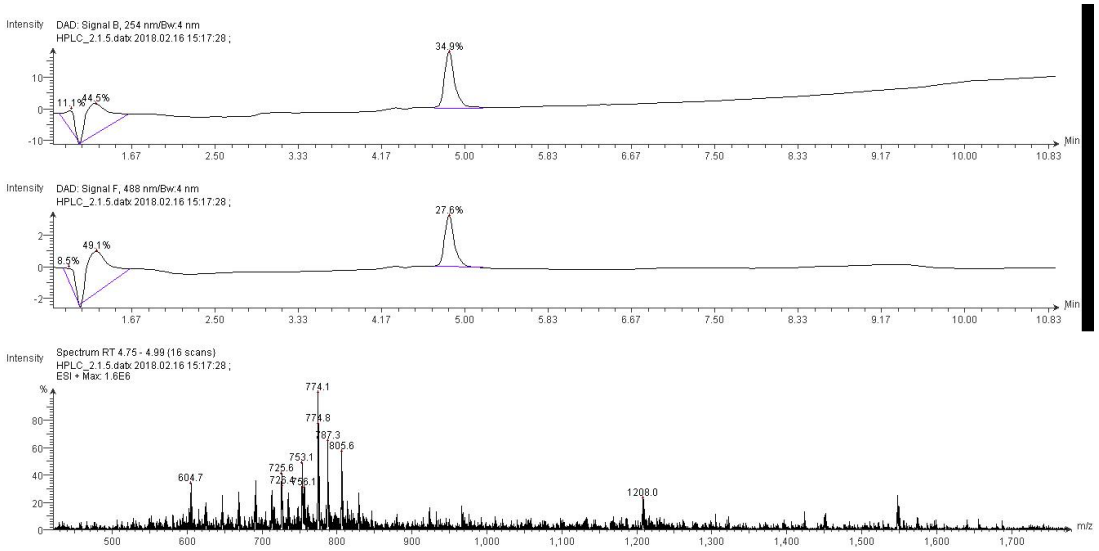

Low-resolution ESI(+) mass spectrum of **RhoVR-SNAP**
Calculated for [M/2+H]+ 1209; Found 1208.0; Calculated for [M/3+H]+ 806; Found 805.6

Schemes and Figures

Scheme A1-1. Overview of RhoVR-SNAP Synthesis

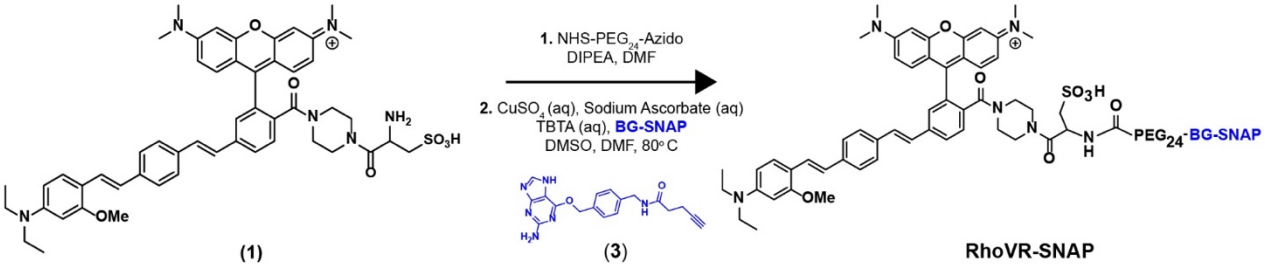

Figure A1-1. *RhoVR1-SNAP loading optimization in HEK cells*

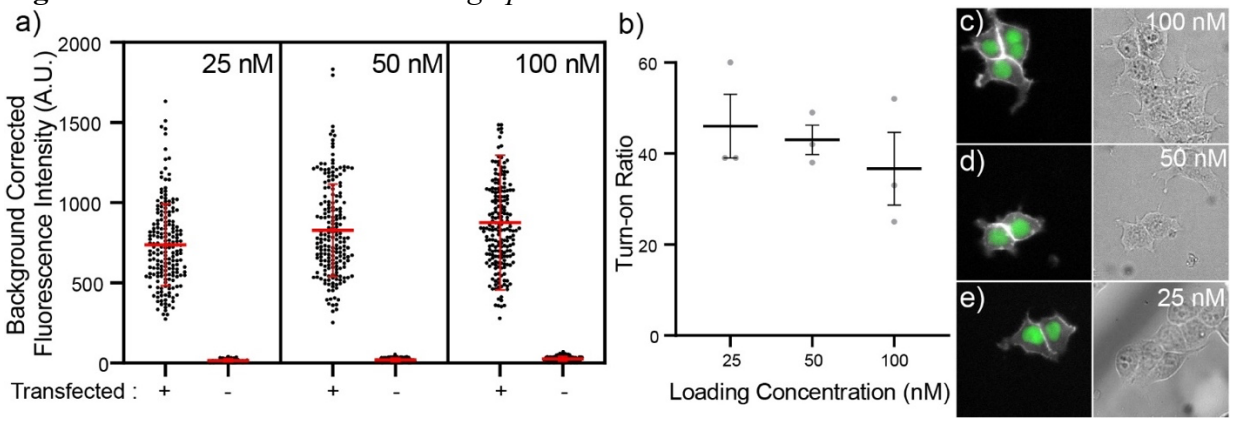

Figure A1-1. RhoVR1-SNAP loading optimization in HEK cells. a) Background corrected fluorescence intensity of SNAPf expressing (+) and non-expressing (-) cells loaded with 25 nM, 50 nM, or 100 nM RhoVR-SNAP. Each data point represents a single cell with n= 190-198 cells per condition over the course of 3 separate experiments. Error bars are standard deviation of the mean. **b)** Average fluorescence ratio of transfected to non-transfected cells from data shown in a). Each gray data point represents the average of 3 coverslips from 1 experiment (3 experiments total), error is represented as the mean ± SEM. There is no statistical significance between mean values using a 2-way ANOVA followed by Tukey's multiple comparisons test, $p > 0.05$. Live cell images of RhoVR-SNAP and nuclear GFP (left) colored in white and green loaded with **c)** 100 nM, **d)** 50 nM, or **e)** 25 nM RhoVR-SNAP alongside the transmitted light image (right) showing non-transfected cells as well. RhoVR-SNAP fluorescence intensity in c-e) is normalized to c).

Table A1-1. *RhoVR1-SNAP Reaction Table*

Notebook	Reagent*	Stock (mM)	Volume used (µL)	µMol	H2O: DMSO	total volume (µL)	Temp (°C)	Time (Hr)	P v S
1	1	16	134	2.1	0.46	604	40	24	piperazine
BD 2-98	2	100	48	4.8					
	3	25	96	2.4					
	4	100	94	9.4					
	5	48	100	4.8					
Notes	no product identified in crude. LCMS is a mess								
2	1	16	130	2.1	0.46	510	80	3.5	piperazine
BD 2-105	2	100	50	5.0					
	3	25	80	2.0					
	4	100	80	8.0					
	5	48	100	4.8					
Notes	Successful method								
3	1	15	60	0.9	0.76	370	60-80	5	sarcosine
BD 3-12	2	100	50	5.0					
	3	25	80	2.0					
	4	100	80	8.0					
	5	48	100	4.8					
Notes	bad ionzation, thought I saw product (m/z=550 &733), tried purifying on waters HPLC- 10-100 protocol, product never came out during collection but came out at end of protocol (~20 min)								
4	1	15	60	0.9	0.76	370	65	5	sarcosine
BD3-14	2	100	50	5.0					
	3	25	80	2.0					
	4	100	80	8.0					
	5	48	100	4.8					
Notes	consistent with BD3-12, purified on HPLC with 50-100 method, saw m/z 1098 and 732 in 3 collected vials, concentration significantly lower than anticipated - not usable								
5	1	15	100	1.5	0.80	720	65	5	sarcosine
BD3-14	2	100	100	10.0					
	3	25	160	4.0					
	4	100	160	16.0					
	5	48	200	9.6					
Notes	No LCMS data- instrument clogged. Tried PTLC purification instead. Method did not work but instead streaked across the plate								
6	1	15	100	1.5	0.80	720	60	3	sarcosine
BD3-14	2	100	100	10.0					
	3	25	160	4.0					
	4	100	160	16.0					
	5	48	200	9.6					
Notes	LCMS unclear- some noticeable peaks in 560 nm, but very dilute (probs during an LCMS clog), worried reaction would increase with byproducts so tried running on a column with 15%MeOH, inconclusive- no final product collected								
8	1	15	130	1.9	0.48	490	80	24	sarcosine
BD3-35	2	100	50	5.0					

	3	25	80	2.0					
	4	100	80	8.0					
	5	48	100	4.8					
Notes	purified on waters HPLC and got pure product in the end with m/z=1098, but too little to work with in cells.								
9 BD3-38	1	15	260	3.8	0.37	1180	80	5	sarcosine
	2	100	200	20.0					
	3	25	160	4.0					
	4	100	160	16.0					
	5	48	200	9.6					
Notes	still didn't go to completion but product peak there (5min in TFA), learned 50-100 protocol no good because too much BG sticks around, ran samples in 50/50 Meoh/meCN, injected 500uLx3, long story of HPLC troubles but end result was 5 vials with different purity. #1 = cleanest, still BG though and weird peak shape, #2 probably has the most product in it, but messy, has BG, and a weird m/z=1088 not 1098, #3 and #4 very messy, weird peak morphology, combined these 2 to try and re-purify but everything seems to decompose. #5 is starting VF primarily								

* Reagent 1 = RhoVR1-N3, 2 = BG-alkyne, 3 = Copper Sulfate, 4 = Sodium Ascorbate, 5 = TBTA

Table A1-1. *RhoVR1-SNAP Stability Assays*

Storage condition (after drying under vacuum)	Stability	LCMS Notes
Stock concentration	*357 μM*	
Room Temperature	~10 % decomp	
Room Temperature + N_2 flush	~10 % decomp	
-20 °C	~10-15% decomp	Peak broadening + small side peaks
-20 °C + N_2 flush	~10-15% decomp	
-80 °C	~10-15% decomp	
-80 °C + N_2 flush	~10-15% decomp	
Stock concentration	*178 μM*	
Room Temperature	~10 % decomp	
Room Temperature + N_2 flush	~10 % decomp	
-20 °C	~10-15% decomp	Peak broadening + small side peaks
-20 °C + N_2 flush	~10-15% decomp	
-80 °C	~10-15% decomp	
-80 °C + N_2 flush	~10-15% decomp	
Stock concentration	*89 μM*	
Room Temperature	~10 % decomp	
Room Temperature + N_2 flush	~10 % decomp	
-20 °C	~10-15% decomp	Peak broadening + small side peaks
-20 °C + N_2 flush	~10-15% decomp	
-80 °C	~10-15% decomp	
-80 °C + N_2 flush	~10-15% decomp	

*Raw LCMS data saved under RPC-snaptag_stability_assay

Spectrum 3. *Representative HPLC of RhoVR-SNAP Decomposition from a 178 uM aliquot dried, flushed with N_2, and stored at -20°C.*

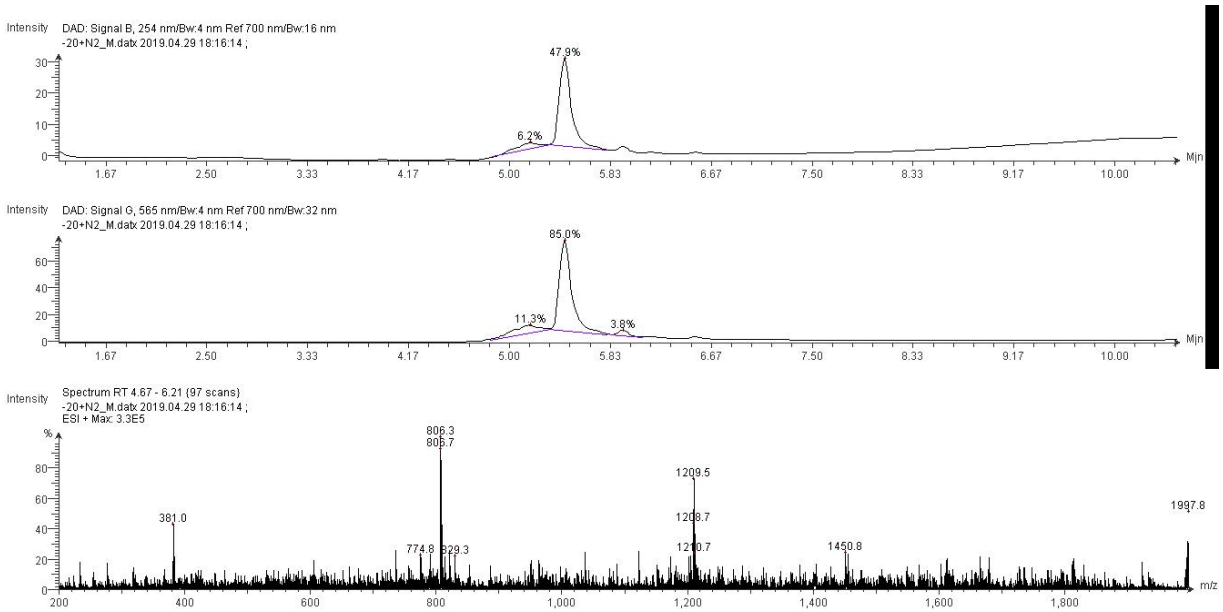

References

1. Liu, P. & Miller, E. W. Electrophysiology, Unplugged: Imaging Membrane Potential with Fluorescent Indicators. *Acc. Chem. Res.* **53**, 11–19 (2020).
2. Deal, P. E. *et al.* Covalently Tethered Rhodamine Voltage Reporters for High Speed Functional Imaging in Brain Tissue. *J. Am. Chem. Soc.* **142**, 614–622 (2020).
3. Ortiz, G. *et al.* A Silicon-Rhodamine Chemical-Genetic Hybrid for Far Red Voltage Imaging from Defined Neurons in Brain Slice A silicon-rhodamine chemical-genetic hybrid for far red voltage imag- ing from defined neurons in brain slice. **8**, (2020).
4. Grenier, V., Daws, B. R., Liu, P. & Miller, E. W. Spying on Neuronal Membrane Potential with Genetically Targetable Voltage Indicators. *J. Am. Chem. Soc.* **141**, 1349–1358 (2019).
5. Keppler, A. *et al.* A general method for the covalent labeling of fusion proteins with small molecules in vivo. (2002). doi:10.1038/nbt765
6. Sun, X. *et al.* Development of SNAP-tag fluorogenic probes for wash-free fluorescence imaging. *ChemBioChem* **12**, 2217–2226 (2011).
7. Sun, X. *et al.* Development of SNAP-tag fluorogenic probes for wash-free fluorescence imaging. *ChemBioChem* **12**, 2217–2226 (2011).

Appendix 2:
Investigation of Possible Fluorescence-based Ratio Metric Voltage Imaging Systems

Introduction

Optical approaches to measure membrane potential typically report electrical events as changes in fluorescence intensity. However, fluorescence intensity alone cannot reliably report an absolute membrane potential value or an exact millivolt (mV) change[1,2]. Intensity measurements between preparations and experiments are complicated by variations in dye loading, membrane composition (affecting dye concentrations), bleaching rates, illumination and optical path settings making absolute membrane potential calibrations complicated and unreliable. Ratiometric imaging approaches attempt to bypass these issues by measuring more than a single intensity change. For example, using electrochromic dyes or a two-component fluorescent system that relies on two emission values allows for quantitative voltage measurements, or more commonly ion concentrations, based on a calibrated ratio. However, most systems have seen limited success in reliably quantifying mV values and are instead still used to qualitatively detect changes in voltage.

In the process of designing Q-BOLT (discussed in Chapter 3), we found the 2-acceptor resonance energy transfer (RET) system reported a ratio change sensitive to membrane potential. In short, this system has a single donor molecule sandwiched between two spectrally distinct acceptors which have their own distinct RET efficiency with the donor[3]. One of the acceptors, dipacrylamine (DPA), is a dark absorber which has a distance dependent change in efficiency based on the electric field of the membrane. The RET efficiency to the second fluorescent acceptor is not dependent on distance, but dependent on the resulting apparent quantum yield of the donor. Since DPA is non-fluorescent there are only two emission values which allows for a single ratiometric readout. However, with Q-BOLT we found the raw change in the ratio value did not produce high enough resolution to accurately determine an absolute membrane potential. The difference in the ratio at -60 mV and +40 mV, for instance, was roughly 0.06 (± 0.02) making it possible to determine a hyperpolarized from a depolarized cell, but practically impossible to make a reliable mV prediction. One of the hypotheses as to why the dynamic range of the ratio was so small comes down to the limited photon count using bioluminescence. As a result, there is a large error in the fluorescent acceptor BRET measurements because of a poor signal to noise ratio.

We wondered if replacing the luciferase in Q-BOLT with a fluorophore would improve the overall photon emission and still retain the highly sensitive dual-RET voltage sensing mechanism. We explored two variations of this where NanoLuc is replaced with a green fluorescent protein (GFP) or with the self-labeling $SNAP_f$-tag protein. We know from previous FRET and BRET studies that sacrificing the efficiency of energy transfer can result in an increase in functional sensitivity[3,4]. With Q-BOLT specifically, we found there is a sweet spot between energy transfer efficiency and maximum voltage sensitivity. If a fluorescent dual-RET voltage sensing mechanism similarly applies to this system, we reasoned the $SNAP_f$ protein in combination with the HaloTag protein would allow for high-throughput screening of compatible fluorophore ligand pairs to find the most voltage sensitive combination, rather than cloning several different constructs with varying fluorescent proteins.

In a second approach, we wanted to explore the possibility of replacing TMR/DPA molecules in Q-BOLT with RhoVR-HaloTag ligands. The use of a targeted VoltageFluor (VF) would effectively combine (1) the rhodamine acceptor (TMR) and (2) rapid voltage sensor (DPA) into one single molecule. Previous attempts at using RhoVR-HaloTag VFs with bioluminescence did produce a large enough BRET efficiency to detect voltage changes (discussed in Chapter 4). However, using a fluorescent protein may generate a large enough FRET signal and potentially allow for qualitative ratio values relative to membrane potential given the controlled 1:1 A/D ratio.

A third approach to fluorescence based ratiometric voltage sensing is to combine two spectrally distinct VoltageFlours (VF). Our group commonly receives questions from other research affiliations wondering if combining two VFs could be used ratiometrically, however this had not been previously explored. We wondered if the raw ratio from two emission values of voltage sensitive BeRST and voltage in-sensitive VF2.0Cl could be calibrated to resolve absolute membrane potential. If successful, this approach could be an easily accessible method for qualitative voltage measurements without needing cellular protein expression.

Results and Discussion

Chemigenetic hybrid approach to ratiometric voltage imaging

We first screened a variety of acceptor rhodamine-based HaloTag (HT) ligands encompassing a range of VFs with varying linker lengths separating the fluorophore from the reactive chloroalkane moiety, non-permeable TMR-HT ligand, and a cell permeable Janelia Fluor 525 (**Scheme A2-2a-e, Fig. A2-1**). Raw emission scans of HEK293T cells expressing HT-GFP-pD imaged in a 96-well plate show one emission max around 500 nm without the addition of a rhomdaine acceptor (**Fig. A2-1a-c**, grey) and a second emission peak around 590 nm or 560 nm in the presence of a TMR or azetidine based fluorophore, respectively (**Fig. A2-1a-c**, red). We found the difference in magnitude of 590 nm emission with RhoVR0-PEG25-HT to be larger than its voltage sensitive counter part RhoVR1-PEG25-HT (**Fig. A2-1a** and **b,** red), suggesting a better FRET efficiency for the former likely due to the lack of PeT quenching. This is also consistent when comparing raw A/D (rhodamine/GFP) ratios across the suite of dyes (**Fig. A2-1d**). There is an increase in the A/D ratio for all rhodamine-HT ligands (**Fig. A2-1d**, red) with a consistent baseline A/D without dye (black). Additionally, the raw ratio values are consistent for each VF with little spread across each replicate, with the exception of RhoVR0-PEG25-HT with ratio values ranging from 0.25 to 1.0. The reason for this is unclear. For an easier comparison we evaluate the FRET ratio: average A/D ratio in the presence of an acceptor divided by the ratio in the absence of an acceptor. The cell permeable JF525 has the largest FRET efficiency and RhoVR1 with the shortest polyethylene glycol linker (PEG0) has the lowest FRET efficiency (**Fig. A2-1e**, 8 and 1 respectively). We speculate JF525 has a larger FRET efficiency and raw A/D ratio for two reasons: improved spectral overlap with GFP and the ability to internalize which increases the number of molecules participating in FRET.

Live cell imaging shows intracellular and membrane localized GFP expression (**Fig. A2-2b**). Intracellular fluorescence from trafficking fluorescent proteins is common and could potentially be improved using alternative membrane anchoring motifs or secretion signals. The addition of non-permeable TMR-HT shows specific membrane staining of only transfected cells (**Fig. A2-2a-c**). Transient expression of a similar construct that replaces GFP with a second self-labeling protein shows similar results. Cells transfected with HT-SNAPf-DAF show excellent membrane fluorescence with the addition of a non-permeable AlexaFluor-488 SNAP-tag (NEB) substrate and TMR-HT (**Fig. A2-2d-f**). These data indicate successful expression, localization, and functionality of the fusion proteins.

Optimization of membrane localized FRET using epifluorescence microscopy was not investigated due to COVID-19 setbacks. We have set a foundation for future advancements on this project by establishing protein fusion expression, localization, and functionality at the plasma membrane. Additionally, HT-GFP-pD bulk plate reader assays provide a starting point for selecting the best rhodamine acceptor to continue with voltage sensitive studies. For instance,

RhoVR1-PEG9-HT shows the largest VF A/D ratio and may be a good candidate. However, assuming a PEG linker averages 0.3 nm per segment, then the rough (minimum) length between the VF and reactive chloroalkane would be 2.7 nm. The linker needs to be long enough to allow membrane insertion and in doing so would have to account for the size of HT and GFP, estimated to be roughly 3.3 nm and 4.2 nm in length[5,6]. For this reason, the PEG9 linker may not allow for VF insertion into the membrane, however increased flexibility between the proteins may accommodate for this. Alternatively, the RhoVR1-PEG25-HT VF should have a flexible linker long enough to allow for proper membrane insertion. While this VF has a low FRET efficiency (~1.5) the non-voltage sensitive counterpart (RhoVR0) has an efficiency >2.5x larger (~4) suggesting a potential dynamic range of ratios much greater than what we could achieve with Q-BOLT.

Chemical approach to ratiometric voltage imaging using dual VoltageFluors

The third approach to ratiometric voltage sensing is to combine two spectrally distinct VoltageFlours (VF), BeRST1 and VF2.0Cl (**Scheme A2-2g** and **h**). HEK cells were loaded with equimolar concentrations of two VoltageFluors to investigate the possibility of a purely chemical ratiometric strategy. A linear response in the raw A/D ratio is seen with holding potentials from -80 mV to +80 mV (**Fig. A2-3a**). Unfortunately, the variation in the ratio values is large, the voltage response small (.02 change per 100 mV), and as a result we are not able to predict an absolute membrane potential value from cell to cell with any certainty (**Fig. A2-3b**). The relative voltage changes of a single cell, however, can be predicted to some degree. The fractional change in the ratio ($\Delta R/R$) improves the voltage readout (20% per 100 mV) with a higher consistency between voltage changes relative to a baseline of -60 mV (**Fig. A2-3c** and **d)**. After normalizing the -60 mV ratio to 0 for an individual cell, the average difference between the actual and estimated membrane potential based on $\Delta R/R$ is ~10 mV (**Fig. A2-3d**).

Using two untethered VoltageFluors for absolute voltage measurements does not produce consistent raw ratio values. We hypothesize there is likely not a one-to-one ratio between the A/D pair within the membrane due to loading variations, even within the same coverslip. The low raw sensitivity of the system makes it impossible to decipher a difference between -60 mV and -40 mV for example. In the future, this system could be improved by synthetically tethering the two VFs together to reduce variations in loading concentration, however overall solubility of the dye may become an issue. Additionally, pairing BeRST with a reverse-PeT VF may enhance the ratio change, improving the likelihood of decerning between two holding potentials solely based off a raw ratio.

The combination of BeRST with VF2.0Cl is attractive given the experimental simplicity of simply bath loading dye. However, variations in loading concentration and cellular localization within the membrane make it impossible to ensure 1:1 stoichiometry. To achieve a consistent baseline ratio there must be a consistent acceptor:donor stoichiometry from cell-to-cell within a single coverslip, but also across different experiments. Synthetic coupling of the two VFs could circumvent this issue, however solubility of the resulting compound may pose new and separate challenges. The chemigenetic method using two self-labeling enzymes (HT and $SNAP_f$) may be the most promising among the three approaches explored here. The HT-$SNAP_f$ fusion ensures equal stoichiometry which is not as easily controlled with the two other methods. Fusion of HT to GFP works well and the stoichiometry on the extracellular side of the membrane may be equal, however internal GFP fluorescence may vary from cell-to-cell making calibration and analysis challenging. It should also be mentioned that varying rates of photobleaching during longer exposures may add further difficulties in calibrating ratiometric measurements. Absolute

membrane potential measurements may not be possible for constant-illumination recordings. More likely, the hybrid method could allow for small snap shots to track membrane potential throughout a cellular process, the cell cycle for instance. These data are a promising start, but more research is still needed to investigate consistent ratio values and voltage sensing functionality.

Experimental Methods

Cell culture and dye loading

HEK293T cell lines were obtained from the UC Berkeley Cell Culture Facility and discarded after 25 passages. Cells were dissociated during passages using 0.05% Trypsin-EDTA with phenol red (Thermo Fisher Scientific) at 37°C, and then maintained in Dulbecco's Modified Eagle Medium (DMEM) with 4.5 g/L D-glucose supplemented with 10% FBS (Seradigm (VWR); Radnor, PA) and 2 mM 668 GlutaMAX (Gibco) in a 5% CO2 incubator at 37°C.

For all imaging experiments, cells were plated onto 25 mm diameter #1.5 glass coverslips (Electron Microscopy Sciences) in 6 well tissue culture plates (Corning; Corning, NY). To maximize cell attachment, coverslips were treated before use with 1-2 M HCl for 2-5 hours and washed overnight three times with 100% ethanol and three times with deionized water. Coverslips were sterilized by heating to 150°C for 2-3 hours. Before use, coverslips were incubated with poly-D-lysine (Sigma-Aldrich, made as a 0.1 mg/mL solution in phosphate-buffered saline with 10 mM Na_3BO_3) for 2-10 hours at 37°C and then washed twice with water and twice with Dulbecco's phosphate buffered saline (dPBS, Gibco). HEK293T cells were seeded 24 hours before microscopy experiments.

RhoVR and tetramethyl rhodamine HaloTag ligands were previously synthesized by our group[3,7]. Janelia Fluor 525 was purchased from TOCRIS and SNAP-Surface 488 from New England Biolabs. For all experiments, cells were loaded with 500 nM dye in HBSS for 15 minutes at 37°C and 5% CO2, washed 2x with HBSS, and replaced with fresh HBSS. For NanoLuc containing constructs, furimazine substrate (Promega) was added to NanoGlo buffer in a 1:20 dilution, mixed, added to pre-labeled cells and imaged directly after.

Epifluorescence microscopy and CLARIOstar Plus+ microplate reader

All imaging was performed on an inverted epifluorescence microscope AxioObserver Z-1 (Zeiss), equipped with a Spectra-X Light engine LED light (Lumencor), controlled using μManager (V1.4, open-source, Open Imaging). Bioluminescence emission was collected using a 460/30 nm (Semrock) emission filter. For GFP, AF488, and VF2.1Cl images, excitation light was delivered at 475/34 nm using an LED and collected with an emission filter (bandpass; 540/50 nm; 500 ms exposure time, 2ms for electrophysiology experiments) after passing through a 510 LP dichroic mirror. Tetramethyl rhodamine dyes were excited with 550/15 nm light and collected with an emission filter (bandpass; 650/60 nm; 500 ms exposure time) and 594 LP dichroic. The far red BeRST VF was excited at 635/22 nm and emission collected through a QUAD filter set (432/525/595/730) and dichroic (409/493/573/652). Images were acquired using Plan-Apochromat 20/0.8 air objective (20x, Zeiss) and captured on an OrcaFlash4.0 sCMOS camera (sCMOS; Hamamatsu).

Bulk measurements were taken with a CLARIOstar plus plate reader (courtesy of the Martin Lab at UC Berkeley). Emission cans were collected from 490 – 625 nm at 10 Hz with GFP excitation at 470/15 nm. All spectra were normalized to the max peak emission. Ratios were determined from emission values collected using 515/20 and 599/20 filters with exposure times kept at 0.1 seconds (10 Hz).

Electrophysiology

Pipettes were pulled from borosilicate glass with filament (Sutter Instruments, Novato, CA) resistances ranging from 4 to 7 MΩ with a P97 pipette puller (Sutter Instruments). The internal solution composition is as follows, in mM (pH 7.25, 285 mOsmol/L): 125 potassium gluconate, 10 KCl, 5 NaCl, 1 EGTA, 10 HEPES, 2 ATP sodium salt, 0.3 GTP sodium salt. EGTA (tetraacid form) was prepared as a stock solution in either 1 M KOH or 10 M NaOH before addition to the internal solution. Pipettes were positioned with an MP-225 micromanipulator (Sutter Instruments).

Electrophysiology recordings were made with an Axopatch 200B amplifier and digitized with a Digidata 1550B (Molecular Devices). Signals were filtered with a 5 kHz low-pass Bessel filter. Correction for pipette capacitance was performed in the cell attached configuration. Images were acquired while in voltage-clamp mode at the designated holding potential for 2-4 seconds. Holding potentials applied varied from -80mV to +80 mV, with +20 mV increments and a -60mV holding potential between each step. Potentials were applied in random order, and a membrane test was conducted between each step to verify the quality of the patch. Recordings of single cells were only included if they maintained a 10:1 ratio of membrane resistance (Rm) to access resistance (Ra) and an Ra value below 30 MΩ throughout the recording, although most recordings maintained a 20:1 ratio or better.

Cloning and transient transfections

HEK293T cells plated in a 6 well tissue culture dish were incubated at 37°C in a humidified incubator for at least 24 hours prior to transfection. Once cells reached ~60-75% confluency, transfections were performed with Lipofectamine 3000, using half the recommended p3000 and a quarter of the lipofectamine volumes suggested from the manufacturer's protocol (Thermo Fisher Scientific). We found reducing the amount of lipofectamine significantly increased cell health without dramatically reducing the transfection efficiency. Cells were allowed to grow an additional 5-10 hours after transfection before being plated onto glass coverslips for microscopy experiments (described above).

For expression in HEK cells, all constructs were sub-cloned into a pcDNA3 vector with a leading N-terminal IgK secretion signal and a single pass pDisplay transmembrane domain or a GPI-anchor (the decay accelerating factor, DAF) fused at the C-terminal of the protein fusion. The name of each construct, corresponding order of each domain, and Benchling link is as follows:

IgK – HaloTag – (GS linker) – GFP – pDisplay (*benchling*)
IgK – HaloTag – (GS linker) – SNAPf – DAF (*benchling*)

Schemes and Figures

Scheme A2-1. *Ratiometric voltage sensing strategies*

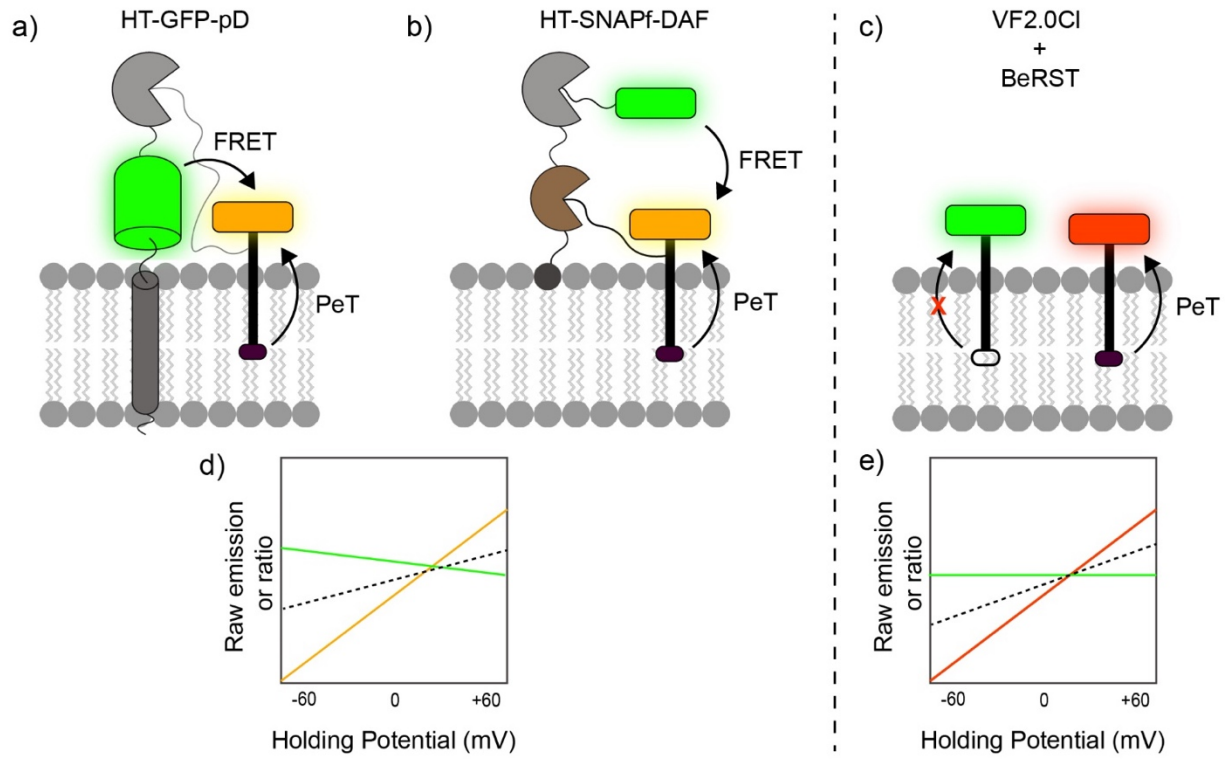

Scheme A2-1. Ratiometric voltage sensing strategies. a) and **b)** Chemigenetic approaches to ratiometric voltage sensing combing HaloTag (HT, light grey) and GFP (green) or SNAP-tag (SNAPf, brown) proteins. **a)** A HaloTag-GFP fusion anchored to the membrane using a single alpha helical domain, pDisplay (dark grey), requires the addition of only a RhoVR-HaloTag VoltageFluor (orange). GFP fluorescence and VF FRET emissions are modulated by a voltage sensitive photo-induced electron mechanism (PeT). The same voltage mechanism applies for **b)** the HT-SNAPf construct (anchored using a DAF GPI anchor, dark grey) but allows for easy fluorophore modulation. For simplicity, GFP is replaced with a fluorescein-based HT ligand which acts as a spectrally similar FRET donor. With increasing membrane potential (mV) **d)** its hypothesized the RhoVR VF emission from FRET increases linearly (orange line) based on PeT, while GFP fluorescence simultaneously decreases (green line) with increasing FRET efficiency (or reduction in PeT quenching). Ideally the ratio (dotted black line) will show a large increase and with an equivalent protein:dye ratio may allow for consistent absolute membrane potential estimates based on raw ratio values. An alternative **c)** chemical approach combines the non-voltage sensitive VF2.0Cl (green) with a far-red voltage sensitive BeRST VF (red). With increasing membrane potential **e)** VF2.0Cl emission should remain relatively constant (green line) while only the fluorescence from BeRST will increase (red line) resulting in an increase in the ratio (dotted black line).

Scheme A2-2. *Chemical structures of indicators*

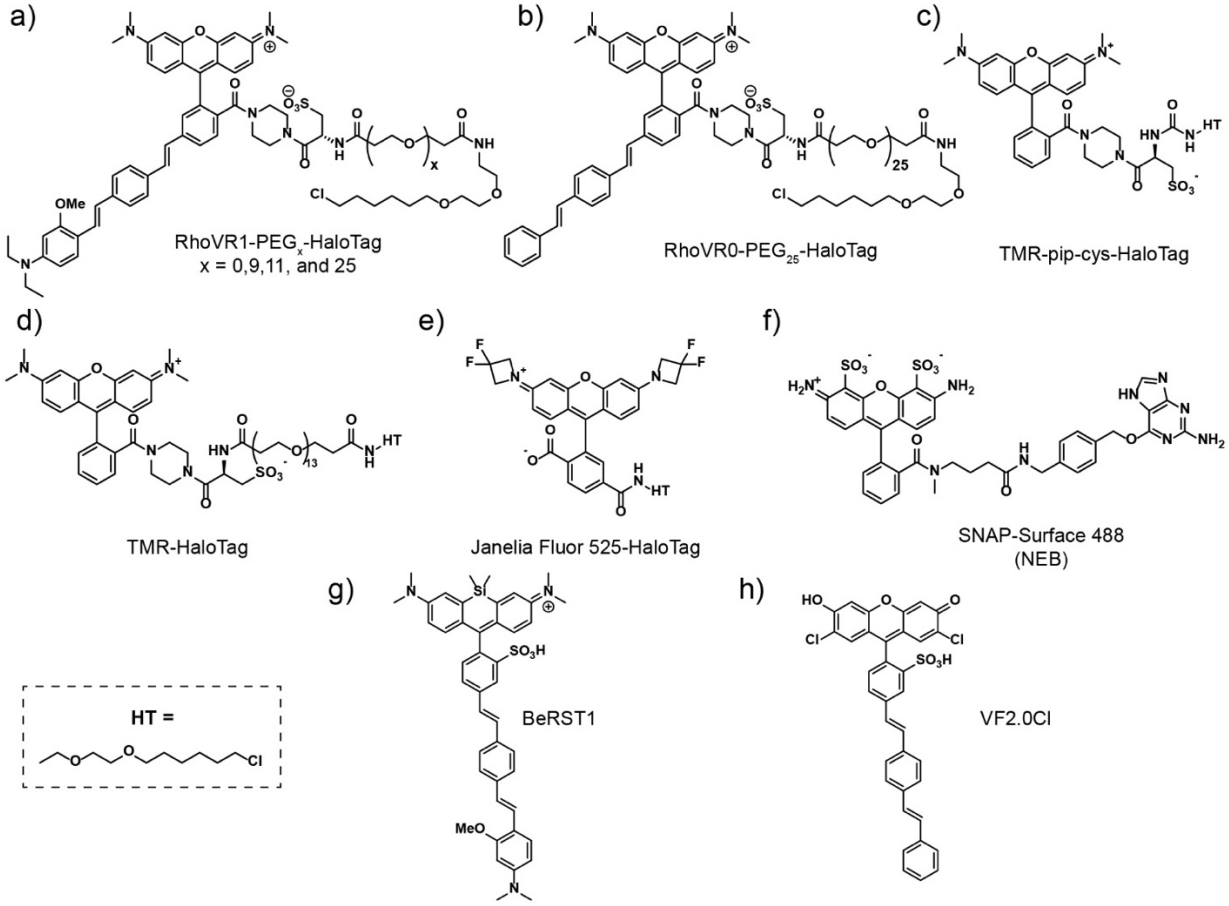

Figure A2-1. *FRET rhodamine acceptor screening using bulk imaging*

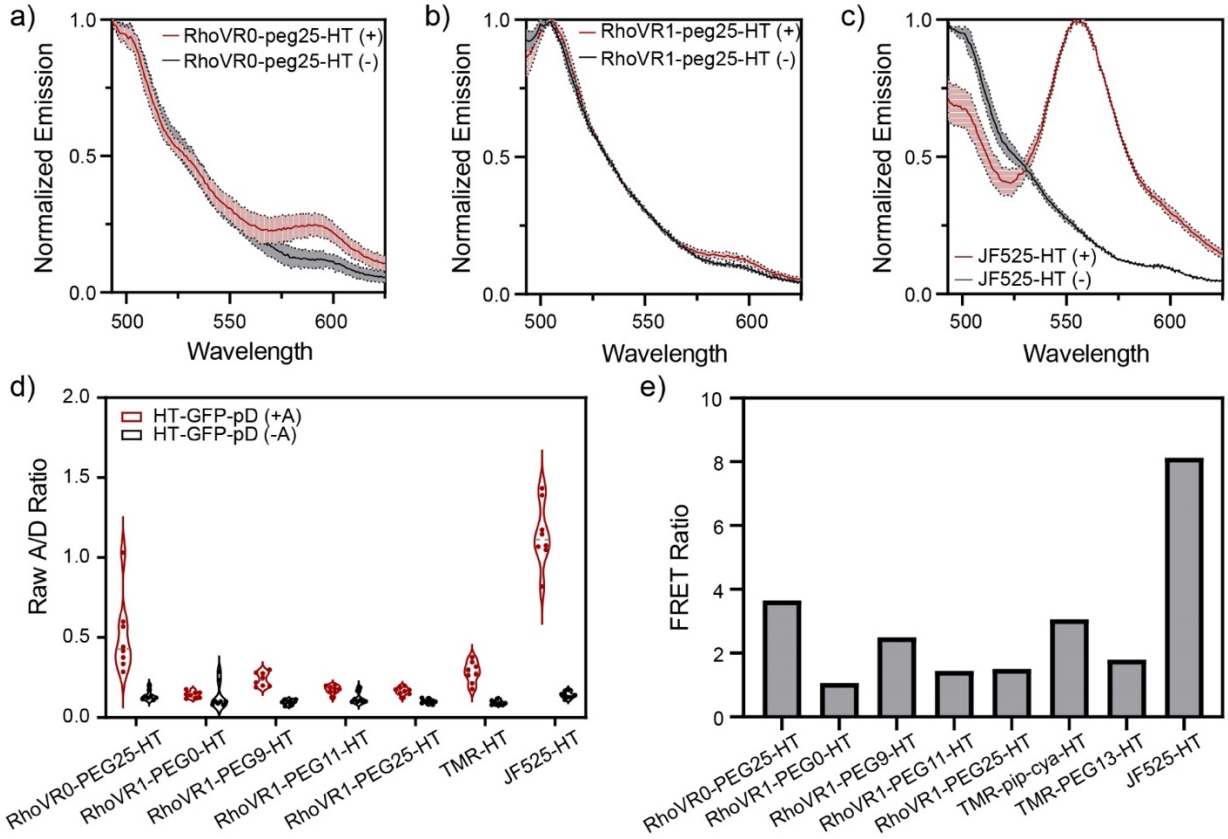

Figure A2-1. FRET rhodamine acceptor screening using bulk imaging. **a-c)** Normalized emission scans from 490-625 nm of HEK cells expressing HT-GFP-pD with or without a rhodamine-HaloTag (HT) acceptor (red and grey, GFP emission max = 500 nm, RhoVR-HT emission max = 590 nm, JF_{525} emission max = 560 nm). **d)** Raw acceptor-donor (A/D) ratios from wells before (black) and after the addition of various rhodamine-HaloTag (red). **e)** FRET ratios calculated from the data in d) determined by dividing average ratios in the presence of an accepter (red) by the ratios without an acceptor (black). n = 8 wells per condition.

Figure A2-2. *Ratiometric construct expression and localization in HEK cells*

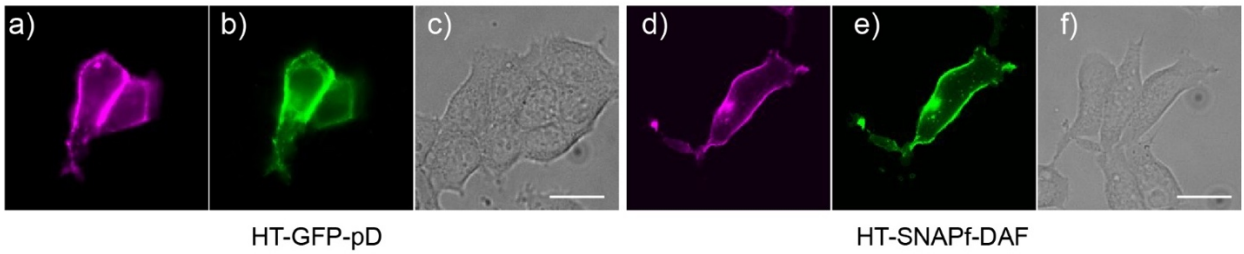

Figure A2-2. Ratiometric construct expression and localization in HEK cells. Live cell epifluorescent images of **a)** TMR-HT, **b)** GFP, and **c)** transmitted light emission in HEK expressing HT-GFP-pD. Similar images of HEK cells expressing HT-SNAPf-DAF and labeled with **d)** TMR-HT, **e)** AF-488 SNAP, and **f)** cell permeable JF525. Scale bars are 20 μm.

Figure A2-3. *Chemical-based ratiometric calibrations using BeRST and VF2.0Cl to determine absolute membrane potential*

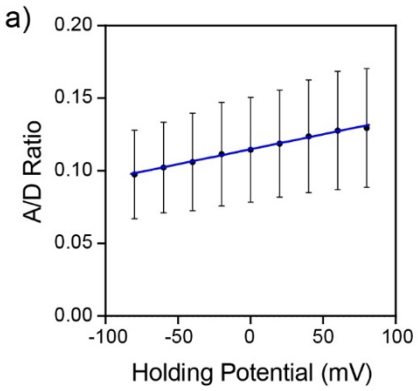

b)

Holding Potential (mV)	Measured Ratio cell 1	Measured Ratio cell 2	Estimated mV cell 1	Estimated mV cell 2
-80	0.059	0.188	-28	38
-60	0.064	0.195	-25	42
-40	0.064	0.206	-25	47
-20	0.069	0.218	-23	53
0	0.069	0.222	-23	55
20	0.072	0.228	-21	58
40	0.076	0.239	-19	64
60	0.076	0.249	-19	69
80	0.079	0.251	-18	70

Equation of best fit line + Use ratio to estimate mV

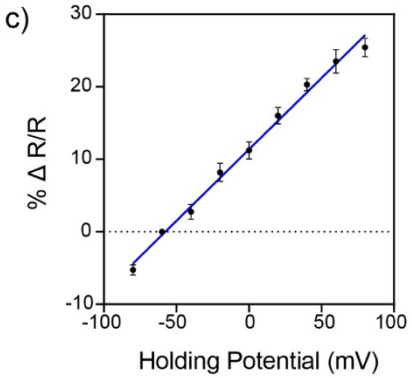

d)

Holding Potential (mV)	Fractional Change cell 1	Fractional Change cell 2	Estimated mV cell 1	Estimated mV cell 2
-80	-0.069	-0.038	-96	-80
-60	0.000	0.000	-60	-60
-40	0.007	0.054	-56	-32
-20	0.086	0.114	-15	-1
0	0.082	0.136	-17	11
20	0.141	0.168	13	27
40	0.191	0.222	39	56
60	0.198	0.274	43	82
80	0.240	0.283	65	87

Equation of best fit line + Use ratio to estimate mV

Figure A2-3. Chemical-based ratiometric calibrations using BeRST and VF2.0Cl to determine absolute membrane potential. a) Average raw BeRST:VF2.0Cl (A/D) ratio as a function of voltage in HEK cells held from -80 mV to +80 mV (n=4 cells). **b)** Two representative cells and their respective ratio values at each holding potential (mV) and the resulting estimated membrane potential value using the equation from the best fit line (blue, y= .0002x + 0.1146, R^2 = 0.02795). **c)** Average fractional change in the A/D ratio from data in a) as a function of voltage. **d)** Fractional change of the ratio for each individual cell relative to their -60 mV value. The two representative cells are the same shown in b). Similarly, these fractional change values are used to estimate the membrane potential using the line of best fit (blue, y= .001924x + .1154, R^2 = 0.96). Error bars are SEM.

References

1. Ehrenberg, B. & Loew, L. M. Absolute spectroscopic determination of cross-membrane potential. *J. Fluoresc.* **3**, 265–269 (1993).
2. Lazzari-Dean, J., Gest, A. & Miller, E. Optical determination of absolute membrane potential. *bioRxiv* 519736 (2019). doi:10.1101/519736
3. Benlian, B. R. *et al.* Small Molecule-Protein Hybrid for Voltage Imaging via Quenching of Bioluminescence. *ACS Sensors* (2021). doi:10.1021/acssensors.1c00058
4. Machleidt, T. *et al.* NanoBRET-A Novel BRET Platform for the Analysis of Protein-Protein Interactions. *ACS Chem. Biol.* **10**, 1797–1804 (2015).
5. Hink, M. A. *et al.* Structural dynamics of green fluorescent protein alone and fused with a single chain Fv protein. *J. Biol. Chem.* **275**, 17556–17560 (2000).
6. Yazaki, J. *et al.* HaloTag-based conjugation of proteins to barcoding-oligonucleotides. *Nucleic Acids Res.* **48**, 2–13 (2020).
7. Deal, P. E. *et al.* Covalently Tethered Rhodamine Voltage Reporters for High Speed Functional Imaging in Brain Tissue. *J. Am. Chem. Soc.* **142**, 614–622 (2020).

Appendix 3:
Alternative Approaches to Improve Ratio Metric Bioluminescent Voltage Imaging with Q-BOLT

Introduction

Photon emission and collection is a limiting factor in measuring membrane potential using Q-BOLT-based probes (Chapter 2). Voltage changes can be monitored via bioluminescence quenching between NanoLuc and the lipophilic voltage sensor DPA, or through bioluminescence resonance energy transfer (BRET) with the addition of a TMR HaloTag-ligand. Under optimal conditions these voltage responses are highly sensitive (up to 100% ΔBRET/BRET per 100 mV)[1]; however, the signal to noise limits practical applications *in vivo.* Previous studies screening structural modifications of the luciferin or directed evolution of the luciferase have drastically improved luminescence output.[2,3] However, the NanoLuc-furimazine pair used in Q-BOLT is one of the best and brightest, leaving little room for luminescence optimization to improve the overall BRET signal. Energy transfer efficiency is also heavily influenced by acceptor-donor orientation and distance which is certainly not optimal in Q-BOLT. We reasoned an improved BRET efficiency could be achieved by bringing the HaloTag and NanoLuc proteins side-by-side, rather than on-top of one another (**Scheme A3-1**).

The two strategies we used to achieve this goal involve 1) a single protein fusion using a double-pass transmembrane domain and 2) bicistronic protein fusions using versatile interacting peptide (VIP) tags.[4,5] Most membrane targeting motifs used in our group have utilized a single pass transmembrane domain or a lipid anchor. Separate NanoLuc and HaloTag proteins with individual anchoring motifs could easily be expressed at the membrane but may not localize close enough together for efficient BRET or express at a one-to-one ratio.

Both these issues could be addressed by using a double-pass transmembrane domain with each protein fused at the N- and C- terminals or by using high affinity coiled-coil VIP tags. Theoretically, a double pass transmembrane domain should be possible based on secondary protein structure and the propensity to form hydrophobic alpha helices. In other words, there is not a conserved primary amino acid sequence for transmembrane helices. We wondered if we could take the first two helices of an already known multi-pass membrane protein and fuse NanoLuc and HaloTag on the N- and C- terminals, with the hopes of translocating the fusion to the plasma membrane with both termini on the extracellular side (**Scheme A3-1b**). To do this we took the sequence containing the first two helices of the Ace2 rhodopsin, a commonly used protein sensor for that can be easily expressed to the cell membrane[6], and promoted membrane localization using three combinations of the IgK and Kir secretion signals. Alternatively, we also tried to build a Q-BOLT system using VIP technology which takes advantage of high affinity coiled-coil interactions between two peptide tags, coil E and coil R[5]. We aimed to fuse HaloTag and NanoLuc to the N-terminal of each coil E and coil R tag (**Scheme A3-1c**), on the same DNA plasmid, to bring the proteins side-by-side, in close proximity to one another, and in a one-to-one ratio.

Results and Discussion

Three double-transmembrane domain (dTMD) constructs derived from the first two helices of the rhodopsin, Ace2, were tested for expression with varying secretion targeting motif combinations: (1) IgK only, (2) KirSS only, and (3) both IgK and KirSS. In all constructs NanoLuc was linked to the N-terminal of the transmembrane spanning domains and HaloTag to the C-terminal. However, regardless of the secretion signal expression of the fusion proteins appeared to be toxic in HEK293T cells for all three constructs (**Fig. A3-1**). All cells labeled with a rhodamine-HaloTag ligand appeared dead.

Expression of the VIP tags fused to NanoLuc and HaloTag has not yet been explored. While this modification to Q-BOLT is promising, cloning of this construct has not been completed.

For ease of cloning, we designed two plasmids with the following domain orders: (1) IgK-HaloTag-HA-pDisplay-CoilE and (2) Igk-myc-NanoLuc-pDisplay-CoilR. The isotope tags, HA and myc, were included for location and expression verification incase functionality of the HaloTag or NanoLuc proteins was hindered. We successfully subcloned plasmid (2) into a pcDNA3 backbone, however insertion of the Coil E peptide after pDisplay has not been successful for unknown reasons. We also designed a plasmid similar to construct (2) that replaces NanoLuc with GFP, however a full plasmid has yet to be pieced together. Cloning fragments and primers are included in detail under the experimental section below.

Experimental Methods

Cell culture, transient transfections, and dye loading

HEK293T cell lines were obtained from the UC Berkeley Cell Culture Facility and discarded after 25 passages. Cells were dissociated during passages using 0.05% Trypsin-EDTA with phenol red (Thermo Fisher Scientific) at 37°C, and then maintained in Dulbecco's Modified Eagle Medium (DMEM) with 4.5 g/L D-glucose supplemented with 10% FBS (Seradigm (VWR); Radnor, PA) and 2 mM 668 GlutaMAX (Gibco) in a 5% CO2 incubator at 37°C.

For all imaging experiments, cells were plated onto 25 mm diameter #1.5 glass coverslips (Electron Microscopy Sciences) in 6 well tissue culture plates (Corning; Corning, NY). To maximize cell attachment, coverslips were treated before use with 1-2 M HCl for 2-5 hours and washed overnight three times with 100% ethanol and three times with deionized water. Coverslips were sterilized by heating to 150°C for 2-3 hours. Before use, coverslips were incubated with poly-D-lysine (Sigma-Aldrich, made as a 0.1 mg/mL solution in phosphate-buffered saline with 10 mM Na_3BO_3) for 2-10 hours at 37°C and then washed twice with water and twice with Dulbecco's phosphate buffered saline (dPBS, Gibco). HEK293T cells were seeded 24 hours before microscopy experiments.

Transfections were performed with Lipofectamine 3000, using half the recommended p3000 and a quarter of the lipofectamine volumes suggested from the manufacturer's protocol (Thermo Fisher Scientific). We found reducing the amount of lipofectamine significantly increased cell health without dramatically reducing the transfection efficiency. Cells were treated with the transfection solution at least 1 hour after plating and imaged 18-24 hours later.

Cells were loaded with 500nM TMR-HaloTag dye (synthesis described in Chapter 3) in HBSS for 15-20 minutes at 37°C and 5% CO2. Cells were washed 2x with HBSS and replaced with fresh HBSS for imaging. Cells were used immediately after loading the dye and no cells remained at room temperature for longer than an hour.

Live cell microscopy

All imaging was performed on an inverted epifluorescence microscope AxioObserver Z-1 (Zeiss), equipped with a Spectra-X Light engine LED light (Lumencor), controlled using μManager (V1.4, open-source, Open Imaging). Bioluminescence emission was collected using a 460/30 nm (Semrock) emission filter (10 second exposure). Tetramethyl rhodamine was excited with 550/15 nm LED light and collected with an emission filter (bandpass; 650/60 nm; 500 ms exposure time) and 594 LP dichroic. Images were acquired using Plan-Apochromat 20/0.8 air objective (20x, Zeiss) and captured on an OrcaFlash4.0 sCMOS camera (sCMOS; Hamamatsu).

Cloning

All dTMD constructs were sub-cloned into a pCAG vector with transmembrane domains from the first two helices of Ace2 rhodopsin. Constructs contained either a leading N-terminal IgK

secretion signal, a C-terminal Kir secretion signal (KirSS), or both. The VIP construct was cloned into a pcDNA3 backbone and only included the IgK secretion signal. Following the N-terminal secretion signal is either HaloTag or NanoLuc, an isotope tag (HA or myc), a single pass alpha helical transmembrane domain (pDisplay), and a VIP tag (Coil E/R). The two peptide tagged fusions are separated by a self-cleaving T2A peptide. The name of each construct, corresponding order of each domain, and Benchling link are as follows:

1. IgK – NanoLuc$_{outisde}$ – TMD1 – loop$_{inside}$ – TMD2 – HaloTag$_{outisde}$ (*benchling*)
2. NanoLuc$_{outisde}$ – TMD1 – loop$_{inside}$ – TMD2 – HaloTag$_{outisde}$ – KirSS (*benchling*)
3. IgK – NanoLuc$_{outisde}$ – TMD1 – loop$_{inside}$ – TMD2 – HaloTag$_{outisde}$ – KirSS (*benchling*)
4. IgK – HaloTag – HA – pDisplay – CoilE – T2A – IgK – myc – NanoLuc – pDisplay – CoilR (*benchling*)

Cloning details for the unfinished VIP tag fusions (4):

#	Gene	Forward primer	Reverse Primer	Nuclease
1	IgK-HT-HA-pD	TAATACGACTCACTATAGGG	AGAAGAAGCCACGTGGTGGATCC CTGGAAATCGAAGCAGC	--
2	Coil E	CCTCATCATGCTTTGGCAGAAGAAGC CACGTGGTGGATCCCTGGA	TATAGGACTCGATACGGC	--
3	T2A	AATATAGGACTCGATACGGCCCCCTC GGGGGAGGCGAGGGTCGGGGCT	CCCGGGGTCGACAATGGAGACAG ACACACTCCTGCTATGGGTACT	--
4	IgK-myc-NLuc-pD-Coil R	ATGGAGACAGACACACTCCT	CCTCGACTGTGCCTTCTA	--
6	pcDNA3	--	--	KpnI/Xho I

Schemes and Figures

Scheme A3-1. *Alternative models for improved Q-BOLT voltage imaging*

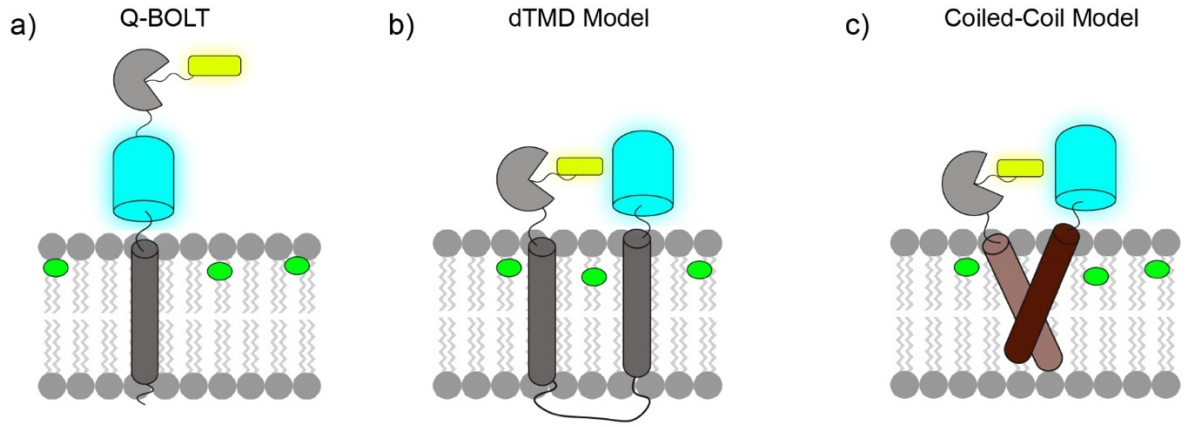

Scheme A3-1. Alternative models for improved Q-BOLT voltage imaging. a) Basic model of Q-BOLT with the HaloTag domain (HT; grey) and non-permeable HT-ligand (yellow) oriented above the NanoLuc luciferase (cyan) with dipacrylamine (DPA; green) within the membrane. Alternative models place the two protein domains, and as a result the HT-ligand acceptor and luciferase donor, side by side via **b)** a double alpha helical transmembrane domain or **c)** a coiled-coil dimerization model using VIP tags (dark and light red).

Figure A3-1. *Characterization of dTMD constructs in HEK cells*

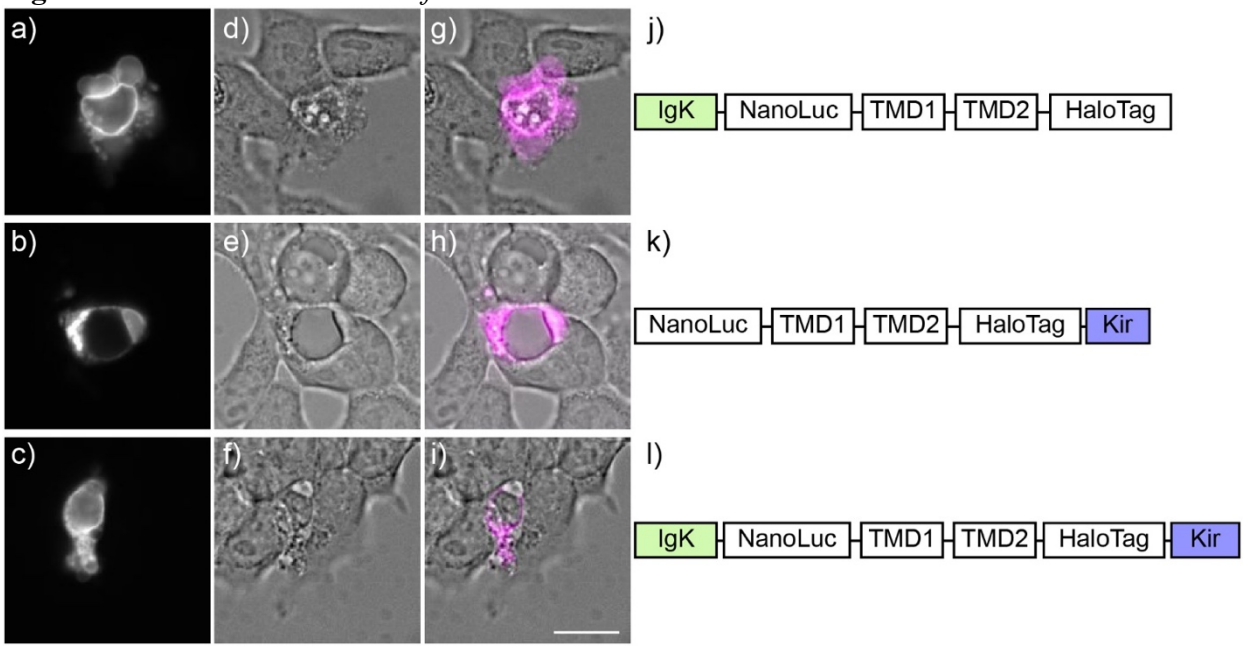

Figure A3-1. Characterization of dTMD constructs in HEK cells. a-c) Live cell fluorescence images of HEK cells labeled with 500 nM TMR-pip-cya-HaloTag, alongside the respective **d-f)** transmitted light and **g-i)** merged images after transient transfection of a NanoLuc-dTMD-HaloTag containing **j)** an N-terminal leading secretion signal (IgK), **k)** a C-terminal potassium channel membrane trafficking and ER export signal (Kir), or l) both secretion and export signals. Scale bar is 15 μm.

References

1. Benlian, B. R. *et al.* Small Molecule-Protein Hybrid for Voltage Imaging via Quenching of Bioluminescence. *ACS Sensors* (2021). doi:10.1021/acssensors.1c00058
2. Hall, M. P. *et al.* Engineered luciferase reporter from a deep sea shrimp utilizing a novel imidazopyrazinone substrate. *ACS Chem. Biol.* **7**, 1848–1857 (2012).
3. Suzuki, K. *et al.* Five colour variants of bright luminescent protein for real-time multicolour bioimaging. *Nat. Commun.* **7**, 13718 (2016).
4. Zane, H. K., Doh, J. K., Enns, C. A. & Beatty, K. E. Versatile Interacting Peptide (VIP) Tags for Labeling Proteins with Bright Chemical Reporters. *Chembiochem* **18**, 470–474 (2017).
5. Doh, J. K. *et al.* VIPER is a genetically encoded peptide tag for fluorescence and electron microscopy. *Proc. Natl. Acad. Sci. U. S. A.* **115**, 12961–12966 (2018).
6. Deo, C. & Lavis, L. D. Synthetic and genetically encoded fluorescent neural activity indicators. *Current Opinion in Neurobiology* **50**, (2018).

Appendix 4:
Genetic Targeting of Optical Voltage Sensors at Intracellular Organelle Membranes

Introduction

The electrochemical gradient maintained across a cell's membranous bilayers is fundamental in excitable cell-to-cell communication and in common cellular processes like migration, differentiation, and cell cycle regulation[1,2]. Likewise, intracellular membrane-bound organelles can maintain ion gradients creating a voltage difference within the lumen relative to the cytosol. While a comprehensive profile of the precise mechanisms detailing the functional roles of each organellular membrane potential remains elusive, mitochondria are a great example of the most extensively studied. We know the mitochondrial membrane potential (V_{Mito}) is essential for cellular respiration and, when dysregulated, can result in neurodegenerative diseases, cancer, and metabolic disorders[3,4]. On the other hand, relatively less is known about the mechanistic details and roles of phagosome and lysosomal membrane potential (V_{Lys}) changes, though more investigative studies are emerging. From these studies we know proper lysosomal function requires constant luminal maintenance which includes ionic homeostasis, with an estimated V_{Lys} 20-40 mV more positive than the cytosol[5]. It's postulated that V_{Lys} may be an important controller of lysosomal acidification, catabolite export, and trafficking; however, more in depth studies measuring V_{Lys} during these processes are needed[5,6].

Optical methods are a promising approach to measure organelle membrane potentials given the reduced invasiveness, especially compared to traditional electrode-based measurements. Commonly used optical indicators produce a readout of voltage differences based on changes in fluorescence intensity, FRET efficiency, or dye localization. However, reliable indicators for intracellular measurements are lacking and limited partly due to a lack of organelle targeting specificity or pH sensitivity. To address this, we present the progress of two mitochondrial and lysosomal voltage indicators inspired by previous sensors developed within our lab and others.

Mitochondrial targeting

Our group synthesized a new mitochondrial indicator, SPIRIT RhoVR1, composed of the VoltageFluor RhoVR1 coupled to a labile acetoxymethyl (AM) ester group[7]. The overall cationic charge of SPIRIT RhoVR1 drives the VF into the negatively charged environment of the mitochondrial matrix where the AM ester is cleaved by endogenous esterases. Removal of the AM ester reveals the RhoVR1 carboxylate and traps the now net-neutral VF within the inner membrane of the mitochondria to sense voltage through the conventional PeT-based mechanism of our VF dyes. While we demonstrate SPIRIT RhoVR1 has excellent mitochondria localization, retention, and reversible responses to hyper- and depolarization events, it is highly possible for cytosolic esterases to hydrolyze the VF before reaching the mitochondrial matrix. Premature hydrolysis leaves free RhoVR1 within the cytosol to load into alternative organellular membranes which may hamper the signal to noise ratio and voltage response of properly localized SPIRIT RhoVR. Here we chose a chemical-genetic hybrid approach to improve targeting by replacing the AM ester with a bulkier cyclopropyl methyl ester (CPME) moiety, RhoVR-CPM, paired with exogenously expressed pig-liver esterase (PLE) enzyme. Previous studies show PLE is capable of cleaving bulky esters both intra- and extracellularly, and can specifically remove CPME from a VF[8,9]. Replacement of the smaller AM ester in SPIRIT RhoVR1 should reduce hydrolysis by native esterases within the cytosol and result in RhoVR1 unmasking only in cells expressing mitochondrial matrix targeted PLE.

Lysosomal targeting

In recent reports by Matamala et al., the group extended the application of the chemical-hydrid hVoS system combing the voltage sensitive dipacrylamine, DPA, with a fluorescent protein to report voltage changes in membrane potential based on FRET efficiency within organelles

($hVoS_{org}$)[10,11]. DPA is a dark absorber which has both lipophilic and anionic characteristics. The small molecule localizes within lipid bilayers and redistributes between the inner and outer leaflets based on the electrical field potential. Matamala et al. reasoned that DPA must have an equilibrium with all membranes, not just the plasma membrane, and so membrane potential should be measurable at organelles too. Our work creating the bioluminescent voltage sensor, Q-BOLT, was also inspired by the original hVoS system but replaces the fluorescent protein with a bioluminescent luciferase[12]. Here we show successful targeting of NanoLuc to the endosomal-lysosomal pathway by fusion to the c-terminus of the lysosomal membrane protein, LAMP1[10]. Fusion to the c-terminus of LAMP1 places the luciferase in the cytosol. With successful localization of the luciferase, we reasoned Q-BOLT could be applied to internal membranes and used to detect voltage changes similar to $hVoS_{org.}$

Results and Discussion

PLE targeting to the mitochondrial matrix

We set out by working on the synthesis of RhoVR-CPM and PLE protein targeting in tandem. Synthetic efforts were done by group member, Julia Martin, but only preliminary efforts on PLE targeting will be discussed. Previous work in our group showed that while PLE needs to traffic through the endoplasmic reticulum (ER) to maintain activity, removal of the ER retention signal and redirection to the plasma membrane using a secretion signal did not destroy enzymatic activity[9]. Replacement of the secretion signal with a transit peptide from human cytochrome c VIII[13] (**Fig. A4-1a**) shows intracellular PLE localization in immunofluorescence stains of permeabilized HEK cells (**Fig. A4-1-b and c**). The colocalization of PLE immunofluorescence and MitoTracker Red is similar but not perfect (**Fig. A4-1-d-g**). The poor spatial resolution of the fluorescent images from immunostaining makes it difficult to distinguish small puncta as seen with the small molecule mitochondrial tracker, creating a rather blurred region of localization. It is unclear if these results indicate suboptimal trafficking and/or artifacts from fixation and staining. Given these data, we believe the mitochondrial matrix targeting sequence (MMTS) from cytochrome c VIII may be trafficking the protein to the matrix, however it is unclear to what extent PLE may be stuck in other organelles, like the ER.

New construct designs are underway to fuse a green or red fluorescent protein (FP) to the c-terminus of PLE. These PLE-FP fusions will enable live cell imaging with known fluorescent organelle indicators to improve targeting verification efforts. Functional assays in living cells with fluorogenic substrates will also confirm PLE enzymatic activity which should colocalize with FP fluorescence.

Lysosomal NanoLuc targeting

HEK293T cells expressing the LAMP1-NanoLuc construct show distinct bioluminescent puncta after the addition of the furimazine substrate (**Fig. A4-2a**). Nuclear localized GFP was used as an indicator to make identification of transfected cells easier, however the addition of the fluorescent lysosomal indicator, Lysoview, appeared to diffuse the nuclear signal throughout the cell (**Fig. A4-2b,** compare nuclear GFP in cell 2 versus no clear nuclear outline in cell 1). The localization pattern is similar to the fluorescence emission from Lysoview (Biotium, **Fig. A4-2c** and **d**) suggesting successful lysosomal targeting. It is worth noting that colocalization is not perfect likely because of organelle movement between acquisitions, given the 10 second exposure time used to capture higher resolution bioluminescent images.

Voltage sensitivity has not yet been investigated. We predict bioluminescence alone should decrease in response to depolarization, in the presence of DPA, however these experiments may

be challenging to using bioluminescence changes alone. Future experiments should take this challenge into consideration and may benefit from adding a FRET pair using HaloTag or fluorescent protein to the c-terminal of NanoLuc to buffer non-functional emission fluctuations.

Experimental Methods

Cell culture, transfection and dye/substrate loading

HEK293T cell lines were obtained from the UC Berkeley Cell Culture Facility and discarded after 25 passages. Cells were dissociated during passages using 0.05% Trypsin-EDTA with phenol red (Thermo Fisher Scientific) at 37°C, and then maintained in Dulbecco's Modified Eagle Medium (DMEM) with 4.5 g/L D-glucose supplemented with 10% FBS (Seradigm (VWR); Radnor, PA) and 2 mM 668 GlutaMAX (Gibco) in a 5% CO2 incubator at 37°C. Transfection of plasmids was carried out using Lipofectamine 3000 (Invitrogen) ~18-24 h after plating cells onto plastic. For all imaging experiments, cells were plated 12-24 hours after transfection onto 25 mm diameter #1.5 glass coverslips (Electron Microscopy Sciences) in 6 well tissue culture plates (Corning; Corning, NY). To maximize cell attachment, coverslips were treated before use with 1-2 M HCl for 2-5 hours and washed overnight three times with 100% ethanol and three times with deionized water. Coverslips were sterilized by heating to 150°C for 2-3 hours. Before use, coverslips were incubated with poly-D-lysine (Sigma-Aldrich, made as a 0.1 mg/mL solution in phosphate-buffered saline with 10 mM Na_3BO_3) for 2-10 hours at 37°C and then washed twice with water and twice with Dulbecco's phosphate buffered saline (dPBS, Gibco). HEK293T cells were seeded 24 hours before microscopy experiments.

Prior to imaging, cells were loaded with dye following manufacturer protocols in HBSS for 20 minutes at 37°C and 5% CO2. Mitotracker red was applied at 1x concentration and Lysoview at 0.5x. Cells were washed with HBSS and replaced with fresh HBSS prior to imaging. Furimazine substrate (Promega) was added to NanoGlo buffer (1:10 dilution), mixed, added to cells and imaged immediately.

Immunostaining and fixation

To detect expression and localization of PLE, HEK cells were fixed with 4% paraformaldehyde in PBS for 10 min and permeabilized with 0.3% v/v Triton-X100 (Sigma Aldrich) in PBS for 2 min. Blocking was done in 5% w/v bovine serum albumin (BSA; Sigma Aldrich) in PBS for 1 h. Primary antibody was incubated at 4 °C overnight, followed by AlexaFluor secondary antibody (Life Technologies) at room temperature for 2 h. All antibodies were used at 1:1000 dilution.

Name	Primary/Secondary	Manufacturer	Catalog #	Isotype
Anti-HA	Primary	CST	2367S	Mouse IgG
Anti-mouse 405S	Secondary	Biotium	20380	Goat IgG

Live cell microscopy

All imaging was performed on an inverted epifluorescence microscope AxioObserver Z-1 (Zeiss), equipped with a Spectra-X Light engine LED light (Lumencor), controlled using μManager (V1.4, open-source, Open Imaging). Bioluminescence emission was collected using a 460/30 nm (Semrock) emission filter (10 second exposure). For SPOT2.1Cl images, excitation light was delivered at 475/34 nm using an LED and collected with an emission filter (bandpass; 540/50 nm; 100 ms exposure time) after passing through a 510 LP dichroic mirror. Images were

acquired using Plan-Apochromat 20/0.8 air objective (20x, Zeiss) and captured on an OrcaFlash4.0 sCMOS camera (sCMOS; Hamamatsu).

Plasmid construction

For expression in HEK cells, PLE with a mitochondrial matrix targeting sequence (MMTS) on the N-terminal and an HA tag on the C-terminal was subcloned into a pcDNA3 vector with a cytomegalovirus (CMV) promoter. The partial MMTS sequence was created by annealing primers together to create a mini gene block (see below). For lysosomal expression, LAMP1 with NanoLuc on the C-terminal was also subcloned into a pcDNA3 vector with the cytomegalovirus (CMV) promoter. Nuclear-targeted GFP (NLS-GFP) was inserted downstream of PLE or NanoLuc, separated by self-cleaving T2A peptide sequence. All constructs were verified by sequencing.

MMTS Gene Block
Annealing Protocol:

Gene	Forward primer	Reverse Primer
MMTS	AGAGGCCGCTGCCCCGCC CGTCGGCACTACAGACGA CTCGCCCTGCTTGGGTGC AGCCT	AGGCTGCAACCCAAGCAGG GCGAGTCGTCTGTAGTGCC GACGGGCGGGGCAGCGGCCTCT

Dissolve each oligonucleotide in a volume of Annealing Buffer so that each has the same concentration.
The concentration of each oligonucleotide needs to be 2X the desired concentration of the duplex oligonucleotide.

Annealing Buffer Composition (1X)

10 mM Tris, pH 7.5 - 8.0
50 mM NaCl
1 mM EDTA

---

1. Mix equal volumes of the equimolar oligonucleotides in a PCR tube.
2. Use the following thermal profile:
    a. Heat to 95 °C and maintain the temperature for 2 min.
    b. Cool to 25 °C over 45 min.
    c. Cool to 4 °C for temporary storage.
3. Centrifuge the PCR tube briefly to draw all moisture away from the lid and measure concentration using a nanodrop.
4. Use the gene block in the following Gibson assembly.

The following sequences and primer pairs were used (5' to 3'):
(intermediate construct) MMTS-PLE-HA-DAF-T2A-NLS-GFP

Fragment #	Gene	Forward primer	Reverse Primer	Nuclease
1	Backbone to MMTS	ATTTACGGTAAACTG CCCAC	CGGGCGGGGCAGCG GCCTCTTAACAGCGG CATGGTGGCGGTACCA	--
2	MMTS	Annealed Gene Block		--
3	PLE-HA-DAF	CCCTGCTTGGGTTGCA GCCTGCACCAAGGTTC GCTATGGTGTGGCTGC TG	AAGTGGTTCCACTTCCTTTATT	--
4	pcDNA3 backbone	--	--	NdeI (5.457 kb)
Benchling: https://benchling.com/s/seq-GP0WiNLZrlsaJlbmyJoy				

(version 1- built off intermediate construct above) MMTS-PLE-HA -T2A-NLS-GFP

Fragment #	Gene	Forward primer	Reverse Primer	Nuclease
1	MMTS-PLE-HA	ATTTACGGTAAACTGC CCAC	GTGAGCAGAGAGCCCC GACCCTCAGCATAATC TGGAACATCATATGGATA	
2	T2A-NLS-GFP	TATCCATATGATGTTCC AGATTATGCTGAGGGT CGGGGCT	TAGAAGGCACAGTCGAGG	
3	MMTS-PLE-DAF backbone	--	--	NdeI/XhoI (4.52 kb)
Benchling: https://benchling.com/s/seq-ZMmZxANNzQwknf44PXOg				

LAMP1-NanoLuc-T2A-NLS-GFP

Fragment #	Gene	Forward primer	Reverse Primer	Nuclease
1	LAMP1	CACTATAGGGAGACCC AAGCTTGGTACCGCCA	GCTCCCTCCACCGCTCCCG CCGATGGTCTGATAGCC	

		CCATGG		
2	NanoLuc	GGCGGGAGCGGTGGA GGGAGCAGCGGTGGA GTCTTCACACTCGAAGATTT	CGACGTCGCCACATGTGA GCAGAGAGCCCCGACCCTCCGCCAGAATGCGT	
3	T2A-NLS-GFP	GAGGGTCGGGGCTCTCTGCTCACAT	TAGAAGGCACAGTCGAGG	
4	pcDNA3 backbone	--	--	KpnI/XhoI (4.935 kb)

Schemes and Figures

Scheme A4-1. *Improvements for imaging mitochondrial membrane potential using mitochondrial matrix localized PLE for and RhoVR-CPM*

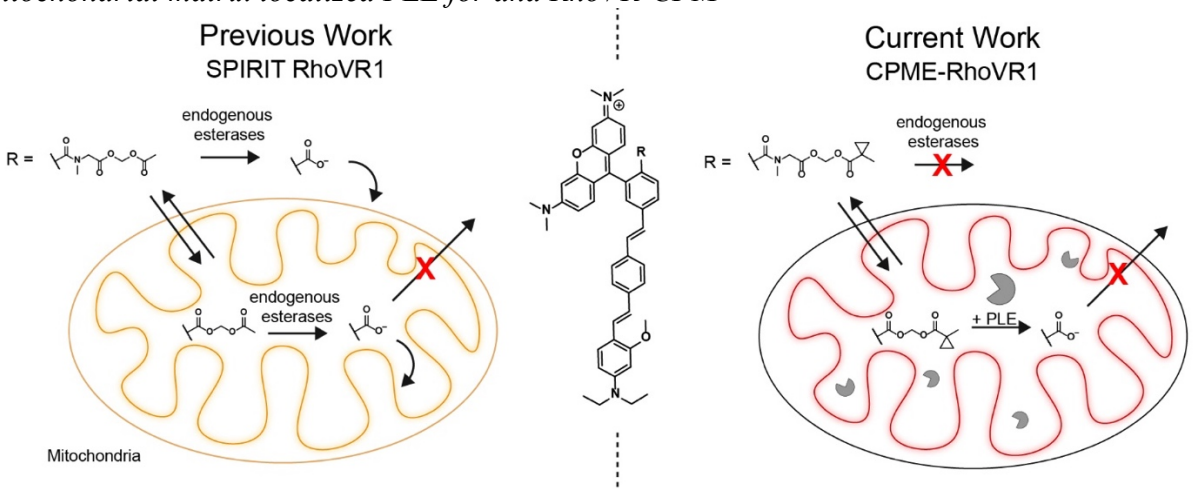

Scheme A4-1. Improvements for imaging mitochondrial membrane potential using mitochondrial matrix localized PLE for and RhoVR-CPM. Previously published work using SPIRIT RhoVR (left) localizes within the mitochondrial matrix where is accumulates within the inner membrane after the AM ester is cleaved by endogenous esterases (orange glow). However, endogenous esterases within the cytosol may pre-emptively remove the AM ester, preventing RhoVR1 from localizing within the inner membrane and instead label the outer mitochondrial membrane (orange, no glow). Current work (right) proposes to use a non-native esterase, PLE (grey), in combination with a bulkier CPM ester to RhoVR1. As a result the CMP ester group would be selectively removed only when the dye enters the matrix, thereby trapping RhoVR1 within to label only the inner membrane.

Scheme A4-2. *Bioluminescence voltage sensing at the lysosome.*

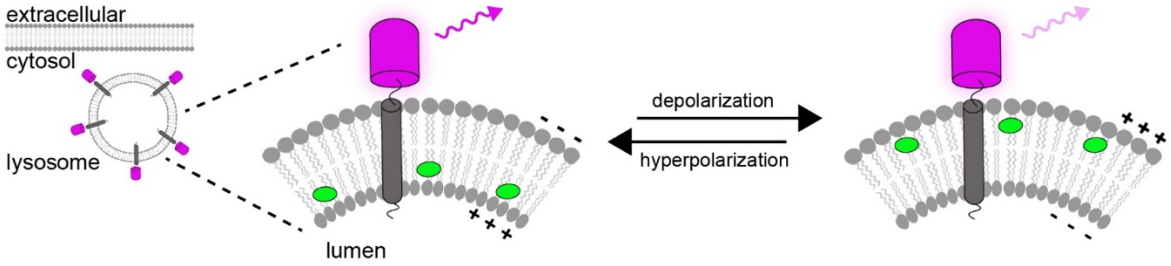

Figure A4-1. MMTS-PLE-HA immunostaining and MitoTracker colocalization

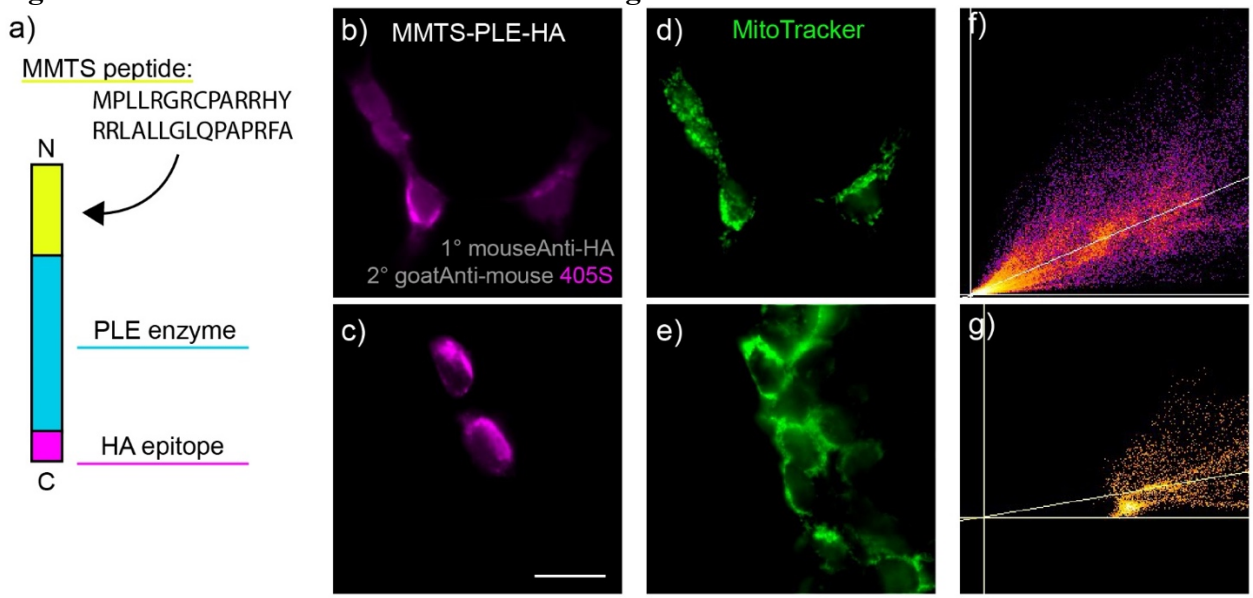

Figure A4-1. MMTS-PLE-HA immunostaining and MitoTracker colocalization. **a)** Schematic of the MMTS-PLE-HA pre-protein starting from the N- (top) to C- (bottom) terminals, mitochondrial matrix targeting sequence (MMTS) peptide in yellow, PLE in cyan, and the HA epitope used for immunostaining in **b)** and **c)** in magenta. **b)** and **c)** Representative epifluorescence images of fixed HEK 293T cells expressing MMTS-PLE-HA identified using a mouse Anti-HA primary antibody, followed by a goat Anti-mouse 405S secondary (magenta). **d)** and **e)** Mitochondria localization stained with MitoTracker Red (green) and ImageJ colocalization analysis between MitoTracker and 405S conjugated antibody emission plotted in **f)** and **g)**. Scale bar is 20 μm.

Figure A4-2. Lysosomal-NanoLuc targeting in live cells

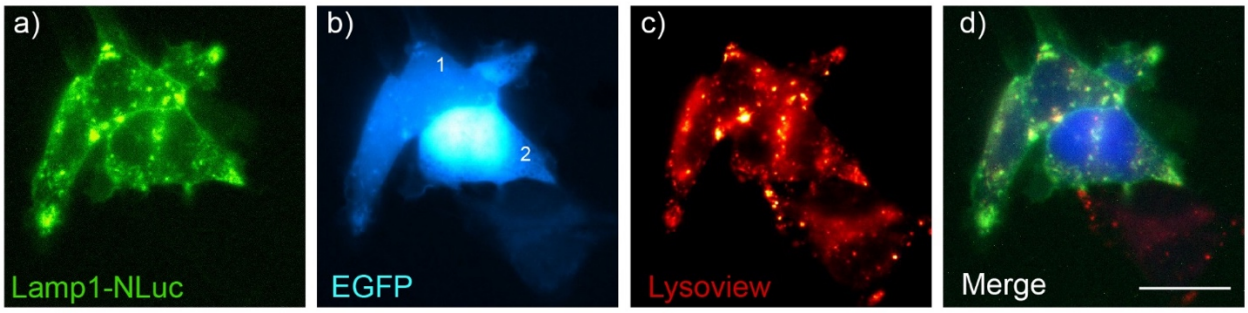

Figure A4-2. Lysosomal-NanoLuc targeting in live cells. a) Bioluminescence emission from Lamp1-NanoLuc expressing cells after the addition of 2x furimazine (~5-10 μM) **b)** Nuclear localized GFP was used as a successful transfection marker (cell 2), although the addition of Lysoview diffused the FP signal throughout some positively transfected cells (cell 1). **c)** Fluorescence from lysosomes of the cells shown in a) and b) labeled with 0.5x Lysoview (Biotium) and **d)** a merged image of all channels with the same color scheme used in a-c. Scale bar is 15 μM.

References

1. Pardo, L. A., Brüggemann, A., Camacho, J. & Stühmer, W. Cell cycle-related changes in the conducting properties of r-eag K+ channels. *J. Cell Biol.* **143**, 767–775 (1998).
2. Blackiston, D. J., McLaughlin, K. A. & Levin, M. Bioelectric controls of cell proliferation: ion channels, membrane voltage and the cell cycle. *Cell Cycle* **8**, 3519–3528 (2009).
3. Lin, M. & Beal, F. Mitochondrial dysfunction and oxidative stress in neurodegenerative diseases. *Nat. Rev.* **443**, (2006).
4. Bhatti, J. S., Bhatti, G. K. & Reddy, P. H. Mitochondrial dysfunction and oxidative stress in metabolic disorders — A step towards mitochondria based therapeutic strategies. *Biochim. Biophys. Acta - Mol. Basis Dis.* **1863**, 1066–1077 (2017).
5. Xu, H. & Ren, D. Lysosomal Physiology. *Annu. Rev. Physiol.* **77**, 57–80 (2015).
6. Koivusalo, M., Steinberg, B. E., Mason, D. & Grinstein, S. In situ measurement of the electrical potential across the lysosomal membrane using FRET. *Traffic* **12**, 972–982 (2011).
7. Klier, P. E. Z., Martin, J. G. & Miller, E. W. Imaging Reversible Mitochondrial Membrane Potential Dynamics with a Masked Rhodamine Voltage Reporter. *J. Am. Chem. Soc.* **143**, 4095–4099 (2021).
8. Tian, L. *et al.* Selective esterase-ester pair for targeting small molecules with cellular specificity. *Proc. Natl. Acad. Sci. U. S. A.* **109**, 4756–4761 (2012).
9. Liu, P., Grenier, V., Hong, W., Muller, V. R. & Miller, E. W. Fluorogenic Targeting of Voltage-Sensitive Dyes to Neurons. *J. Am. Chem. Soc.* **139**, 17334–17340 (2017).
10. Matamala, E., Castillo, C., Vivar, J. P., Rojas, P. A. & Brauchi, S. E. Imaging the electrical activity of organelles in living cells. *Commun. Biol.* **4**, 1–12 (2021).
11. Chanda, B. *et al.* A hybrid approach to measuring electrical activity in genetically specified neurons. *Nat. Neurosci.* **8**, 1619–1626 (2005).
12. Benlian, B. R. *et al.* Small Molecule-Protein Hybrid for Voltage Imaging via Quenching of Bioluminescence. *ACS Sensors* (2021). doi:10.1021/acssensors.1c00058
13. Van Kuilenburg, A. B. P., Muijsers, A. O., Demol, H., Dekker, H. L. & Van Beeumen, J. J. Human heart cytochrome c oxidase subunit VIII Purification and determination of the complete amino acid sequence. *FEBS Lett.* **240**, 127–132 (1988).

Appendix 5:
Bioluminolysis of Fluorogenic VoltageFluors

Introduction

Bioluminescence resonance energy transfer (BRET) has been widely used to study real time cellular dynamics including protein-protein interactions, protein expression patterns, metabolite sensing, and even membrane potential changes[1–4]. More recently, BRET has been used not only as a reporter tool but as a cellular effector and activator. For example, BRET can activate or inhibit neuronal activity via luminopsins, created by the fusion of luciferase and opsin proteins[5]. Energy transfer via BRET is also sufficient to cleave photolabile groups, a mechanism termed bioluminolysis, and can stimulate the release of bioactive molecules *in vivo*[6]. We reasoned this same principle could be extended to BRET-uncaging of our small-molecule photoactivatable optical sensor of transmembrane potential, SPOT2.1.Cl, which is capped with a dimethoxy-o-nitrobenzyl (DMNB) moiety[7].

The chemical structure of SPOT2.1.Cl is analogous to its parent derivative, VF2.1Cl, and localizes at the plasma membrane without internalization. Prior to uncaging, SPOT2.1.Cl is weakly fluorescent at the cell membrane, but upon site directed illumination (390 nm) the DMNB group is cleaved, and SPOT becomes brightly fluorescent[7]. Following photo-uncaging, activated SPOT2.1.Cl maintains a similar voltage response (~20% $\Delta F/F$) to its parent VF2.1Cl derivative[7,8]. This photo-activatability allows for spatial control and targetability of specific cells or subcellular regions, however, in deep tissue preparations light penetration, z-axis resolution, and phototoxicity (especially at shorter wavelengths) becomes a major limitation. For this reason, we thought bioluminolysis may expand our ability to uncage VoltageFluors within deep tissues at specific cell type populations (**Scheme A5-1**). Here describe preliminary efforts to determine if the bright and stable luciferase NanoLuc[9] could uncage SPOT2.1.Cl in transfected HEK cells. Under current conditions, we observe very little uncaging of SPOT2.1.Cl in cell expressing NanoLuc and treated with furimazine.

Results and Discussion

Uncaging SPOT2.1.Cl in HEK293T cells

After oxidation of its coelenterazine based substrate, furimazine, NanoLuc emits a bright blue with a peak of 460 nm. While the emission maximum is red shifted relative to the energy needed to cleave DMNB from SPOT2.1.Cl, the bioluminescence spectrum is broad and so we wondered if there would be enough energy to cleave the capping group. We achieved membrane localized bioluminescence using a previously discussed construct (NanoLuc-pDisplay used in Chapter 3). SPOT2.1.Cl labeled cells incubated with a 1:10 or 1:5 furimazine dilution did not appear to show VF uncaging (**Fig. A5-1**). Surprisingly, after 1 hour of incubation at 37°C bioluminescence is still seen (**Fig. A5-1a** and **c**). We also noticed a visual difference in the longer wavelength channel (540/50 nm emission) between the 1:10 and 1:5 dilutions, but the reasons are unclear. Cells with significantly more furimazine (1:5) seem to have some nuclear localized signal (**Fig. A5-1d**) whereas the fluorescence from cells in the 1:10 dilution seems to be mostly autofluorescence or dim SPOT2.1.Cl (**Fig. A5-1b**). In some instances there seems to be minimally brighter membrane fluorescence at a transfected cell, but overall this method using NanoLuc did not appear to be efficient.

NanoLuc is not an optimal donor given the poor spectral overlap with the DMNB moiety. Future studies should investigate alternative photolabile groups slightly red shifted relative to DMNB, near 430-450 nm. More blue shifted luminescent proteins paired with SPOT2.1.Cl could be an easier route. For example, one alternative could be the use of an obelin photoprotein mutant that has a bioluminescence emission at 390 nm[10]. Photoproteins, like obelin, or alternative

luciferase proteins may pose additional challenges, however, if the protein requires additional cofactors like calcium or ATP. Cleavage of a photolabile group covalently linked to a VoltageFlour should be possible using bioluminescence energy transfer, but more investigation is needed.

Experimental Methods

Cell culture

HEK293T cell lines were obtained from the UC Berkeley Cell Culture Facility and discarded after 25 passages. Cells were dissociated during passages using 0.05% Trypsin-EDTA with phenol red (Thermo Fisher Scientific) at 37°C, and then maintained in Dulbecco's Modified Eagle Medium (DMEM) with 4.5 g/L D-glucose supplemented with 10% FBS (Seradigm (VWR); Radnor, PA) and 2 mM 668 GlutaMAX (Gibco) in a 5% CO2 incubator at 37°C.

For all imaging experiments, cells were plated onto 25 mm diameter #1.5 glass coverslips (Electron Microscopy Sciences) in 6 well tissue culture plates (Corning; Corning, NY). To maximize cell attachment, coverslips were treated before use with 1-2 M HCl for 2-5 hours and washed overnight three times with 100% ethanol and three times with deionized water. Coverslips were sterilized by heating to 150°C for 2-3 hours. Before use, coverslips were incubated with poly-D-lysine (Sigma-Aldrich, made as a 0.1 mg/mL solution in phosphate-buffered saline with 10 mM Na_3BO_3) for 2-10 hours at 37°C and then washed twice with water and twice with Dulbecco's phosphate buffered saline (dPBS, Gibco). HEK293T cells were seeded 24 hours before microscopy experiments.

NanoLuc substrate and dye loading

Cells were loaded with 1 μM dye in HBSS for 20 minutes at 37°C and 5% CO2. Cells were washed 2x with HBSS and replaced with fresh HBSS. After rinsing, furimazine substrate (Promega) was added to NanoGlo buffer, mixed, added to the SPOT2.1.Cl labeled cells and incubated for 1 hr at 37°C. The final substrate concentration for a 1:10 dilution is roughly ~5-10uM, and double that for the 1:5 dilution (estimates based on information provided from Promega).

Live cell microscopy

All imaging was performed on an inverted epifluorescence microscope AxioObserver Z-1 (Zeiss), equipped with a Spectra-X Light engine LED light (Lumencor), controlled using μManager (V1.4, open-source, Open Imaging). Bioluminescence emission was collected using a 460/30 nm (Semrock) emission filter (10 second exposure). For SPOT2.1.Cl images, excitation light was delivered at 475/34 nm using an LED and collected with an emission filter (bandpass; 540/50 nm; 100 ms exposure time) after passing through a 510 LP dichroic mirror. Images were acquired using Plan-Apochromat 20/0.8 air objective (20x, Zeiss) and captured on an OrcaFlash4.0 sCMOS camera (sCMOS; Hamamatsu).

Schemes and Figures

Scheme A5-1. *Synthesis and photoactivation of SPOT*

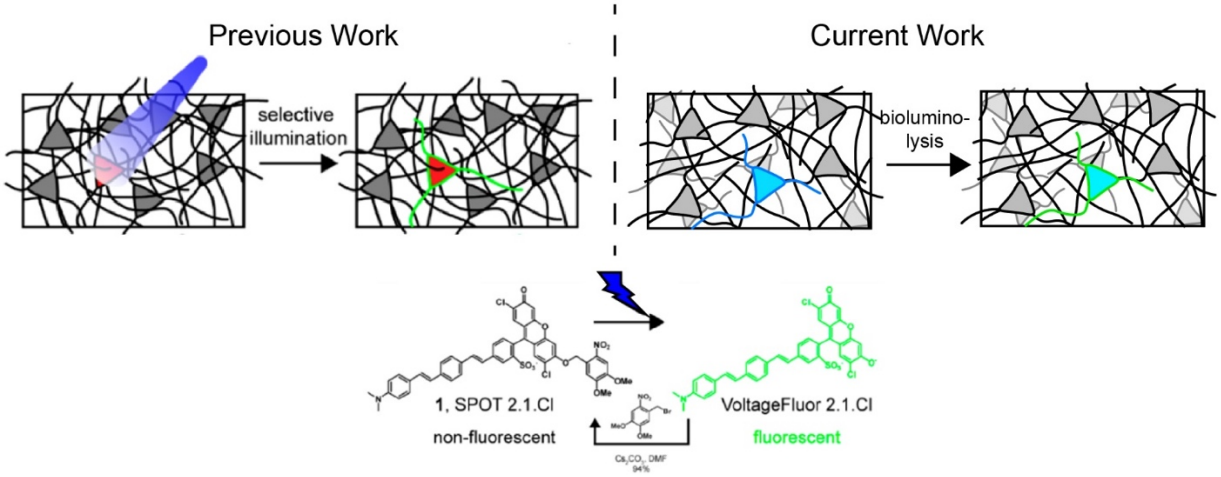

Figure A5-1. ***Bioluminescent uncaging of SPOT2.1.Cl in HEK using NanoLuc***

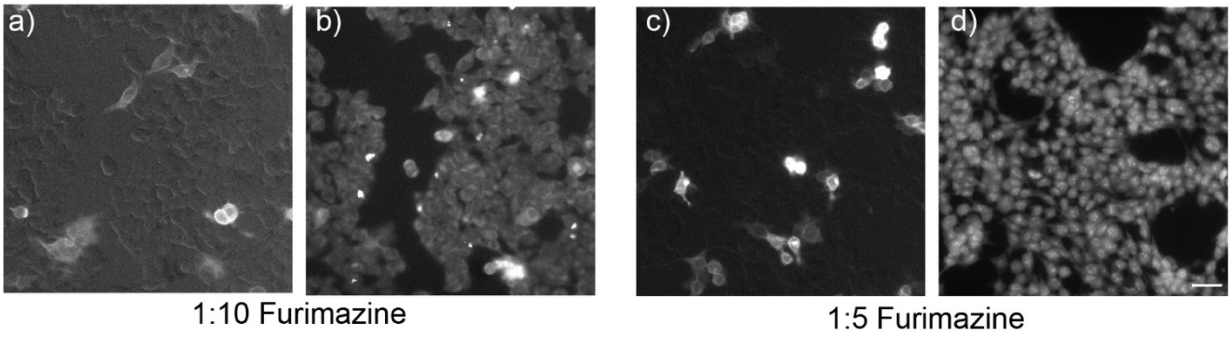

Figure A5-1. Bioluminescent uncaging of SPOT2.1.Cl in HEK using NanoLuc. Live cell imaging of cells pre-loaded with SPOT2.1.Cl and incubated with furimazine at 37°C. **a)** bioluminescence and **b)** fluorescence emission in HEK293T cells after 1 hour incubation with a 1:10 furimazine dilution. **c)** Bioluminescence and **d)** fluorescence emission after 1 hour incubation with a 1:5 furimazine dilution. Scale bar is 40 μm.

References

1. Inagaki, S. *et al.* Genetically encoded bioluminescent voltage indicator for multi-purpose use in wide range of bioimaging. *Sci. Rep.* **7**, 1–11 (2017).
2. Benlian, B. R. *et al.* Small Molecule-Protein Hybrid for Voltage Imaging via Quenching of Bioluminescence. *ACS Sensors* (2021). doi:10.1021/acssensors.1c00058
3. Zhang, G. J. *et al.* Bioluminescent imaging of Cdk2 inhibition in vivo. *Nat. Med.* **10**, 643–648 (2004).
4. Dixon, A. S. *et al.* NanoLuc Complementation Reporter Optimized for Accurate Measurement of Protein Interactions in Cells. *ACS Chem. Biol.* **11**, 400–408 (2016).
5. Berglund, K. *et al.* Luminopsins integrate opto- and chemogenetics by using physical and biological light sources for opsin activation. *Proc. Natl. Acad. Sci.* (2016). doi:10.1073/pnas.1510899113
6. Chang, D. *et al.* Luciferase-Induced Photouncaging: Bioluminolysis. *Angew. Chemie - Int. Ed.* **58**, 16033–16037 (2019).
7. Grenier, V., Walker, A. S. & Miller, E. W. A Small-Molecule Photoactivatable Optical Sensor of Transmembrane Potential. *J. Am. Chem. Soc.* **137**, 10894–10897 (2015).
8. Miller, E. W. *et al.* Optically monitoring voltage in neurons by photoinduced electron transfer through molecular wires. *Proc. Natl. Acad. Sci. U. S. A.* **109**, 2114–2119 (2012).
9. England, C. G., Ehlerding, E. B. & Cai, W. NanoLuc: A Small Luciferase Is Brightening Up the Field of Bioluminescence. *Bioconjug. Chem.* **27**, 1175–1187 (2016).
10. Malikova, N. P. *et al.* Spectral tuning of obelin bioluminescence by mutations of Trp92. *FEBS Lett.* **554**, 184–188 (2003).